IMPROVING LINKAGE OF HEPATIC TOXICITY AND PATHOLOGY ENDPOINTS WITH TOXICOGENOMICS

Christine Louise Powell

A dissertation submitted to the faculty of the University of North Carolina at Chapel Hill in partial fulfillment of the requirements for the degree of Doctor of Philosophy in the Curriculum in Toxicology

Chapel Hill
2007

Approved by:

Ivan Rusyn, M.D., Ph.D.

Richard S. Paules, Ph.D.

James A. Swenberg, D.V.M., Ph.D.

David W. Threadgill, Ph.D.

Michael D. Wheeler, Ph.D.

ABSTRACT

CHRISTINE POWELL: Improving Linkage of Hepatic Toxicity and Pathology Endpoints with Toxicogenomics
(Under the direction of Ivan Rusyn, M.D., Ph.D.)

The science of toxicology is directed toward understanding the mechanisms by which environmental agents cause adverse health effects in humans. Traditional methodologies to assess toxicity have relied on observable adverse effects which have proven to be useful diagnostic indicators; however, frequently they do not provide mechanistic insight necessary to unravel the complex biological networks responsible for the development of disease. Toxicogenomics, a sub-discipline of toxicology which examines the global genomic response of organisms to a toxic insult, when applied in parallel with classical toxicological endpoints can advance the field by providing molecular markers of exposure and response, and defining disease processes. Thus, we hypothesize that molecular signatures defining disease mechanisms and early effects of exposure can be phenotypically anchored to biomarkers of oxidative stress and DNA damage. In Aim 1, a molecular signature of incipient toxicity for an acute sub-toxic dose of acetaminophen was phenotypically anchored to oxidative stress markers based on its mechanism of hepatotoxicity. The detection of early changes in a biologic process at doses and times with no apparent clinical signs of toxicity provides an improved basis to develop predictive markers of effect. In Aim 2, molecular signatures were identified that temporally modeled disease pathology and oxidative stress for a choline-deficient model of rodent hepatocellular carcinoma (HCC). Measures of oxidative DNA damage established a temporal linkage between fibrosis and accumulation of DNA lesions, processes that may contribute to

hepatocyte transformation. Moreover, comparison of rat and human HCC expression profiles, regardless of etiology, demonstrated that advanced stages of liver disease converge onto a common and indistinguishable phenotype. In Aim 3, gene expression profiling combined with measures of oxidative stress established that dietary fatty acids can have a profound yet differential effect on oxidative stress in the liver mediated by their ability to activate PPARα. Many environmental exposures exhibit human toxicity and disease through oxidative-stress signaling pathways. Thus, dietary fatty acids can markedly influence sensitivity or resistance to disease. In summary, toxicogenomics moves the field of toxicology beyond traditional approaches by linking the critical molecular events caused by exposure to environmental factors with disease.

DEDICATION

To my parents, Teresa and T.D. Powell,

whose love and support made all this possible

ACKNOWLEDGEMENTS

I give my sincere appreciation to my mentor, Dr. Ivan Rusyn, for his years of support, wisdom and words of encouragement. I am deeply appreciative for the knowledgeable advice and recommendations contributed by my committee: Dr. Richard S. Paules, Dr. James A. Swenberg, Dr. David W. Threadgill, and Dr. Michael Wheeler. I am indebted to the members of Dr. Ivan Rusyn's laboratory: Mrs. Blair Bradford, Ms. Amanda Burns, Mr. Dan Gatti, Ms. Alison Hege, Mrs. Oksana Kosyk, Ms. Pamela Ross and Ms. Courtney Woods.

I would not have been able to complete the work presented here without the contributions and assistance from the many people I was so fortunate to have collaborated with. It is my great pleasure to recognize the following individuals and their respectable institutions:

- Mr. Robert Schoonhoven, Mrs. Pat Upton, Dr. Jun Nakamura, Dr. Gunnar Boysen and Dr. Kerry-Ann Da Costa of University of North Carolina at Chapel Hill
- Dr. Alexandra N. Heinloth, Dr. Gary A. Boorman and Dr. Michael L. Cunningham of the National Institute of Environmental Health Sciences
- Dr. Ayumi Denda of Department of Nara Medical University
- Dr. Fumiyuki Uematsu and Dr. Dai Nakae of Sasaki Foundation
- Mr. Joel S. Parker of Constella Health Sciences
- Dr. Edward K. Lobenhofer of Paradigm Array Labs

TABLE OF CONTENTS

LIST OF TABLES

LIST OF FIGURES

LIST OF ABBREVIATIONS AND SYMBOLS

8-OH-dG	8-hydroxy-deoxyguanosine
ALT	alanine aminotransferase
AP	apurinic/apyrimidinic
Ape	apurinic/apyrimidinic endonuclease 1
APAP	acetaminophen
ARP	aldehyde reactive probe
BER	base excision repair
CD	choline deficient/choline deficiency
CS	choline sufficient L-amino acid defined
DAG	1,2-*sn*-diacylglycerol
EPA	Environmental Protection Agency
EMSA	electromobility shift assay
FDA	Food and Drug Administration
FDR	false discovery rate
GO	gene ontology
GSH	glutathione
H_2O_2	hydrogen peroxide
HBV	hepatitis B virus
HCC	hepatocellular carcinoma
HCV	hepatitis C virus
HNE	4-hydroxynonenal
HSC	hepatic stellate cells
MDA	malondialdehyde
Mgmt	O^6-methylguanine DNA methyltransferase

Mpg	N-methylpurine DNA glycosylase
NAPQI	N-acetyl-*p*-benzoquinone imine
$NO^{\cdot}$	nitric oxide
NOEL	no observable effect level
$O_2^{\cdot -}$	superoxide anion
Ogg1	8-oxoguanine DNA glycosylase 1
·OH	hydroxyl radical
$ONOO^-$	peroxynitrite
Parp	poly (ADP-ribose) polymerase
PC	phosphotidylcholine
PCNA	proliferating cell nuclear antigen
PKC	protein kinase C
PPARα	peroxisome proliferator-activated receptor alpha
Pol β	polymerase (DNA directed) β
Pol δ	polymerse (DNA directed) δ
PUFA	polyunsaturated fatty acids
ROS	reactive oxygen species
SAM	significance analysis of microarrays
TRC	Toxicogenomics Research Consortium
ω	omega
WY	WY-14643; 4-chloro-6-(2,3-xylidino)-2-pyrimidinylthioacetic acid

CHAPTER I

INTRODUCTION

A. INTEGRATING TOXICOGENOMICS WITH CURRENT TOXICOLOGY TESTING METHODS TO ADVANCE RISK ASSESSMENT

1. Toxicogenomics Defined

The science of toxicology is directed toward understanding the mechanisms by which individual environmental agents cause their effects in humans. Due to technical limitations, the evolution of toxicological science has been relatively slow and was accomplished one chemical or one mechanism of action at a time. In addition to chemicals and drugs, there are other environmental factors and stressors, such as radiation, biological agents, and dietary and lifestyle factors that alone or by interaction contribute to the development of disease. The complex effects of the environment must be characterized to a progressively greater depth for us to understand their biochemical and genetic impact on the cells in which adverse effects are manifested. Thus, new technologies such as genomics, the science of characterizing genes, including variation and gene regulation, and their functions in cells and tissues would contribute greatly to the advancement of toxicology. Toxicogenomics, a sub-discipline of toxicology, elucidates how the entire genome is involved in biological responses of organisms exposed to environmental toxicants/stressors. Toxicogenomics gets its strength from the combination of disciplines and a mixture of traditional and innovative research methods. Genetic susceptibility and the environmental stressors that instigate disease in humans is the focus of much research and are of importance to regulatory agencies. New methods to characterize environmental agents, their cellular and molecular mechanisms, and ultimately their effect on a whole genome scale, are being closely examined by regulatory agencies for integration into their decision making strategies (1). At the present state of development for the field of toxicogenomics, the major advances in understanding toxic effects will still be made one chemical, agent, or mechanism at a time. The promise of this new technology is such that it can be used to generate data on large numbers of chemicals and exposure conditions and to develop an

unprecedented knowledge base that can be used to guide future research, improve environmental health, and aid in regulatory decisions (2, 3).

2. Phenotypic Anchoring of Toxicogenomic Data

The results of the gene expression profiling studies can serve as a guide in the search for specific genes/proteins that could be used as biomarkers of incipient toxicity, or can predict the pathological changes that are yet to be realized by morphological analysis. The linkage of candidate biomarkers (e.g., genes and metabolites) to the actual causal processes that lead to specific toxic effects can be accomplished through studies involving morphological and ultrastructural analysis of the changes, *in situ* hybridization, immunohistochemistry, and the laser-capture microdissection of cells to relate the expression of the putative biomarkers to the specific cells that have undergone these adverse events (4). For example, studies from the National Center for Toxicogenomics have demonstrated the capability of identifying signature patterns of altered gene expression that can be used to predict the classes of chemicals that an animal was exposed to based on an initial training set of chemicals (5, 6). This work led to the hypothesis that it is possible to define signature patterns of altered gene expression that indicate specific adverse effects of chemical, drug, or environmental exposures. The idea is that once signatures are identified using large-scale global microarray analysis, it will then be possible to develop smaller multi-chemical and multi-pathway arrays that can be used to assess the potential toxicity of chemicals in a rapid, prospective manner. The so called “phenotypic anchoring” of gene expression data to toxicological and pathological indices is required to remove some of the subjectivity of conventional molecular expression analyses. It also helps to distinguish the toxicological effect signal from other gene expression changes that may be unrelated to toxicity, such as the varied pharmacological or therapeutic effects of a compound. This distinction could mean better insights into pathways of toxicity and disease processes and

their mechanisms that have been heretofore unattainable.

3. Moving the Field of Toxicogenomics Forward

Predicting adverse health outcomes in humans resulting from chemical exposure has traditionally relied on observable, treatment related adverse events. The adverse event may include gross changes in body or organ weight, histopathological observations, changes in clinical chemistry or hematological parameters, or more commonly, a combination of all of the above. These endpoints have proven to be useful diagnostic indicators; however, frequently they do not provide mechanistic insight necessary to unravel the complex biological networks responsible for the pathogenesis and progression of disease. Moreover, these measures are insensitive to detect low-level toxicity or pre-clinical stages of disease which can lead to inaccurate hazard assessment (7). Since changes in cellular responses brought about by chemical exposure are thought to precede morphological changes, alterations in gene expression may serve as early, sensitive indicators of potential toxicity compared to currently employed methods. Toxicogenomic studies applied in parallel with traditional measures of toxicity can establish important linkages between altered gene transcripts and the pathological sequelae of events leading to toxicity. Information generated from such data sets has the potential to provide insights into mode of action and to identify sensitive biomarkers of exposure. Unfortunately, much of the available toxicogenomic data that has been published to date, with few exceptions, has been limited to a qualitative description of alterations in gene transcripts with little or no correlation to toxicity or contribution to the elucidation of mechanisms of toxicity (8).

The gene signature itself provides little information for understanding the underlying mechanism of toxicity or disease. Assigning biological function (i.e., functional genomics) to gene sets and uncovering how their gene products work together under normal homeostatic conditions and after perturbation by environmental agents are needed to define the complex

exposure-disease relationship. The Gene Ontology (GO) Consortium has developed three vocabularies to describe gene products as a function of their biological processes, their cellular components, and their molecular/biochemical function. Graphical user interfaces such as GoMiner (9) work with GO to identify global molecular and biochemical trends in gene expression data. Then, and most importantly, gene functionality can be phenotypically anchored to measures of toxicity to uncover how sets of genes and their products work together in health and disease. Integrating functional genomics with phenotypic anchors of toxicity presents us with an opportunity to define at unprecedented levels of detail, the molecular events that precede and accompany toxicity, promising to shed light on toxic mechanisms that are presently poorly understood (10). The information gathered from such studies can further reduce the uncertainity factors that are weighted in determining the safety factor to prevent adverse health effects in humans. Regulatory agencies are watching this field closely but will be reluctant to accept such data sets until this field undergoes significiant scientific rigor. As such, proof-of-principle studies must be conducted using well characterized models of toxicity to establish toxicogenomics as a valuable and biologically meaningful tool in toxicology.

B. OXIDATIVE STRESS

1. Oxidative Stress as a Common General Mechanism of Toxicity and Disease

Cells living in an oxygen-rich environment are inundated with various endogenous and exogenous sources of reactive oxygen species (ROS). As a consequence of cellular metabolic and biochemical processes such as mitochondrial respiration, β-oxidation, and cytochrome P450 metabolism, there is a steady production of ROS in the cell (11). Additionally, inflammation, exposure to ultraviolet radiation, γ-irradiation, and the formation of reactive intermediates from xenobiotic metabolism serve as exogenous mediators of ROS

generation (12). ROS are known to play dual role in biological systems, since they can be either harmful or beneficial to living systems (13). Beneficial effects involve physiological roles in the defense against infectious agents, in the function of numerous cellular signaling pathways, and at low concentrations the induction of a mitogenic response. However, oxidative stress can arise when the production of ROS exceeds the cell's antioxidant capacity, resulting in damage to cellular macromolecules such as DNA, proteins, and lipids (14). As a result, cells have evolved numerous defense mechanisms to counteract and limit the levels of reactive oxidants and the cellular damage that can ensue (15). These include enzymatic reduction of ROS by superoxide dismutase, glutathione peroxidase, and catalase, as well as non-enzymatic quenching of ROS by vitamin E, vitamin C, β-carotene, and glutathione (16). Besides these primary defense mechanisms, selective proteolysis of oxidatively damage proteins and various mechanisms of DNA repair act as secondary antioxidant systems to maintain the integrity of protein homeostasis and genetic information. Despite these defense responses against ROS, oxidative damage accumulates during the life cycle, and radical-mediated damage to DNA, proteins, and lipids has been proposed to play a key role in aging and the development of age-dependent diseases such as cancer, atherosclerosis, arthritis, neurodegenerative disorders, diabetes and other conditions. Moreover, exposure to exogenous sourcs of free radicals including drugs, environmental pollutants like ozone and polychlorinated biphenyls, cigarette smoke, and various fungal and bacterial toxins exhibit human toxicity and disease through oxidative stress-sensitive signaling pathways.

While excessive ROS production clearly damages cells, low transcient levels of ROS play a major physiological role in regulating intracellular signaling pathways (17). The induction and propagation of intracellular signaling events is tightly regulated by the cellular redox state which ultimately is governed by ROS levels. Alterations in the redox state are primarily mediated through oxidation of protein sulfhydryl groups resulting in conformational

changes in proteins (18). Such changes mediate oxidants to stimulate receptor tyrosine kinases, even in the absence of ligand, as well as the downstream effectors in signal transduction pathways including ras, growth factor kinase, src/Abl kinase, c-jun-N-terminal kinase, mitogen activated protein kinase (MAPK) and phosphoinositide-3 kinase (PI-3) dependent signaling pathways (19-21). As a result, several redox-regulated transcription factors are activated including AP-1, NF-κB, p53, and HIF-1 (18, 22). These transcription factors control the expression of genes that modulate cell signaling, DNA synthesis, enzyme activation, selective gene expression, regulation of the cell cycle, and cell survival (23). Thus, the cellular redox potential is an important determinant of cell function and disruptions of redox balance may adversely affect the fate and function of the cell.

2. *Reactive Oxygen Species and Biomolecules*

2.1 DNA

DNA damage as a result of oxidative stress is considered to be the most common insult affecting the genome (24, 25). DNA is a particularly sensitive cellular target because of the potential to create cumulative mutations that can disrupt cellular homeostasis. Oxidative DNA damage can include chemical and structural modifications to purine and pyrimidine bases and 2′-deoxyribose, and the formation of single- and double-strand breaks (26). Persistent oxidative DNA damage can result in either arrest or induction of transcription, induction of signaling transduction pathways, replication errors and genomic instability. In a given cell, it is estimated that 10^5 oxidative DNA lesions are formed each day (27). The exact number of oxidative DNA adducts is unknown but over 100 have been identified thus far; however, whether each of these adducts are produced in measurable amounts *in vivo* to be biological relevant remains to be determined (28-31). Oxidative stress-induced mutations are suggested to play a major role in a number of chronic diseases

including carcinogenesis, neurodegenerative disorders, and cardiovascular disease (11, 26, 32).

In living cells, ROS are formed continuously as a consequence of both metabolic and biochemical reactions in addition to external factors. These ROS include oxygen radicals such as superoxide ($O_2^{\cdot-}$), hydroxyl (·OH), peroxyl ($RO_2\cdot$), alkoxyl ($RO\cdot$), and hydroperoxyl ($HO_2\cdot$); and non-radicals that possess strong oxidizing potential or are easily converted to radicals by transition metals that include singlet oxygen ($^1O_2$), hydrogen peroxide (H_2O_2), hypochlorous acid (HOCl), ozone (O_3), and peroxynitrite ($ONOO^-$). DNA damage induced by ROS occurs by way of chemical and structural alterations to purine and pyrimidine bases and 2′-deoxyribose, and the formation of abasic sites and DNA strand breaks, see Figure 1.1 (26).

The interaction of reactive oxidants with DNA can occur in a variety of ways. For instance, some ROS do not interact at all with DNA bases, such as superoxide and hydrogen peroxide (33, 34). Instead, they are believed to elicit their toxicity to DNA by conversion to hydroxyl radicals mediated by transition metal ions (e.g. iron and copper) through Haber-Weiss and Fenton reactions (35, 36). The hydroxyl radical is highly reactive and does not diffuse more than a couple of molecular diameters before reacting with the closest cellular component (36, 37). Therefore, in order to oxidize DNA directly, the hydroxyl radical must be generated immediately adjacent to nucleic acids. An assortment of products could be generated from such reactions since the hydroxyl radical reacts with all bases by either addition or abstraction of hydrogen atoms (33). The most frequent base lesion produced is by addition of a hydroxyl radical to the C8 position of guanine to produce 8-oxo-dG, a marker commonly measured to assess oxidative stress to DNA. This adduct is a mutagenic lesion that preferentially pairs with adenine rather than cytosine resulting in G:C to T:A transversions following replication (38, 39).

Peroxynitrite is a strong DNA oxidizing and nitrating agent that is a product of the

coupling reaction of superoxide and nitric oxide. Damage to DNA by peroxynitrite can include strand breaks, base oxidation, deamination of guanine and adenine, and nitration of guanine bases (40-42). Peroxynitrite has been demonstrated to oxidize purine bases with the formation of oxazolone, 8-oxo-7,8-dihydro-2'-deoxyadenosine, and 8-oxo-dG (43, 44). Moreover, it has been shown that peroxynitrite is at least a 1000 fold more reactive toward 8-oxo-dG than normal 2'-deoxyguanosine generating secondary products of 2-deoxy-β-D-erythro-pentofuranosyl derivatives of cyanuric, parabanic, and oxaluric acid (45, 46). Mutations induced by peroxynitrite using pSP189 shuttle vector were predominately G:C to T:A transversions after replication in both bacteria and mammalian cells (47). Activated macrophages produce both superoxide and nitric oxide; thus, they are a potential source of peroxynitrite. Unlike the hydroxyl radical, peroxynitrite has the ability to diffuse across cells providing a potential linkage between chronic inflammation and carcinogenesis.

Oxidants can react with the sugar moiety of DNA leading to the formation of apurinic/apyrimidinic (AP) sites and single- and double-strand breaks. The hydroxyl radical can abstract hydrogen atoms from all five carbon atoms of 2′-deoxyribose resulting in base loss and/or strand breakage (12). Oxidative DNA adducts can promote cleavage of the *N*-glycosidic bond with deoxyribose which can result in the formation of an AP site. Furthermore, deoxyribose oxidation leads to the formation of base propenal and 3-phosphoglyceraldehyde which can react with DNA to form pyrimidopurinone (M_1G) and etheno-adducts, respectively (48).

Indirect mutagenicity of DNA can occur by lipid peroxidation, a process involving the oxidation of polyunsaturated fatty acids (PUFA). In the presence of transition metal ions, the generation of reactive carbonyl products, including epoxides and aldehydes, can be generated and then covalently bind to DNA. These reactive substances damage DNA by forming exocyclic adducts (49, 50) which have been shown to have genotoxic and mutagenic effects. For example, 4-hydroxynonenal (HNE) can form an etheno-DNA adduct

which can promote chromosomal aberrations and sister chromatid exchanges (51, 52) whereas, malondialdehyde (MDA) can give rise to M_1G that is highly mutagenic resulting in base pair substitutions (51, 52).

2.2 Proteins

One of the hallmarks of chronic or severe oxidative stress is the accumulation of oxidized proteins, which tend to form high-molecular weight aggregates. Protein oxidation is important to cellular homeostasis in the fact that proteins serve vital roles in regulating cell structure, cell signaling, and the various enzymatic processes of the cell. Identification and mechanisms involved in the formation of protein oxidation products has been investigated both *in vivo* and *in vitro* using isolated amino acids and cell free extracts (53-55). The mechanisms involve metal catalyzed oxidation, oxidation induced cleavage, amino acid oxidation, and the conjugation of lipid peroxidation products.

Metal-catalyzed oxidation of proteins is one of the most common mechanisms for inducing protein oxidation, especially for the introduction of carbonyl groups. This process requires the generation of H_2O_2 and the presence of transition metal ions such as iron or copper (56, 57). The ions bind to specific metal binding sites within the protein and through Fenton chemistries react with H_2O_2 to generate $^{\cdot}OH$ that then attacks nearby amino acid residues. Cleavage of peptide bonds can occur if the hydroxyl radical generated from H_2O_2 abstracts a hydrogen atom from the polypeptide backbone forming a carbon-centered free radical (alkyl-radical). This radical can then cross-link with other alkyl radicals and form protein aggregates or can react with O_2 to generate alkyl-peroxyl radical. The peroxyl radicals can then be converted to alkyl peroxides by reactions with the protonated from of superoxide.

The side chains of all amino acids are susceptible to oxidation by ROS/RNS; however, the most sensitive amino acids are those with aromatic side chains (tyrosine,

tryptophan, or phenylalanine) and those containing sulfhydryl groups (histidine, methionine, and cysteine). ROS-induced oxidation of aromatic side-chain amino acids can occur through a variety of intermediates. For example, the oxidation of phenylalanine residues leads to the formation of mono- and di-hydroxy derivatives whereas tryptophan residues are converted to several hydroxyl-derivatives, to formylkynurenine and to nitrotryptophan (56). Tyrosine residues can be attacked by reactive nitrogen species generating 3-nitrotyrosine (58). In contrast to aromatic amino acids, cysteine and methionine residues are oxidized via reactions at the site of sulfhydryl residues (59). This oxidation is reversible as cross-linked derivatives can be repaired by disulfide exchange reactions catalyzed by thiol transferases.

Protein carbonyls may be generated by the oxidation of several amino acid side chains by the formation of Michael adducts between lysine, histidine, and cysteine residues and α,β-unsaturated aldehydes (56). They can also be generated with reducing sugars or glycoxidation of lysine amino groups. Protein carbonyls can further react with the α-amino groups of lysine residues (60) forming intra- or inter-molecular cross-links which can promote the formation of protein aggregates.

2.3 Lipids

Lipid peroxidation is a process involving the oxidation of polyunsaturated fatty acids (PUFAs). The overall process consists of three stages: initiation, propagation, and termination. It is initiated by abstraction of a hydrogen atom that can be mediated by the hydroxyl, peroxyl, and alkoxyl radicals forming lipid hydroperoxides; however, these species are relatively short-lived (61). Conversely, in the presence of transition metals the highly biologically reactive carbonyl products, including epoxides and aldehydes [e.g., crotonaldehyde, acrolein, 4-hydroxynonenal (HNE), and malondialdehyde (MDA)], can be produced and then diffuse from site of production and covalently bind to proteins and DNA (62).

The peroxidation of membrane lipids can be very damaging because it leads to alterations in the biological properties of cell membranes leading to inactivation of membrane bound receptors or enzymes which in turn may impair normal cellular functions. Moreover, it is an autocatalytic process which is terminated only by the recombination of radicals or depletion of substrate (63). Thus, the initial oxidation of only a few lipid molecules can result in significant tissue damage.

3. *Mechanisms of DNA Repair*

Systems of response to DNA damage that reduce the yield of mutations and chromosomal aberrations in damaged cells are collectively known as DNA repair. Repair enzymes recognize and remove DNA adducts, correct the DNA sequence, and rejoin strand breaks. The cell possesses a number of DNA repair mechanisms to deal with oxidative and alkylated DNA lesions, including direct damage reversal (via the enzyme O^6-methylguanine-DNA methyltransferase), base and nucleotide excision, and mismatch repair. Mechanisms for repair of strand breaks include non-homologous end-joining and homologous recombination.

It is believed that the predominant pathway used for removal of oxidized and many of the alkylated bases is base excision repair (BER), see Figure 1.2. The process of BER is initiated by DNA glycosylases [e.g. 8-oxoguanine DNA glycosylase 1 (Ogg1), endonuclease III homolog 1 (NTH1), thymine glycol-DNA- glycosylase (NTH)] which are often promiscuous as far as their substrate specificity is concerned. The glycosylase hydrolyzes the *N*-glycosylic bond between the oxidized base and sugar moiety thus releasing the free damaged base and giving rise to an AP site. AP endonuclease (APE) acts upon the AP site generating a single strand break by cleaving the phosphodiester backbone 5′ to the AP site, leaving behind a 3′-hydroxyl group and a 5′-deoxyribose phosphate group (dRP). At this point the BER pathway can proceed through two different sub-pathways: short-patch and

long-patch BER. These pathways are differentiated by the enzymes involved and the number of nucleotides removed. Short-patch BER replaces a single nucleotide by polymerase β (Pol β) and the newly synthesized DNA sealed by DNA ligase III/XRCC1 heterodimer (64). Long-patch BER inserts 2 to 13 nucleotides by concordant action of Pol β, PCNA, Fen 1, and ligase 1.

Even though DNA lesions and misincorporations are dealt with by a complex system of DNA repair enzymes, the process of repair proceeds through several intermediate steps that involve the formation of secondary lesions which are also mutagenic and clastogenic (i.e., abasic sites and single strand breaks) (65). There are a number of consequences of induction/deficiency in DNA repair that are important for the process of carcinogenesis. Although induction would lead to enhanced repair, it has been suggested that this can be deleterious and promote mutagenesis (66). If enzymes that act consecutively on different steps of repair are up-regulated unevenly, a state of imbalanced DNA repair might occur and lead to accumulation of both mutagenic and clastogenic lesions (67, 68). It should also be noted that not all polymerases have the same fidelity with some being more prone to introducing incorrect nucleotides (69).

4. Oxidative DNA Damage and Cancer

Cancer pathogenesis is a multi-step process involving mutations in critical genes required for maintaining cellular homeostasis and the clonal expansion of these mutated cells (70). The foremost is the ability to induce DNA damage that can lead to mutations if replication proceeds without proper repair. Oxidative stress-induced DNA damage can lead to mutations and is suspected to be a major cause of cancer (32, 71). Furthermore, persistent oxidative DNA damage can alter signaling cascades, gene expression, induce or arrest transcription, and increase replication errors and genomic instability, all of which have been described in the progression of cancer development.

Chronic inflammation from infection or injury is believed to contribute to about one in four of all cancer cases worldwide (72). Inflammation activates a variety of immune cells which induce a number of oxidant-generating enzymes such as NADPH oxidase, inducible nitric oxide synthase, and myeloperoxidase that are capable of producing high concentrations of ROS (e.g., superoxide anion, hydrogen peroxide, nitric oxide, and peroxynitrite). The increased production of ROS can increase the yield of mutations in DNA and also serve as an intracellular signal to promote mitogenesis (73). A number of viral and microbial diseases such as hepatitis C, *Helicobacter pylori*, and human papillomavirus are associated with an increased risk of liver, colon, and cervical cancer, respectively (74). Furthermore, they are all associated with an increase in the DNA adduct, 8-oxo-dG. To reduce the cancer risk, treatment strategies have targeted to alleviate the inflammation (e.g., anti-inflammatory agents such as interferons) or oxidant production (e.g., antioxidants such as ascorbic acid, β-carotene, and α-tocopherol) (75, 76).

Chlorinated compounds, metal ions, barbiturates, phorbol esters, aromatic hydrocarbons, and some peroxisome proliferators are chemical carcinogens that have been shown to induce oxidative stress and damage *in vitro* and *in vivo* (77). The mode of action of many chemical carcinogens is by generating ROS through redox cycling via electron transfer groups such as quinones, metal complexes, aromatic nitro compounds, and conjugated imines. Benzene is classified as a human carcinogen and inhalation or dermal occupational exposures have been associated with acute leukemia and lymphoma (78). While the mechanism of action for benzene is still not clearly understood, the induction of chromosomal aberrations in hematopoietic stem cells is believed to be a critical element. The metabolism of benzene produces a number of phenolic and quinone species that can undergo a one electron reduction to a very unstable semiquinone that rapidly reduces oxygen to superoxide, which regenerates the quinone and completes one redox cycle. Thus, this continuous cycle leads to an increase in ROS production and potential for

oxidative DNA damage. Measurements of the DNA adduct, 8-oxo-7,8-dihydro-2'-deoxyguanine (8-oxo-dG), have been reported in cell cultures and bone marrow *in vivo* after treatment with benzene (79).

The presence of multiple pathways of repair for DNA damage demonstrates its important role in maintaining genomic stability. Therefore, it would be expected that reduced enzymatic activity or a defective enzyme in DNA repair would increase the likelihood of mutations and as a result increase risk of disease. Indeed, there are a number of hereditary diseases (e.g., Xeroderma Pigmentosum, Trichothiodystrophy, Cockayne's Syndrome, and Fanconi's Anemia), although extremely rare, that are characterized by an increased cancer risk due to deficiencies in nucleotide excision repair (NER). For example, Xeroderma Pigmentosum is a human disease with multiple defects in the NER pathway responsible for the removal of UV radiation-induced DNA damage and thus, individuals with this disease have a 1000-fold increased risk of developing skin cancer compared to the general population. More common are subtle changes in DNA repair phenotype derived from single nucleotide polymorphisms (SNPs) that are increasingly considered as cancer susceptibility genes (80). An increased risk of esophagus, lung, and prostate cancer has been linked to SNP S326C in the human Ogg1 DNA repair gene, responsible for the removal of oxidized guanines. Another repair gene, XRCC1 with a SNP R194W, has been linked to increased risk of bladder, breast, lung, and stomach cancer.

5. Measurements of Oxidative Damage

The measurements of oxidative stress and oxidative DNA damage are vast and as such can not be covered in depth in this chapter. Thus, we have limited the discussion to only those endpoints used in the research studies for this dissertation.

5.1 Detection and Quantification of 8-hydroxy-deoxyguanosine by LC-MS/MS

The revelation of the ability of oxidants to damage DNA and the appreciation of its importance in disease has pressed the need for the development of sensitive analytical methods to detect and quantify levels of DNA adducts. The ability to draw any cause-and-effect conclusions regarding the role of oxidative stress to DNA and a particular chemical agent or disease state depends on knowing the precise endogenous or control levels of adducts that are to be used as biomarkers. Unfortunately, determining the background levels for the most commonly occurring and measured DNA adduct, 8-oxo-dG, has been difficult to ascertain up until recent efforts by ESCODD. Historical reports by enzymatic and chromatographic methods used to assay this particular DNA adduct have basal level estimates spread over three orders of magnitude (81). Importantly, it was shown that the grossly inflated values were most likely due to erroneous oxidation during DNA isolation and processing which can be limited by the inclusion of radical scavengers (82). The introduction of this modification to these standard procedures has brought chromatographic values closer in line with enzymatic methods that do not require DNA isolation (e.g., Comet assay). However, there still remains an approximate seven-fold difference between these two methods in control levels for 8-oxo-dG. It is likely that true endogenous levels for this DNA lesion are approximately 1 per million guanines.

Technological advances in mass spectrometry in the past decade have led to the emergence of LC-MS/MS as the method of choice for detecting and quantifying DNA adducts. Compared to HPLC-ECD, LC-MS/MS offers several advantages including the ability to provide structural information and the inclusion of internal standards resulting in greater specificity and improved quantitation. Recently, a capillary LC-MS/MS method has been developed for the detection and quantification for 8-oxo-dG. This method involves the enzymatic digestion of DNA with $^{15}N_5$-8-oxo-dG as internal standard and is followed by either isolation of 8-oxo-dG by HPLC (20 to 50 μg DNA required) or immunoaffinity (only 2 to

10 μg DNA required) chromatography. The isolated fraction is injected into the LC-MS/MS using electrospray ionization (ESI), and measured by selective reaction monitoring (SRM). Reported endogenous 8-oxo-dG levels in calf thymus DNA, untreated rat liver, and human HeLa cells were consistently between 2 to 3 adducts per 10^6 dG (Swenberg, unpublished data).

5.2 Apurinic/Apyrimidinic (AP) Sites

Slot blot assays for sugar back-bone lesions are based on the ability of an aldehyde reactive probe (ARP) to recognize the open ring structure of 2′-deoxyribose formed when a base is lost (83). Thus, this assay allows the measurement of abasic (AP) sites and with the addition of lesion-specific endonucleases (e.g., FPG or endonuclease III) allows detection of oxidized purines and pyrimidines. The measurement of AP sites is performed on isolated genomic DNA, followed by treatment with ARP, transferred to nitrocellulose membrane, reacted with streptavidin-conjugated horseradish peroxidase, and enzymatic activity measured by chemiluminescence. Quantification is based on an internal standard containing a known number of AP sites. This method can underestimate DNA damage if enzymatic reactions do not go to completion.

5.3 Expression of DNA Repair Genes as a Biomarker of Oxidative DNA Damage

While many analytical techniques that assess oxidative DNA damage at the level of base or sugar are vulnerable to technical difficulties, the expression of BER genes, a biological response to DNA damage, holds promise as a sensitive *in vivo* biomarker. Because this pathway encompasses broad specificity and multiple routes of repair, it allows greater sensitivity in the ability to detect oxidative DNA damage compared to previously mentioned analytical techniques. Studies measuring the expression of BER genes have been used to identify sources for DNA-damaging oxidants (84) as well as establishing links

between chronic inflammation, dysregulation of DNA repair, and microsatellite instability (85).

5.4 Immunohistochemistical Detection of Oxidative Damage

Antibodies specific for stable oxidative DNA and protein adducts can be visualized in cells in paraffin-embedded tissues and a qualitative assessment can be made using imaging software. There are a number of commercially available antibodies to measure oxidative modifications of DNA and proteins, including 8-OH-dG, 3-nitrotyrosine, HNE, and MDA. Antibodies are limited in specificity if there is cross-reactivity between structurally similar DNA adducts or with other constituents of the cell. Thus, the application of this method must include proper positive and negative controls for accurate interpretation of results.

5.5 Glutathione

Glutathione (GSH) is an intracellular low-molecular weight thiol that protects cells from free radical attack by reducing disulfide bonds formed within cytoplasmic proteins to cysteines by acting as an electron donor. It is found almost exclusively in its reduced form since the enzyme which reverts it from its oxidized form (GSSG), GSH reductase, is constitutively active and inducible upon oxidative stress. As a measure of sulhydryl status, GSH has been used as an indicator of the cellular redox state. Several methods have been developed to identify and quantify GSH in fluid and tissue samples including spectrophotometric and flurometric assays often applied to HPLC analysis, and more recently developed GC-MS and LC-MS techniques (86). There a number of commercially available high-throughput colormetric kits to measure GSH. The assay is based on the glutathione recycling system by 5-5'-dithiobis-2-nitrobenzoic acid (DTNB) and GSH reductase. DTNB and GSH react to generate 2-nitro-5-thiobenzoic acid and GSSG. Since 2-nitro-5-thiobenzoic acid is a yellow colored product, GSH concentration can be determined

by measuring absorbance at 412nm. GSH can be regenerated by GSH reductase, and reacts with DTNB to generate more product which dramatically improves the sensitivity of total GSH detected.

C. RATIONALE AND SPECIFIC AIMS

A discord between adverse findings in clinical data with those generated using in vivo animal models fosters the search for better methods to evaluate chemical safety. This is especially true for the liver, as it has been found to have one of the poorest correlates between *in vivo* animal studies and human toxicities (87). Not surprisingly, drug-induced liver toxicity is one of the leading causes for the termination of clinical trials and removal of drugs from the market. As oxidative stress is recognized as common general mechanism of human toxicity and disease, it can be speculated that it has a role in the discordance of observable adverse effects between animals and humans. It is proposed that the information gathered from toxicogenomic studies has the potential to provide novel insights into the mode of action and generate markers of impending toxicity at doses and times that are currently unattainable. This information can then be used to more accurately model potential adverse effects across species ultimately improving the risk assessment process. Currently, genomic technologies have demonstrated their utility in classification (5, 6, 88) and diagnostics (89, 90), but significant contributions toward deciphering mechanisms of toxicity and aiding risk assessment have yet to materialize. This is not surprising, since most studies have failed to use appropriate bioinformatic tools to integrate disparate data sets as well as phenotypically anchor the data to adverse outcomes (8). *Thus, we hypothesize that molecular signatures defining disease mechanisms and early effects of exposure can be phenotypically anchored to biomarkes of oxidative stress and DNA damage.* To test this hypothesis, we proposed three specific aims each of which would evaluate a model of oxidant-induced liver injury to address a key toxicological question as described below.

Specific Aim 1. Current toxicology tests have limited ability to assess subtle forms of toxicity that may occur at low doses. Employing toxicogenoimc approaches has the ability to lower the no observable effect level (NOEL) detected compared to existing methods. Although this ability to observe subtle alterations at earlier times and/or lower doses has its advantages, it also presents itself with confounding implications in the ability to segregate different states of homeostasis from states of deregulation which may cause pathological effects. Recently, a proof-of-concept study (91) was conducted whereby rats administered the hepatotoxicant, APAP, found that a sub-toxic dose (150 mg/kg) elicits subtle alterations in gene transcripts related to oxidant stress that are exacerbated with toxic doses (1500 to 2000 mg/kg). The livers from these animals demonstrated no apparent toxicity based on changes in histology or clinical chemistry. This study presented an opportunity to evaluate the validity of gene expression studies as a sensitive marker of incipient toxicity. Thus, in *Aim 1* our hypothesis was that a gene signature for oxidative stress at a sub-toxic dose would be phenotypically anchored to markers of oxidative stress and DNA damage based on the proposed mechanism of APAP-induced hepatotoxicity.

Specific Aim 2. The choline-deficient (CD) diet is an extensively studied non-chemical-induced, non-genotoxic model of rodent hepatocellular carcinoma (HCC) that produces a well-defined temporal pattern of pathological changes involving the consecutive emergence of a fatty liver, apoptosis, compensatory proliferation, fibrosis, and cirrhosis that is markedly similar to the sequence of events typified by human HCC. As pathological processes are active events under genetic control, gene expression analysis provides a powerful means of monitoring these processes and identifying key molecular events required to achieve specific pathological outcomes. Oxidative stress is considered a critical mediator in the pathological sequence of events. Thus, it was our hypothesis in *Aim 2* to

establish a temporal correlation of pathology and oxidative DNA damage in a CD-model of rat HCC using gene expression profiling.

Specific Aim 3. An emerging issue in toxicology is the role of nutrition as a modulator of environmental exposures. This is of particular concern as over the past half century a significant proportion of the population in the U.S. is clinically defined as overweight or obese. It has been suggested that a temporal shift in ω-6:ω-3 PUFA intake ratios have contributed to the growing obesity epidemic (92); however, the mechanisms by which different dietary fatty acids affect the molecular processes of human disease have not been fully elucidated. Thus, it was our hypothesis in *Aim 3* that a high-fat diet of ω-6 PUFA fed to mice would increase oxidative stress and oxidative DNA damage in the liver. As oxidative-stress signaling pathways are a common mechanism for human toxicity and disease, it would be expected that a diet that promotes a pro-oxidant state in tissues would impart some inherit susceptibility to disease.

Figure 1.1

Schematic diagram of types of DNA damage that may be induced by reactive oxygen species

Abbreviations: reactive oxygen species, ROS; 4-hydroxy-2-nonenal, 4-HNE; malondialdehyde, MDA; pyrimidopurinone, M_1G; etheno-deoxyguanosine, edA; etheno-deoxyadenosine, edA; human 8-oxoguanine DNA glycosylase 1, hOgg1; N-methylpurine DNA glycosylase, MPG; 2,6-diamino-4-hydroxy-5-formamidopyrimidine, FapyG; 8-oxo-7,8-dihydro-2'-guanosine, 8-oxo-G.

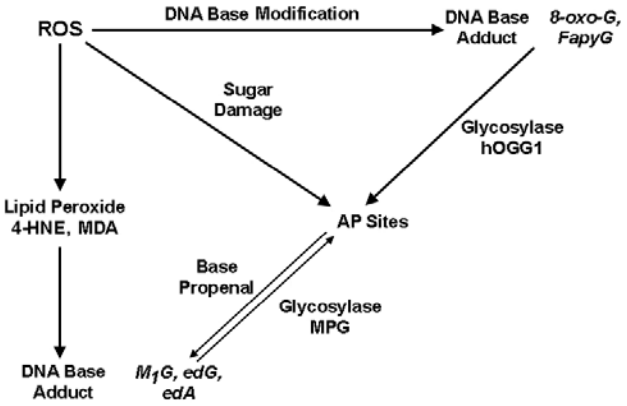

Figure 1.2

Schematic diagram of base excision repair pathways for removal of oxidized DNA lesions formed as a result of a chemical exposure that causes oxidative stress

The sequence of modifications of DNA is depicted in bold, whereas the molecular events that occur at each step are shown in italics. The gene products that participate at each step of repair are also displayed.

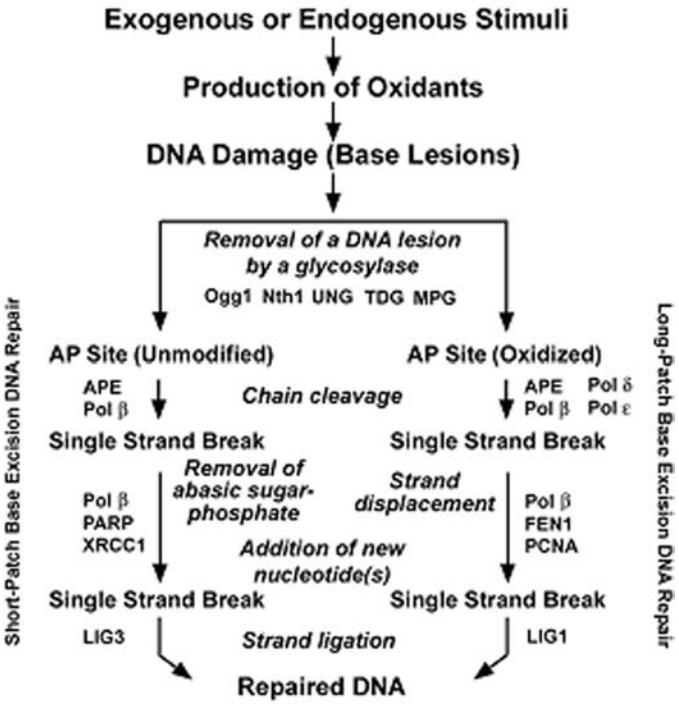

CHAPTER II

PHENOTYPIC ANCHORING OF ACETAMINOPHEN-INDUCED OXIDATIVE STRESS WITH GENE EXPRESSION PROFILES IN RAT LIVER

A. Abstract

Toxicogenomics provides the ability to examine in greater detail the underlying molecular events that precede and accompany toxicity, thus allowing prediction of adverse events at much earlier times compared to classical toxicological endpoints. Acetaminophen (APAP) is a pharmaceutical that has similar metabolic and toxic responses in rodents and humans. Recent gene expression profiling studies with APAP found an oxidative stress signature at a sub-toxic dose that we hypothesized can be phenotypically anchored to conventional biomarkers of oxidative stress. Liver tissue was obtained from experimental animals used to generate microarray data where male rats were given APAP at sub-toxic (150 mg/kg), or overtly toxic (1500 and 2000 mg/kg) doses and sacrificed at 6, 24, or 48 h. Oxidative stress in liver was evaluated by a diverse panel of markers that included assessing expression of base excision repair (BER) genes, quantifying oxidative lesions in genomic DNA, and evaluating protein and lipid oxidation. A sub-toxic dose of APAP produced significant accumulation of nitrotyrosine protein adducts. Both sub-toxic and toxic doses caused a significant increase in 8-hydroxy-deoxyguanosine (8-OH-dG) as well as significant decrease in glutathione (GSH) content. Only toxic doses of APAP significantly induced expression levels of BER genes. None of the doses examined resulted in a significant increase in the number of abasic sites or in the amount of lipid peroxidation. The accumulation of nitrotyrosine and 8-OH-dG adducts along with reduced GSH content in the liver phenotypically anchors the oxidative stress gene expression signature observed with a sub-toxic dose of APAP, lending support to the validity of gene expression studies as a sensitive and biologically-meaningful endpoint in toxicology.

B. Introduction

Toxicogenomics is an area in toxicology that elucidates how the entire genome is involved in biological responses of organisms exposed to environmental toxicants. Expectations for this new field have been high with promises of obtaining in much greater detail the molecular events that precede and accompany toxicity, thus allowing prediction of a toxic insult at much earlier stages than classical measures. Initial studies have been encouraging with gene-specific signatures that predict and classify unknown hepatotoxicants based on a preliminary training set of chemicals (6). This work has led to the hypothesis that it is possible to define signature patterns of altered gene expression that indicate specific adverse effects of chemicals, drugs, or environmental exposures.

In order for gene expression profiling to become a well recognized and valuable tool in toxicology, it should be characterized for its ability to reflect the results derived from classical toxicology assays (*e.g.*, histopathology, and clinical chemistry) in a dose- and time-dependent manner (4). Such phenotypic anchoring removes subjectivity from interpretation of expression data by distinguishing between the toxicological effect signal from other gene expression changes that may be unrelated to toxicity, such as the therapeutic effects of a compound. Unfortunately, much of the available toxicogenomic data that has been published to date, with few exceptions, has been limited to a description of alterations in gene expression patterns.

Toxicology studies, in themselves, are quite complex with sources of variability resulting from the dose and delivery of the chemical under study, the choice of animal species, and the differences in biological and pathological responses of various tissues (93). The combination of this with the known technical variability in genomic studies (94) underscores the importance of careful validation of alterations in gene expression

patterns. In most cases, expression data can be phenotypically anchored using classical toxicological methods; however, the apparent lack of sensitivity for most toxicity assays will make this difficult for altered expression patterns observed at sub-toxic doses. Thus, corroboration of such expression data sets will require the use of more sensitive, complex assays.

The results of gene expression profiling studies can serve as a guide in the search for specific genes and/or proteins that could be used as biomarkers of incipient toxicity, or can predict the pathological changes that are yet to be realized by morphological analysis. Recently, a proof of concept study was designed whereby rats, the preferred model organism in toxicity testing, were administered the well characterized hepatotoxicant, acetaminophen (APAP), and demonstrated that alterations in expression patterns at a low, sub-toxic dose (*i.e.*, no apparent toxicity was detected by histopathology or clinical chemistry) may reveal signs of subtle cellular injury that are exacerbated at higher doses (91). Specifically, it was found that altered gene expression patterns were suggestive of mitochondrial dysfunction and oxidative stress and with increasing dose there was concomitant increase in the magnitude of response and number of genes represented within the same vital cellular pathways. However, the specificity of these gene expression changes to the mechanism of APAP hepatotoxicity cannot be discerned without further research. Here, we have undertaken a study to substantiate these findings of a gene expression signature for oxidative stress by a sub-toxic of APAP in rat liver using a panel of sensitive biomarkers of oxidative stress and oxidative DNA damage. The results of our studies show that a reduction in glutathione (GSH) content in the liver alongside with the accumulation of nitrotyrosine protein adducts and 8-hydroxy-deoxyguanosine lesions in DNA, events known to be a part of the mode of action of APAP, provide good and early phenotypic anchors for gene

expression signature of APAP-induced oxidative stress, even at a sub-toxic dose.

C. MATERIALS AND METHODS

Animals and treatments

The studies detailed herein were performed using liver tissues (stored at -80°C) from previously published report (91) where male Fisher 344 rats were administered a single acute dose of acetaminophen by gavage at sub-toxic (150 mg/kg) or overtly toxic (1500 and 2000 mg/kg) doses in 0.5% aqueous methyl cellulose. Animals were sacrificed 6, 24, or 48 hrs following dosing at which point frozen and formalin-fixed liver samples were collected.

Determination of Liver Tissue Glutathione Levels

Approximately 50 mg frozen liver tissue was homogenized in 5% sulfosalicyclic acid, centrifuged at 8k x g for 10 min, and the supernatant assayed for reduced glutathione content following manufacturer's protocol (BioVision, Mountain View, CA).

Immunohistochemistry

Formalin-fixed, paraffin-embedded sections (6 μm) were mounted on glass slides. Sections were deparaffinized in xylene, rehydrated in a series of graded alcohol concentrations, and placed in phosphate-buffered saline (PBS) with 1% Tween 20. Immunostaining was performed using DAKO EnVision System HRP (Dako Cytomation, Carpinteria, CA) with primary antibody [1:200 nitrotyrosine (Molecular Probes; Eugene, OR); 1:200 malondialdehyde (MDA; Alpha Diagnostic, San Antonio, TX); and 1:200 8-hydroxyguanosine (Research Diagnostics; Flanders, NJ)] diluted in PBS containing 1% bovine serum albumin and incubated overnight at 4°C. Slides were counterstained with hematoxylin. In order to ensure the quantitative measurement of each immunoreaction,

all sections from each animal and group to be compared were processed in parallel. Antibody specificity was determined by incubating each antibody with its respective antigen before immunostaining. Quantitative analysis of immunostained liver sections was performed using BIOQUANT software (BIOQUANT Image Analysis, Nashville, TN) by averaging percent area stained to total area within pericentral regions at 200× with exception for 8-OH-dG where percentage of positively stained nuclei to total nuclei in pericentral regions was determined.

Isolation of DNA

DNA was extracted by a procedure slightly modified from the method reported previously (95). To minimize formation of oxidative artifacts during isolation, 2,2,6,6-tetramethylpiperidinoxyl (TEMPO, 20 mM final concentration) was added to all solutions and all procedures were performed on ice. Briefly, frozen tissues were thawed and homogenized in PBS with a Tehran homogenizer (Wheaton Instruments, Millville, NJ). After centrifugation at 2,000 x g for 10 min, the nuclear pellets were incubated in lysis buffer (Applied Biosystems, Foster City, CA) overnight at 4°C with proteinase K (500 mg/ml; Applied Biosystems). DNA was extracted twice with a mixture of phenol/chloroform/water followed by ethanol precipitation. The extracted DNA was incubated in PBS (pH 7.4) with RNase A followed by DNA precipitation with cold ethanol. Then, the DNA pellet was resuspended in sterilized double distilled water. The DNA solution was stored at -80°C until assayed. The DNA extraction method used in this study is unlikely to modify the original number of AP sites and single strand breaks in genomic DNA from intact tissues or cells, based on re-extraction data of DNA exposed to high concentrations of methylmethane sulfonate (Swenberg and Nakamura, unpublished).

Apurinic/apyrimidinic (AP) sites

AP sites were measured following a procedure reported by Nakamura and Swenberg (83). Briefly, 8 µg of DNA in 150 µl of phosphate-buffered saline was incubated with 1 mM aldehyde reactive probe at 37°C for 10 min. After precipitation using cold ethanol, DNA was resuspended in TE buffer (10 mM Tris-HCl, pH 7.4, containing 1 mM EDTA). DNA (250 ng) in TE buffer was heat-denatured and loaded on a nitrocellulose membrane (110 ng DNA/slot, Hybond-C Super, Amersham Pharmacia Biotech, Piscataway, NJ). The nitrocellulose membrane was soaked with 5×SSC and then baked in a vacuum oven for 30 min. The membrane was preincubated with 10 ml of Tris-HCl containing bovine serum albumin for 15 min and then incubated in the same solution containing streptavidin-conjugated horseradish peroxidase at room temperature for 45 min. After rinsing the nitrocellulose membrane, the enzymatic activity on the membrane was visualized by enhanced chemiluminescence reagents (Amersham). The nitrocellulose filter was exposed to x-ray film, and the developed film analyzed using a Kodak Image Station 440. Quantitation was based on comparisons to internal standard DNA containing a known amount of AP sites.

Detection and Quantification of 8-OH-dG by Capillary LC-MS/MS

The measurement of 8-OH-dG by LC-MS/MS was adapted from the method described by Liao (96). To digest DNA into individual nucleosides, DNA (30 to 50 µg) was dissolved in 80 mM Tris-HCl buffer/20 mM MgCl2 (pH 7.0) with 2.75 pmoles [$^{15}N_5$]-8-OH-dG internal standard prior to digestion with 40U of DNase I for 10 min at 37°C. Next, 2.7 mU of phosphodiesterase I and 2U of alkaline phosphatase were added and incubated for an additional 1h. The released 8-OH-dG was purified by reverse phase HPLC using a Beckman Ultrasphere ODS C18 column (5 um, 4.6 x 250 mm, Beckman, Fullerton, CA). The isocratic mobile phase was 7% MeOH in 10 mM ammonium formate

(pH 4.3) with a flow rate 1 mL/min. Fractions were collected 2 min preceding and following the elution of 8-OH-dG. The quantitative analysis of 8-OH-dG by capillary LC-electrospray-MS/MS was performed with an 1100 capillary high-performance liquid chromatograph (Agilent, Wilmington, DE) coupled to a TSQ-Quantum triple quad mass analyzer (ThermoFinnigan, San Jose, CA). A 3.5 μm Zorbax XDB-C18 column (0.3 mm x 150 mm; Agilent) was operated with a binary mobile phase of 2% 10 mM ammonium formate (pH 4.3) and 98% methanol followed by a linear gradient increase of methanol from 2% to 30% from 0 to 5 min, holding at 30% for 10 min, and immediate return to initial conditions that was held for 15 min. Both analyte and internal standard were detected by single reaction monitoring of the transition of nucleoside to base adduct *m/z* 284.2 to 168.2 and *m/z* 289.2 to 173.2, respectively. MS conditions were as follows: spray voltage, 2200 V; heated capillary temperature, 350°C. All reagents were purchased from Sigma-Aldrich (St. Louis, MO) and were ACS grade or higher.

Ribonuclease protection assays

Total RNA was isolated using RNeasy total RNA (Qiagen, Valencia, CA) and dissolved in RNase-free water. Samples were stored at -80°C until assayed. The quality of preparations was determined using an Agilent Bio-Analyzer® (Agilent Technologies, Palo Alto, CA). The RNase protection assays were performed on 20 μg of individual total RNA samples using a RiboQuant™ multi-probe RNase protection assay kit (rBER, BD PharMingen, San Diego, CA) essentially as described elsewhere (84). Riboprobes were synthesized in the presence of [^{32}P]dUTP to yield labeled antisense RNA probes. Protected fragments were separated on 5% polyacrylamide nucleic acid separation gels, dried and exposed to x-ray film. The intensity of protected bands was quantified using Kodak 1D Image Analysis Software (New Haven, CT) and normalized to the intensity of housekeeping gene L32.

Statistical analysis

Results are reported as means ± SD with n = 3 in each group. Treatment groups were compared using one-way ANOVA analysis followed by Tukey's multiple comparison post-hoc test, where appropriate. A $p<0.05$ was selected before the study to determine statistical differences between groups.

D. Results

A previous toxicogenomic study of APAP-induced toxicity in rat liver revealed an oxidative stress signature with a sub-toxic dose at 6h that was also present after exposure to overtly toxic doses (91). Specifically, this gene signature included the induction of cAMP inducible gene 1, heterogenous nuclear ribonucleoproteins A1/B1, phospholipase C gamma1, metallothionein (MT1a), phytoene dehydrogenase, and H2AX histone family. To substantiate the link of this oxidative stress gene expression signature to incipient liver toxicity, we examined the liver tissue from this earlier study to measure a diverse panel of endpoints for oxidative stress and DNA damage. The previous study found that livers of animals treated with a sub-toxic (150 mg/kg) dose of APAP were histologically indistinguishable from controls. In contrast, rats treated with 1500 and 2000 mg/kg exhibited mild to moderate centrilobular necrosis and inflammatory lesions that was most prominent at 24h and coincided with a significant increase in serum alanine aminotransferase (ALT) activity, (2952 IU/L ± 261 and 5047 ± 728, respectively).

Glutathione depletion by the reactive metabolite of APAP, *N*-acetyl-*p*-benzoquinone imine (NAPQI), is thought to play an important causal role in APAP-induced hepatotoxicity. As such, liver tissue from rats given a single acute dose by gavage of vehicle or APAP at sub-toxic, 150 mg/kg, or overtly toxic, 1500 mg/kg, doses

at 6 and 24 hrs post-dosing were analyzed for reduced GSH content. APAP treatment at sub-toxic and overtly toxic doses led to a 30 and 58% depletion of GSH content, respectively, compared to control animals at 6 hrs post-dosing (Table 2.1). By 24 hrs, GSH content had returned to control levels.

Peroxynitrite, an oxidant and nitrating species, is formed from the reaction of superoxide and nitric oxide (NO·) which can lead to the formation of 3-nitrotyrosine protein adducts (97, 98). Liver sections from rats given a single acute dose by gavage of vehicle or APAP at sub-toxic (150 mg/kg) or overtly toxic (1500 and 2000 mg/kg) doses were examined for the presence of nitrotyrosine protein adducts by immunohistochemistry. Control animals as well as those given an overtly toxic dose of APAP exhibited minimal to non-detectable levels of nitrotyrosine (Figure 2.1A, 2.1C-D); in contrast, rats given a sub-toxic dose of APAP exhibited extensive localized staining of hepatocytes within pericentral regions of the liver lobule (Figure 2.1B, 2.1E) which resolved to control levels by 48hrs. Microscopic examination showed the presence of nitrotyrosine adducts within both cellular and nuclear compartments of hepatocytes. Quantitative analysis of liver sections from control animals showed that nitrotyrosine comprised less than 5% of total cellular area in pericentral regions of the liver lobule as opposed to those given a sub-toxic dose of APAP where nitrotyrosine comprised 80% and 30% of total cellular area at 6 and 24 hrs post-dosing, respectively (Figure 2.1F).

The covalent binding of NAPQI to mitochondrial proteins can lead to an increased production of reactive oxygen species (ROS) that can react with DNA (99). First, we examined 8-OH-dG, a widely-used marker of oxidative DNA damage, by immunohistochemical detection (Figures 2.2A-C). Microscopic examination of liver sections from control animals revealed sporadic distribution of positively stained nuclei but sections from animals given either sub-toxic or overtly toxic dose had a concentration of positively stained nuclei within the pericentral region (Figure 2.2D).

Image analysis was performed to determine the percentage of positively stained nuclei (Figure 2.2E). Both sub-toxic and overtly toxic doses of APAP led to a significant accumulation of 8-OH-dG adducts at 6 hrs post-dosing.

Then, we determined the amounts of 8-OH-dG after APAP treatment using a recently developed capillary LC-MS/MS method as described in Materials and Methods. A calibration curve was obtained by using 275.5 fmoles internal standard and variable amounts of 8-OH-dG ranging from 0.5 to 228 fmoles/μl. The ratio of the peak areas of 8-OH-dG versus internal standard was plotted against the known amounts of 8-OH-dG yielding a linear calibration curve with a correlation coefficient of 1.0 (Figure 2.3A). Endogenous levels of 8-OH-dG in control rat liver were ~ 1 adduct per 10^6 dG (Figure 2.3B), in agreement with recent consensus reports from European Standards Committee on Oxidative DNA Damage (100). Analysis of liver tissues from rats treated with a sub-toxic and overtly toxic dose of APAP found a 3 to 4-fold increase in 8-OH-dG adducts, respectively, over control (Figure 2.3B), confirming our results with immunohistochemical detection.

It is believed that the predominant pathway used for removal of oxidized bases from DNA is the base excision repair (BER) pathway. A multi-probe RNase protection assay for BER enzymes was used, since this approach distinguishes the presence of multiple expressed DNA repair genes simultaneously from a single sample, thus allowing for sensitive comparative analysis of different mRNA products both within and between samples. Sub-toxic dose - 150 mg/kg (data not shown), had no effect on expression of BER genes as compared to controls; however, a time- and dose-dependent increase (1.5 to 3-fold) in mRNA for proliferating–cell nuclear antigen (*Pcna*), poly ADP-ribose polymerase (*Parp*), AP endonuclease 1, 8-oxoguanine DNA glycoslyase 1 (*Ogg1*), and polymerases β and δ was observed for 1500 mg/kg dose of APAP (Table 2.2). In addition, expression of *Mgmt*, an enzyme involved in the direct

repair of alkylated guanine residues and not involved in repair of oxidative DNA lesions, was unaffected in all treatments examined, conferring specificity to BER pathway.

Next, to determine whether the number of mutagenic and clastogenic apurinic/apyrimidinic (AP) sites was increased following exposure to APAP, AP sites were measured using a slot blot assay. AP sites can be generated spontaneously by chemical depurination of labile bases and enzymatically by DNA glycosylases in a process of BER. In addition, ROS may induce sugar lesions directly by hydrogen abstraction of deoxyribose, frequently resulting in oxidized AP sites (101). Although APAP at overtly toxic doses induced BER genes as shown above, there were no significant increases in the number of AP sites generated for any of the treatments (Figure 2.4).

Through the metabolic activation of APAP, both superoxide and peroxynitrite are generated that subsequently may initiate lipid peroxidation by Fenton chemistry (97). Lipid peroxidation was evaluated by immunostaining for malondialdehyde (102) in liver sections from rats given vehicle, or a single acute dose by gavage of APAP at sub-toxic (150 mg/kg) and overtly toxic (1500 mg/kg) doses at 6, 24, or 48 hrs (Figure 2.5A-C). Quantitative image analysis (Figure 2.5D) found no statistically significant difference (one-way ANOVA, $p<0.05$) between treatment groups and controls.

E. Discussion

In the present study, we investigated whether altered gene expression patterns that are suggestive of oxidative stress at a sub-toxic dose of APAP, when no apparent toxicity was detected using routine histopathological and clinical chemistry measurements, could be phenotypically anchored by using a panel of sensitive biomarkers for oxidative stress and oxidative DNA damage. Our results substantiate the previously reported gene expression profiling data (91) demonstrating that the sub-toxic

dose of APAP does induce oxidative stress as demonstrated by the significant accumulation of nitrotyrosine protein adducts and 8-OH-dG DNA lesions and the reduction in GSH content at 6 hrs post-dosing. This confirms that gene expression signatures can potentially serve as predictive indicators of toxicity with increasing expression and exacerbation of a gene signature. Thus, the data support the potential role of gene expression profiling as a sensitive and biologically-relevant endpoint in toxicology.

APAP is a common over-the-counter medication used for its analgesic and antipyretic properties; however, it is also one of the leading causes of drug-induced liver failure (103). At pharmacological doses, APAP is metabolized by sulfation and glucuronidation, and to a lesser extent, by cytochrome CYP2E1 that produces a reactive metabolite, NAPQI, which is detoxified by conjugation with GSH (99, 104). APAP-induced hepatotoxicity occurs when GSH reserves are exhausted allowing covalent binding of NAPQI to critical cellular proteins as APAP-cysteine adducts (105), ultimately disrupting their cellular function, see Figure 2.6. Many of these covalently bound proteins are within the mitochondria (106) resulting in reduced respiration (107) and increased superoxide production (108). Superoxide either reacts with nitric oxide to produce peroxynitrite, which is responsible for protein nitration (109), or dismutates to hydrogen peroxide whereby it can oxidize cellular macromolecules. The presence of nitric oxide, which is induced by APAP (110), is thought to block propagation of lipid peroxidation (111). It has been postulated that loss of mitochondrial function and concomitant generation of oxidative stress are central to APAP-induced hepatotoxicity (112).

It is well recognized that the metabolic activation of APAP leading to GSH depletion is an important step in APAP-induced liver toxicity. As expected, an overtly toxic dose of APAP given to rats significantly reduced GSH content to 60% less than

control at 6 hrs post-dosing. Most surprisingly, a sub-toxic dose also significantly reduced GSH, albeit to a lesser extent. These data support earlier gene expression studies for oxidant stress at sub-toxic dose although the

A number of studies have reported elevated levels of nitrotyrosine protein adducts that precede and accompany APAP-induced hepatotoxicity in mice (109, 113). In this study, only rats given a sub-toxic dose of APAP, not overtly toxic doses, had significantly elevated levels of nitrotyrosine protein adducts in liver compared to controls. These data support the presence of oxidant stress as indicated by earlier gene expression studies for a sub-toxic dose of APAP but demonstrates that the oxidant species formed in the presence of sub-toxic and overtly toxic doses of APAP in the rat are not identical. It has been shown that nitration of tyrosine residues is not limited to peroxynitrite exposure but can occur via peroxidase enzymes such as glutathione peroxidase (114) which is impaired during APAP toxicity. Alternatively, it has been demonstrated that APAP is highly effective at preventing tyrosine nitration by peroxynitrite (115, 116). Thus, in this study overtly toxic doses of APAP, unlike sub-toxic doses, may be able to out compete tyrosine for peroxynitrite which may explain the differences observed with nitrotyrosine levels between these two dosing groups. Moreover, this data would suggest that nitrotyrosine is not associated with APAP-induced hepatotoxicity in the rat; an observation that is in direct opposition to what has been observed in numerous studies with mice. This may well reflect a mechanistic difference in APAP metabolism between these two rodent species.

The generation of ROS by either APAP metabolism or resulting mitochondrial damage can lead to direct or indirect oxidative DNA damage. Immunohistochemical and mass spectrometry methods found a significant accumulation of the potentially mutagenic DNA lesion, 8-OH-dG, at sub-toxic and overtly toxic doses of APAP.

Accumulation of 8-OH-dG lesions preceded the onset of hepatic injury as reported by ALT and histopathology. The formation of 8-OH-dG from APAP exposure potentially results from mitochondrial oxidant stress where both superoxide and peroxynitrite are produced and can either directly or indirectly oxidize guanines in DNA (35, 43).

Recently, the quantified expression of base excision DNA repair (BER) genes was shown to be a sensitive *in vivo* biomarker of chemical-induced oxidative stress (84). Moreover, because this pathway encompasses broad specificity and multiple routes of repair, it allows greater sensitivity in the ability to detect oxidative DNA damage. The measurement of multiple genes involved in the BER pathway by an RNase protection assay was able to detect up-regulation of gene expression that correlated with the onset of centrilobular hepatic necrosis in addition to the rise and fall of ALT. However, the assay was unable to detect significant increases of BER genes at a sub-toxic dose where genomic profiling generated an oxidative stress signature that consisted primarily of genes that are involved in protecting the cell from oxidative stress. It is known that the redox state of the cell is one of many mechanisms involved in activating transcription factors involved in regulating the expression of DNA repair genes (117). Thus, it may be that at sub-toxic doses of APAP the apparent increase in expression of anti-oxidants, such as metallothioneins, may be sufficient in maintaining a redox equilibrium.

The accumulation of apurinic/apyrimidinic (AP) sites can result from oxidative DNA damage through an intermediary step of BER pathway, enzymatic cleavage, and chemical depurination. The induction of BER pathway and, in particular, AP endonuclease gene by APAP was not, however, corroborated by the accumulation of AP sites by any of the APAP treatments examined. A lack of evidence for an increase in AP sites may be manifested in the limited dose and time regimens examined in this study. Since the development of APAP toxicity typically occurs within the first 6h of exposure,

the detection of abasic sites would be limited if repair occurred rapidly. Alternatively, the repair pathway could involve another route whereby generation of an abasic site is obsolete. The dissociation between expression of BER genes and accumulation of AP sites is not an unusual phenomenon and has been observed with other chemical hepatotoxicants (84).

The role of lipid peroxidation in APAP-induced hepatotoxicity has been controversial (118-120). Mitochondrial dysfunction leads to both increased production of superoxide and formation of peroxynitrite that are both capable of initiating lipid peroxidation; however, biochemical studies have shown that nitric oxide can prevent the propagation of lipid peroxidation reactions (111). This is supported by the fact that inhibiting nitric oxide production during APAP exposure leads to enhanced lipid peroxidation (120). Our studies revealed that lipid peroxidation, as measured by the presence of malondialdehyde, was not observed to be significant for any doses or times examined. Despite the generation of ROS/RNS by APAP, our work does not support the role of lipid peroxidation as a mediator of APAP-induced hepatotoxicity.

It should be considered that alterations in gene expression that are potentially indicative of cellular injury with an adverse outcome but are unsubstantiated by classical measures of toxicity may be a mere reflection of the tissue's capacity to cope. As demonstrated in this study, an APAP-induced oxidant signature generated by a sub-toxic dose was corroborated using sensitive biomarkers for oxidative stress and DNA damage. However, the presence of genes having an anti-oxidant role within this signature may explain the lack of observable toxicity by classical measures. In order to discern whether gene expression alterations in critical cellular pathways represent benign homeostatic adjustments, indications of the potential for adverse effects or in fact represent adverse effects, especially at doses and times with no observable toxicity, will

require the application of more sophisticated and sensitive tools that provide a mechanistic link between a chemical and the observed toxic effect.

In general, the acceptance of microarray expression data as a relevant endpoint in toxicological studies requires careful interpretation and validation. It has been suggested that this should be achieved using classical toxicological endpoints such as histopathology and clinical chemistry (121). One of the great promises of toxicogenomics is that it will be able to detect and predict toxicity at much earlier stages compared to existing methods; however, restricting validation of expression data to only classical endpoints, with their inherent lack of sensitivity, would bring the advancement of toxicogenomics as well as toxicology to an impasse. Most importantly, the enhanced sensitivity of microarray studies to detect subtle, early alterations in vital cellular pathways that may be indicative of adverse effects, but display no observable toxicity by conventional measures, can have serious ramifications in policy and regulatory decision making.

In summary, we show that incipient signs of oxidative stress can be observed with a sub-toxic dose of APAP based on the significant accumulation of both nitrotyrosine protein adducts and 8-OH-dG DNA lesions, markers anchored on the mechanism of APAP-induced liver toxicity. The use of sensitive biomarkers of oxidative stress and oxidative DNA damage revealed not only that mechanistic differences may exist in APAP metabolism between sub-toxic and overtly toxic doses in rats but also among rodent species. Gene expression profiling is a sensitive tool capable of detecting subtle cellular disturbances at doses and times unobtainable by classical toxicological measures. Thus, it has the potential to serve an essential role in predicative toxicology by generating gene signatures as biomarkers of incipient toxicity.

Table 2.1

Reduced glutathione concentration in rat liver following acetaminophen treatment

	μmoles rGSH/g liver		
Time	**Control**	**150 mg/kg**	**1500 mg/kg**
6h	5.5 ± 0.43	3.8 ± 0.13*	2.3 ± 0.15*
24h	5.2 ± 0.68	5.9 ± 0.02	4.6 ± 0.75

Rats were administered a single acute dose of acetaminophen by gavage at sub-toxic (150 mg/kg) or overtly toxic (1500 mg/kg) doses in 0.5% aqueous methyl cellulose (vehicle control). Liver tissue collected at 6 or 24h post-dosing was analyzed for reduced glutathione (rGSH) content as described in Materials and Methods. Hepatic rGSH concentration is expressed as μmoles/g liver ± standard deviation from 3 animals per group. *Statistical difference ($p < 0.01$) from control group using one-way ANOVA followed by Tukey's multiple comparison post-hoc test.

Table 2.2

Expression of DNA repair genes in rat liver after treatment with an overtly toxic dose (1500 mg/kg) of acetaminophen

DNA Repair Gene	Control	6h	24h	48h
Ogg1, 8-oxoguanine DNA glycosylase 1	3.8 ± 0.8	3.9 ± 0.8	**8.2 ± 2.8***	**10.2 ± 1.5***
Mpg, N-methylpurine DNA glycosylase	6.0 ± 0.4	5.2 ± 1.3	4.8 ± 2.7	4.0 ± 0.8
Ape, purinic/apyrimidinic endonuclease 1	23.5 ± 1.4	21.6 ± 5.2	**34.8 ± 2.8***	30.8 ± 1.7
Pol β, polymerase (DNA directed) β	13.2 ± 0.9	11.9 ± 1.3	**18.7 ± 1.8***	15.8 ± 1.2
Pol δ, polymerase (DNA directed) δ	1.5 ± 0.3	1.7 ± 1.7	**6.0 ± 1.6***	**8.8 ± 2.8***
Pcna, proliferating cell nuclear antigen	20.7 ± 2.1	22.5 ± 2.6	33.6 ± 7.9	**50.9 ± 7.6***
Parp, poly (ADP-ribose) polymerase	15.3 ± 0.5	**21.4 ± 1.3***	**27.6 ± 3.8***	**29.1 ± 1.6***
Mgmt, O^6-methylguanine DNA ethyltransferase	29.8 ± 1.3	24.1 ± 5.7	32.2 ± 6.6	32.1 ± 0.1

Total RNA was isolated from liver samples and analyzed by RNase protection assay. The results are mean ± standard deviation from 3 animals per group. The relative expression of each gene was normalized to the expression of the housekeeping gene L32. The control is pooled RNA from three biological replicates and then 6, 24, and 48h time points averaged together. The results from animals given a sub-toxic dose of APAP (150 mg/kg) are not presented since they were not significantly different from controls. *Statistical difference ($p < 0.05$) from control group using one-way ANOVA followed by Tukey's multiple comparison post-hoc test.

Figure 2.1

A Sub-toxic dose of acetaminophen significantly increases nitro-tyrosine protein adducts in rat liver

Representative micrographs (200×) of liver tissue from rats immunostained for nitrotyrosine after treatment with (A) methyl cellulose control or (B) 150 mg/kg acetaminophen at 6, 24, and 48hrs post-dosing and (C) 1500 mg/kg and (D) 2000 mg/kg acetaminophen at 6 hrs post-dosing*. Representative micrograph (40×) of liver tissue from rats after treatment with 150 mg/kg acetaminophen demonstrating centralobular localization of nitrotyrosine staining (D). Immunostained liver sections for control (□) and 150 mg/kg (■) APAP were quantified by averaging percent area stained to total area at 200× in pericentral regions (F). Data are presented as mean $\pm$ SD, n = 3 biological replicates per group. Data significantly different from control, $p < 0.01$, is denoted by asterisk. *Analysis of overtly toxic doses of APAP at 24 and 48 hrs post-dosing was not performed due to the extensive presence of necrotic tissue that often stains non-specifically. CV, central vein; PV, portal vein.

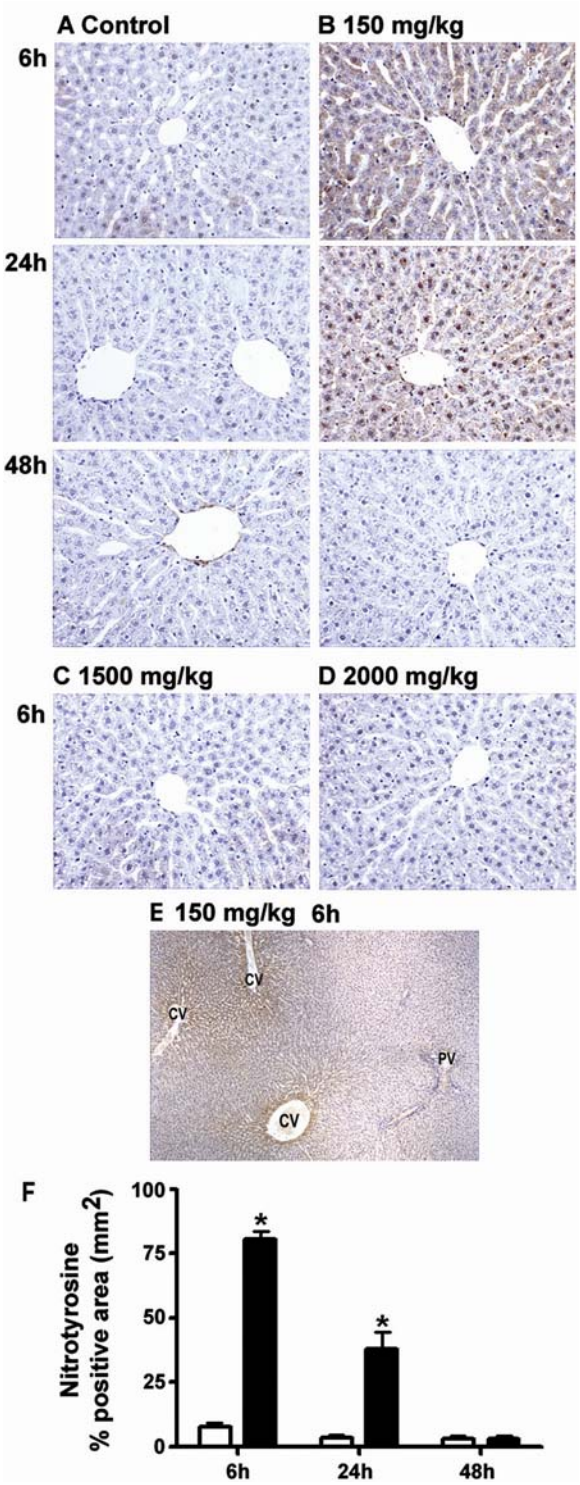
A Control
B 150 mg/kg
6h
24h
48h
C 1500 mg/kg
D 2000 mg/kg
6h
E 150 mg/kg 6h
CV
CV
CV
PV
F
Nitrotyrosine
% positive area (mm2)
100
75
50
25
0
*
*
6h
24h
48h

Figure 2.2

Rat liver genomic DNA significantly accumulates 8-OH-dG adducts after 6 hrs treatment with sub-toxic and overtly toxic doses of acetaminophen

Representative micrographs (200×) of liver tissue immunostained for 8-OH-dG from rats treated with (A) methyl cellulose control, (B) 150 mg/kg, or (C) 1500 mg/kg acetaminophen 6 hrs post-dosing. Representative micrograph (40×) of liver tissue from rats after treatment with 150 mg/kg acetaminophen demonstrating centralobular localization of 8-OH-dG adducts (D). Immuno-stained liver sections for control (□), 150 mg/kg (■), or 1500 mg/kg (■) APAP were quantified by averaging percent nuclei stained to total nuclei within pericentral regions at 200× (E). Data are presented as mean ± SD, n = 3 biological replicates per group. Data significantly different from control, $p < 0.05$, is denoted by asterisk. ND = not determined. CV, central vein; PV, portal vein.

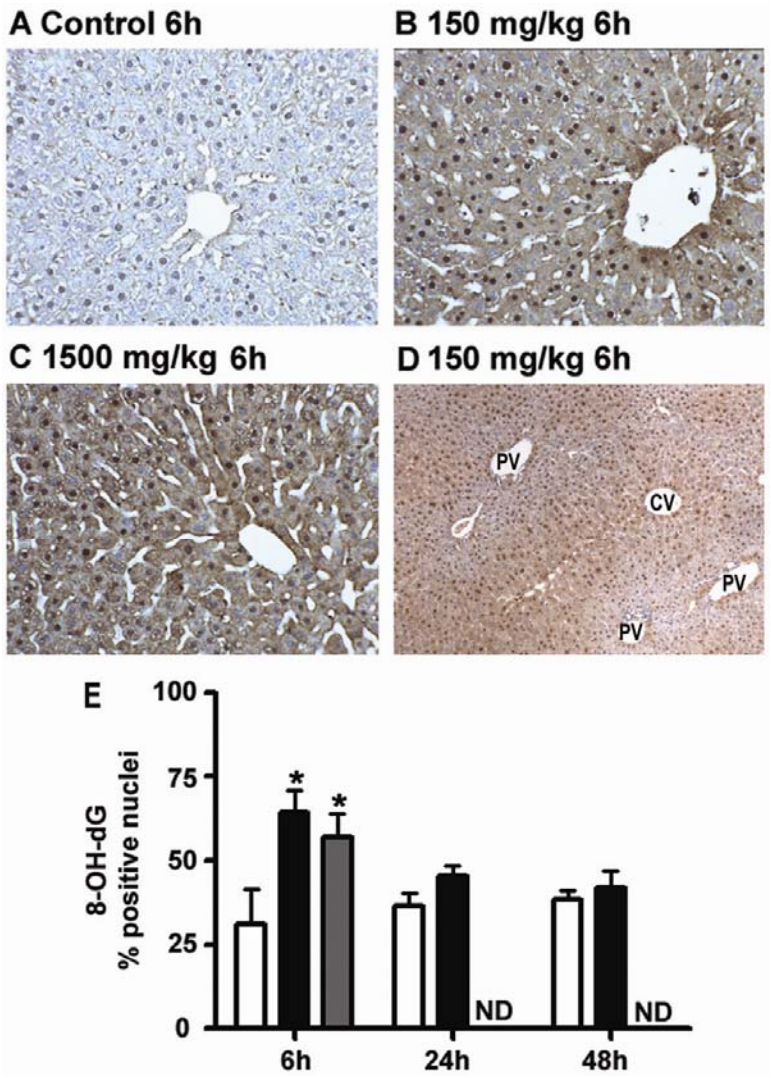

Figure 2.3

A sub-toxic dose of APAP significantly accumulates 8-OH-dG DNA adducts in rat liver as measured by capillary LC-MS/MS

(A) Standard calibration curve for 8-OH-dG by capillary LC-MS/MS. The ratio of the peak areas of 8-OH-dG (AS) to 275.5 fmoles [$^{15}N_5$]-8-OH-dG (AI) as the internal standard plotted against the amount of 8-OH-dG ranging from 5.5 to 228 fmoles/μl. (B) Quantitative measure of 8-OH-dG DNA adducts in rat liver from control (□), 150 mg/kg (■), or 1500 mg/kg (■) APAP. Data are presented as mean ± SD from 3 animals per group. *Statistical difference ($p < 0.05$) from control group using one-way ANOVA followed by Tukey's multiple comparison post-hoc test.

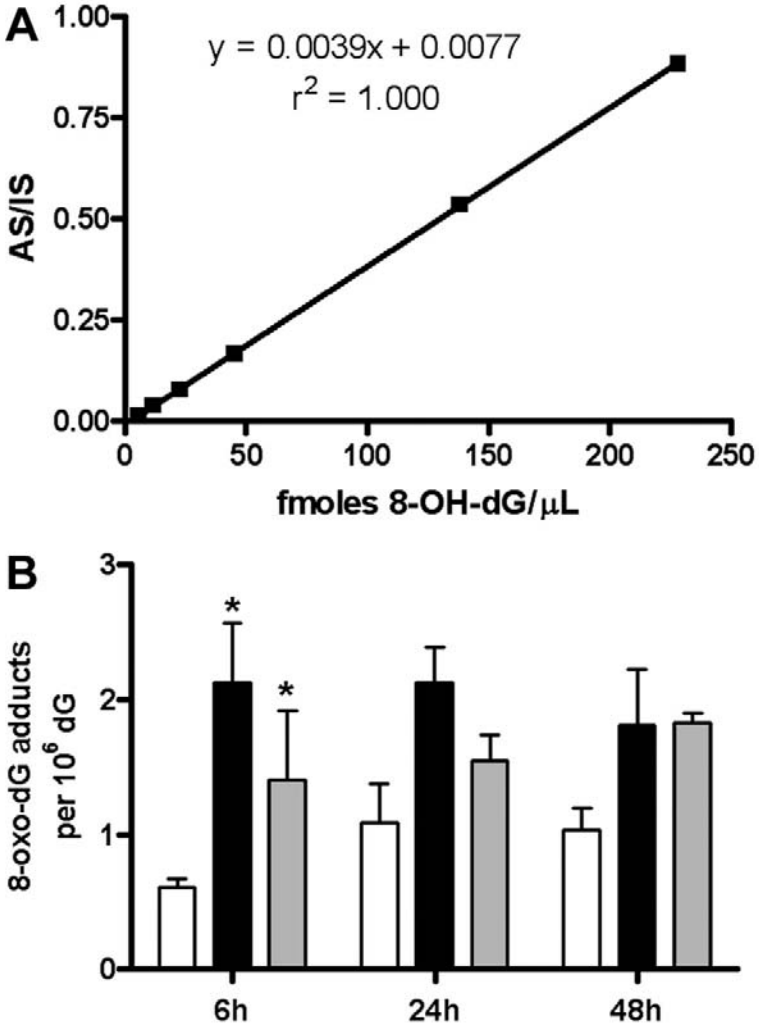

Figure 2.4

Acetaminophen has no effect on the accumulation of apurinic/apyrimidinic (AP) sites in rat liver

The number of AP sites in genomic DNA isolated from livers of control (□) and 150 mg/kg (■), or 1500 mg/kg (■) APAP at 6, 24, and 48h. The control is pooled RNA from three biological replicates and then 6, 24, and 48h time points averaged together. Data is given as mean ± SD, n = 3. Statistical analysis by one-factor ANOVA ($p < 0.05$) found no significant difference between acetaminophen treated groups and control.

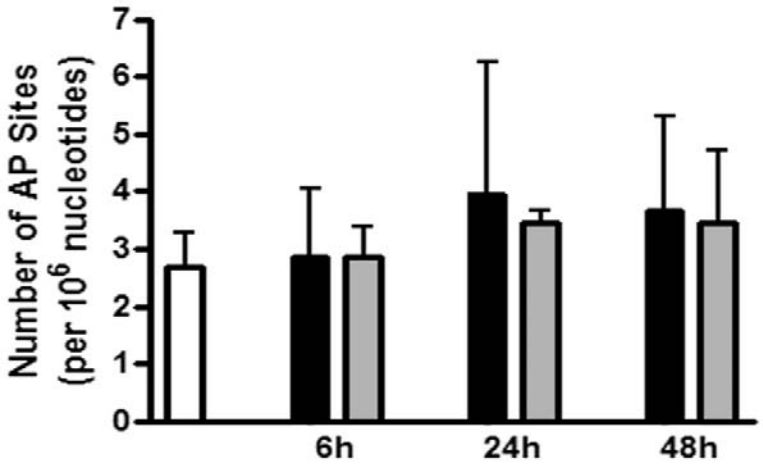

Figure 2.5

Acetaminophen does not promote lipid peroxidation in rat liver

Representative micrographs (200×) of liver tissue immunostained for malondialdehyde from rats treated with (A) methyl cellulose control, (B) 150 mg/kg, or (C) 1500 mg/kg acetaminophen 6 hrs post-dosing. Immunostained liver sections for control (□), 150 mg/kg (■), or 1500 mg/kg (■) APAP were quantified by averaging percent area stained to total area at 200× in pericentral regions (D). Data are presented as mean ± SD, n = 3 biological replicates per group. Statistical analysis by one-factor ANOVA ($p < 0.05$) found no significant difference between acetaminophen treated groups and control. ND = not determined.

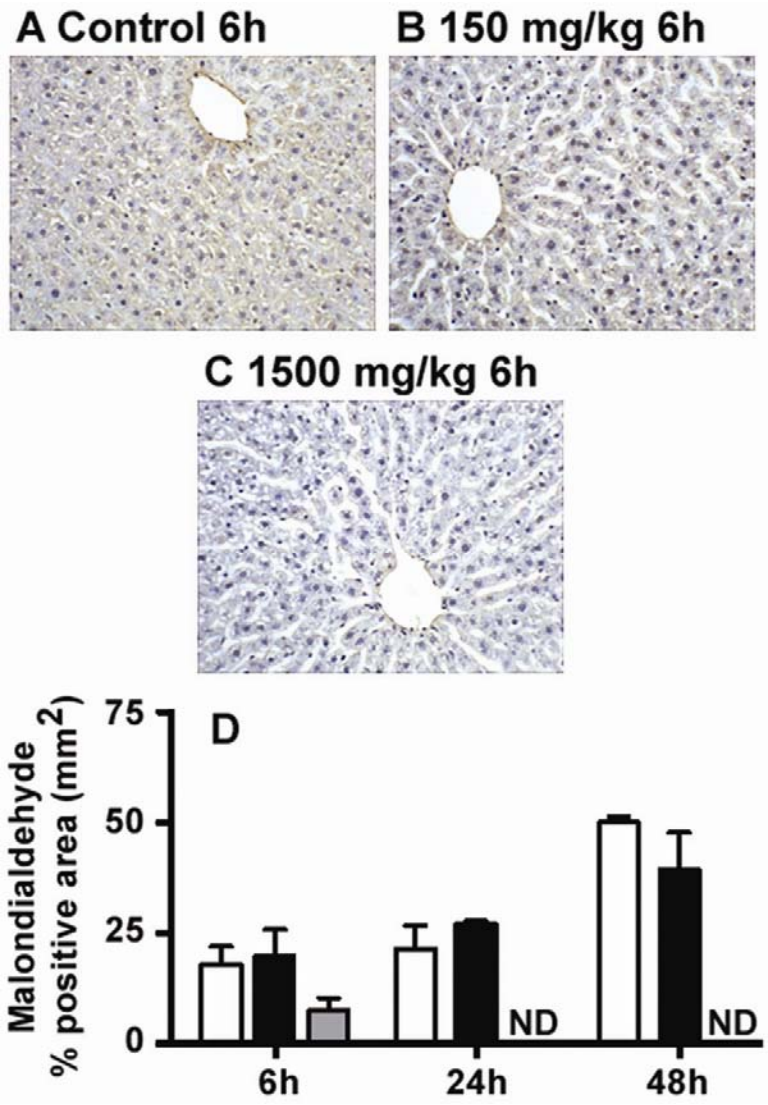

Figure 2.6

Phenotypic anchors of gene expression profiling for oxidative stress are a reflection of the proposed mechanism of APAP-induced hepatotoxicity

APAP is metabolized by cytochrome P450s to a reactive metabolite, *N*-acetyl-*p*-benzoquinone imine (NAPQI), which depletes glutathione (GSH) and covalently binds to cellular proteins as APAP-cysteine adducts. Mitochondrial injury leads to increased production and release of reactive oxygen and nitrogen species that promotes oxidative stress and DNA damage. The depletion of GSH and coupling reaction of superoxide ($O_{2\cdot}^-$) and nitric oxide ($NO\cdot$) leads to formation of peroxynitrite ($ONOO^-$) that reacts with protein tyrosine residues. It has been proposed that the production of $NO\cdot$, induced by APAP, terminates lipid peroxidation propagation. The concomitant loss of mitochondrial function and generation of oxidative stress are postulated to have a central role in APAP-induced hepatoxicity. The sequence of events involved in APAP-induced hepatatoxicity are shown in *bold,* whereas the markers of oxidative stress and oxidative DNA damage measured in this study are shown in *italics*. ∗, markers that anchored gene expression signature suggestive of oxidative stress with a sub-toxic dose of APAP. The scheme is a summation of previously published reports on APAP-induced hepatotoxicity, see Discussion.

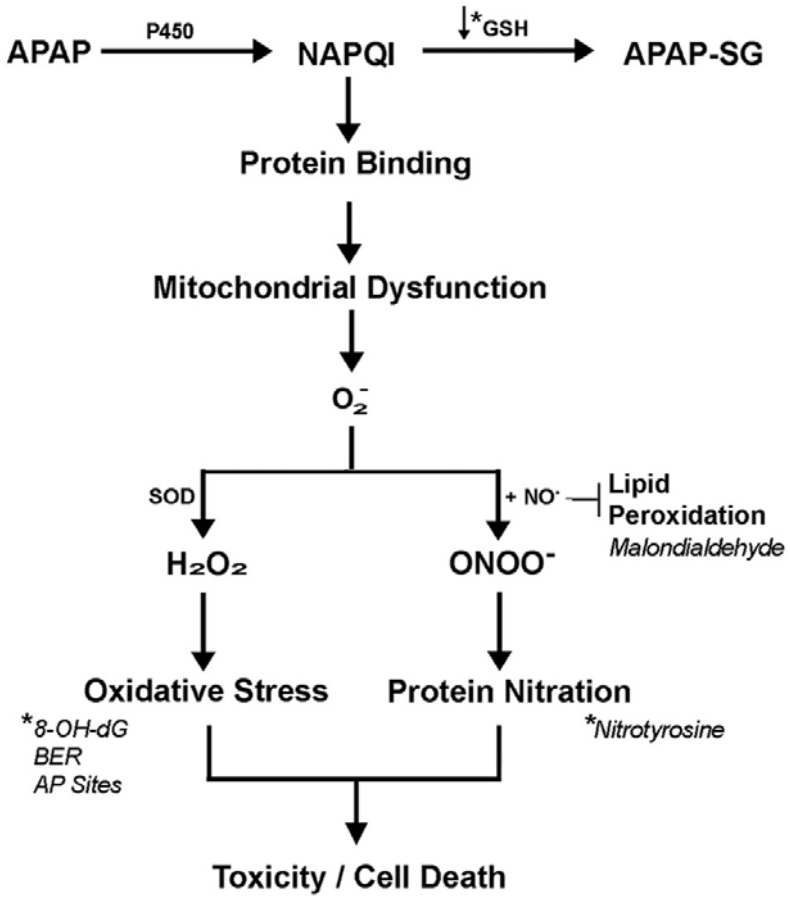

CHAPTER III

TEMPORAL CORRELATION OF PATHOLOGY AND DNA DAMAGE WITH GENE EXPRESSION IN A CHOLINE-DEFICIENT MODEL OF RAT LIVER INJURY

A. Abstract

Hepatocellular carcinoma (HCC) is the terminal event in chronic liver diseases that include repeated cycles of cellular injury and regeneration. While much is known about the cellular pathogenesis and etiologic agents leading to HCC, the molecular events are not well understood. The choline-deficient (CD) model of rodent HCC involves the consecutive emergence of a fatty liver, apoptosis, compensatory proliferation, fibrosis, and cirrhosis that is markedly similar to the sequence of events typified by human HCC. Moreover, oxidative stress is thought to play a pivotal role in the progression of the disease. Here, we hypothesize that gene expression profiling can temporally mirror the histopathology and oxidative DNA damage observed with this model. We show that clusters of highly co-regulated genes representing distinct cellular pathways for lipid biosynthesis and metabolism, apoptosis, cell proliferation and tissue remodeling temporally correlate with the well-defined sequential emergence of pathological alterations in the progression of liver disease. Additionally, an oxidative stress signature was observed which was corroborated in a time-dependent manner with increases in oxidized purines and abasic sites in DNA. Collectively, expression patterns were strongly driven by pathology demonstrating that patterns of gene expression in advanced stages of liver disease are primarily driven by histopathological changes and to a much lesser degree by the original etiological agent. In conclusion, gene expression profiling coupled with the CD model of HCC provides a unique opportunity to unveil the molecular events associated with various stages of liver injury and carcinogenesis and to distinguish between causal and consecutive changes.

B. Introduction

The choline deficient (CD) diet is an extensively studied non-chemical induced, non-genotoxic model of rodent hepatocellular carcinoma (HCC) that produces a well-defined temporal pattern of pathological changes (Figure 3.1). It is characterized by an initial increase in triglycerides resulting in macro-vesicular fat deposition (steatosis) that quickly diffuses throughout the entire liver within 4 to 5 days (122). By 4 weeks, increased fat storage and oxidative stress are thought to contribute to hepatocellular injury which prompts apoptosis (123) and is coupled with compensatory liver regeneration (124). Fibrosis develops as activated hepatic stellate cells increase collagen production disrupting liver architecture, and eventually leads to cirrhosis by 30 weeks of treatment (125). Lastly, carcinomas develop with a 100% incidence by 52 weeks (126). The sequence of pathological events is remarkably similar to the progression of human HCC associated with hepatitis B (HBV) and C (HCV) viral infections, non-alcoholic fatty liver disease, and alcohol abuse.

The development and progression of HCC in the CD model is not well understood due to the complexity of genetic and epigenetic events that occur in hepatocytes. Nevertheless, repeated cycles of hepatocyte injury and regeneration, oxidative stress to DNA (127), chronic activation of protein kinase C (128), activation of arachidonic acid cascade, in particular cyclooxygenase-2 (129), and hypomethylation of c-fos, c-myc, and c-Ha-ras (130, 131) have been reported to occur. However, the definitive role of each of these processes in disrupting liver homeostasis and progression to HCC has yet to be elucidated.

Molecular profiling of cancer by high density microarray analysis is a powerful tool for identifying new biomarkers with diagnostic and predictive value as well as increasing our understanding of the mechanisms of carcinogenesis (132). Genomic studies of breast, lung, and colon cancers have identified unique gene networks and

regulatory pathways useful in classifying tumors into clinically relevant sub-types (133-135). Furthermore, the corroboration of altered expression patterns with phenotypic endpoints such as histology, pathology, and clinical chemistry have provided the much needed validation of molecular profiling data (4).

HCC is the fifth leading cause of cancer death worldwide. Early diagnosis is difficult since most people are asymptomataic during the early stages of the disease and there are no diagnostic markers currently available, contributing to the high mortality rate. Moreover, the lack of appropriate and reproducible animal models for HCC impedes the development of diagnostic markers and therapies. Transcriptional profiling coupled with an appropriate animal model for HCC provides an opportunity to identify novel molecular markers with diagnostic and prognostic value. Here, we show that gene expression profiling of CD model of HCC can be phenotypically anchored to the well-defined sequential emergence of histopathological changes and associated oxidative stress to DNA. The gene expression changes observed with this model are remarkably similar to human HCC expression data from diverse etiologies. Collectively, the expression patterns in advanced liver disease are strongly driven by pathology and not etiology. Thus, understanding the early molecular events leading to such events is key for medical intervention.

C. Experimental Procedures

Animals and treatments

The studies detailed herein were performed using tissue samples (stored at -80°C) from previously published report (136) where male Fisher 344 rats were administered with either a choline sufficient L-amino acid defined (CS) diet, or CD L-amino acid defined diet and water *ad libitum* for 12, 30, or 80 weeks; or samples generated specifically for this study (3 days and 4 weeks) using the identical procedure.

RNA Isolation

Total RNA was isolated using RNeasy kit (Qiagen, Valencia, CA). Samples were stored at -80°C until assayed. The quality of preparations was determined using Bio-Analyzer® (Agilent Technologies, Palo Alto, CA).

Microarray Experiments

Gene expression analysis of isolated RNA from liver tissue was performed using Affymetrix® Rat 230A microarrays (Affymetrix, Santa Clara, CA) at Functional Genomics Core at UNC-CH using standard procedures specified by the manufacturer (neuroscience.unc.edu/core_facilities/functional/).

Microarray Data Analysis

Preliminary analysis was performed using MAS 5.0 software (Affymetrix). Array quality was determined by examination of 3' to 5' intensity ratios of selected genes. Data was normalized to global probe intensity using a robust multi-array average (RMA) method (137) and expression data were $\log_2$-transformed and gene-median centered. Hierarchical clustering analysis was conducted using Cluster (rana.lbl.gov/EisenSoftware.htm) to perform gene-centered, average-linkage clustering (138); the data was visualized using Java TreeView (jtreeview.sourceforge.net).

Two independent statistical tests were applied to identify the unique gene expression profiles of CD and CS. First, the method of Sorlie et al. (139) was utilized to define genes intrinsic to an experimental group versus control, where a group is defined as unique combination of the type of diet (CD or CS) and duration of treatment (4, 12, 80 weeks and tumors). This method gives the best (lowest) scores to those genes whose variation is low within a group, but high across multiple groups. The resulting list is expected to encompass subsets of genes whose expression is common to all samples within each group. To establish a false discovery rate (FDR) for this computational

approach (i.e., to establish statistical significance), the group label for each sample was randomly permuted and the set of intrinsic scores was calculated from the resulting groupings. This process was repeated twenty times. A threshold of the intrinsic scores was determined by identifying the score that gave the greatest number of significant calls with less than 5% occurrence in the permuted results. In addition, a two-class, unpaired Significance Analysis of Microarrays [SAM; (140)] was performed as described for intrinsic gene identifier. The SAM algorithm differs from the intrinsic scores defined above since more weight is placed on differences in fold changes between the groups. Delta values were adjusted to obtain the gene list with a < 5% FDR. All microarray raw data tables are available at the UNC Microarray Database (genome.unc.edu).

RNase Protection Assays

Expression of base excision DNA repair genes was analyzed using RNase protection assay with rat multi-probe template set (rBER, BD PharMingen, San Diego, CA) as described elsewhere (84).

Detection of Apurinic/Apyrimidinic (AP) Sites and Oxidized Purines

Genomic DNA was extracted by a procedure slightly modified from the method reported previously (95). To minimize formation of oxidative artifacts during isolation, 2,2,6,6-tetramethylpiperidinoxyl (TEMPO, 20 mM) was added to all solutions and all procedures were performed on ice. The AP and OGG1 slot blot assays were performed as previously described (83, 141).

D. Results and Discussion

Hierarchical analysis of gene expression data distinguishes CS and CD treated groups. It has been well established that a CD diet causes HCC in rats and produces a well-defined temporal pattern of pathological changes involving steatosis, hepatocyte injury, fibrosis and cirrhosis (Figure 3.1). To assess whether expression

profiling temporally mirrors the altered pathological changes observed with the liver disease induced by this treatment, we applied a high-throughput Affymetrix Rat 230A array to liver tissues from control CS or CD diet-fed Fisher 344 rats. Liver tissues were chosen at 4, 12, and 80 weeks, as were tumors larger than 5 mm at 80 weeks, to reflect the various stages of liver injury. It should be noted; however, that the gene expression profiling was performed on whole liver making it difficult to discern the contribution of individual cell types. Furthermore, 30 and 80 week liver samples may not be devoid of tumors 5 mm or less and may contain necrotic and apoptotic hepatocytes in addition to other cell types associated with liver cirrhosis.

Identification of gene clusters temporally expressed in liver of CD treated rats. Two independent statistical tests, intrinsic gene identifier (134) and SAM (140), were performed to identify genes whose expression profiles were unique to CD at any time point using the 6,045 fully annotated transcripts on the array. Intrinsic gene identifier analysis showed that expression levels of 3,102 genes segregated at least a single time point (e.g., 4, 12, 80 weeks, or tumors) compared to its corresponding control group. SAM identified 4,673 genes of which 88% (2,739 genes) were also detected by an intrinsic gene identifier analysis. Genes from both lists were assigned into functional categories using Gene Ontology (GO) and enriched KEGG pathways using Onto-Pathway-Express (142). Considerable overlap between the two methods was observed as the enriched KEGG pathways identified by both analyses were identical (Appendix 5).

The intrinsic gene list was subjected to clustering analysis using a centered, average-linkage hierarchical algorithm. The resulting dendrogram (Figure 3.2) revealed two major branches separating the experimental groups, CS and CD. Interestingly, heterogeneity between tumor samples was observed with T2 and T3 samples (two distinct tumors from the same animal) being similar to each other but somewhat different

from other tumors and 80 week CD samples. Data mining using GO annotations for intrinsic genes (NetAffx™ Analysis Center, affymetrix.com) was used to assign functional classes and to determine the cellular and molecular pathways defining treatment separation. Several clusters of highly up-regulated genes evoked by CD were associated with apoptosis, cell proliferation, protein synthesis, and tissue remodeling. Conversely, metabolism, lipid synthesis, and ion transport pathways were selectively down-regulated compared to CS.

To determine whether molecular profiling would model the temporal changes in histopathology observed with CD, genes with a functional assignment associated with lipid biosynthesis or metabolism (excluding ion transport pathways), apoptosis, cell proliferation, and tissue remodeling were compiled. Supervised hierarchical clustering was conducted to view temporal changes in expression of genes associated with abovementioned biological processes (Figure 3.3, Appendix 1). This result demonstrates that dramatic alterations in gene expression occur as early as 4 weeks in CD samples.

Gene expression patterns reveal CD attributes to altered lipid metabolism. Accumulation of lipid mostly comprised of triglycerides occurs in hepatocytes within days of administering a CD diet to rats (143). This has been attributed to the compromised ability to synthesize phosphatidylcholine (PC), a major constituent of lipoprotein envelopes, whereby secretion of triglycerides from the liver is inhibited. PC plays a major role as a structural component of cellular membranes and as a source of second messengers, it can influence both normal physiological and pathological processes including carcinogenesis.

Indeed, GO-assisted search identified 160 genes within the intrinsic gene list with a functional assignment to either lipid biosynthesis or metabolism (Figure 3.3A). After 4 weeks of CD diet, an induction of genes for fatty acid (Cpt1a, Cte1, Fabp2, Fads1, and

Mte1) and cholesterol (Apoa1, Abcg1, and Vldlr) metabolism occurred most likely as a result of the accumulation of intracellular lipids. At 12 weeks, there was an additional increase in expression of phospholipases (Pla2g4a, Plce1, Pspla1, and Dpep1) that release second messengers and metabolic precursors from membrane phospholipids. For example, activation of membrane receptors coupled to phospholipase C release 1,2-*sn*-diacylglycerol (DAG) from intact membrane phospholipids which are potent activators of protein kinase C (PKC). PKC targets include proteins involved in the control of gene expression, cell division, and differentiation (144) and alterations in PKC signaling have been attributed to tumorigenesis (145). Interestingly, it has been demonstrated that CD rats accumulate high levels of DAG in cellular membranes and this coincides with increased PKC levels and activity (128). Phospholipase A2 releases arachidonic acid from cellular phospholipids, a precursor to the biologically potent eicosanoids, prostaglandins and thromboxanes of which several members were highly expressed (Ptgfrn, Ptgs1, Tbxas1, Ltc4s). At 80 weeks, there was an increase in expression of phospholipases (Plcg1 and Pla2g6) and phosphoesterases (Pde4b and Pter). Over the course of CD diet, there was a transient down-regulation of genes associated with steroid and fatty acid synthesis and lipid transport (Appendix 1).

Gene expression patterns reveal CD activates apoptotic pathways. There have been numerous reports of induction of apoptosis with CD diet through both p53-dependent and -independent pathways. Supervised hierarchical clustering of genes associated with apoptosis revealed a strong induction of pro-apoptotic genes at 4 weeks of CD diet (Figure 3.3B) such as caspases, apoptosis activating factor 1 (APAF1), tissue necrosis factor, and p53. Tumor samples did not express p53 or mitochondrial mediated apoptotic genes such as APAF1 and caspases; however, there were a small number of

genes up-regulated in tumor samples associated with death receptor-mediated pathway including TNF and NGF receptor superfamilies and Cflar.

In vitro studies with CWSV-1 rat hepatocytes have demonstrated that the rate of apoptosis is inversely correlated with cellular PC content (123). Moreover, it has been shown that inhibition of PC biosynthesis by CD diet leads to apoptosis by an increase in intracellular ceramide levels in neurons (146); however, our data shows an increase in expression of genes related to ceramide metabolism including acid ceramidase (Asah) and UDP-glucose ceramide glucosyltransferase (Ugcg) suggesting that ceramide is not an important mediator of apoptosis in this model. Additionally, the induction of apoptotic genes coincided with a predominance of genes associated with positive regulators of the cell cycle (Figure 3.3C, Appendix 1) such as cyclins, oncogenes, and cyclin dependent kinases.

Gene expression patterns reveal CD mediates tissue repair through activation of hepatic stellate cells. Recurrent hepatocellular injury is a hallmark of the CD diet that chronically activates cellular and molecular mechanisms of tissue repair leading to fibrosis and cirrhosis of the liver. Analysis of gene expression patterns revealed a highly expressed cluster of genes related to the initiation and promotion of fibrosis at 4 and 12 weeks of CD treatment (Figure 3.3D), including transforming growth factor β, which promotes the proliferation of fibroblasts and hepatic stellate cells and the extracellular matrix components collagens, proteoglycans, fibronectin, laminins, and matrix metalloproteinases (147, 148). Moreover, hepatic stellate cell-specific genes were up-regulated, including stellate activation associated cell protein, α-smooth muscle actin, vimentin, and tissue inhibitors of metalloproteinases, supporting their involvement in fibrosis (149, 150).

Gene expression reveals liver injury transition states in CD rats. Above, we identified gene clusters that temporally mirrored the histopathological alterations observed with the CD model in rat liver. Here, we examined the genes associated with the initial transition from normal liver to a state of chronic liver injury and ultimately leads to the second transition to HCC. To define these two major transition states, we performed unpaired SAM analysis between CS samples versus CD non-tumor samples (i.e., transition state 1), and CD non-tumors versus CD tumors (i.e., transition state 2). Next, to cross-compare these genes lists we generated a Venn diagram (Figure 3.4) to identify genes that are shared or unique in these two liver injury transition events. Lastly, the gene lists were submitted to GoMiner (9) to identify significantly enriched biological processes (Appendix 2).

SAM analysis of expression changes during transition state 1 identified 2,302 and 5,882 genes to be significantly up- or down-regulated, respectively. GO mapping found a significant enrichment in biological processes related to proliferation, cell death, and tissue remodeling. In contrast, processes related to cell communication, in particular, G-protein coupled signal transduction and ion transport pathways, were significantly down-regulated, most likely a reflection of the loss of cell membrane structure due to the inability to synthesize phospholipids. For transition state 2, SAM identified 581 and 212 genes to be significantly up- or down-regulated, respectively. Processes related to cell proliferation alongside with transcription-coupled nucleotide excision repair were significantly increased. In contrast, processes related to oxidative DNA damage and repair and apoptosis were down-regulated potentially signifying increased genomic instability and survival of cells in liver tumors.

Interestingly, there were 1,101 genes shared between the two transition states, but their expression changes were directionally opposite. Specifically, 518 and 583 genes were significantly up- or down-regulated in transition state 1 and vice versa. There

were a number of processes related to cell motility, cytoskeleton reorganization, and immune response up-regulated in transition state 1, a reflection of the underlying molecular events that occur after extensive cellular injury. In contrast, transition state 2 showed a significant enrichment in metabolic processes that would be required to sustain tumor growth.

CD-induced hepatocarcinogenesis is preceded by oxidative stress to DNA. It has been shown that treatment of rodents with a CD diet causes oxidative stress to DNA that is predominantly removed and repaired by the base excision repair (BER) pathway. To confirm that oxidative stress to DNA is present in CD rats, changes in expression of DNA repair genes, a sensitive *in vivo* marker of oxidative stress to DNA (151), was evaluated. A significant increase in expression of proliferating–cell nuclear antigen, AP endonuclease 1, 8-oxoguanine DNA glycosylase 1 (Ogg1), and polymerase β was observed in CD-fed animals (Table 3.1). Additionally, expression of O^6-methylguanine-DNA methyl transferase, an enzyme involved in the direct repair of alkylated guanine residues, was enhanced. Previous reports have shown increases in DNA methyl transferase expression with preneoplastic and neoplastic livers of rodents fed a CD diet which is the result of a hypomethylated promoter (152).

In parallel, the intrinsic gene list for GO functional assignments associated with oxidative stress was examined and identified 92 genes. Hierarchical clustering of these genes revealed a temporal separation of genes that are over expressed in liver at 4 and 12 weeks, 12 and 80 weeks, and tumor samples (Figure 3.5). The 4 and 12 week cluster reflects an up-regulation of cellular antioxidant defenses such as heat shock protein (Hspa1b, Hspcb, Hsp60, and Hspa1a) and glutathione peroxidase (Gpx2 and Gpx3) genes. At 12 and 80 weeks, an increase in genes linked to DNA damage including the DNA repair genes apurinic/apyrmidinic endonuclease 1, DNA polymerase delta, and the

DNA-damage-inducible transcript 4 was observed. Surprisingly, the expression of Ogg1 was not increased in the microarray data; however, the concordant temporal upregulation of a number of DNA repair genes with CD is evidence of a biological response for oxidative DNA damage in this model.

In tumors, an up-regulation in DNA repair genes including mismatch repair protein, polymerase epsilon, and mediator of DNA damage checkpoint 1 was found. Additionally, a number of cellular antioxidants were up-regulated including thioredoxins and glutathione S-transferases. Interestingly, thioredoxins have been demonstrated to promote proliferation and growth of tumors through induction of growth factors and cytokine activity (153).

Although there have been previous reports documenting the accumulation of 8-oxo-dG DNA adducts in liver of rats given a CD diet, the data must be interpreted with caution since previous reports may be erroneous due to *ex vivo* oxidation during DNA isolation, as reported by the European Standards Committee on Oxidative DNA Damage (ESCODD) (154). Thus, we measured oxidized purines in DNA using an isolation procedure that was shown to minimize artifactual *ex vivo* oxidation. Figure 3.6A illustrates that background level of oxidized purines was below 1 x 10^6 nucleotides, in agreement with ESCODD-reported values (100). Significant increases in oxidized purines were observed in animals given CD diet for 12 weeks and in tumor samples. Abasic sites in DNA are generated spontaneously by chemical depurination of labile oxidized bases and enzymatically by DNA glycosylases. To determine whether the number of mutagenic and clastogenic AP sites is increased following CD treatment, AP sites were measured. Significant increases (> 2.5 fold) in the number of AP sites were seen in 12 and 30 week CD treated rat liver (Figure 3.6B).

Generation of oxidants and the resulting state of oxidative stress in the cell induces both genotoxic and epigenetic events that can promote the process of

carcinogenesis. Oxidative stress to DNA is one of the earliest changes observed in rodent liver on a CD diet, with accumulations of 8-oxo-deoxyguanosine (8-oxo-dG), a mutagenic lesion capable of G:C to T:A transversions (155, 156). Additionally, end products of lipid peroxidation such as malondialdehyde and 4-hydroxy-2-nonenal have been reported to form in liver of CD-treated animals (122) resulting in exocyclic DNA adducts that are known to be mutagenic and genotoxic, respectively (157). Here, we have demonstrated that gene expression profiling revealed differential expression of oxidative stress related genes for CD. Specifically, microarray expression data showed an induction of several DNA repair genes involved in the BER pathway after 12 week CD treatment and beyond suggesting that DNA damage had occurred. This was confirmed with increases in AP and oxidized purines in liver DNA. The increase in expression of DNA repair genes and the accumulation of DNA lesions at 12 weeks corresponds to the development of fibrosis and cirrhosis of the liver. Recent studies demonstrated a correlation between increases in DNA repair expression and the histological stage of fibrosis in liver biopsies (158). Moreover, increases in 8-oxo-dG adducts and expression of DNA repair genes was reported in the surrounding tissue of liver tumors (159). Thus, the fibrotic process may be a contributing factor to the transformation of hepatocytes towards a neoplastic phenotype.

CD-induced rat HCC and human HCCs are similar at the level of gene expression. To determine how CD model of rat HCC recapitulates human HCC, gene expression patterns with data from a human HCC study (160) were compared. This study encompassed 102 primary liver tumors and 74 non-tumor liver samples. For this comparison, Ensembl genome browser (ensembl.org) was used to identify rat and human gene orthologs that were present on both microarray platforms. Of the 2,121 genes that were identified as differentially expressed in CD-induced tumors (i.e.,

transition state 2), 492 orthologous genes were selected. Gene expression ratios were standardized to a mean ± s.d. of 0 ± 1 in each data set. Hierarchical clustering analysis of the integrated data sets (Figure 3.7) showed two major clusters, one representing human and CD rat HCC samples, and the other, with a few exceptions, representing non-tumor human liver tissues. Tumors from humans with HBV, HCV, as well as non-infected individuals, were interspersed within the HCC cluster. Furthermore, two distinctive nodes with highly expressed genes were evident in HCC samples as compared to non-tumor liver tissue. Biological processes that were enriched in these nodes were identified using GO mapping. These included angiogenesis, cell-matrix adhesion, G-protein and tyrosine kinase signaling cascades, and protein metabolism. Thus, these data suggest that gene expression changes in CD-induced tumors in rats are similar to human HCC gene expression phenotype and may be potentially used to distinguish between human tumor and non-tumor samples.

Gene expression distinguishes between causal and consecutive events in liver disease. While much is known about the cellular pathogenesis and etiologic agents leading to HCC; the molecular events that contribute to the disease are not well understood. Thus, the use of appropriate animal models coupled with global gene expression profiling can provide the opportunity to serially dissect the molecular events associated with liver injury and disease. Here, we have demonstrated that microarray gene expression data can be phenotypically anchored to the sequential pathological alterations observed during the development of rodent HCC induced by a CD diet. The hierarchical clustering analysis of this expression data set was strongly driven by the histopathological changes that are observed during the progression of HCC by CD diet. Thus, this data provides the opportunity to decipher the genomic changes required to elicit such phenotypic endpoints.

Since the liver pathological changes observed in rodents on a CD diet are similar to that observed by agents (e.g., HBV, HCV and alcohol) causing chronic human liver injury, we suggest that similar expression patterns would be observed in advanced stages of human liver disease regardless of etiology. Indeed, gene expression patterns of CD-induced liver tumors are phenotypically similar to human HCC from diverse etiologies (i.e., HBV, HCV, and HBV/HCV negative individuals). The fact that these liver tumors were interspersed among each other within the HCC branch demonstrates that regardless of the initial confounding etologic agent eventually these diseases converge onto a common and indistinguishable phenotype.

In conclusion, we have shown that gene expression profiling can temporally model the well-defined sequential emergence of pathology and oxidative stress observed with the CD model of rodent HCC. Moreover, the development of fibrosis and cirrhosis temporally coincided with the accumulation of oxidative DNA lesions; processes which may contribute to hepatocyte transformation. Molecular profiling of tumors will not identify the early molecular changes required for transformation; however, the CD model of HCC in the rat provides an opportunity to serially dissect the molecular events related to the onset of liver injury and carcinogenesis that is also relevant to progression of human HCC.

Table 3.1

Expression of DNA repair genes in rat liver after treatment with a control choline sufficient (CS) or choline deficient (CD) diets

	1 week		*12 weeks*		*80 weeks*	
DNA Repair Genes	***CS***	***CD***	***CS***	***CD***	***CS***	***CD***
OGG1, 8-oxoguanine DNA glycosylase 1	1.6 ± 0.1	**1.9 ± 0.1***	1.9 ± 0.4	2.6 ± 0.5	0.9 ± 0.9	**2.6 ± 0.4***
MPG, N-methylpurine DNA glycosylase	3.2 ± 2.9	2.0 ± 0.2	2.0 ± 1.2	3.1 ± 0.8	1.0 ± 0.2	5.2 ± 3.4
APE, apurinic/apyrimidinic endonuclease 1	6.6 ± 0.7	8.4 ± 1.0	7.5 ± 2.2	12.3 ± 5.1	4.3 ± 0.1	**13.8 ± 3.6***
Pol β, polymerase (DNA directed) β	5.6 ± 1.2	4.8 ± 0.7	4.5 ± 1.2	**8.6 ± 2.1***	3.8 ± 0. 9	9.5 ± 5.2
PCNA, proliferating cell nuclear antigen	4.4 ± 0.7	8.6 ± 3.2	4.4 ± 1.6	**12.4 ± 5.1***	3.9 ± 1.7	8.1 ± 3.1
PARP, poly (ADP-ribose) polymerase	10.6 ± 1.2	10.6 ± 0.1	10.4 ± 2.8	14.0 ± 3.5	7.8 ± 1.9	9.7 ± 2.6
MGMT, O^6-methylguanine DNA methyltransferase	13.1 ± 1.5	**17.3 ± 0.9***	14.0 ± 3.5	**27.5 ± 8.7***	19.4 ± 1.2	**33.5 ± 13.2***

RNase protection assay was performed on total RNA isolated from liver samples. The results are mean ± standard deviation from 3 animals per group. The relative expression of each gene was normalized to the expression of the housekeeping gene L32. *Statistical difference ($P < 0.05$) from a corresponding CS group using student's t-test.

Figure 3.1

Pathological stages of liver disease progression in a rat model of HCC

The choline deficient L-amino acid defined diet is a non-genotoxic model of rodent hepatocarcinogenesis. Choline deficiency produces a well-defined temporal pattern of histopathological changes beginning with a fatty liver (steatosis), hepatocellular injury, apoptosis with compensatory proliferation, fibrosis and cirrhosis. Pre-neoplastic foci with a glutathione S-transferase positive (GST-P) phenotype eventually give rise to the development of hepatocellular adenomas and carcinomas within a year of administering the diet.

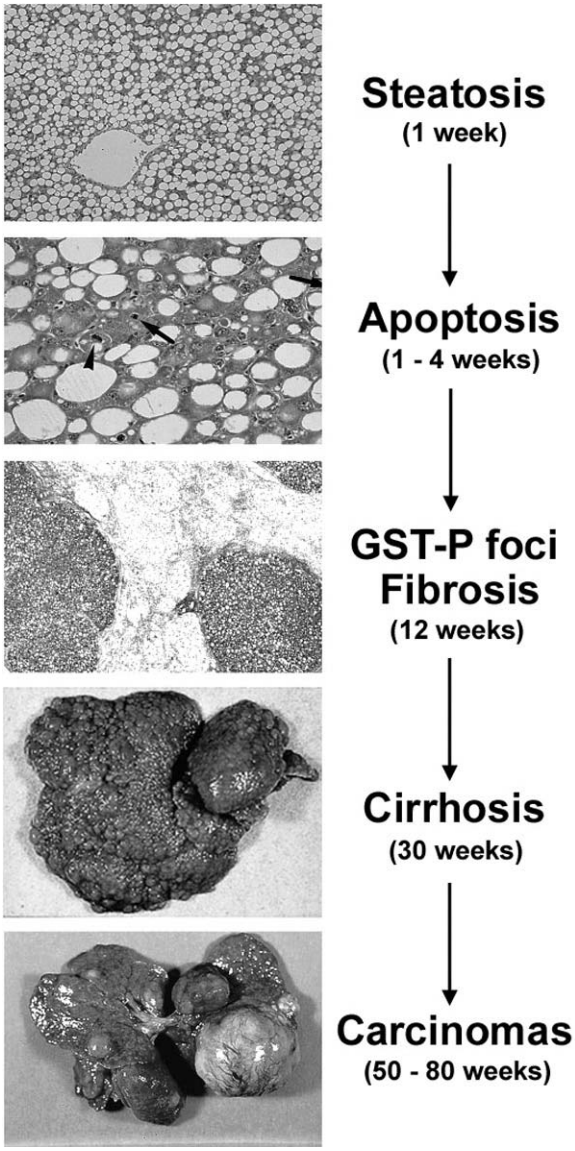

Figure 3.2

Hierarchial clustering of choline sufficient (CS) and choline deficient (CD) liver samples using "intrinsic" gene set

Intrinsic analysis identified genes whose expression levels vary the least within a single treatment group but are highly variable between treatments (FDR < 5%). Hierarchial clustering analysis was conducted on a list of 3,100 non-redundant genes identified through such analysis. Functional classes were assigned to each gene using Gene Ontology (GO) and revealed that the highly up-regulated genes were related to cell proliferation, apoptosis, protein synthesis, and tissue remodeling where as down-regulated genes were related to metabolism, lipid synthesis, and ion transport. For unsupervised hierarchical clustering of entire rat array see Appendix 4.

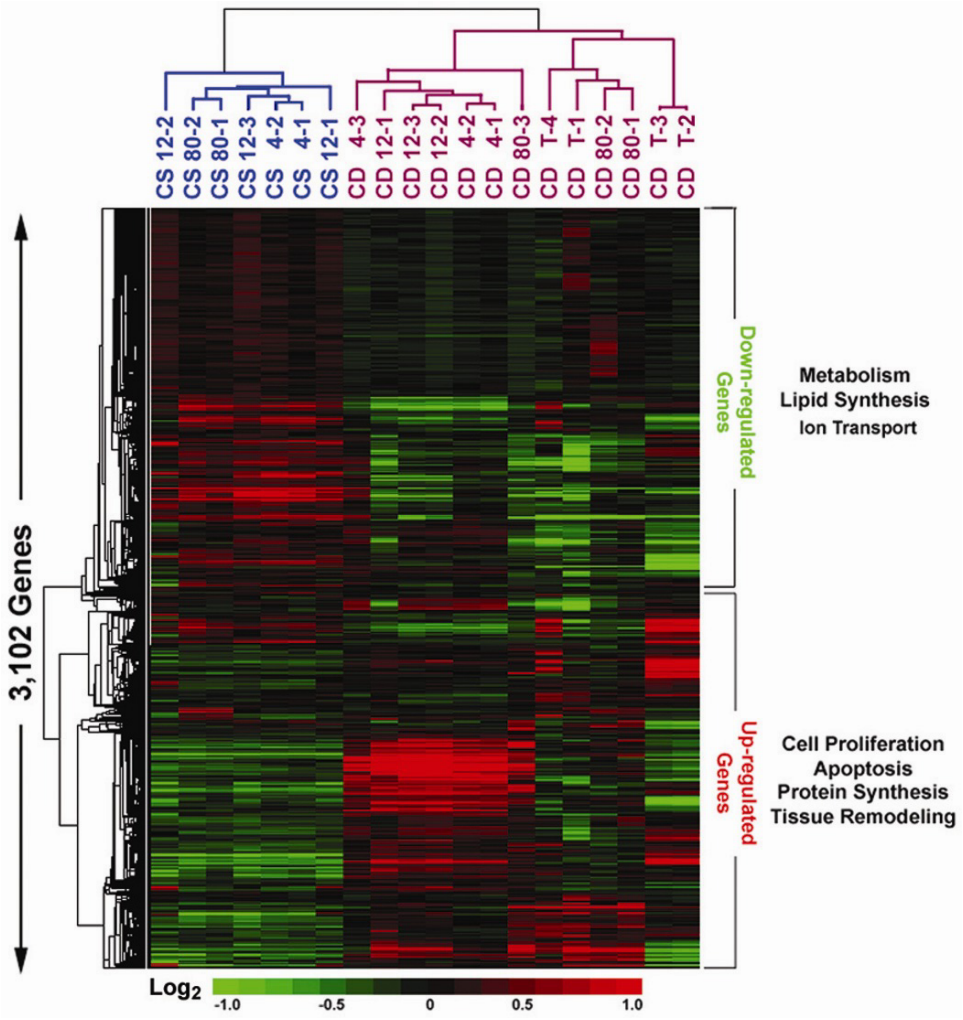

Figure 3.3

Supervised hierarchical clustering of altered cellular and molecular pathways associated with choline deficiency

Gene Ontology (GO) was used to assign functional classes to “intrinsic” gene set to identify cellular pathways related to the histopathological events evoked by choline deficiency. These cellular pathways include lipid biosynthesis and metabolism (A), apoptosis (B), cell proliferation (C), and tissue remodeling (D).

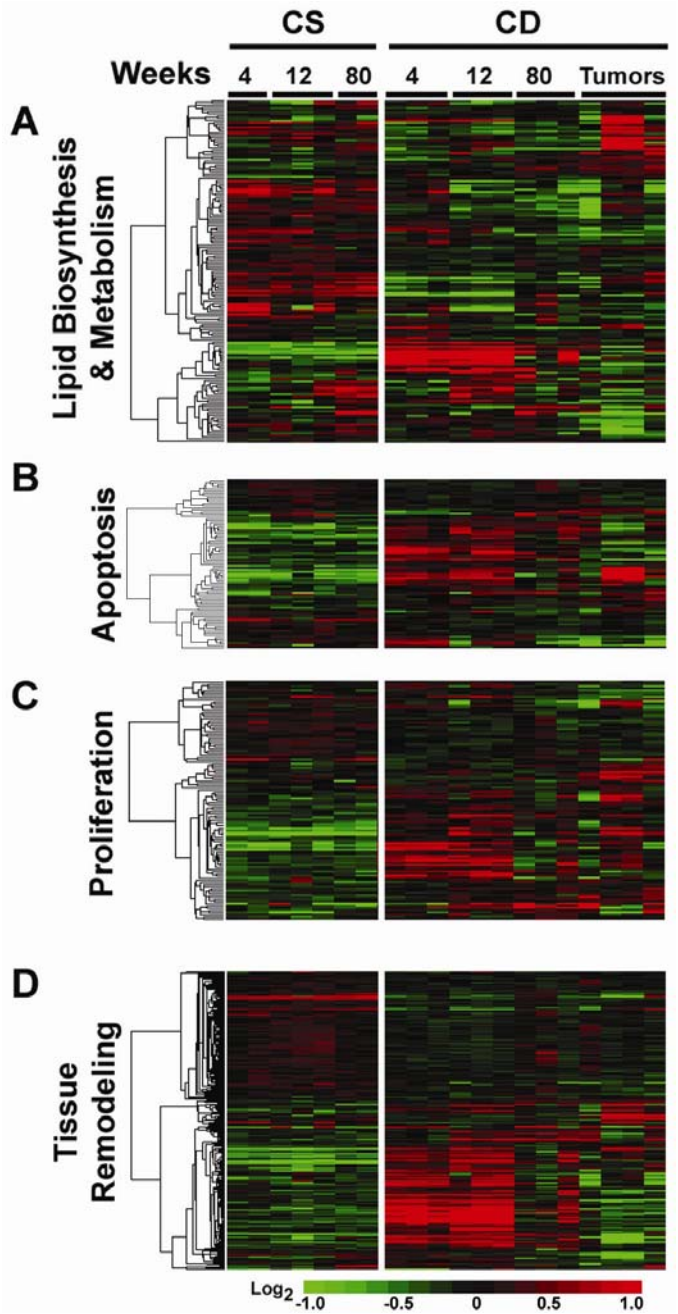

Figure 3.4

Venn diagram illustrating the distribution of gene alterations between liver injury transition states in choline deficient rats

Significant gene lists were generated using SAM (FDR < 5%) for each transition state as described in text and cross-compared. Values represent number of genes significantly induced (red) or repressed (green) that are either unique or shared by the two transition states. There were 1,101 genes shared between the two injury states but their expression changes were directionally oppositite. Gene lists were submitted to GoMiner (9) to identify significantly enriched biological processes ($p < 0.05$), of which a few are shown. The number of genes associated with each process is given in parenthesis. A complete listing of enriched biological processes is available in Appendix 2.

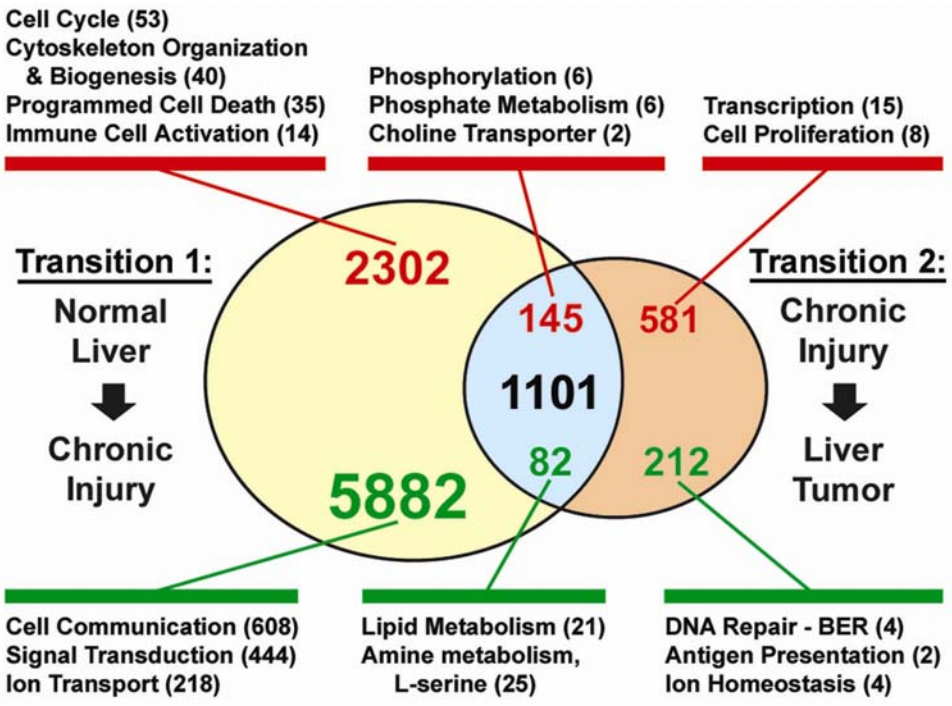

Figure 3.5

Temporal expression of oxidative stress genes in rat liver evoked by a choline deficient diet

Gene Ontology (GO) identified 92 genes within the “intrinsic” gene set associated with oxidative stress from rat liver samples treated with a control choline sufficient (CS) or choline deficient (CD) diet for 4 to 80 weeks. Tumor (T) samples were collected from CD treated rats at 80 weeks. Supervised hierarchical clustering was conducted and is shown in Figure 5A. Colored bars on right side of A illustrate the location of clusters shown in B-D. The clusters of temporally expressed genes expanded for 4 and 12 weeks (B), 12 and 80 weeks (C), and tumor samples (D).

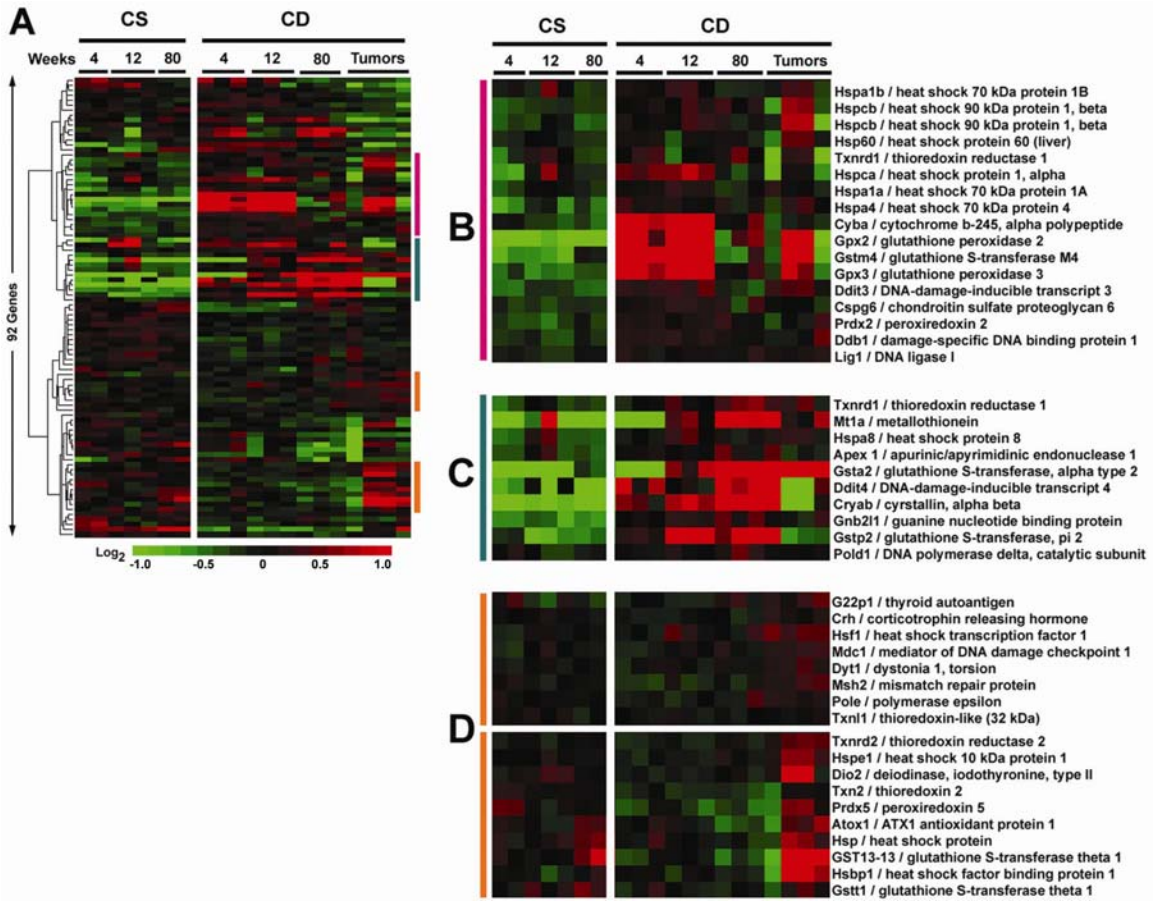

Figure 3.6

Choline deficiency promotes the accumulation of oxidative DNA lesions in rat liver

Genomic DNA was isolated from livers of control CS diet (□) and CD (■) treated rats, and tumors (■) and the number of (A) Ogg1-sensitive sites (B) or apurinic/apyrimidinic (AP) sites (B) determined as described in "Materials and Methods". Data are presented as means ± standard deviation from 2-3 animals per group. *Statistical difference ($P < 0.05$) from corresponding control group by Student's t test.

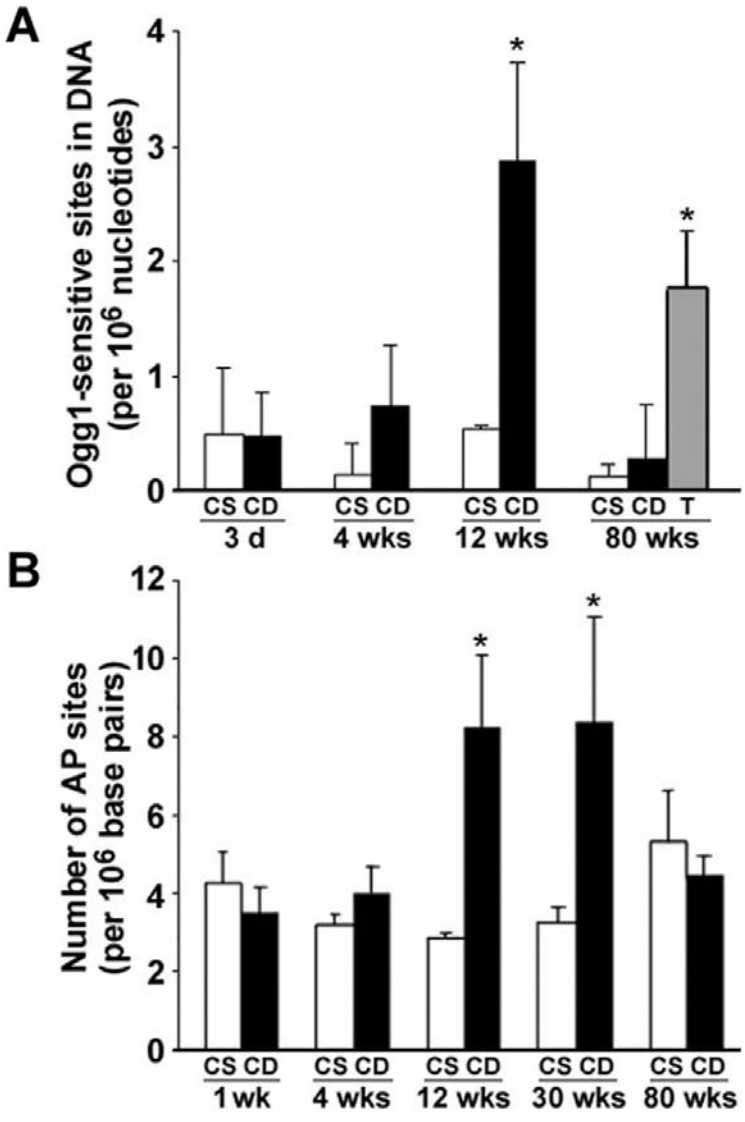

Figure 3.7

Clustering analysis of rat and human HCCs

Unsupervised hierarchical cluster analysis of integrated rat (this study) and human (160) HCC datasets. Ensembl genome browser was used to identify orthologous genes present on both arrays (492 genes) and expression ratios were standardized to a mean ± standard deviation of 0 ± 1 prior to clustering. The two areas highlighted on the heatmap represent clusters of genes that are highly expressed in both rat and human HCC. Biological processes associated with these gene clusters are shown. A complete list of genes is available in Appendix 3.

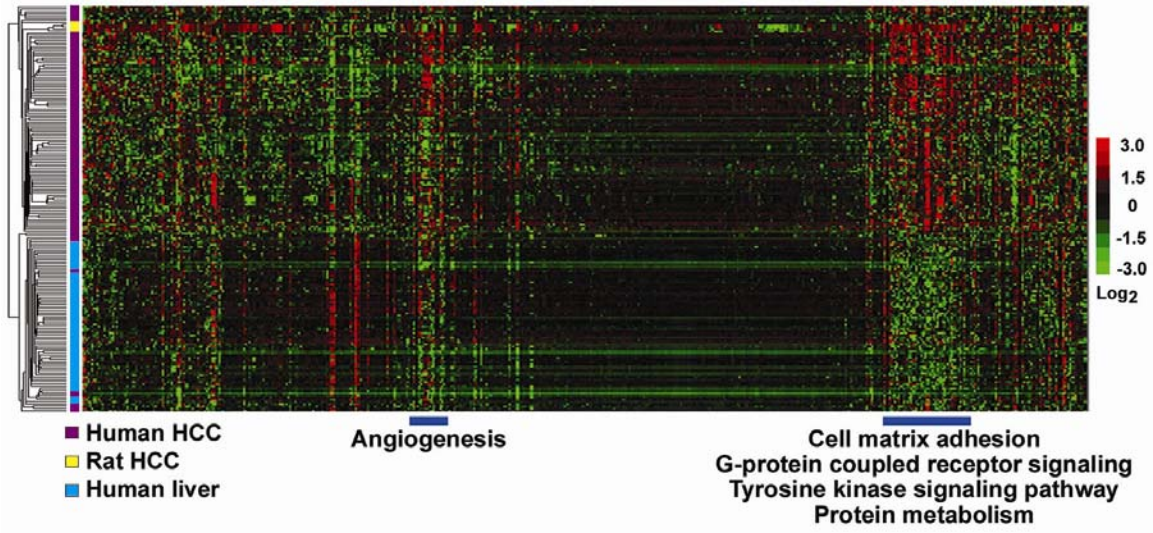

CHAPTER IV

PPARα-REGULATED MOLECULAR NETWORKS ARE RESPONSIBLE FOR THE DIFFERENTIAL EFFECTS OF DIETARY FATTY ACIDS ON OXIDATIVE STRESS AND DNA DAMAGE IN MOUSE LIVER

A. ABSTRACT

Epidemiological and animal model research shows that ω-3 and ω-6 polyunsaturated fatty acids (PUFA) can have a profound effect on physiological processes linked to obesity and metabolic disorders. The mechanisms underlying the differential effects between these two PUFA are thought to include the ability to generate bioactive lipids, modulate gene expression through nuclear receptors, and increase cellular oxidant injury. To identify potential mechanistic differences between the two PUFA, male C57BL/6J mice were administered a high fat diet (23.5% from fat) containing corn (ω-6 PUFA) or fish oil (ω-3 PUFA) for up to 3 weeks and gene expression profiling was performed on liver. Pathway mapping of significantly altered genes showed that a diet rich in fish oil induced biological processes related to fatty acid oxidation, glutathione metabolism and oxidative stress; in contrast, corn oil significantly repressed these processes while inducing inflammatory response. These data suggested that PUFA can modulate the cellular redox state in liver. Thus, oxidative stress biomarkers in the liver were evaluated. It was determined that a corn oil-containing diet leads to increases in expression of DNA repair genes (AP endonuclease 1 and uracil DNA glycosylase) and the number of 8-OH-dG DNA adducts with concomitant decrease in reduced GSH content. Fish oil leads to reduction in 8-OH-dG DNA adducts while no induction of DNA repair genes was observed. Molecular and biochemical assays demonstrated that fish oil, but not corn oil, trans-activated PPARα. Moreover, comparison of gene expression data with known PPAR pan-agonist, WY-14,643, determined that over 50% of the genes altered by fish oil treatment were driven by PPARα. Included within this gene list were many anti-oxidants such as glutathione-S-transferases, heat shock and proteasome proteins. In summary, dietary fatty acids can modulate the cellular redox state and the direction may be dependent on their ability to trans-activate PPARα.

B. INTRODUCTION

Metabolic syndrome has emerged as a public health issue worldwide as it is considered an important predictor for the development of chronic debilitating diseases such as type-II diabetes mellitus, cardiovascular disease, and certain types of cancer (161). It can be characterized as a group of metabolic abnormalities which include insulin resistance along with abdominal adiposity, dyslipidemia and a systemic pro-inflammatory state (162). Its prevalence coincides with the rapidly growing obesity epidemic (163) which has arisen due to the prevailing sedentary lifestyles and unhealthy dietary habits in industrialized societies. Obesity, considered as a central component in this syndrome, is a chronic metabolic and nutritional disorder with multi-factorial etiology, involving genetic and environmental factors. Increased dietary fat intake is considered to be causal but more substantial evidence now indicates that the type, not the amount, of fat is important in the risk of chronic disease (164). As such, it is imperative to understand the mechanistic differences in biological effects of different types of fats in relation to the development of obesity and related co-morbidities.

As obesity rates rose over the past half century the intake ratio of the essential dietary fatty acids, ω-6 and ω-3 polyunsaturated fatty acids (PUFA), has also changed dramatically to between 10:1 to 20:1 (92, 165). These two types of fatty acids compete directly with one another for enzymes and for incorporation into the cell, where they can influence cell signaling pathways and receptor function. As well, the metabolic derivatives of these two fatty acids have diverse biological functions, typically antagonistic to each other, and can modulate a variety of physiological and pathophysiological processes. PUFA can alter plasma lipid levels, cardiovascular function, insulin action, neuronal development, and the function and regulation of the immune system. PUFA have shown therapeutic efficacy in chronic diseases such as arthritis (166), cardiovascular disease (167), diabetes (168), and carcinogenesis (169).

Obesity and related metabolic disorders have been associated with several important common pathogenic mechanisms of disease including hyperlipidemia, systemic inflammation (170), and oxidative stress (171). Numerous epidemiological studies as well as animal models have shown that ω-3 and ω-6 PUFA affect these pathogenic processes (172). The dietary intake of PUFA and most importantly, the dietary PUFA ratio can directly or indirectly modulate the accumulation of visceral and intracellular lipid content by stimulating adipogenesis, activating transcription factors, and altering intracellular signaling events (173). PUFA are considered important modulators of the immune system as they are used to synthesize eicosanoids, short-lived hormone-like lipids that include prostaglandins and leukotrienes, with potent inflammatory and chemotactic functions. The conjugated double bonds in PUFA are highly susceptible to free radical-mediated lipid peroxidation. Since these reactions are self-propagating, the initial oxidation of only a few lipid molecules can result in significant tissue damage. The by-products of this chain reaction, such as malondialdehyde (MDA) and 4-hydroxynonenal (HNE), can readily diffuse from the site of production and covalently bind to DNA and proteins potentially disrupting or altering vital cellular functions. Moreover, these by-products are potent chemoattractants promoting macrophage infiltration and inflammation (174).

In the present study, it was determined that ω-3 and ω-6 PUFA differentially modulate the cellular redox state in mouse liver which may be dependent on their ability to trans-activate PPARα. As oxidative stress is an important common mechanism in the development of human diseases, it further emphasizes the importance of understanding the role of dietary intervention in the prevention of human disease.

C. MATERIALS AND METHODS

Animals and treatments. Adult (aged 6-8 weeks) male wild-type C57Bl/6J mice were purchased from Jackson Laboratories (Bar Harbor, ME). Mice were fed with a commercial AIN-76A diet [control, 5% fat (Harlan TEKLAD, Madison, WI)] or modified AIN-76A diet (Table 4.1) where 23.5% of fat was provided as either corn oil (Mazola® Corn Oil, Cordova, TN) or fish oil (OmegaPure™ Refined Menhaden Fish Oil, kindly donated by OmegaProtein, Houston, TX) for 1 or 3 weeks. Diets were supplemented by the manufacturer with 1000 ppm mixed-tocopherols and 200 ppm tertiary butyl hydroquinone to prevent oxidation. To assure quality and consistency of oils, diets were prepared fresh daily and all leftovers removed. Fatty acid hydroperoxide values were monitored (175) and determined to be < 3 mEq/kg. All mice were maintained in a temperature- and light-controlled facility, and permitted *ad libitum* consumption of food and water. At the end of the study, liver and body weight measurements were collected. A portion of liver tissue was preserved in formalin for histological sections and the remaining tissue was snapped frozen in liquid nitrogen and stored at –80°C for later analyses. All animals were given humane care in compliance with NIH and institutional guidelines and studies were performed according to protocols approved by the appropriate institutional review board.

Extraction and measurement of fatty acids: Lipids were extracted using the method of Bligh and Dyer (176). The lower (chloroform) phase was transferred to a clean tube and evaporated to dryness under nitrogen. The residual lipids were saponified and the fatty acids trans-methylated by sequential 1 ml addition of 4.25 % NaOH in $CHCl_3$:MeOH (2:1, v/v) and 1N HCl in saline (177). The samples were mixed vigorously then centrifuged at 1500 x g for 5 min. The lower phase containing the fatty acid methyl esters was carefully transferred to a clean, dry tube and evaporated to dryness under nitrogen. Fatty acid methyl esters were then resuspended in 50 µl undecane, and analyzed using capillary gas chromatography (GC). Fatty acid methyl

esters were analyzed by Fast GC on a Perkin Elmer AutoSystem XL Gas Chromatograph (Shelton, CT), split injection, with helium as the carrier gas. The methyl esters were separated on a capillary column coated with 70% cyanopropyl polysilphenylene – siloxane (10 m x 0.1 mm ID- BPX70 0.2 μm; SGE, Austin, TX); injector 240ºC and detector 280ºC. Data were analyzed with the Perkin Elmer Totalchrom Chromatography Software, version 6.2. Heptadecanoic acid (17:0) was added to the samples as an internal standard to correct for recovery and quantitation. Individual fatty acids were identified by comparing their retention to authentic standards (Nu Chek Prep, Elysian, MN).

RNA Isolation: Total RNA was isolated using RNeasy kit (Quiagen, Valencia, CA) and dissolved in RNase-free water. Samples were stored at -80°C until assayed for no more than 2 months to minimize degradation. The quality of preparations was determined using an Agilent Bio-Analyzer (Agilent Technologies, Palo Alto, CA).

Microarrays: Total RNA was isolated from mouse liver and gene expression analysis performed using Agilent 22K mouse arrays (G4121B, Agilent) following standard protocols specified by the manufacturer. A mouse standard RNA [(Icoria, Research Triangle Park, NC); (94)] was used as an internal reference to normalize expression ratios across all arrays. Images were obtained from an Agilent microarray scanner, features extracted by Agilent image analysis software, and the data was deposited into the UNC microarray database (https://genome.unc.edu). Data was then batch extracted, Lowess normalized (178) and subjected to cluster analysis (138). Genes were omitted from further analysis if they were either absent or flagged for poor feature quality in at least two of the three biological replicates in each experimental group. About 17,400 genes were selected for further analyses based on these quality metrics. Missing data were imputed using the SAM add-in for Excel (Microsoft Corp., Redmond, WA) plug-in with 100 permutations and *k*-nearest neighbors (KNN) with $k = 5$.

Unpaired SAM analysis of control liver samples at 1 and 3 weeks demonstrated no significant difference in expression as the lowest false discovery rate obtained was 60% (82 genes). As such, all subsequent statistical analyses were performed with 1 and 3 week control samples grouped as a single entity. Significant gene lists were subjected to average-linkage hierarchical clustering analysis using Pearson correlation and the data visualized in Java Treeview (138).

RNase Protection Assays: Expression of base excision DNA repair genes was analyzed with an RNase protection assay using mouse multi-probe template set (mBER, BD PharMingen, San Diego, CA) essentially as described in (84). Riboprobes were synthesized in the presence of [^{32}P]dUTP to yield labeled antisense RNA probes. The RNase protection assays were performed on 30 µg total RNA samples using a RiboQuant^{TM} multi-probe RNase protection assay kit (BD PharMingen). Protected fragments were separated on 5% polyacrylamide nucleic acid separation gels, dried and exposed to x-ray film. The intensity of protected bands was quantified using Kodak 1D Image Analysis Software (New Haven, CT) and normalized to the intensity of housekeeping gene L32.

Determination of Liver Tissue Glutathione Levels: Frozen liver tissue (~ 50mg) was homogenized in 5% sulfosalicyclic acid, centrifuged at 8k x g for 10 min, and the supernatant assayed for total or reduced glutathione content following specified protocol supplied by the manufacture (BioVision, Mountain View, CA).

Immunohistochemistry: Formalin-fixed, paraffin-embedded liver sections (6 µm) were mounted on glass slides. Sections were deparaffinized in xylene, rehydrated in a series of graded alcohol concentrations, and placed in PBS with 1% Tween 20. Immunostaining was performed using DAKO EnVision System HRP (Dako Cytomation, Carpinteria, CA) with primary antibody [1:100 PCNA (Dako Cytomation; 1:200 8-

hydroxyguanosine (Research Diagnostics; Flanders, NJ)] diluted in PBS containing 1% bovine serum albumin and incubated overnight at 4°C. Slides were counterstained with hematoxylin. In order to ensure the quantitative measurement of each immunoreaction, all sections from each animal and group to be compared were processed in parallel. Antibody specificity was determined by incubating each antibody with its respective antigen before immunostaining. Quantitative analysis of immunostained liver sections was performed using BIOQUANT software (BIOQUANT Image Analysis, Nashville, TN) by averaging percent positively stained nuclei to total nuclei within 10 random fields at 200×.

DNA Isolation: DNA was extracted by a procedure slightly modified from the method reported previously (95). To minimize formation of oxidative artifacts during isolation, 2,2,6,6-tetramethylpiperidinoxyl (TEMPO, 20 mM final concentration) was added to all solutions and all procedures were performed on ice. Briefly, frozen tissues were thawed and homogenized in PBS. After centrifugation at 2,000 x g for 10 min, the nuclear pellets were incubated in lysis buffer (Applied Biosystems, Foster City, CA) overnight at 4°C with proteinase K (500 mg/ml; Applied Biosystems). DNA was extracted twice with a mixture of phenol/chloroform/water followed by ethanol precipitation. The extracted DNA was incubated in PBS (pH 7.4) with RNase A followed by DNA precipitation with cold ethanol. Then, the DNA pellet was resuspended in sterilized double distilled water. The DNA solution was stored at -80°C until assayed.

Detection and Quantification of 8-OH-dG by Capillary LC-MS/MS: The measurement of 8-OH-dG by LC-MS/MS was performed essentially as described in (179). Briefly, DNA (50 μg) was digested into individual nucleosides and 8-OH-dG purified by reverse phase HPLC using Beckman Ultrasphere ODS C18 column (5 um, 4.6 x 250 mm, Beckman, Fullerton, CA). Quantitative analysis of 8-OH-dG was

performed with an 1100 capillary high-performance liquid chromatograph (Agilent, Wilmington, DE) coupled to a TSQ-Quantum triple quad mass analyzer (ThermoFinnigan, San Jose, CA). Both analyte and internal standard were detected by single reaction monitoring of the transition of nucleoside to base adduct *m/z* 284.2 to 168.2 and *m/z* 289.2 to 173.2, respectively.

Electrophoretic mobility shift assay (EMSA) for PPARα: Nuclear protein extracts were prepared using the method described by Dignam et al., (180) and EMSA was performed using a DNA-protein binding detection kit [Panomics Electromobility Gel-Shift Kits (Redwood City, CA)] according to manufacture's protocol. Briefly, the 10 µl reaction mixture contained 1X binding buffer, 10 µg nuclear extract, and 1 µg Poly d(I-C) and was pre-incubated for 5 min on ice prior to adding 10 ng PPARα biotin-labeled probe (5'-AAAAACTGGGCCAAAGGTCT-3'). Specificity of the binding was determined by competition experiments, which were carried out by adding a 20-fold molar excess of unlabelled PPARα to the reaction mixture before labeled probe was added. Samples were electrophoresed through 6% non-denaturing TBE polyacrylamide gel and transferred to nylon membrane. The membrane was incubated with streptavidin-HRP conjugate at 1:1000 for 15 min. Protein-DNA complexes were visualized by exposing to x-ray film.

Acyl-CoA oxidase activity: Activity of the peroxisomal enzyme acyl-CoA oxidase was measured as described in (181). The activity was measured from the amount of formaldehyde formed by the peroxidation of methanol by hydrogen peroxide, a product of peroxisomal β-oxidation. Protein concentration was determined using a BCA assay (Pierce Biotechnology Inc, Rockford, IL).

D. RESULTS

Dietary fatty acid treatment effects on liver morphology and biochemistry. Male C57Bl/6J mice, in groups of 5, were given either a control low fat diet (5%) or high fat diets (23.5%) of either corn oil (ω-6 PUFA) or fish oil (ω-3 PUFA) for 1 or 3 weeks. Diets were prepared fresh daily to prevent rancidity and in vitro fatty acid peroxidation of diets after 24 hours of preparation were < 3 mEq/kg. Food intake and body weights of the mice were not affected by the type of dietary lipid (data not shown). Liver to body weight ratio (Table 4.2) significantly increased in mice administered high-fat diets of corn oil or fish oil. This was most pronounced with a high-fat diet of fish oil with a 1.5-fold increase over control was observed at both 1 and 3 weeks. To determine the role of proliferation and cellular hypertrophy on the observed increased liver weight, the % PCNA positively stained nuclei and number of nuclei per field, respectively, was measured. Proliferation as compared to control low-fat diet was unaffected by dietary treatments. The significant decrease in nuclei per field following fish oil treatment compared to controls at both 1 and 3 weeks would infer that the observed gain in liver weight was attributable to an increase in parenchymal cell size.

To determine the changes in fatty acid composition following dietary treatment, total liver lipids were analyzed by gas chromatography, Table 4.3. Temporal differences were not observed between 1 and 3 weeks for the various dietary treatments and for clarity, the data dicussed here reflects the values from the 3 week time point. It was surprising to observe only modest changes in fatty acid conent between a control low-fat and high-fat diet of corn oil even though the diet composition was formulated with a 4.7-fold increase in % fat. The ω-6:ω-3 PUFA ratios were 4.7 and 7.0 for control and corn oil, respectively, attributable to the 82.5% increase in hepatic linoleic acid (18:2n-6) content from corn oil diet. In contrast, a high-fat diet of fish oil significantly altered the fatty acid composition in the liver compared to control. The ω-6:ω-3 PUFA ratio was

dramatically reduced from 7.0 to 0.94. As expected hepatic linoleic acid (18:2n-6) content was diminished to almost half along with significant increases in the long-chained PUFA docosahexaenoic acid (186%) and the monounsaturated fatty acid 13-docosenoic acid (1,535%).

Temporal and treatment-dependent changes in gene expression. Gene expression profiling was performed on liver tissue collected at 1 or 3 weeks following dietary treatments. A multi-class Significant Analysis of Microarrays [SAM; (140)] test was performed to identify genes whose expression levels were significantly differentially changed within at least one treatment group (i.e., control, corn oil, or fish oil) and within a single time point (i.e., 1 week or 3 weeks). The list of significantly altered genes with a false discovery rate (FDR) of less than 5% and 1.5 fold change consists of 4,537 genes. Clustering analysis was performed on this gene set, Figure 4.1A. The dendrogram shows that the samples segregated based on dietary treatment with one exception and within those clusters further separation was based on duration of treatment. To identify temporal changes in gene expression, SAM analysis was performed on 1 and 3 week liver samples from control, corn oil, or fish oil treated mice. The analysis revealed that the expression phenotypes for livers from mice administered a control-low fat diet or a high-fat diet of fish oil at 1 and 3 weeks were not significantly different. The lowest obtainable FDR was 60% (82 genes) and 7% (14 genes) for control and fish oil, respectively. A total of 824 genes were differentially expressed for corn oil between 1 and 3 weeks. The majority of these genes, 768, were induced at 3 weeks of corn oil treatment. GoMiner (9) analysis was performed on the entire gene list to identify significantly enriched Gene Ontology (GO) biological processes ($P < 0.05$; minimum of 3 gene transcripts per category). From this, it was observed that intracellular movement via endocytosis and exocytosis were up-regulated along with one-carbon metabolism (Figure 4.1B).

To identify treatment-dependent changes in gene expression in livers from mice given high-fat diets of corn oil or fish oil at 1 and 3 weeks, SAM analysis was performed. Comparison of expression data at 1 week showed that 1,339 genes were differentially expressed between the two treatment groups (Figure 4.1C). Within this gene set, GO analysis revealed that fish oil induced biological categories related to fatty acid oxidation, apoptosis, epigenetic gene regulation, and glutathione and xenobiotic metabolism. In contrast, corn oil induced categories related to responses to stress, wounding, and unfolded proteins as well as innate immune response. Comparison of expression data at 3 weeks showed that 436 genes, a 3-fold reduction compared to 1 week, were differentially expressed between the two treatment groups. The biologically processes described at 1 week are similar at 3 weeks with the exception of epigenetic gene regulation, apoptosis, and glutathione metabolism which no longer appear on the list.

Gene expression analysis reveals discordant effect on anti-oxidant defense genes by ω-3 and ω-6 PUFA. Analysis of the biological pathways evoked by corn oil and fish oil within the liver revealed dissimilar responses to oxidative stress, and glutathione and xenobiotic metabolism. To further examine the treatment responses on oxidative stress-related pathways, GO was used to identify genes within the microarray that have an association with oxidative stress. A total of 163 genes were identified of which 81 were found to be significantly differentially expressed among the different treatment groups. Supervised hierarchical clustering of this gene set was performed and two major gene clusters were identified that were specific to fish oil or corn oil and are shown in Figures 4.2A-B. Several enzymatic and non-enzymatic antioxidant defenses were induced by a diet rich in fish oil. These genes fall into several categories including phase II detoxification enzymes (i.e. glutathione S-transferases), anti-oxidants (i.e., catalase, GSH peroxidase, and GSH reductase), molecular chaperones/proteasome systems (i.e. heat shock proteins and proteosomal protein sub-units). Furthermore, DNA

repair enzymes (i.e., Tdg, Ung, and Ape) and anti-inflammatory response proteins (i.e., heme oxygenase) were induced in the liver in mice given a high-fat diet of corn oil. Also, several genes related to metal metabolism, metallothioneins, thioredoxins, and heme oxygenase, were induced as well.

High-fat diets rich in ω-6 PUFA cause pro-oxidant state in mouse liver. Analysis of the oxidative stress-related gene set revealed that corn oil and fish oil based diets lead to discordant responses in antioxidant defense systems within the liver suggesting alterations in the cellular redox state. Total and reduced GSH content were measured in liver tissue from mice fed a control low-fat diet or diets rich in corn oil or fish oil (Table 4.4). Total GSH levels across all dietary treatments and time points were not significantly different and ranged between 6.8 and 7.4 μmoles GSH equivalents/g tissue. Reduced GSH content in the liver; however, was found to be significantly reduced by corn oil by 3- and 2-fold at 1 and 3 weeks, respectively, compared to corresponding time-matched controls.

As shown in Figure 4.2B, a high-fat diet of corn oil induced several DNA repair genes in liver of which several belong to the base excision repair (BER) pathway. BER is the predominant mechanism used for the removal of oxidized bases from DNA. A diet rich in corn oil but not fish oil significantly induced the expression of two BER genes, uracil DNA glycosylase (UNG) and AP endonuclease 1 (APE), as compared to corresponding time-matched controls at both 1 and 3 weeks, Table 4.5. These two genes were also observed to be significantly induced by corn oil in microarray analysis. Expression of O^6-methylguanine DNA methyltransferase (Mgmt), an enzyme involved in the direct repair of alkylated guanine residues and not involved in repair of oxidative DNA lesions, was found to be induced by fish oil at 3 weeks. This would be consistent with previous report (182) whereby induction of antioxidant gene expression modulated

Mgmt activity levels at least, in part, by augmented mRNA levels.

Next, a widely-used marker of oxidative DNA damage is 8-hydroxy-deoxyguanosine (8-OH-dG) which was measured using immunohistochemical detection (Figure 4.3A-B). Microscopic examination of liver sections from all dietary treatments showed sporadic distribution of positively stained nuclei with no lobular localization. Quantitative analysis of 8-OH-dG DNA adducts in livers of mice administered a control low-fat diet had 50-60% positively stained nuclei. These levels were significantly increased by a high-fat corn oil diet to almost 80% by 3 weeks. Most surprisingly, a diet rich in fish oil significantly reduced the percentage of positively stained nuclei compared to controls by almost 2-fold. As immunohistochemical detection is considered semi-quantitative and susceptible to non-specific reactions, 8-OH-dG adducts were also measured using capillary LC-MS/MS. The number of 8-OH-dG in livers from control mice were ~ 1 adduct per 10^6 dG (Figure 4.3B), in agreement with consensus reports from European Standards Committee on Oxidative DNA Damage (100). Analysis of liver tissues from mice following a high-fat diet of corn oil found a significant increase in these DNA adducts, approximately 2-fold over controls. There was no significant difference in adducts in livers from mice given control or fish oil based diets.

Activation of PPARα plays a role in the differential effects of ω-3 or ω-6 PUFA. Analysis of microarray data suggested that fish oil, but not corn oil, activated peroxisome proliferator-activated receptor alpha (PPARα) as GO processes related to fatty acid oxidation and peroxisome organization and biogenesis were significantly enriched by fish oil. It has been shown that fatty acids and their eicosanoid derivatives can regulate gene transcription through PPARs (183). To determine the degree of involvement of PPARα in regulating gene expression by high fat diets of ω-3 or ω-6 PUFA, expression data from livers of mice treated with a potent PPARα pan-agonist,

WY-14,643 (WY; 50 mg/kg) for 1 or 4 weeks (Woods et al., unpublished data), was compared to the expression data generated in this study. SAM analysis of control and WY treated samples identified 1,275 gene transcripts to be differentially expressed. Since the study described herein and the WY study were performed using the same microarray platform, probe set ids were used to intersect the two significant gene lists to generate a single non-redundant shared gene list. A total of 845 genes were identified. Unsupervised hierarchical clustering was conducted on this gene set and is shown in Figure 4.4A. The dendrogram shows that the expression phenotypes from livers of mice given fish oil or WY are similar. To cross-compare the gene alterations between fish oil and WY, a venn diagram (Figure 4.4B) was constructed from the significant gene lists generated using SAM analysis (FDR <5%, 1.5 fold-change). Of the 719 genes that were differentially expressed by fish oil, 68% of those were shared with WY. GO analysis of the PPARα-regulated gene set shared between fish oil and WY showed induction of biological processes related to fatty acid metabolism, cofactor metabolism, and oxygen and reactive oxygen species (ROS) metabolism while responses to stress and immune response were repressed. Fish oil, however, did not induce processes related to cell proliferation or apoptosis in the liver as was demonstrated with WY treatment.

There are conflicting reports on the potency of ω-3 and ω-6 PUFA to transactivate PPARα (184-186). Thus, the effects of high-fat diets rich in ω-3 and ω-6 PUFA on DNA binding activity of PPARα in liver of mice are shown in Figure 4.5A. Gel shift assays demonstrated that fish oil considerably increased PPARα binding activity compared to control and corn oil diet treated mice. Competition assay using excess unlabeled DNA oligo blunted PPARα binding activity confirming the translocation and activation of PPARα following fish oil treatment in mice. These data correlated with the 5-fold increase in activity of the classical PPARα–regulated gene acyl-CoA oxidase,

Figure 4.5B. There was no significant difference in DNA binding activity or acyl-CoA activity with a high-fat diet of corn oil.

E. DISCUSSION

Nutrient-gene interactions have become a key issue in the modulation and prevention of human disease. It has been suggested that a temporal shift in ω-6:ω-3 PUFA intake ratios over the past half century have contributed to the growing obesity epidemic; however, the mechanisms by which different dietary fatty acids affect the molecular processes of human disease have not been fully elucidated. In the present study, molecular profiling was performed on liver tissue of mice treated with either high-fat diets of corn oil or fish oil to identify the molecular processes modulated by PUFA treatment. It was determined that three key GO categories affected included fatty acid oxidation, cofactor metabolism, and immune response. As obesity has been linked to pathogenic mechanisms including hyperlipidemia, oxidative stress, and systemic inflammation these data would suggest that dietary fatty acids can influence key cellular and molecular events that underlie this disease.

Oxidative stress is a common mechanism of liver disease and it can evolve from fatty acid oxidation and inflammation while the level of oxidants is modulated by the antioxidant capacity and cofactor supply of the cell. Analysis of expression data for oxidative stress-related genes revealed that fish oil, to a significantly greater extent than corn oil, induced a number of antioxidant and stress-inducible genes capable of inactivating ROS and protecting or removing oxidized macromolecules in the cell. Included were various isoforms of GSH S-transferases and thiol reductases, enzymes required for recycling GSH and reducing oxidized proteins and lipid hydroperoxides. Also, secondary defenses to restore cellular homeostasis by stabilizing or excising

damaged proteins (i.e., heat shock chaperone proteins and proteasomal pathways) were increased. In contrast, corn oil resulted in the induction of 6 DNA repair genes, all members of the BER pathway, the predominant pathway to excise and repair oxidative DNA lesions. As many of these cellular defense systems are known to be induced under conditions of physiological or chemical stress including oxidative stress, it would suggest that both types of dietary fatty acids result in an increase in oxidants. However, these data would imply that only fish oil evokes changes in gene expression profiles to defend against excess ROS production and potentially detrimental shifts in cellular redox state.

The induction of phase II detoxification and antioxidant enzymes is a major protective mechanism against increased production of ROS. The transcriptional activation of these stress response genes has been linked to the *cis*-acting transcriptional enhancer called the ARE which, in turn, is positively regulated by the transcription factor Nrf2. The mouse strain used in these studies, C57Bl/6J, has been shown to carry a single nucleotide polymorphism within the Nrf2 promoter that results in reduced constitutive and induced expression compared to C3H/HeJ (187). Examination of nuclear Nrf2 protein levels and protein-DNA binding activity in livers from mice given high-fat diets of corn oil or fish oil were either undetectable or unchanged among treatment groups (data not shown), which is consistent with previous report with 7-day WY treatment (188). This would suggest an alternative mechanism involved in the regulation of antioxidant defense system in this mouse model. A potential candidate is PPARα, as it is preferentially activated by ω-3 PUFA and has been shown to regulate genes in common with the stress-inducible transcription factors, Nrf2 and HSF (188). Moreover, studies using PPARα-null mice have shown decreased resistance to oxidant-induced liver injury (188, 189) suggesting that the hepatoprotective effects of PPARα may be under transcriptional regulation.

The PPARα regulatory network largely encompasses lipid metabolism and glucose homeostasis pathways, Figure 4.6. Microarray and biochemical analysis showed that high-fat diets of fish oil but not corn oil lead to increased fatty acid oxidation through trans-activation of PPARα. This process results in the proliferation of peroxisomes and the coordinate induction of hepatic genes involved in the β-oxidation of fatty acids in peroxisomes, mitochondria, and other cellular components. The main gene targets of PPARα include acyl-coA oxidase (Aco), carnitine palmitoyltransferase 1 (Cpt1), which are in involved in β-oxidation and Cyp4a1, which is involved in ω-oxidation of fatty acids. It has been shown using peroxisome proliferators such as WY that fatty acid oxidation results in disproportionate increase in oxidant production through several H_2O_2 generating enzymes (i.e., Acox1 and Cpt1a) and H_2O_2 degrading enzymes (Cat) with disruption of GSH peroxidase leading to increased oxidative stress. To defend against PPARα activation and ROS production several defense mechanisms appear to concomitantly up-regulated. These include increases in glutathione-S-transferases, ROS metabolizing enzymes (Cat, Gpx), heat shock proteins (Hspca, Hspb2) including proteasome maintenance proteins, and uncoupling proteins (UCP1, UCP2, UCP3). The hepatoprotective effects against oxidant-induced liver injury by PPARα may be mediated by augmenting anti-oxidant expression levels. Furthermore, as WY and fish oil induce this same gene set, it would suggest that PPARα is the driving force behind the transcriptional changes responsible for up-regulation of cellular anti-oxidant defense mechanisms in mouse liver. There may be some concern with dietary intervention with fish oil as the positive effects appear to be mediated through PPARα, the same pathway used by peroxisome proliferators (PP) to induce liver growth and carcinogenesis in rodents (190). However, fish oil did not promote proliferation or oxidative stress in the liver which has been presented with more typical PP.

In addition to regulating lipid homeostasis, PPARα has been shown to possess anti-inflammatory properties. It is important in controlling the duration of inflammation induced by arachidonic acid, an eicosanoid derivative of ω-6 PUFA, as PPARα knock-out mice displayed a prolonged response to inflammatory stimuli (191). Studies have shown that administration of PPARα ligands, including WY, augment IL-4 expression (192) along with blunting c-Jun activation (193) which abrogates the expression of pro-inflammatory cytokines such as IL-6, TNFα, IFN-γ and NO synthase. Moreover, they diminish NF-kB levels (194) and DNA binding activity by increasing the expression of IκBα (195). The PPARα regulatory network (Figures 4.6A-C) clearly demonstrates that PPARα ligands, such as fish oil and WY, repress the expression of pro-inflammatory cytokines. These data would support GO analysis of PUFA expression data and would suggest that corn oil treatment results in a pro-inflammatory state. Inflammation activates a variety of immune cells, which induce a number of oxidant-generating enzymes such as NADPH oxidase, inducible nitric oxide synthase, and myleoperoxidase. These enzymes are capable of producing high concentrations of ROS which include superoxide anion, hydrogen peroxide, nitric oxide, and peroxynitrite. Thus, the increase in inflammatory mediators may be a considerable source of ROS accounting for the pro-oxidant state established in the liver following corn oil treatment.

The production of ROS in excess of the antioxicant capacity of the cell can shift the cellular redox state. It is known that decreases in GSH content, a useful indicator of oxidative stress, can result in tissue damage as cellular macromolecules would be vulnerable to free radical attack. Moreover, changes in the redox state of intracellular thiols, especially GSH, influence the actions of redox sensitive transcription factors contributing to alterations in gene transcription. Indeed, depletion of reduced GSH by corn oil treatment at both 1 and 3 weeks generated a protracted pro-oxidant state in the

liver. This condition most likely contributed to the elevated levels of 8-OH-dG DNA adducts. Surprisingly, this was not accompanied by an increase in 8-oxoguanine DNA glycosylase 1 (Ogg1) expression, an enzyme responsible for excising oxidized guanines from DNA. It has been demonstrated that shifts in the cellular redox state can reduce transcriptional activity of Ogg1 by decreased binding of Sp1 transcription factor to its promoter (196) in addition to abolishing Ogg1 protein activity (197). This enzyme is particularly sensitive to thiol modifying agents as 8 cysteine residues reside within the active site. The shift in the cellular redox state by corn oil treatment would account for the inability to induce Ogg1 expression and the resultant accumulation of 8-OH-dG adducts. A most intriguing observation was the reduction in 8-OH-dG adducts following fish oil treatment in comparison to a low-fat control diet. It can be speculated that this is the result of a steady-state in anti-oxidant capacity as reduced GSH content was unaffected. This, in part, was contributed to by the increase in expression of genes responsible for regulating GSH levels such as glutamate-cysteine ligase, the rate-limiting enzyme in GSH synthesis, and GSH reductase which recycles GSH from its oxidized form.

The accumulation of oxidative DNA lesions, if unrestrained, can contribute to disease development. As such, the cell has developed an elaborate system known as DNA repair to reduce the yield of mutations and chromosomal aberrations. This includes BER which functions as a tightly coordinated sequence of events where oxidative DNA damage is removed and repaired. It has been shown to be DNA-damage inducible (198) and a sensitive biomarker of oxidative DNA damage (151, 199). During the process of BER, a glycosylase such as Ogg1 or Ung excises an incorrect base from DNA creating a transient abasic site. Ape1 cleaves the DNA backbone leaving behind a single strand break to allow incorporation of the correct nucleotide. Pol β, the rate-limiting step in BER (200), replaces the nucleotide and DNA ligase seals the gap. In this study, the

expression levels of Ung, which is responsible for excising misincorporated uracil from DNA, were increased in the livers of mice given a high-fat diet of corn oil. It has been demonstrated that folate deficient diets result in increased rates of uracil misincorporation into DNA and DNA hypomethylation (201) by disrupting one-carbon compound metabolism. Dysregulation of this metabolic pathway can negatively affect DNA metabolism and integrity as it serves two critical cellular functions, de novo synthesis of deoxynucleotides and SAM-dependent DNA methylation. Two genes within this pathway required for thymidine synthesis, 5,6-dihydrofolate reductase (Dhfr) and thymidylate synthetase (Tyms) were transcriptionally repressed in the liver of mice administered high-fat diet of corn oil. It is unknown at this time as to how corn oil treatment disrupts one-carbon metabolism but it could be speculated that changes in cofactor supply and/or sensitivity to cellular redox state may play a role.

It could be inferred from the DNA repair expression data that corn oil alters the balance and coordination of BER by stimulating the initiation of BER (Ung and Ape1) without subsequent stimulation of the rate limiting step (Pol β). The inability to detect AP sites in the liver (data not shown) of these mice demonstrates that Ape1 activity was adequate to process the abasic site and, in the process, generate a single strand break. Thus, a state of altered BER would generate an environment conducive to the accumulation of genotoxic and clastogenic lesions. As Pol β expression and activity are dependent on cellular deoxynucleotide triphosphate levels, the resultant imbalance in BER may be due to a dysregulation in thymidine synthesis. An imbalance in DNA repair has serious implications as it is associated with increased genomic instability, a hallmark of carcinogenesis. These data provide evidence for gene-nutrient interactions that could potentially be harmful by increasing rate of DNA mutations.

Recent epidemiological studies on obesity have shown that body mass index (202, 203) and fat accumulation (171) closely correlate with markers of systemic oxidative stress. Moreover, increased oxidative stress in accumulated fat is, in part, responsible for the dysregulation of adipocytokines which participate in the pathogenesis of obesity-associated metabolic syndrome (171). Herein this study, we propose that increased oxidative stress and DNA damage in liver of mice treated with high-fat diet of ω-6 PUFA may serve as an early instigator in molecular and cellular processes leading to obesity and obesity-related co-morbidities. These effects may be ameliorated through increased dietary intake of ω-3 PUFA as they have an adaptive reaction against increased oxidative stress by inducing antioxidant genes.

Table 4.1

Diet formulations

Diet Ingredient	Low Fat Diet 5% Corn Oil g/kg	High Fat Diet 23.5% Corn or Fish Oil g/kg
Casein	200	250
DL-methionine	3	3.75
Corn Starch	520	312
Dextrose, monohydrate	130	78
Cellulose	50	62.5
Corn Oil	50	30
Various Fat Source	0	205
Mineral Mix	35	43.75
Vitamin Mix	10	12.5
Choline Bitartrate	2	2.5
Total	**1000**	**1000**

Table 4.2

Effect of high-fat ω-3 and ω-6 PUFA diets on hepatic morphology

	Control		Corn Oil		Fish Oil	
	1 wk	3 wk	1 wk	3 wk	1 wk	3 wk
% Liver to Body Wt	4.0 ± 0.31	4.0 ± 0.21	4.2 ± 0.36	4.7 ± 0.22[b]	5.9 ± 0.65[b]	5.9 ± 0.63[b]
nuclei per field (cellular hypertrophy)	274 ± 28	285 ± 17	308 ± 19	241 ± 28	210 ± 28[a]	242 ± 18[a]
% PCNA nuclei	1.2 ± 0.20	1.3 ± 0.33	1.4 ± 0.26	1.3 ± 0.22	1.4 ± 0.40	1.3 ± 0.27

C57Bl/6 male mice were given AIN-76A diet (5% fat; control diet) or diets supplemented with either corn or fish oil (23.5% fat) for 1 to 3 weeks. Body and liver weights were determined at end of 1 or 3 weeks. Hemotoxylin-eosin stained liver sections were used to assess hepatocyte hypertrophy by counting the number of nuclei per random field at 200×. Proliferation was measured as an index of percent PCNA positively stained nuclei to total nuclei. Data are represented as means ± standard deviation from 5 animals per group. Statistical difference ($^{a}P < 0.05$; $^{b}P < 0.01$) compared to corresponding control group using one-way ANOVA.

Table 4.3

Fatty acid composition of liver total lipids following treatment with high fat diets of either corn oil or fish oil

	1 week			3 weeks		
Fatty Acid	**Control**	**Corn Oil**	**Fish Oil**	**Control**	**Corn Oil**	**Fish Oil**
14:0	321 ± 69	179 ± 37	415 ± 149	426 ± 132	195 ± 78	341 ± 58
14:1	20 ± 9	ND	19 ± 10	28 ± 10	ND	19 ± 3[a]
16:0	14802 ± 1348	13807 ± 1327	13580 ± 1199	17359 ± 3517	13860 ± 2942	13265 ± 739
16:1 n-7	1549 ± 649	577 ± 101	592 ± 398	1450 ± 780	371 ± 167	1195 ± 189
18:0	6317 ± 460	7695 ± 129[a]	5468 ± 483[d]	7175 ± 1030	8154 ± 445	5227 ± 343[a,e]
18:1 n-9	8690 ± 2085	7355 ± 400	5145 ± 914[a]	13275 ± 6105	7603 ± 2375	4621 ± 330
18:2 n-6	10752 ± 815	20693 ± 670[c]	6839 ± 558[c,d]	10760 ± 1390	19639 ± 3908[a]	6401 ± 549[a,e]
18:3 n-3	200 ± 16	199 ± 22	146 ± 95	226 ± 37	259 ± 54	124 ± 51[d]
20:0	184 ± 26	261 ± 35	241 ± 54	193 ± 14	172 ± 72	223 ± 24
20:1n-9	265 ± 35	245 ± 17	136 ± 48[a,d]	316 ± 54	276 ± 58	88 ± 22[b,e]
20:2n-6	232 ± 13	295 ± 35[a]	82 ± 10[c,f]	305 ± 118	369 ± 49	89 ± 20[a,e]
20:3cis n-6	774 ± 90	530 ± 60[a]	381 ± 89[b]	964 ± 267	832 ± 243	330 ± 61[a]
20:3transn-6	ND	28 ± 48	ND	120 ± 29	50 ± 86	36 ± 62
20:4n-6	4486 ± 610	8788 ± 572	3218 ± 127[c,f]	6026 ± 2059	9883 ± 1090	2279 ± 190[b,e]
20:5n-3	102 ± 10	106 ± 5	25 ± 39[a,d]	82 ± 41	57 ± 19	ND
22:0	76 ± 66	61 ± 6	358 ± 113[b,e]	116 ± 10	78 ± 4	391 ± 98[b,e]
22:1n-9	128 ± 86	115 ± 4	2194 ± 761[b,e]	158 ± 36	127 ± 11	2584 ± 358[c,f]
22:5	53 ± 15	17 ± 1	32 ± 8	52 ± 17	23 ± 5	42 ± 31
22:6n-3	3284 ± 917	4138 ± 151	10404 ± 1611[b,e]	3551 ± 1147	4032 ± 178	10186 ± 84
24:0	852 ± 1178	133 ± 10[a]	633 ± 89	860 ± 1172	144 ± 20	661 ± 75
24:1n-9	ND	ND	56 ± 26[a]	20 ± 35	31 ± 6	ND
Total n-6	16244 ± 5731	30171 ± 8414	11071 ± 2879[a]	18175 ± 6307	30547 ± 8623	8681 ± 3245[a,d]
Total n-3	3585 ± 1593	4442 ± 2019	10575 ± 5957	3858 ± 1962	4348 ± 2239	10310 ± 5845
n-6/n-3 ratio	4.5	6.7	1.0	4.7	7.0	0.94

Values represent means ± standard deviation (nmoles fatty acid/g liver), n =3. Saturated fatty acids (14:0, 16:0, 18:0, 20:0, 22:0); monounsaturated fatty acids (14:1n-7, 16:1n-7, 18:1n-9, 20:1n-9, 22:1n-9, 24:1n-9); polyunsaturated fatty acids [PUFA (18:2n-6, 18:3n-3, 20:2n-6, 20:3n-6, 20:4n-6, 20:5n-3, 22:6n-3)]; n-6 long-chain PUFA (20:4n-6); n-3 long-chain PUFA (20:5n-3, 22:6n-3). The significance of the differences between mean values was assessed by one-way ANOVA and Tukey's post-hoc test: $^{a}p< 0.05$, $^{b}p < 0.01$, $^{c}p < 0.001$ vs controls or $^{d}p < 0.05$, $^{e}p < 0.01$, $^{f}p < 0.001$ vs corn oil treatment. ND = not detected.

Table 4.4

Effects of high-fat ω-3 and ω-6 PUFA diets on liver glutathione content

	Glutathione Eqv (μmoles/g tissue)	Control	Corn Oil	Fish Oil
1 week	Total	7.3 ± 0.94	7.4 ± 0.74	6.2 ± 0.93
	Reduced	5.2 ± 0.53	1.6 ± 0.86*	5.8 ± 1.14
3 weeks	Total	6.8 ± 1.20	7.0 ± 0.98	6.8 ± 1.23
	Reduced	6.4 ± 1.45	2.9 ± 0.75*	5.4 ± 1.09

Total and reduced glutathione content (μmoles/g tissue) was measured in mouse liver tissue following treatment with high fat diets of corn oil (ω-6) or fish oil (ω-3) for 1 or 3 weeks. Results are expressed as means ± standard deviation from 5 animals per group. *Statistical difference ($P < 0.05$) compared to corresponding control group using one-way ANOVA followed by Tukey's multiple-comparison post-hoc test.

Table 4.5

Expression of base excision DNA repair genes are induced by high-fat diets rich in ω-6 PUFA

	1 week			*3 weeks*		
DNA Repair Genes	***Control***	***Corn Oil***	***Fish Oil***	***Control***	***Corn Oil***	***Fish Oil***
OGG1, 8-oxoguanine DNA glycosylase 1	6.7 ± 0.2	6.5 ± 0.5	4.7 ± 2.1	4.8 ± 1.8	5.0 ± 1.1	7.1 ± 0.51
MPG, N-methylpurine DNA glycosylase	4.9 ± 1.6	2.9 ± 0.6	4.1 ± 1.0	4.1 ± 1.2	3.7 ± 1.1	5.0 ± 0.7
TDG, thymine DNA glycosylase	9.7 ± 1.0	11.6 ± 1.2	6.1 ± 2.0	7.8 ± 1.6	8.6 ± 1.6	7.4 ± 5.6
UNG, uracil DNA glycosylase	3.3 ± 0.6	13.0 ± 1.4[b]	2.5 ± 0.9	2.8 ± 0.7	6.8 ± 1.2[b]	2.5 ± 1.2
APE, apurinic/apyrimidinic endonuclease 1	10.0 ± 3.2	20.1 ± 1.5[b]	6.8 ± 1.8	10.5 ± 3.6	18.7 ± 4.4[a]	10.9 ± 4.6
Nthl1, E. coli endonuclease III-like 1	4.1 ± 0.5	3.4 ± 0.8	3.6 ± 0.7	3.3 ± 0.4	2.6 ± 1.0	3.5 ± 0.2
Pol β, polymerase (DNA directed) β	16.4 ± 3.1	19.7 ± 1.9	18.9 ± 0.5	16.7 ± 5.7	16.9 ± 2.7	14.2 ± 1.3
PCNA, proliferating cell nuclear antigen	19.6 ± 4.2	14.8 ± 1.8	18.5 ± 5.7	16.1 ± 2.7	16.8 ± 2.1	15.3 ± 0.41
MGMT, O^6-methylguanine DNA methyltransferase	14.2 ± 1.3	8.0 ± 3.7	16.8 ± 4.0	10.4 ± 2.0	9.1 ± 1.7	19.1 ± 3.4[a]

RNase protection assay was performed on total RNA isolated from liver samples The results are mean ± standard deviation from 3 animals per group. The relative expression of each gene was normalized to the expression of the housekeeping gene L32. *Statistical difference ([a]P < 0.05; [b]P < 0.001) from corresponding control group using one-way ANOVA followed by Tukey's multiple comparison post-hoc test.

Figure 4.1

Temporal and treatment-dependent changes in gene expression in mouse liver following treatment with high-fat diets of ω-3 and ω-6 PUFA

(A) Unsupervised hierarchical clustering of significantly differentially expressed genes in liver from mice fed a control low-fat diet (5% corn oil) or high fat diets of either corn oil (ω-6) or fish oil (ω-3) for 1 or 3 weeks. Significant Analysis of Microarrays (SAM) (140) was performed to identify genes whose expression levels were significantly different (FDR < 5% with 1.5 fold change) among any treatment group compared to corresponding control. The color of each gene is proportional to the mean expression level (in $\log_2$ units, see color bar) of the gene across the entire set of samples (red - median, black – no change, and green - below median value). The dendrogram shows that samples clustered into three groups based on dietary treatment. To identify temporal (B) and treatment-dependent (C) changes in gene expression among and between high-fat diets, SAM two-class unpaired analysis was performed. These gene lists were submitted to GoMiner (9) to identify significantly enriched biological processes ($P<0.05$). A few of these processes are shown within color coded circles (red – upregulated; green – down-regulated) to its respective treatment as indicated. The number of genes associated with each process is given in parentheses. SAM analysis found no temporal difference in gene expression for fish oil where the lowest obtainable FDR was 6.3% (14 genes).

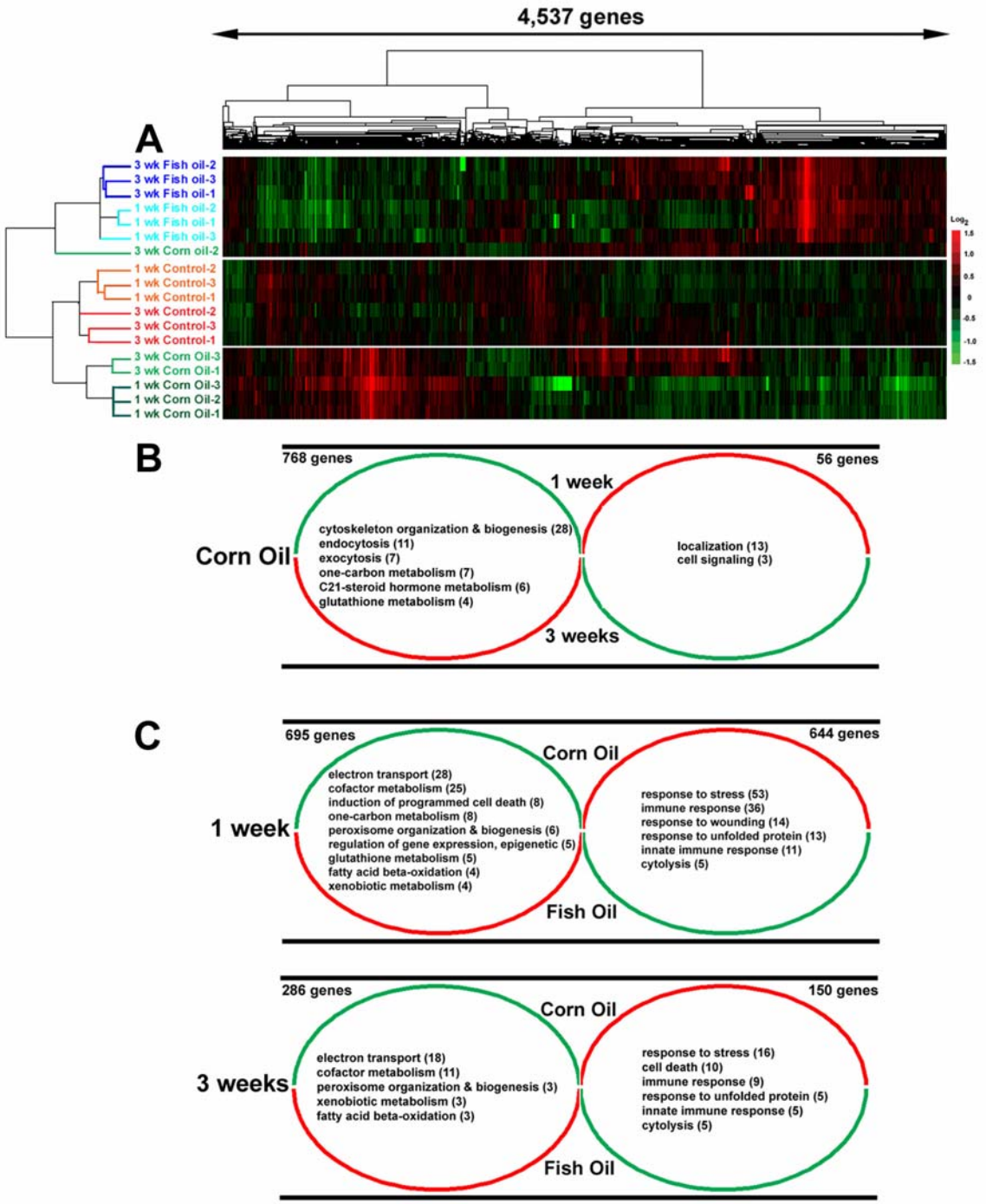
4,537 genes
A
3 wk Fish oil-2
3 wk Fish oil-3
3 wk Fish oil-1
1 wk Fish oil-2
1 wk Fish oil-1
1 wk Fish oil-3
3 wk Corn oil-2
1 wk Control-2
1 wk Control-3
1 wk Control-1
3 wk Control-2
3 wk Control-3
3 wk Control-1
3 wk Corn Oil-3
3 wk Corn Oil-1
1 wk Corn Oil-3
1 wk Corn Oil-2
1 wk Corn Oil-1
Log2
1.5
1.0
0.5
0
-0.5
-1.0
-1.5
B
768 genes
1 week
56 genes
Corn Oil
cytoskeleton organization & biogenesis (28)
endocytosis (11)
exocytosis (7)
one-carbon metabolism (7)
C21-steroid hormone metabolism (6)
glutathione metabolism (4)
localization (13)
cell signaling (3)
3 weeks
C
695 genes
Corn Oil
644 genes
1 week
electron transport (28)
cofactor metabolism (25)
induction of programmed cell death (8)
one-carbon metabolism (8)
peroxisome organization & biogenesis (6)
regulation of gene expression, epigenetic (5)
glutathione metabolism (5)
fatty acid beta-oxidation (4)
xenobiotic metabolism (4)
response to stress (53)
immune response (36)
response to wounding (14)
response to unfolded protein (13)
innate immune response (11)
cytolysis (5)
Fish Oil
286 genes
Corn Oil
150 genes
3 weeks
electron transport (18)
cofactor metabolism (11)
peroxisome organization & biogenesis (3)
xenobiotic metabolism (3)
fatty acid beta-oxidation (3)
response to stress (16)
cell death (10)
immune response (9)
response to unfolded protein (5)
innate immune response (5)
cytolysis (5)
Fish Oil

Figure 4.2

A high-fat diet of ω-3 PUFA leads to an induction of anti-oxidant defense genes in mouse liver

Gene ontology (GO) identified 163 genes on the microarray with an association with oxidative stress. SAM multi-class analysis identified 81 of those genes to be significantly differentially expressed (FDR < 5% with 1.5 fold change) within at least one treatment group. Supervised hierarchical clustering was performed using this gene list. The dendrogram showed that genes segregated into two main clusters based on dietary treatment. The gene clusters induced by fish oil (A) or corn oil (B) treatment are shown.

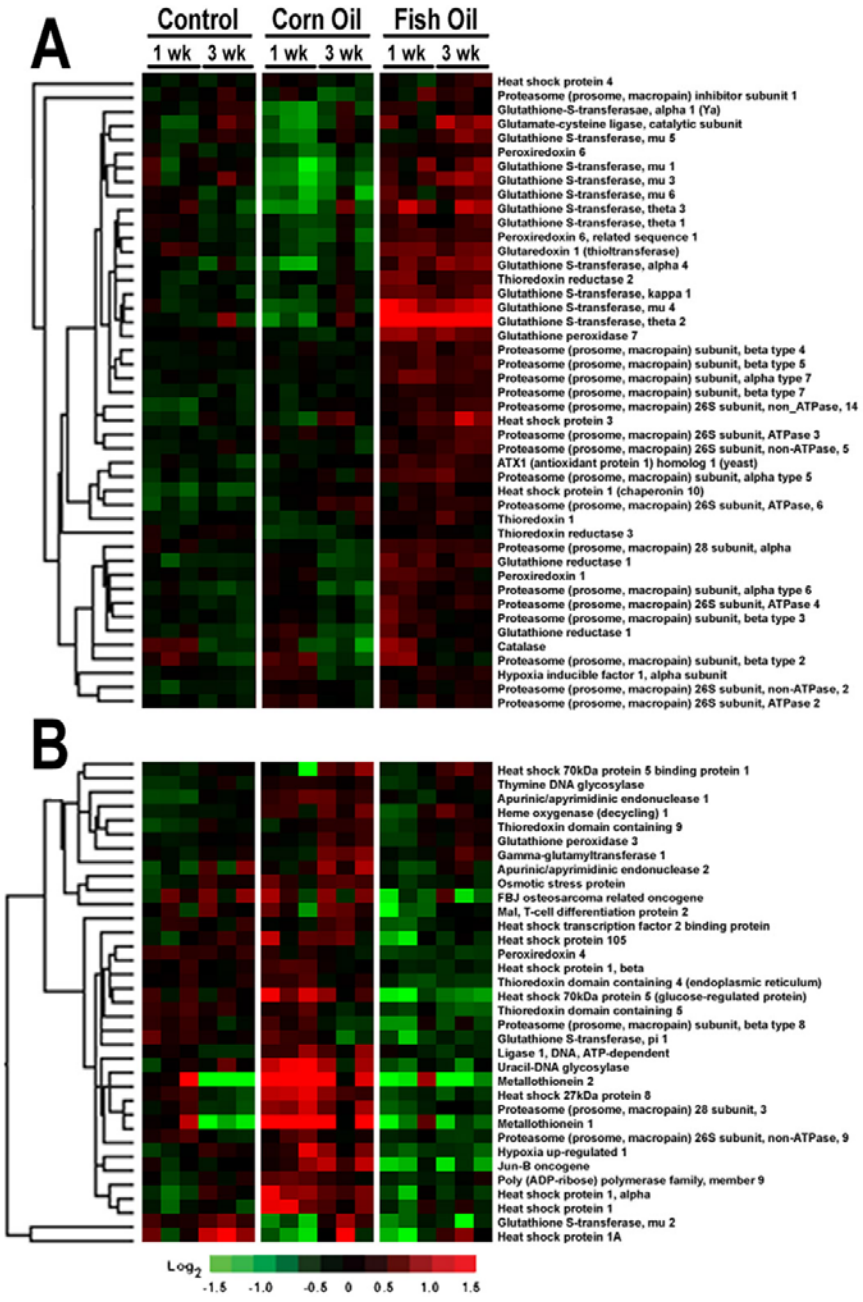

Figure 4.3

The type of PUFA influences the degree of accumulation of 8-OH-dG DNA adducts in liver compared to control low-fat diet

Representative micrographs (200×) of 8-OH-dG stained liver sections (A) from mice fed for 3 weeks with low-fat control diet, or high fat diets of either corn oil (ω-6), or fish oil (ω-3). Quantification of 8-OH-dG DNA adducts from immunostained liver sections using Bioquant image analysis software by averaging percent nuclei stained to total nuclei at 200x (bar graph) or number of adducts in genomic liver DNA determined by capillary LC-MS/MS analysis (line graph) are shown (B). Results are expressed as mean ± standard deviation from 5 animals per group. *Statistical difference ($P < 0.05$) compared to corresponding control group using one-way ANOVA followed by Tukey's multiple comparison post-hoc test.

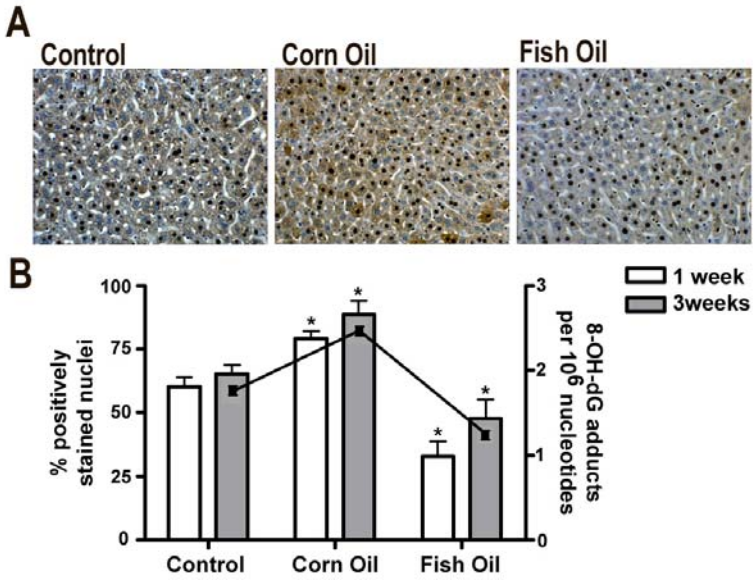

Figure 4.4

Gene expression phenotypes in livers from mice given a high-fat diet of ω-3 PUFA or PPARα agonist, WY-14,643, are similar

(A) Unsuperivsed hierarchical clustering of integrated gene expression data sets from this study and data from livers of mice treated with PPARα pan agonist, WY-14,643 (50 mg/kg) for 1 or 4 weeks. Dendrogram shows two major sample clusters demonstrating that liver gene expression phenotypes are most similar between fish oil and WY-14,643. (B) Venn diagram illustrating the distribution of gene alterations between fish oil and WY-14,643. Significant gene lists were generated using SAM (FDR < 5%) for each treatment and cross-compared. Values represent the number of genes significantly induced (red) or repressed (green) that are either unique or shared between the two treatment groups. Gene lists were submitted to GoMiner (9) to identify significantly enriched biological processes (P < 0.05 and a minimum of 3 gene transcripts), of which a few are shown. The number of genes within a given process is shown in parentheses.

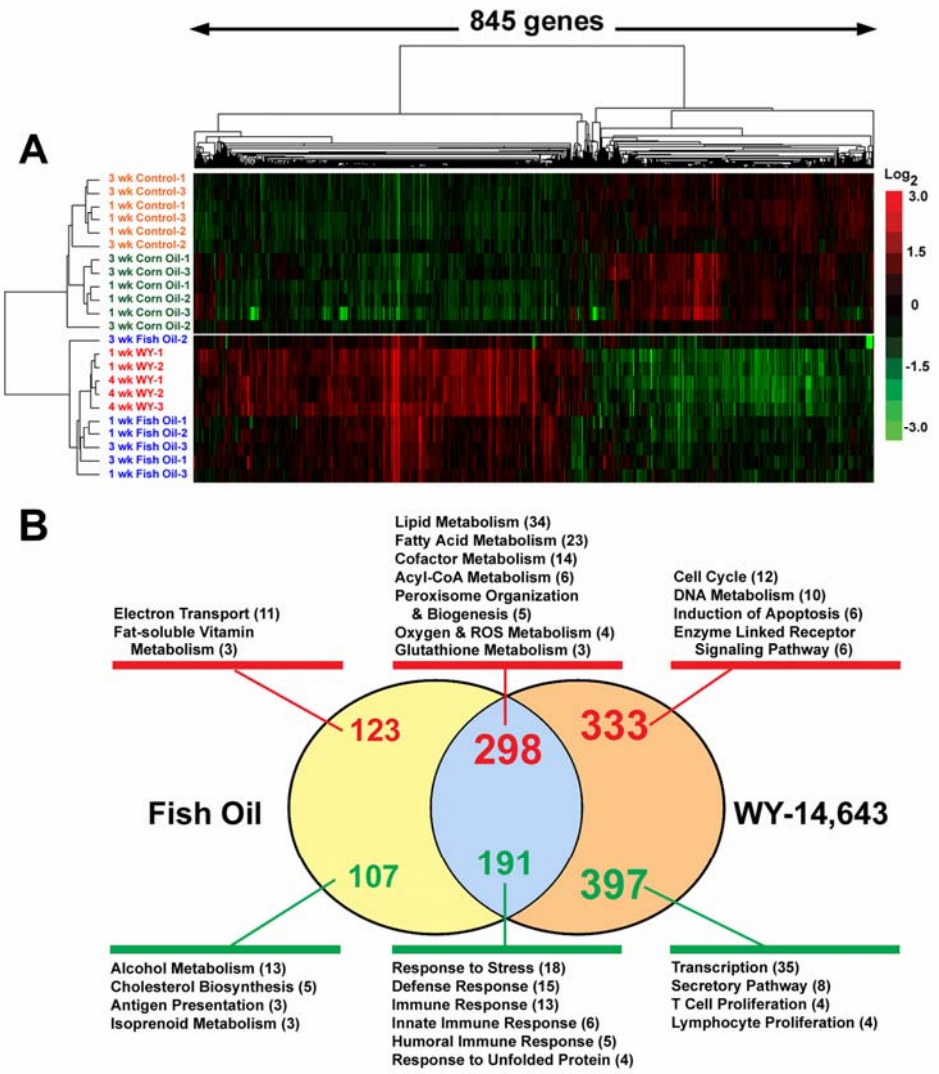

Figure 4.5

Activation of PPARα in liver with ω-3 PUFA dietary treatment

(A) Mice were administered a control low-fat diet or high-fat diets of either corn oil (ω-6) or fish oil (ω-3) for 1 or 3 weeks. Liver nuclear protein extracts were prepared and PPARα activity was determined by EMSA using biotin-labeled consensus sequence oligonucleotide as described in Materials and Methods. For unlabeled probe competition, nuclear extracts from mice administered a fish oil diet were used, denoted by arrows. Results are representative of two biological replicates. (B) Activity of acyl-CoA oxidase (ACO), a PPARα-regulated gene, measured biochemically in livers from mice fed control low fat diet or high fat diets of corn oil or fish oil for 1 or 3 weeks. Results are expressed as mean ± standard deviation from 3 animals per group. *Statistical difference ($P < 0.05$) compared to corresponding control group using one-way ANOVA followed by Tukey's multiple comparison post-hoc test.

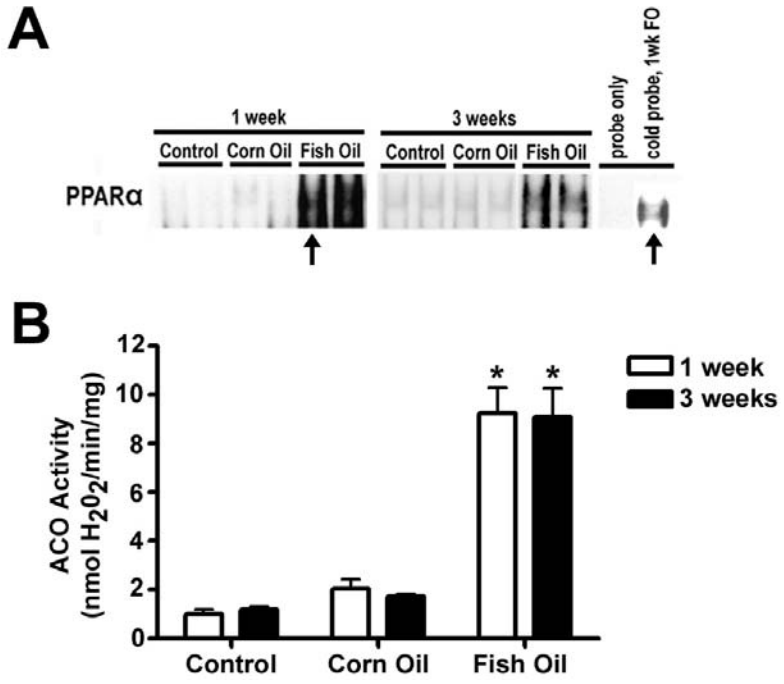

Figure 4.6

Gene expression modulation of PPARα-regulated networks by PUFA

Gene expression modulation of PPARα regulated networks by high-fat diets of corn oil or fish oil and a PPARα pan-agonist, WY-14,643. Gene expression data from liver of mice fed with high-fat diets of either corn oil (A) or fish oil (B) for 3 weeks and from mice treated with Wy-14,643 for 4 weeks (C) were averaged and genes within network scheme color-coded according to level of expression (red – induced, green – repressed, gray – unchanged, and yellow – gene absent from array). Genes within the inner blue circle are known to either directly or indirectly promote or attenuate oxidative stress. Those encircled in orange are lipid metabolism genes while those encircled in red are modulators of inflammation. Network scheme was prepared using Pathway Studio® 4.0 software (204) based on PubMed and other public datasources.

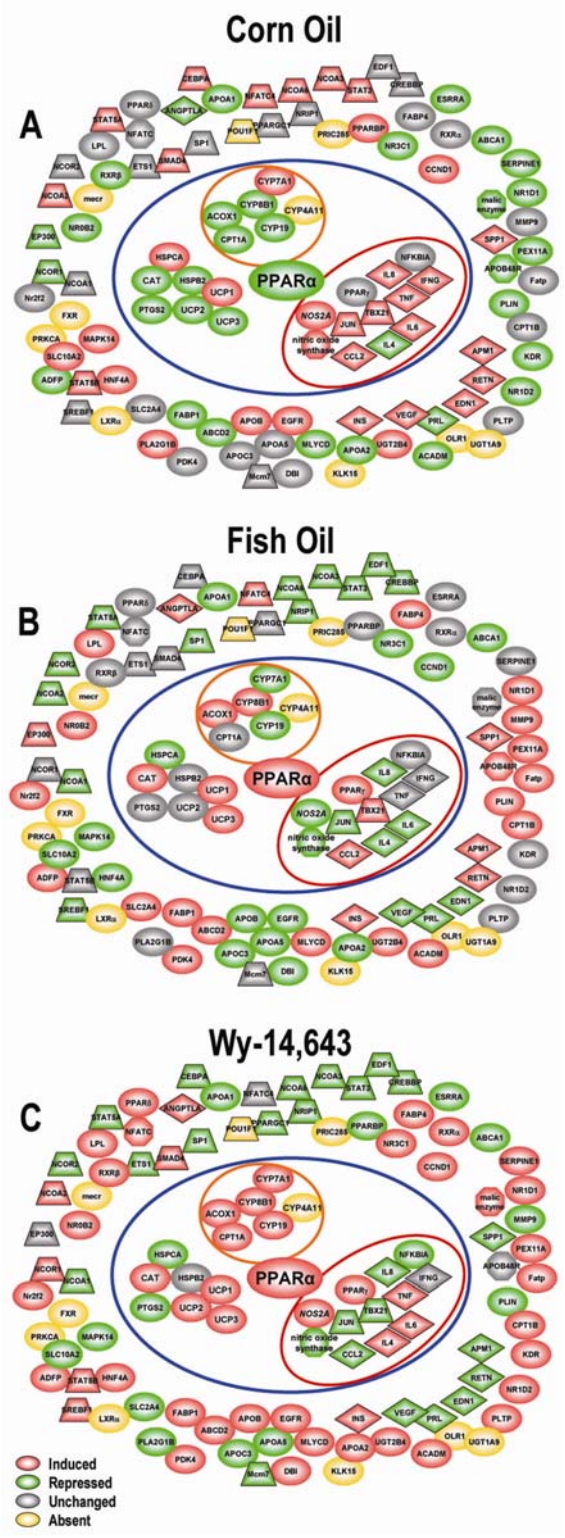
Corn Oil
A
PPARα
Fish Oil
B
PPARα
Wy-14,643
C
PPARα
Induced
Repressed
Unchanged
Absent

CHAPTER V

DISCUSSION

A. Conclusion and Perspectives

Considerable mechanistic gaps exist in our ability to characterize the complex associations among environmental exposures, genetics, and adverse health outcomes. Toxicity and disease is most frequently not the product of a singly perturbed gene or protein but instead is the result of complex interweaving networks of biological processes involving genes, proteins, and metabolites. Thus, establishing direct linkages between exposure and adverse health outcomes requires a comprehensive understanding of the diverse and complex responses leading to pathogenesis. The results obtained from microarray profiling experiments can provide a molecular framework of toxicity upon which phenotypic endpoints of toxicity can assist to derive the mechanism of action. The research studies detailed herein are distinct in their own right but were designed to demonstrate the power and versatility of toxicogenomic studies to assist in understanding the evolution and progression of oxidant-induced liver toxicity and disease. Incorporating the results from microarray profiling experiments with phenotypic markers for oxidative stress and DNA damage allowed us to improve the linkages between oxidant-induced hepatic toxicity and pathology and most importantly, provide insight into the molecular networks involved in eliciting observed pathologies.

1. Predictive Markers of Early Effect

The sensitivity afforded by toxicogenomic studies provides an unprecedented window into the early events preceding toxicity that can serve as predictive markers of exposure or early effect. For instance, previous studies using APAP-induced hepatotoxicity in the rat demonstrated that cellular pathways perturbed at low doses of APAP may be indicative of overt toxicity occurring at higher doses (91). Indeed, in our work the gene signature indicative for oxidative stress was successfully phenotypically anchored to markers of oxidative stress for both low and overtly toxic doses of APAP

(179). Taken together, these studies demonstrate that gene expression profiling can assess toxicity more comprehensively by detecting subtle indicators of potential adverse effects in the absence of overt toxicity. From a risk assessment point of view, the ability of microarray studies to detect subtle changes with ever lower doses should lead to improved extrapolation methods as toxicity studies to evaluate chemical safety can be conducted using more relevant human exposure levels.

Although, a disconnect between traditional measures of observable toxicity with alterations in gene expression supported by unconventional phenotypic endpoints will bring forth a critical reassessment for how we define toxicity. In our study, the observed state of oxidative stress was short-lived subsiding within 24h of exposure along with the reversal of altered expression changes. A major challenge is to determine which molecular events that change with low doses are necessary for pathological outcomes, versus those that are adaptive, beneficial, and/or unrelated to the development of pathologies (205). Discriminating between these lines will require an extensive dose-response study upon which the data can then be used to determine points of departure, establish thresholds of toxicity, and predict exposure levels required to initiate the cascade of molecular responses leading to an adverse outcome. There are still many challenges ahead for how we interpret alterations in gene expression but we must be especially careful to refrain from classifying every expression change as an adverse event.

2. Assessing Degree of Conservation for Mechanisms of Toxicity

A surprising revelation from our toxicogenomic study on APAP-induced hepatotoxicity was the dose- and species-dependent discord in detecting 3-nitrotyrosine protein adducts, an indirect measure of peroxynitrite formation. The detection of 3-nitrotyrosine has been repeatedly measured in the livers of mice administered a toxic

dose of APAP and is considered a critical mediator for liver injury (206). Surprisingly, in our study using the rat, nitrated protein residues were only detected following a sub-toxic dose which, in turn, would infer that the oxidant species formed in the presence of sub-toxic and overtly toxic doses of APAP are not identical. The culmination of these studies would suggest that there are mechanistic differences in APAP metabolism that are both dose- and species-dependent. Assessing the degree of conservation for the mechanism of APAP-induced hepatotoxicity would facilitate the implementation of mechanistically based uncertainty factors that account for both within- and across-species variability. If repeated studies demonstrate that the mechanism of APAP-toxicity is not conserved across rodent species then it can be speculated that neither species would serve well to accurately access human health hazards. These types of discrepancies have fostered the search for new tools to identify best-fit models for evaluating potential adverse outcomes in humans. A similarity in gene expression patterns could be used to select the most appropriate animal model prior to the conduct of toxicity studies based on the premise that shared expression often implies shared function (7).

3. Identification of Best-fit Animal Models through Comparative Genomics

To date, very few studies in toxicology exploit comparative genomic approaches to identify best-fit animal models to study toxicity or disease. Comparative expression analysis was performed on CD-induced rat HCC (207) with data from human HCC study (160) which included 102 primary tumors and 74 non-tumor liver samples. Clustering analysis of orthologous genes revealed that CD-induced rat HCC and human HCC share similar expression phenotypes. Moreover, functional analysis of similarly expressed genes revealed biological processes consistent with known cancer biology. A particular hallmark of rat HCC was the up-regulation of tyrosine kinase signaling pathways which recently has been linked to a sub-class of human HCC patients with

poor survival (208). Similar studies have also been performed using genetically-modified (transgenic and knock-outs) and chemically-induced models of mouse HCC (209). The results from these studies discriminated the mouse models into three classes of which two of them closely recapitulated the molecular patterns for two sub-classes of human HCC. Taken together, these results support the concept that best-fit models for human cancer studies can be identified by applying genome-scale comparison of gene expression patterns. The clear gain to be realized from such an approach is to connect molecular pathogenic features of human cancer to rodent models with increased confidence.

4. Improving the Linkage Between Oxidant-induced Hepatic Toxicity and HCC

The similarity in gene expression changes between rat and human HCC would indicate that the underlying transcriptional regulation in gene expression changes is conserved and therefore, the CD-induced rat HCC is a suitable model for studying the biology of hepatocarcinogenesis. It is well established that regardless of etiology (i.e., HBV, HCV, and alcohol), the progression to HCC proceeds through a series of pathological changes including fatty liver, repeated cycles of cellular injury and repair, fibrosis, and cirrhosis. The gene expression patterns for the CD-model of HCC were strongly driven by the histopathological changes, as described above, accompanied by progressional shifts in antioxidant defenses, specifically DNA repair genes, suggesting progressively increasing genomic instability. Increases in AP sites and oxidized purines confirmed these results and established a temporal link between fibrosis and the accumulation of DNA lesions. Recent studies have demonstrated a correlation between increases in DNA repair expression and histological stage of fibrosis in liver biopsies (158). Thus, we would propose that the fibrotic process may be a contributing factor to the transformation of hepatocytes towards a neoplastic phenotype. It would be

particularly interesting to follow-up these studies to determine if a correlation exists between grade of fibrosis and the number of oxidative DNA lesions.

5. Role of Dietary Oils as Vehicles to Conduct Toxicological Studies

Nutritional modulation of toxicity or disease has become an emerging issue in toxicology. The growing obesity epidemic (163) is of particular concern as it is associated with increased systemic oxidative stress (171), a condition that may predispose individuals to increased susceptibility to environmental toxicity or disease. A contributory factor to the rise in obesity rates has been the disproportionate intake ratios of ω-6:ω-3 PUFA. Molecular profiling supported by measures of oxidative stress demonstrated that ω-6 PUFA results in a pro-oxidant state in mouse liver most likely established by increased production of pro-inflammatory mediators. Pathway mapping of expression data suggested that the differential effects on oxidative stress by the two dietary fatty acids were mediated by PPARα. Using a comparative genomics approach with a known PPARα agonist, we were able to demonstrate that ω-3 but not ω-6 PUFA shared similar expression patterns and biological functions which included an up-regulation of anti-oxidant defense mechanisms. These data would then infer that the observed differential effects on oxidative stress are mediated by their ability to trans-activate PPARα. As oxidative-stress signaling pathways are a common mechanism for human toxicity and disease, it would be expected that the composition of dietary fatty acids in tissues would impart some inherit resistance or susceptibility to disease. Indeed, several in vivo animal models have shown that increased intake of ω-6 PUFA is associated with increased risk for cyclosporine-mediated nephrotoxicity (210) and potentiates PCB-induced vascular toxicity (211) and aliphatic nitrile toxicity (212). This potentiation of drug and environmental toxicity by corn oil brings into question whether it is an appropriate vehicle to conduct toxicology studies. It has been a mainstay for

decades as the vehicle of choice to administer unpalatable or volatile chemicals. However, this practice is unlikely to change due to the difficulty in identifying suitable vehicles for administering lipophilic compounds which lack any observable side effects.

B. Challenges and Limitations

1. Study Limitations

One of the promises of toxicogenomics is to predict toxicity at earlier times and doses than currently employed methods. In our work with APAP, the phenotypic anchoring of a gene signature for oxidative stress at a sub-toxic dose builds support for gene expression profiling as a sensitive indicator to detect potentially adverse effects in the absence of overt toxicity (179). The conclusions drawn from this study were limited in scope due to the fact that an appropriate dose-response was not conducted. This is of particular importance as we demonstrated a discrepancy in the accumulation of 3-nitrotyrosine protein adducts suggesting that the mechanism of toxicity may not be conserved among sub-toxic to moderate to overtly toxic doses of APAP. Establishing predictive markers of early effect requires the ability to determine which molecular events are needed to initiate the cascade of events leading to pathology. Delineating these points of departure require temporal and dose-response studies that are linked with the appropriate phenotypic markers of toxicity. Such information would provide us with the ability to determine which gene expression changes are required to initiate toxicity and provide a foundation to build potential biomarkers of APAP exposure.

Cancer research requires the use of animal models that most accurately reproduce the human condition. The CD diet is an extensively studied non-genotoxic, non-chemical induced model of rodent HCC that recapitulates the sequelae of pathological events observed in human HCC associated with viral infection and alcohol abuse. This diet is administered over the course of a year and may be considered a

particular harsh treatment as one-carbon metabolism and fatty acid oxidation pathways are severely impaired. Although the histopathology between this model and progression of human HCC may appear similar, the mechanisms that bring about such changes may not. The comparative expression analysis between CD-induced rat HCC and human HCC was severely limited in statistical power as this study included only 4 rat tumors, 2 of those being distinct tumors from the same animal. Secondly, annotation of the rat genome has lagged behind the human and mouse and this most likely limited our ability in identifying all gene orthologs between rat and human HCC data sets.

The major focus of Aim 3 was identifying and understanding how ω-3 and ω-6 PUFA mediate their differential effects on oxidative stress in the mouse liver. In the C57Bl/6J mouse strain it was discovered that PPARα was activated by fish oil but not corn oil treatment and suggested that it was the driving force behind the transcriptional changes responsible for the up-regulation of cellular anti-oxidant defense mechanisms. Although, this observation may be limited to this mouse model and others that have deficiencies in the transcriptional activation of Nrf2, a transcription factor which is responsible for the activation of stress response genes. Previous studies have shown that PPARα and Nrf2 transcriptional regulate similar genes (188). Thus, repeating these studies in an Nrf2 competent mouse line, in addition to PPARα null, would assist in determining the degree of involvement of PPARα in mediating the hepatoprotective effects against oxidative stress. It should also be considered that the amount of dietary fat provided to these mice was considerably high in relation to daily human consumption. This was particular true for fish oil as n-6/n-3 ratios were reduced to 1 and may have contributed to the degree of PPARα activation observed in this study. As epidemiological studies are showing that n-6/n-3 ratios are more important in determining disease risk, it would be pertinent to determine the ratio that delivers the best health benefits.

2. Current Challenges and Limitations of Toxicogenomic Studies

2.1 Standardization of Toxicogenomic Protocols and Data Analysis

Since the inception of DNA microarrays in the early 1990s, several thousand papers describing data from microarrays are published each year. Yet, after 15 years of research and development a major criticism of microarray data that still lingers has been the lack of consensus on the reproducibility and accuracy of the derived data. The repeatability and reproducibility of microarray experiments, comparability across platforms, and best practices for not only experimental design and sample preparation but also for data acquisition, statistical analysis, and interpretation remain inadequately characterized (213). A lack of resolution of these issues has hampered translation of microarray technologies into the regulatory and clinical settings (214).

Consortiums of academic institutions, regulatory and governmental agencies, and the private sector have begun to address these fundamental issues. The Microarray Quality Control Project (MAQC), External RNA Controls Consortium (ERCC) and the Toxicogenomics Research Consortium (TRC) have all launched initiatives aimed to establish a set of quality assurance and quality control criteria to assess and assure data quality, to identify critical factors affecting data quality, and to optimize and standardize microarray procedures (213). To date, several large cross-format studies have already been published (94, 215, 216) which have set out to evaluate the performance for up to 12 different microarray platforms in profiling the expression of identical RNA samples within and across different laboratories. Each of these studies concluded that with careful experimental design using standardized protocols for sample preparation, data acquisition and data normalization that microarray data can indeed be reproducible and comparable among different formats and laboratories. Commercial platforms demonstrated the highest level of reproducibility between laboratories when used together with standardized protocols (94, 216). Initiatives for reference RNA materials

which can be incorporated into the microarray workflow process are currently in progress (217). These materials can then be used by microarray facilities to monitor the technical performance and comparability of data sets generated over time. It is anticipated that the results from these studies will establish universal quality control standards that will provide improved confidence in the consistency and reliability of gene expression data sets.

The validity of microarray studies are generally measured as the concordance and discordance of the data with quantitative real-time PCR (qRT-PCR), a method commonly accepted as the “gold standard” of relative gene expression measurements (218). Studies performed by MAQC revealed an excellent fold-change correlation for differentially expressed genes with medium-to-high expression levels with qRT-PCR (216). Moreover, it was determined that discordant responses in differential gene expression among the various microarray platforms were largely attributable to differences in probe hybridization and platform detection thresholds (219). The detection of genes with low expression levels varied considerably across microarray platforms which was largely dependent on the ability to reliably detect expression. Despite the use of standardized protocols across platforms, there were still considerable differences in significant gene lists. Thus, many issues remain open for investigation in the processing and analysis of microarray data.

One of the fundamental goals of gene expression profiling experiments is to identify those genes that are differentially expressed within the system being studied. Microarray studies are uniquely characterized by small sample sizes, multiple hypothesis testing, and high-dimensional biological data which presented important new challenges to statisticians as traditional statistical approaches were ill-suited. Fold-change was the first method used to evaluate whether genes were differentially expressed and was popular for many years primarily due to its simplicity. Today, it is now widely accepted to

be an inadequate test statistic as it does not incorporate variance and offers no associated level of confidence (220). The preference of statistical significance metric (P value) has frequently been used as a gene selection method although, it is biased to random noise and platform-dependent systematic errors (214). The reliance of P value alone has resulted in the apparent lack of agreement in expression data between laboratories and microarray platforms (214, 221). Results from the MAQC human data sets (215, 216) and TRC rat toxicogenomic data set (221) indicate that fold-change ranking with a non-stringent P value cutoff can be successful in identifying reproducible gene lists. Unfortunately, reproducibility of gene lists does not necessarily equate to accuracy. The lack of reference data sets impedes the independent validation of data analysis methods for their merits and limitations.

The outcome of microarray studies can be affected by many technical, instrumental and computational factors and it is imperative to understand these limitations and variables. Recent concerted efforts have demonstrated that microarray results are comparable across laboratories when standardized protocols are followed. Clearly, microarrays have a long way to go before they can be used to support regulatory decision-making but the contributions made thus far by the MAQC and TRC have provided a solid foundation from which to build.

2.2 Gene Expression is a Limited Biological Measurement

Gene expression data captures only a snapshot in time the changes in mRNA expression levels that occur in response to a given stimulus under study. It is unknown as to whether the observed changes occurred as a result of fluctuations in transcriptional activity, changes in mRNA stability, or changes in cell populations within a given tissue. Moreover, the information gathered from microarray studies does not provide insight into whether or how these changes in expression levels impact cellular functions. An indirect

understanding of global and molecular trends in gene expression data can be made through Gene Ontology (GO) vocabularies which describe gene products as a function of their biological processes, their cellular components, and their molecular/biochemical function provide. This information of gene functionality can then be used to uncover how sets of genes and their products work together in health and disease. As the emerging fields of proteomics and metabolomics catch up with genomics, the integration of such data sets will provide an unprecedented systems biology approach to elucidate complex disease pathways.

2.3 Interpretation of Toxicogenomic Data Requires Phenotypic Anchoring

Toxicology studies are quite complex with sources of variability resulting from the dose and delivery of the chemical under study, the choice of animal species and differences in biological and pathological responses of various tissues (93). The combination of this with the known technical variability in genomic studies (94) underscores the importance of careful validation of alterations in gene expression patterns. A recent toxicogenomic study (TRC, unpublished data) using a well characterized and studied hepatotoxicant, APAP, conducted across seven different centers within the US determined that animal-to-animal variability accounted for one of the largest sources of variability in microarray studies, despite the use of standardized protocols to minimize experimental and technical variables. The extent of liver injury induced by APAP as measured by necrosis and ALT activity varied appreciably across centers and animals. Yet, applying correlation-based analysis to associate liver toxicity to gene expression was demonstrated to be a powerful tool in identifying a selection of genes that respond to APAP treatment. This type of statistical approach of linking expression data with pathology was critical for extracting biological meaningful data with confidence.

The gene signature itself provides little information for understanding the underlying mechanism of toxicity or disease. Linking differentially expressed genes with phenotypic markers of toxicity is required to understand how sets of genes and their products work together in generating adverse health outcomes. Moreover, expression changes are dynamic and subject to reversible temporal changes that can be displaced in time relative to toxicity. This is further complicated when only a subpopulation of the treatment group experiences the toxic effect, as in the case of carcinogenesis. The interpretation of toxicogenomic data will continue to be a difficult task but when put in context with phenotypic endpoints of toxicity can facilitate the development of potential biomarkers of exposure and effect, elucidate molecular mechanisms, and classify new chemical entities.

C. Future Directions

Toxicogenomics continues to evolve especially as advances are made in the fields of bioinformatics and computational biology which develop the powerful tools required to integrate disparate data sets across time, dose, and phenotypic markers. Such methods are now making it possible to provide a systematic evaluation of the effects of variant genetic sequences on responses to toxicants. Genetic linkage and association studies between individuals with and without disease has been used to identify a number of disease susceptibility genes (222, 223), as well as polymorphisms that determine individual diversity in drug responses (224). Toxicologists are now realizing the potential of genetically controlled inbred mouse populations as a surrogate for studying genetic variation in the human population. It is anticipated that the results from toxicogenetic studies involving chemical exposures to large panels of inbred mouse strains will identify polymorphisms responsible for sensitivity to toxicity to particular

agents and identification of chemical-induced genetic changes associated with particular diseases (205).

D. Summary

In summary, toxicogenomics moves the field of toxicology beyond traditional approaches by linking the critical molecular events caused by exposure to environmental factors with the sequelae of events leading to toxicity. This mechanistic information for toxicant action is crucial for understanding adverse health effects in humans and for making more informed regulatory decisions regarding exposure levels. This field is rapidly maturing as regulatory agencies such as Food and Drug Administration (FDA) and Environmental Protection Agency (EPA) are now encouraging the submission of complementary toxicogenomic data (8). Nevertheless, there is still considerable unease with some stakeholders on the use of toxicogenomic data in risk assessment and will bring forth continued scrutiny on the interpretation and incorporation of toxicogenomic data sets into regulatory decision making (8). One thing we can be confident about is that the tools of the genomic era are here to stay.

APPENDICES

APPENDIX 1

Gene lists of cellular pathways evoked by choline deficiency in rat liver

Data mining using Gene Ontology (GO) from NetAffx™ Analysis Center was used to assign functional classes to each gene to determine the cellular and molecular pathways. To determine whether molecular profiling would model the temporal changes in histopathology observed with choline deficiency, genes with a functional assignment associated with lipid biosynthesis or metabolism, apoptosis, cell proliferation, and tissue remodeling were compiled into a single non-redundant list. Supervised hierarchical clustering was conducted to view temporal changes in expression of genes associated with abovementioned biological processes (see Figure 3.4). Average gene expression ratios (log_2-transformed) between choline deficient (CD) and choline sufficient (CS) for each corresponding time point and tumors are shown.

			Log Ratio (CD/CS)			
Unigene ID	**Gene Symbol**	**Description**	**4 wks**	**12 wks**	**80 wks**	**Tumors**
Lipid Biosynthesis & Metabolism						
Rn.2854	Decr1	2,4-Dienoyl Coa Reductase 1, Mitochondrial	-0.05	-0.20	-0.27	-0.87
Rn.7879	Decr2	2-4-Dienoyl-Coenzyme A Reductase 2, Peroxisomal	-0.58	-0.34	-0.59	-1.11
Rn.29594	Hmgcs2	3-Hydroxy-3-Methylglutaryl-Coenzyme A Synthase 2	-0.25	-0.22	-0.18	-0.66
Rn.9215	Aacs	Acetoacetyl-Coa Synthetase	-0.06	-0.24	0.04	0.53
Rn.56980	Slc33a1	Acetyl-Coa Transporter	0.13	-0.32	-0.06	-0.33
Rn.4054	Acat1	Acetyl-Coenzyme A Acetyltransferase 1	-0.03	-0.09	0.17	-0.40
Rn.3786	Acaa2	Acetyl-Coenzyme A Acyltransferase 2 (Mitochondrial 3-Oxoacyl-Coenzyme A Thiolase)	0.14	0.39	0.00	-0.57
Rn.44372	Acac	Acetyl-Coenzyme A Carboxylase	-0.86	-1.58	0.17	0.12
Rn.44372	Acac	Acetyl-Coenzyme A Carboxylase	-0.77	-2.00	-0.39	-0.32
Rn.44359	Acacb	Acetyl-Coenzyme A Carboxylase Beta	-0.48	-0.46	-0.05	-0.40
Rn.6302	Acadm	Acetyl-Coenzyme A Dehydrogenase, Medium Chain	0.22	0.17	-0.72	-0.36
Rn.6215	Acsl1	Acyl-Coa Synthetase Long-Chain Family Member 1	-0.60	-0.46	-0.64	-0.77
Rn.6215	Acsl1	Acyl-Coa Synthetase Long-Chain Family Member 1	-0.80	-0.74	-0.79	-1.00
Rn.54820	Acsl3	Acyl-Coa Synthetase Long-Chain Family Member 3	1.12	1.95	0.18	1.24
Rn.33697	Acsl6	Acyl-Coa Synthetase Long-Chain Family Member 6	-0.02	-0.30	-0.30	-0.02
Rn.13649	Acad9	Acyl-Coenzyme A Dehydrogenase Family, Member 9	0.01	0.06	-0.16	-0.29
Rn.31796	Acox1	Acyl-Coenzyme A Oxidase 1, Palmitoyl	0.11	-0.02	-0.25	-0.21
Rn.10622	Acox2	Acyl-Coenzyme A Oxidase 2, Branched Chain	-1.13	-0.94	-1.12	-0.40
Rn.10546	Acox3	Acyl-Coenzyme A Oxidase 3, Pristanoyl	-0.47	-0.79	-0.49	-0.64
Rn.104556	LOC289036	Adiponectin Receptor 1	-0.20	0.25	-0.61	-0.45
Rn.101807	LOC312670	Adiponectin Receptor 2	-0.46	-0.25	-0.20	-0.26
Rn.101967	ADRP	Adipose Differentiation-Related Protein	0.23	0.64	-1.42	-1.36
Rn.101967	ADRP	Adipose Differentiation-Related Protein	-0.03	0.18	-0.24	-0.62
Rn.10308	Apoa1	Apolipoprotein A-I	0.60	1.03	0.51	0.58
Rn.89304	Apoa2	Apolipoprotein A-Ii	-0.39	-0.35	-1.16	-1.25
Rn.15739	Apoa4	Apolipoprotein A-Iv	-1.46	-2.82	-0.47	-0.29
Rn.48763	Apoa5	Apolipoprotein A-V	-0.27	-0.55	-0.52	-0.44
Rn.8887	Apoc1	Apolipoprotein C-I	-0.45	-0.38	-0.54	-0.33
Rn.262	Apom	Apolipoprotein M	-0.66	-0.93	-0.97	-0.36
Rn.11318	Alox15	Arachidonate 12-Lipoxygenase	-0.36	-0.30	0.08	-0.07

Unigene ID	Gene Symbol	Description	Log Ratio (CD/CS) 4 wks	12 wks	80 wks	Tumors
Rn.9662	Alox5	Arachidonate 5-Lipoxygenase	-0.12	-0.23	-0.30	-0.25
Rn.2184	Cyp2c23	Arachidonic Acid Epoxygenase	-1.26	-0.88	-0.78	-0.42
Rn.29771	Acly	Atp Citrate Lyase	-1.05	-1.37	-0.28	-0.57
Rn.7024	Abcd3	Atp-Binding Cassette, Sub-Family D (Ald), Member 3	-0.49	0.56	-0.28	0.38
Rn.8398	Abcg1	Atp-Binding Cassette, Sub-Family G (White), Member 1	1.26	1.10	0.67	0.23
Rn.74258	Abcg5	Atp-Binding Cassette, Sub-Family G (White), Member 5 (Sterolin 1)	-0.05	0.03	-0.29	0.92
Rn.4896	Crot	Carnitine O-Octanoyltransferase	0.15	0.19	-0.90	-1.50
Rn.4896	Crot	Carnitine O-Octanoyltransferase	0.03	-0.30	-1.11	-2.75
Rn.2856	Cpt1a	Carnitine Palmitoyltransferase 1, Liver	0.34	0.25	0.03	0.47
Rn.6028	Cpt1b	Carnitine Palmitoyltransferase 1B	0.37	-0.09	-0.15	-0.04
Rn.11326	Cte1	Cytosolic Acyl-Coa Thioesterase 1	3.12	3.89	2.13	0.99
Rn.11208	Dgkz	Diacylglycerol Kinase Zeta	-0.20	0.28	0.26	0.30
Rn.1840	Dgka	Diacylglycerol Kinase, Alpha (80 Kda)	-0.53	-0.24	0.12	-0.05
Rn.11413	Dgkb	Diacylglycerol Kinase, Beta	-0.25	-0.25	-0.04	0.01
Rn.3285	Dbi	Diazepam Binding Inhibitor	0.02	-0.09	-1.21	-1.04
Rn.6051	Dpep1	Dipeptidase 1 (Renal)	0.04	0.07	-0.13	-0.17
Rn.80835	Dci	Dodecenoyl-Coenzyme A Delta Isomerase	0.64	0.80	-0.61	-0.51
Rn.80835	Dci	Dodecenoyl-Coenzyme A Delta Isomerase	0.02	-0.24	-0.13	0.02
Rn.6847	Echs1	Enoyl Coenzyme A Hydratase, Short Chain, 1, Mitochondrial	-0.57	-0.69	-1.00	-0.53
Rn.3671	Ehhadh	Enoyl-Coenzyme A, Hydratase/3-Hydroxyacyl Coenzyme A Dehydrogenase	0.22	1.20	-0.61	-1.23
Rn.3252	Fdft1	Farnesyl Diphosphate Farnesyl Transferase 1	-0.86	-0.39	0.01	-0.09
Rn.89119	Faah	Fatty Acid Amide Hydrolase	-0.64	-0.63	-0.51	-0.07
Rn.91358	Fabp2	Fatty Acid Binding Protein 2, Intestinal	1.74	1.81	0.83	0.25
Rn.4258	Fabp4	Fatty Acid Binding Protein 4, Adipocyte	3.26	3.71	2.18	1.21
Rn.10008	Fabp6	Fatty Acid Binding Protein 6, Ileal (Gastrotropin)	-0.25	-0.36	-0.04	0.03
Rn.28161	Fads1	Fatty Acid Desaturase 1	0.16	0.74	-0.51	-0.60
Rn.32872	Fads2	Fatty Acid Desaturase 2	-0.11	0.30	-0.49	-0.94
Rn.4243	rELO1	Fatty Acid Elongase 1	-0.78	-1.14	-1.39	-1.34
Rn.46942	rELO2	Fatty Acid Elongase 2	-2.03	-1.24	0.66	-0.14
Rn.5820	Grn	Granulin	1.19	1.48	0.83	0.56
Rn.11253	Hadhb	Hydroxyacyl-Coenzyme A Dehydrogenase/3-Ketoacyl-Coenzyme A Thiolase/Enoyl-Coenzyme A Hydratase (Trifunctional Protein), Beta Subunit	0.27	0.14	0.15	-0.51
Rn.2700	Hsd17b10	Hydroxysteroid (17-Beta) Dehydrogenase 10	-0.50	-0.40	-0.76	-0.28
Rn.10515	Hsd17b2	Hydroxysteroid (17-Beta) Dehydrogenase 2	0.21	-1.03	0.72	-0.51
Rn.10895	Hsd17b3	Hydroxysteroid (17-Beta) Dehydrogenase 3	-0.11	-0.31	-0.17	-0.29
Rn.2082	Hsd17b4	Hydroxysteroid (17-Beta) Dehydrogenase 4	-0.13	-0.07	-0.39	-0.42
Rn.7040	Hsd17b7	Hydroxysteroid (17-Beta) Dehydrogenase 7	-0.46	-0.48	-0.45	-0.21
Rn.98478	Hsd17b8	Hydroxysteroid (17-Beta) Dehydrogenase 8	-0.52	-0.09	-0.27	0.04
Rn.10857	Hsd17b9	Hydroxysteroid (17-Beta) Dehydrogenase 9	-0.56	-1.43	-1.44	-0.71
Rn.10780	Idi1	Isopentenyl-Diphosphate Delta Isomerase	0.37	0.40	0.41	0.76
Rn.92789	Hadhsc	L-3-Hydroxyacyl-Coenzyme A Dehydrogenase, Short Chain	0.05	-0.22	-0.41	-0.67
Rn.10481	Lcat	Lecithin Cholesterol Acyltransferase	-0.73	-0.45	-0.29	0.01
Rn.38594	Ltc4s	Leukotriene C4 Synthase	0.07	0.37	-0.95	-1.17
Rn.48656	Lipa	Lipase A, Lysosomal Acid	0.32	0.27	0.25	0.31
Rn.1195	Lipc	Lipase, Hepatic	-0.55	-0.70	-0.74	-0.45
Rn.1256	Lcn7	Lipocalin 7	-0.18	0.02	-0.05	-0.32

Unigene ID	Gene Symbol	Description	Log Ratio (CD/CS) 4 wks	12 wks	80 wks	Tumors
Rn.48863	Lbp	Lipopolysaccharide Binding Protein	2.41	1.87	0.94	0.94
Rn.3834	Lpl	Lipoprotein Lipase	2.73	3.44	1.83	0.94
Rn.48696	Lisch7	Liver-Specific Bhlh-Zip Transcription Factor 7	0.72	0.85	0.00	0.07
Rn.26430	Lrp2	Low Density Lipoprotein Receptor-Related Protein 2	0.06	0.03	-0.06	0.94
Rn.23204	Lrp3	Low Density Lipoprotein Receptor-Related Protein 3	-0.32	-0.48	-0.39	0.29
Rn.21381	Lrp4	Low Density Lipoprotein Receptor-Related Protein 4	0.21	0.25	0.36	0.52
Rn.10293	Lrpap1	Low Density Lipoprotein Receptor-Related Protein Associated Protein 1	0.17	-0.09	-0.32	-0.26
Rn.10293	Lrpap1	Low Density Lipoprotein Receptor-Related Protein Associated Protein 1	-0.02	-0.29	0.03	-0.10
Rn.10293	Lrpap1	Low Density Lipoprotein Receptor-Related Protein Associated Protein 1	-0.11	-0.21	-0.06	-0.52
Rn.37524	Mte1	Mitochondrial Acyl-Coa Thioesterase 1	0.98	1.02	0.33	-0.53
Rn.37524	Mte1 /// Cte1	Mitochondrial Acyl-Coa Thioesterase 1 /// Cytosolic Acyl-Coa Thioesterase 1	1.69	1.98	0.72	-0.35
Rn.14519	Pex11a	Peroxisomal Biogenesis Factor 11A	0.08	0.31	-0.48	-1.04
Rn.14519	Pex11a	Peroxisomal Biogenesis Factor 11A	0.11	-0.02	-0.23	-0.65
Rn.29982	Pex12	Peroxisomal Biogenesis Factor 12	-0.36	-0.47	-0.19	-0.05
Rn.7844	Pex14	Peroxisomal Biogenesis Factor 14	-0.22	-0.39	-0.23	-0.18
Rn.11773	Pex3	Peroxisomal Biogenesis Factor 3	-0.25	-0.36	-0.23	-0.30
Rn.17644	Pcscl	Peroxisomal Ca-Dependent Solute Carrier-Like Protein	-0.36	0.25	-1.49	0.71
Rn.10292	Pxmp2	Peroxisomal Membrane Protein 2	-1.02	-0.96	-0.72	-0.84
Rn.4065	Pxmp3	Peroxisomal Membrane Protein 3	0.09	0.03	-0.20	-0.26
Rn.19267	Pecr	Peroxisomal Trans-2-Enoyl-Coa Reductase	-0.41	-0.70	-0.65	-0.36
Rn.96181	Ppard	Peroxisome Proliferator Activated Receptor Delta	-0.22	-0.15	0.01	-0.16
Rn.19436	Ebp	Phenylalkylamine Ca2+ Antagonist (Emopamil) Binding Protein	-1.17	-0.59	-0.66	0.40
Rn.22158	Pten	Phosphatase And Tensin Homolog	-0.02	0.12	-0.28	-0.01
Rn.61687	Ppap2a	Phosphatidate Phosphohydrolase Type 2A	-0.43	0.14	-0.35	-0.46
Rn.3301	Ppap2c	Phosphatidic Acid Phosphatase Type 2C	0.12	0.27	0.02	0.26
Rn.23872	Pib5pa	Phosphatidylinositol (4,5) Bisphosphate 5-Phosphatase, A	0.16	-0.05	0.05	0.01
Rn.44448	Pik3r3	Phosphatidylinositol 3-Kinase P55 Subunit	0.06	-0.08	0.08	-0.01
Rn.11015	Pik4ca	Phosphatidylinositol 4-Kinase, Catalytic, Alpha Polypeptide	0.00	0.31	-0.10	-0.20
Rn.51538	Pigm	Phosphatidylinositol Glycan, Class M	0.13	0.05	-0.03	0.01
Rn.59136	Pigs	Phosphatidylinositol Glycan, Class S	-0.12	0.04	-0.08	-0.01
Rn.9771	Pitpn	Phosphatidylinositol Transfer Protein	0.03	0.22	-0.42	-0.50
Rn.2399	Pitpnb	Phosphatidylinositol Transfer Protein, Beta	0.45	0.16	0.08	0.20
Rn.30025	Pip5k2b	Phosphatidylinositol-4-Phosphate 5-Kinase, Type Ii, Beta	0.06	-0.08	-0.02	0.00
Rn.94783	Pip5k2c	Phosphatidylinositol-4-Phosphate 5-Kinase, Type Ii, Gamma	-0.27	0.10	0.04	0.30
Rn.10696	Pspla1	Phosphatidylserine-Specific Phospholipase A1	0.00	0.47	-0.26	-0.88
Rn.37733	Pde4b	Phosphodiesterase 4B	0.02	0.10	-0.47	0.43
Rn.915	Pgd	Phosphogluconate Dehydrogenase	-1.09	0.09	0.25	-0.03
Rn.9738	Pgam2	Phosphoglycerate Mutase 2	0.14	-0.08	0.14	0.04
Rn.46424	Pla2g2c	Phospholipase A2, Group 2C	-0.18	-0.37	-0.07	-0.11
Rn.11346	Pla2g2a	Phospholipase A2, Group Iia (Platelets, Synovial Fluid)	-0.34	-0.62	-0.07	-0.38
Rn.10162	Pla2g4a	Phospholipase A2, Group Iva (Cytosolic, Calcium-Dependent)	1.05	1.81	0.51	0.18
Rn.20244	Pla2g5	Phospholipase A2, Group V	-0.19	-0.34	-0.12	0.11
Rn.44692	Pla2g6	Phospholipase A2, Group Vi	-0.06	-0.03	0.28	0.41
Rn.6828	Pla2g10	Phospholipase A2, Group X	0.00	-0.37	-0.24	-0.29

Unigene ID	Gene Symbol	Description	Log Ratio (CD/CS) 4 wks	12 wks	80 wks	Tumors
Rn.45523	Plcb1	Phospholipase C, Beta 1	0.45	-0.28	0.41	0.35
Rn.64650	Plce1	Phospholipase C, Epsilon 1	-0.11	0.32	-0.63	-0.70
Rn.11243	Plcg1	Phospholipase C, Gamma 1	-0.01	0.04	0.21	0.35
Rn.44484	Pter	Phosphotriesterase Related	0.27	0.29	-0.55	1.40
Rn.7279	Phyh	Phytanoyl-Coa Hydroxylase (Refsum Disease)	-0.19	-0.40	-0.59	0.54
Rn.24751	Pafah1b2	Platelet-Activating Factor Acetylhydrolase Alpha 2 Subunit (Paf-Ah Alpha 2)	0.19	-0.07	-0.22	-0.37
Rn.17971	Pafah1b3	Platelet-Activating Factor Acetylhydrolase, Isoform 1B, Alpha1 Subunit	0.19	0.44	0.25	0.48
Rn.48685	Ptgdr2	Prostaglandin D2 Receptor	0.06	-0.15	-0.07	0.06
Rn.11400	Ptgds	Prostaglandin D2 Synthase	-0.15	-0.07	0.45	0.21
Rn.7730	Ptges	Prostaglandin E Synthase	0.06	-0.23	0.40	0.08
Rn.6332	Ptgfrn	Prostaglandin F2 Receptor Negative Regulator	0.05	0.34	-0.95	-1.22
Rn.73051	Ptgis	Prostaglandin I2 (Prostacyclin) Synthase	0.09	-0.06	0.04	-0.22
Rn.44404	Ptgs1	Prostaglandin-Endoperoxide Synthase 1	-0.20	0.50	-0.78	-0.89
Rn.64583	Prkaa2	Protein Kinase, Amp-Activated, Alpha 2 Catalytic Subunit	-0.76	-0.83	-0.22	0.09
Rn.3619	Prkab1	Protein Kinase, Amp-Activated, Beta 1 Non-Catalytic Subunit	-0.61	-0.52	0.13	0.58
Rn.48744	Prkab2	Protein Kinase, Amp-Activated, Beta 2 Non-Catalytic Subunit	-0.10	-0.24	0.04	-0.04
Rn.40816	Rxrg	Retinoid X Receptor Gamma	-0.45	-0.46	0.27	0.12
Rn.22142	Rdh10	Retinol Dehydrogenase 10 (All-Trans)	-0.01	-0.45	0.00	-0.24
Rn.94108	RoDHII	Retinol Dehydrogenase Type Ii (Rodh Ii)	1.00	0.03	-0.69	0.20
Rn.46850	Sec14l2	Sec14-Like 2 (S. Cerevisiae)	-0.53	-0.87	-0.54	-0.82
Rn.1167	Acads	Short Chain Acyl-Coenzyme A Dehydrogenase	0.01	-0.14	-0.20	0.09
Rn.3289	Slc25a20	Solute Carrier Family 25 (Carnitine/Acylcarnitine Translocase), Member 20	-0.24	-0.15	-0.39	-0.46
Rn.8368	Slc25a1	Solute Carrier Family 25, Member 1	-0.13	-0.22	-0.46	-0.35
Rn.1047	Slc27a1	Solute Carrier Family 27 (Fatty Acid Transporter), Member 1	-0.14	0.07	-0.07	-0.10
Rn.3608	Slc27a2	Solute Carrier Family 27 (Fatty Acid Transporter), Member 2	0.12	-0.06	-0.21	-0.20
Rn.33239	Sqle	Squalene Epoxidase	0.30	0.32	0.41	0.75
Rn.1023	Scd1	Stearoyl-Coenzyme A Desaturase 1	-0.71	-1.29	-0.71	-0.57
Rn.83595	Scd2	Stearoyl-Coenzyme A Desaturase 2	1.72	2.46	1.66	0.00
Rn.4620	Srd5a1	Steroid 5 Alpha-Reductase 1	-2.06	-1.36	-0.65	-1.27
Rn.2193	Ssg1	Steroid Sensitive Gene 1	1.02	2.23	0.13	-0.74
Rn.6312	Sts	Steroid Sulfatase	-0.84	-0.94	-0.65	1.12
Rn.11399	Star	Steroidogenic Acute Regulatory Protein	-0.06	-0.32	-0.05	-0.07
Rn.31887	Scp2	Sterol Carrier Protein 2	-0.11	-0.32	-0.44	-0.27
Rn.31887	Scp2	Sterol Carrier Protein 2	-0.09	-0.28	-0.57	-0.03
Rn.95306	Srebf1	Sterol Regulatory Element Binding Factor 1	0.14	-0.64	-0.78	-0.73
Rn.95306	Srebf1	Sterol Regulatory Element Binding Factor 1	0.07	-0.08	-0.44	-0.24
Rn.41474	Sult4a1	Sulfotransferase Family 4A, Member 1	-0.49	-0.25	-0.34	-0.24
Rn.16283	Tbxas1	Thromboxane A Synthase 1	0.33	0.31	0.05	-0.17
Rn.9975	Vldlr	Very Low Density Lipoprotein Receptor	0.66	0.49	0.92	0.33
Rn.9975	Vldlr	Very Low Density Lipoprotein Receptor	0.45	0.67	0.65	0.26
Apoptosis						
Rn.2104	App	amyloid beta (A4) precursor protein	-0.09	-0.03	0.20	-0.10
Rn.64522	Apaf1	apoptotic protease activating factor 1	1.30	0.99	0.28	-0.34
Rn.4279	Appbp1	APP-binding protein 1	-0.34	-0.29	0.08	-0.11

Unigene ID	Gene Symbol	Description	Log Ratio (CD/CS) 4 wks	12 wks	80 wks	Tumors
Rn.91239	Birc4	baculoviral IAP repeat-containing 4	0.41	0.54	0.10	0.98
Rn.13007	Bcl10	B-cell CLL/lymphoma 10	0.49	0.81	0.68	0.23
Rn.9996	Bcl2	B-cell leukemia/lymphoma 2	0.91	0.14	-0.65	-0.56
Rn.27923	Btg2	B-cell translocation gene 2, anti-proliferative	-0.17	-0.38	-0.06	0.04
Rn.27923	Btg2	B-cell translocation gene 2, anti-proliferative	0.84	1.30	0.60	1.83
Rn.8897	Btg3	B-cell translocation gene 3	-0.21	-0.22	0.03	0.02
Rn.83607	Bmf	Bcl2 modifying factor	-0.17	-0.27	-0.05	-0.28
Rn.2060	Bnip3	BCL2/adenovirus E1B 19 kDa-interacting protein 3	0.04	-0.06	-0.33	-0.18
Rn.827	Bnip3l	BCL2/adenovirus E1B 19 kDa-interacting protein 3-like	-0.04	-0.14	0.14	-0.16
Rn.14598	Bak1	BCL2-antagonist/killer 1	0.62	0.57	0.07	-0.01
Rn.10323	Bcl2l1	Bcl2-like 1	0.52	0.17	0.34	0.22
Rn.10323	Bcl2l1	Bcl2-like 1	-0.15	-0.19	-0.10	-0.10
Rn.44267	Bcl2l2	Bcl2-like 2	0.50	0.91	0.64	0.47
Rn.44461	Bok	Bcl-2-related ovarian killer protein	0.42	0.35	-0.04	-0.23
Rn.44461	Bok	Bcl-2-related ovarian killer protein	0.06	-0.05	-0.25	-0.17
Rn.19770	Bcl2a1	BCL2-related protein A1	0.26	-0.25	-0.18	-0.57
Rn.10119	Galgt1	beta-4N-acetylgalactosaminyltransferase	0.54	-0.23	-0.43	-0.67
Rn.89639	Bid3	BH3 interacting (with BCL2 family) domain, apoptosis agonist	-0.08	-0.21	-0.07	-0.18
Rn.108186	Btbd14b	BTB (POZ) domain containing 14B	0.31	-0.01	-0.35	-0.50
Rn.28010	Cflar	CASP8 and FADD-like apoptosis regulator	0.57	-0.06	0.28	0.44
Rn.37508	Casp1	caspase 1	1.55	1.79	0.89	0.20
Rn.81078	Casp12	caspase 12	0.52	1.06	0.35	0.17
Rn.1438	Casp2	caspase 2	0.65	0.72	0.18	-0.02
Rn.10562	Casp3	caspase 3	1.42	1.09	0.34	1.77
Rn.10562	Casp3	caspase 3	1.69	1.39	0.52	1.99
Rn.88160	Casp6	caspase 6	1.00	0.66	0.58	1.07
Rn.32199	Casp9	caspase 9	-0.67	-0.50	-0.76	-0.79
Rn.32199	Casp9	caspase 9	-0.12	-0.53	0.71	0.46
Rn.53995	Casp7	caspase-7	0.31	0.29	0.17	0.21
Rn.6479	Cebpb	CCAAT/enhancer binding protein (C/EBP), beta	-0.18	-0.26	0.12	0.35
Rn.60353	Dapkl	Death-associated like kinase	1.04	0.68	0.19	-0.29
Rn.1531	Dap	death-associated protein	-0.03	0.08	-0.02	0.41
Rn.7262	Dad1	defender against cell death 1	0.06	0.35	-0.20	-1.02
Rn.67077	Dffb	DNA fragmentation factor, 40 kD, beta polypeptide (caspase-activated DNase)	-0.06	0.13	-0.31	0.00
Rn.48799	Dffa	DNA fragmentation factor, alpha subunit	-0.40	0.08	-0.17	-0.12
Rn.45601	Edg8	endothelial differentiation, sphingolipid G-protein-coupled receptor, 8	0.46	1.18	0.73	-0.64
Rn.22800	Faim	Fas apoptotic inhibitory molecule	0.96	0.47	-0.03	-0.49
Rn.59459	Gnrh1	gonadotropin-releasing hormone 1	1.07	0.90	0.81	0.26
Rn.64578	Birc3	inhibitor of apoptosis protein 1	0.80	0.19	0.50	-0.17
Rn.9911	Mapk10	mitogen activated protein kinase 10	0.48	-0.53	0.85	0.40
Rn.44266	Mapk8ip	mitogen activated protein kinase 8 interacting protein	0.07	0.07	-0.02	-0.16
Rn.11081	Map3k1	mitogen activated protein kinase kinase kinase 1	0.64	0.33	0.23	0.30
Rn.4158	Asah	N-acylsphingosine amidohydrolase (acid ceramidase)	-0.07	-0.03	-0.22	-0.14
Rn.4158	Asah	N-acylsphingosine amidohydrolase (acid ceramidase)	1.38	0.82	0.65	0.44
Rn.127149	Asah2	N-acylsphingosine amidohydrolase 2	0.91	0.98	1.30	1.44
Rn.3126	Ngfrap1	nerve growth factor receptor associated protein 1	0.33	0.28	0.00	0.10
Rn.18572	Smpd2	neutral sphingomyelinase	0.19	-0.18	-0.12	-0.16

Unigene ID	Gene Symbol	Description	Log Ratio (CD/CS) 4 wks	12 wks	80 wks	Tumors
Rn.32919	Nsmaf	neutral sphingomyelinase (N-SMase) activation associated factor	0.34	0.18	0.31	0.40
Rn.2411	Nfkb1	Nuclear factor kappa B p105 subunit	-0.26	-0.32	-0.03	-0.13
Rn.40242	LOC246143	p75-like apoptosis-inducing death domain protein PLAIDD	0.02	0.41	0.24	-0.02
Rn.40242	LOC246143	p75-like apoptosis-inducing death domain protein PLAIDD	0.37	0.49	0.14	-0.09
Rn.6959	Pdcd2	Programmed cell death 2	0.12	0.28	0.24	0.36
Rn.90142	Pdcd4	programmed cell death 4	0.80	0.91	0.28	-0.17
Rn.8124	Pdcd8	programmed cell death 8 (apoptosis-inducing factor)	-0.41	0.06	-0.50	-0.32
Rn.98279	Prkcd	protein kinase C, delta	-0.10	-0.18	-0.16	-0.06
Rn.1495	Ppp1cc	protein phosphatase 1, catalytic subunit, gamma isoform	-0.22	-0.19	-0.03	-0.10
Rn.73852	Ppp1r14a	protein phosphatase 1, regulatory (inhibitor) subunit 14A	1.44	1.91	0.87	1.64
Rn.2773	Ppp1r14b	protein phosphatase 1, regulatory (inhibitor) subunit 14B	-0.01	-0.13	-0.17	0.02
Rn.87667	Ppp1r14c	protein phosphatase 1, regulatory (inhibitor) subunit 14c	0.02	-0.21	-0.15	-0.11
Rn.8898	Ppp2r2d	protein phosphatase 2, regulatory subunit B, delta isoform	-0.26	-0.23	-0.28	-0.10
Rn.817	Ptma	prothymosin alpha	0.63	0.68	0.59	0.56
Rn.91176	P2rx1	purinergic receptor P2X, ligand-gated ion channel, 1	0.29	0.35	0.15	0.12
Rn.92406	Smp2a	rat senescence marker protein 2A gene, exons 1 and 2	-0.07	0.12	-0.29	-0.03
Rn.91057	Rara	retinoic acid receptor, alpha	0.77	0.99	0.65	0.76
Rn.1300	Stk17b	serine/threonine kinase 17b (apoptosis-inducing)	-0.02	-0.04	0.00	-0.06
Rn.107226	Sh3kbp1	SH3-domain kinase binding protein 1	-0.08	-0.24	0.16	-0.10
Rn.22706	Siat9	sialyltransferase 9 (CMP-NeuAc:lactosylceramide alpha-2,3-sialyltransferase; GM3 synthase)	-0.12	-0.21	-0.07	-0.04
Rn.18522	Sphk1	sphingosine kinase 1	-0.03	-0.12	-0.09	-0.10
Rn.2398	Tieg	TGFB inducible early growth response	-0.07	-0.40	-0.18	-0.05
Rn.10	Tgm2	tissue-type transglutaminase	0.99	1.16	0.97	0.36
Rn.10	Tgm2	tissue-type transglutaminase	0.01	0.05	-0.04	-0.08
Rn.9792	Tnfrsf11b	tumor necrosis factor receptor superfamily, member 11b (osteoprotegerin)	0.07	0.16	-0.04	0.25
Rn.11119	Tnfrsf1a	tumor necrosis factor receptor superfamily, member 1a	0.02	0.33	0.13	0.25
Rn.54443	Tp53	tumor protein p53	0.80	1.05	0.93	0.73
Rn.24091	Ugcg	UDP-glucose ceramide glucosyltransferase	0.56	0.28	0.36	0.23
Rn.9744	Ugt8	UDP-glucuronosyltransferase 8	0.57	0.38	0.33	0.34
Rn.9744	Ugt8	UDP-glucuronosyltransferase 8	0.89	0.44	0.45	0.63
Rn.88756	Ets1	v-ets erythroblastosis virus E26 oncogene homolog 1 (avian)	-0.32	-0.08	0.22	0.29
Proliferation						
Rn.11204	Bmyc	Avian Myelocytomatosis Viral (V-Myc) Related Oncogene	0.50	0.65	0.34	0.58
Rn.103225	Brca2	Breast Cancer 2	0.98	1.16	0.62	0.45
Rn.1303	Cdh1	Cadherin 1	0.30	0.13	0.14	0.30
Rn.8046	Csnk1d	Casein Kinase 1, Delta	1.17	1.13	0.07	0.30
Rn.12365	Csnk1e	Casein Kinase 1, Epsilon	1.02	0.82	0.16	0.39
Rn.11380	Hsd3b7	Cca2 Protein	0.21	1.61	0.26	-0.24
Rn.64487	Arhgef9	Cdc42 Guanine Nucleotide Exchange Factor (Gef) 9	0.34	0.60	0.17	0.08
Rn.105815	Cdc42bpb	Cdc42-Binding Protein Kinase Beta	0.71	1.27	0.76	1.30
Rn.7070	---	Cdk104 Mrna	1.35	2.22	1.07	1.67
Rn.15195	Cdk105	Cdk105 Protein	1.72	2.61	1.49	2.00
Rn.25368	Cdk5rap2	Cdk5 Activator-Binding Protein	0.46	0.11	0.33	0.28

Unigene ID	Gene Symbol	Description	Log Ratio (CD/CS) 4 wks	12 wks	80 wks	Tumors
Rn.9262	Cdc20	Cell Cycle Protein P55Cdc	0.34	0.55	0.31	0.04
Rn.9262	Cdc20	Cell Cycle Protein P55Cdc	-0.06	-0.23	-0.11	-0.13
Rn.6934	Cdc2a	Cell Division Cycle 2 Homolog A (S. Pombe)	0.09	-0.04	-0.17	0.02
Rn.54977	Cdc5l	Cell Division Cycle 5-Like (S. Pombe)	1.36	1.39	0.65	0.11
Rn.31842	Cgref1	Cell Growth Regulator With Ef Hand Domain 1	0.17	0.26	0.51	0.56
Rn.87514	Cgrrf1	Cell Growth Regulator With Ring Finger Domain 1	-0.13	0.20	-0.09	-0.19
Rn.9232	Ccnb1	Cyclin B1	0.74	0.95	0.45	0.54
Rn.9232	Ccnb1	Cyclin B1	0.44	0.41	0.07	0.20
Rn.106758	Ccnc	Cyclin C	-0.04	0.21	-0.04	0.38
Rn.22279	Ccnd1	Cyclin D1	0.16	0.44	0.40	0.72
Rn.22279	Ccnd1	Cyclin D1	0.21	0.32	-0.17	1.22
Rn.22279	Ccnd1	Cyclin D1	0.07	-0.14	-0.18	-0.14
Rn.96083	Ccnd2	Cyclin D2	0.21	0.26	0.10	0.25
Rn.3483	Ccnd3	Cyclin D3	0.95	0.34	-0.50	-0.15
Rn.11012	Gak	Cyclin G Associated Kinase	0.12	0.32	-0.38	-0.66
Rn.5834	Ccng1	Cyclin G1	0.02	-0.11	0.17	-0.04
Rn.6115	Cdk4	Cyclin-Dependent Kinase 4	0.22	0.51	0.32	0.32
Rn.10089	Cdkn1a	Cyclin-Dependent Kinase Inhibitor 1A	-0.31	-0.18	0.15	0.42
Rn.29897	Cdkn1b	Cyclin-Dependent Kinase Inhibitor 1B	-0.14	0.01	-0.06	-0.25
Rn.29897	Cdkn1b	Cyclin-Dependent Kinase Inhibitor 1B	0.39	0.33	0.67	0.45
Rn.92509	Cdkn1c	Cyclin-Dependent Kinase Inhibitor 1C, P57	0.15	0.26	0.08	0.15
Rn.105626	Cdkn2b	Cyclin-Dependent Kinase Inhibitor 2B (P15, Inhibits Cdk4)	-0.11	0.23	0.38	0.11
Rn.63865	Cdkn2c	Cyclin-Dependent Kinase Inhibitor 2C (P18, Inhibits Cdk4)	0.56	0.48	0.60	0.57
Rn.11274	Dbp	D Site Albumin Promoter Binding Protein	0.14	0.03	0.00	-0.32
Rn.27546	Dek	Dek Oncogene (Dna Binding)	-0.14	-0.11	0.11	0.18
Rn.20467	Lig1	Dna Ligase I	-0.20	-0.37	0.06	-0.15
Rn.88690	Pold1	Dna Polymerase Delta, Catalytic Subunit	0.06	0.40	0.39	0.53
Rn.92497	Prim1	Dna Primase, P49 Subunit	0.09	0.17	0.18	0.33
Rn.11027	Dnch1	Dynein, Cytoplasmic, Heavy Chain 1	1.56	1.02	0.47	0.59
Rn.44896	Dnch2	Dynein, Cytoplasmic, Heavy Polypeptide 2	1.86	0.76	0.43	0.27
Rn.11273	Dncic1	Dynein, Cytoplasmic, Intermediate Chain 1	2.48	1.55	0.42	0.46
Rn.35769	Pin	Dynein, Cytoplasmic, Light Chain 1	-1.50	-0.14	-0.88	-0.94
Rn.2064	Dncli1	Dynein, Cytoplasmic, Light Intermediate Chain 1	0.48	0.48	0.19	0.32
Rn.4223	Dkc1	Dyskeratosis Congenita 1, Dyskerin	-0.04	0.11	0.07	0.04
Rn.52317	E2f5	E2F Transcription Factor 5	0.02	0.00	0.12	0.31
Rn.37227	Egfr	Epidermal Growth Factor Receptor	-0.16	-0.12	-0.20	-0.38
Rn.42897	Ereg	Epiregulin	0.11	0.74	1.39	0.63
Rn.36412	Fabp1	Fatty Acid Binding Protein 1, Liver	0.30	0.46	-0.05	0.06
Rn.1699	Fbln5	Fibulin 5	0.17	0.16	0.25	0.09
Rn.11008	Frap1	Fk506 Binding Protein 12-Rapamycin Associated Protein 1	-0.16	0.06	-0.14	0.24
Rn.22304	Bat3	Hla-B-Associated Transcript 3	-0.22	-0.18	-0.01	0.11
Rn.22304	Bat3	Hla-B-Associated Transcript 3	0.48	-0.16	0.08	-0.02
Rn.964	Igf2	Insulin-Like Growth Factor 2	0.10	0.10	0.27	0.16
Rn.34026	Igfbp1	Insulin-Like Growth Factor Binding Protein 1	-0.12	-0.20	0.00	-0.08
Rn.26369	Igfbp3	Insulin-Like Growth Factor Binding Protein 3	0.04	-0.25	0.01	0.09
Rn.1593	Igfbp5	Insulin-Like Growth Factor Binding Protein 5	0.31	0.27	0.01	0.17
Rn.6446	Ilkap	Integrin-Linked Kinase-Associated Serine/Threonine	1.94	1.55	0.59	0.80

Unigene ID	Gene Symbol	Description	Log Ratio (CD/CS) 4 wks	12 wks	80 wks	Tumors
		Phosphatase 2C				
Rn.7990	LOC246046	Liver Regeneration P-53 Related Protein	0.41	0.21	0.26	0.40
Rn.7990	LOC246046	Liver Regeneration P-53 Related Protein	0.66	0.74	0.53	0.48
Rn.4338	Lyn	Lyn Protein Non-Receptor Kinase	0.30	0.13	0.09	0.27
Rn.81062	Mcf2l	Mcf.2 Cell Line Derived Transforming Sequence-Like	0.31	-0.13	-0.08	0.66
Rn.5850	Map2k1	Mitogen Activated Protein Kinase Kinase 1	0.33	0.42	0.05	0.20
Rn.82693	Map2k2	Mitogen Activated Protein Kinase Kinase 2	-0.13	-0.26	-0.06	-0.08
Rn.40328	Map3k12	Mitogen Activated Protein Kinase Kinase Kinase 12	0.68	0.38	0.13	0.44
Rn.42944	Mapk12	Mitogen-Activated Protein Kinase 12	0.81	0.47	0.65	0.37
Rn.33262	Raf1	Murine Leukemia Viral (V-Raf-1) Oncogene Homolog 1 (3611-Msv)	-0.18	-0.20	-0.08	-0.27
Rn.88821	Fbxo2	Neural F Box Protein Nfb42	0.25	0.45	0.37	0.25
Rn.4073	Nbl1	Neuroblastoma, Suppression Of Tumorigenicity 1	0.52	0.60	1.72	0.92
Rn.8395	Nfkbib	Nuclear Factor Of Kappa Light Chain Gene Enhancer In B-Cells Inhibitor, Beta	0.56	0.53	0.76	0.46
Rn.66392	Numa1	Nuclear Mitotic Apparatus Protein 1	0.56	0.53	0.76	0.46
Rn.4110	Ns	Nucleostemin	-0.05	-0.19	-0.17	-0.18
Rn.25935	Per2	Period Homolog 2 (Drosophila)	-0.19	-0.42	-0.07	2.20
Rn.1476	Pmp22	Peripheral Myelin Protein 22	0.07	-0.17	-0.02	-0.37
Rn.10999	Pdgfa	Platelet Derived Growth Factor, Alpha	0.43	0.74	0.18	0.20
Rn.64626	Pdgfc	Platelet-Derived Growth Factor, C Polypeptide	0.47	0.92	0.26	0.05
Rn.9346	Polb	Polymerase (Dna Directed), Beta	0.13	-0.03	0.81	0.77
Rn.40977	Pole	Polymerase (Dna Directed), Epsilon	0.17	0.05	-0.16	0.24
Rn.19327	Polg	Polymerase (Dna Directed), Gamma	0.00	0.24	0.32	0.34
Rn.106248	Polr2g	Polymerase (Rna) Ii (Dna Directed) Polypeptide G	0.05	-0.43	0.01	0.03
Rn.28212	Polr2f	Polymerase Ii	-0.23	-0.41	-0.52	-0.01
Rn.48808	Porf1	Preoptic Regulatory Factor-1	-0.20	-0.56	-0.62	-0.15
Rn.82757	Prok1	Prokineticin 1 Precursor	-0.07	0.06	0.08	0.60
Rn.223	Pcna	Proliferating Cell Nuclear Antigen	-0.02	0.95	2.18	2.16
Rn.20465	PAL31	Proliferation Related Acidic Leucine Rich Protein Pal31	0.45	1.20	0.27	0.40
Rn.20465	PAL31	Proliferation Related Acidic Leucine Rich Protein Pal31	0.38	0.27	0.25	0.26
Rn.12281	Prkcdbp	Protein Kinase C, Delta Binding Protein	0.03	-0.24	-0.03	-0.03
Rn.2024	Ppp1ca	Protein Phosphatase 1, Catalytic Subunit, Alpha Isoform	-0.17	-0.45	-0.17	-0.18
Rn.34888	Pim1	Proviral Integration Site 1	0.21	0.36	0.25	0.45
Rn.107698	Ran	Ran, Member Ras Oncogene Family	-0.27	0.20	0.19	0.42
Rn.108215	Stk6	Serine/Threonine Kinase 6	0.28	0.18	-0.20	-0.21
Rn.14527	Sycp2	Synaptonemal Complex Protein 2	-0.19	-0.26	-0.27	-0.43
Rn.5890	Tep1	Telomerase Associated Protein 1	-0.44	-0.39	-0.18	-0.22
Rn.10576	Thpo	Thrombopoietin	-0.34	-0.35	-0.25	-0.17
Rn.90996	Top2a	Topoisomerase (Dna) 2 Alpha	-0.15	0.37	0.43	0.63
Rn.90996	Top2a	Topoisomerase (Dna) 2 Alpha	0.47	0.79	0.62	0.81
Rn.91572	Top1	Topoisomerase (Dna) I	0.17	0.15	-0.07	0.10
Rn.13425	Tm4sf4	Transmembrane 4 Superfamily Member 4	-0.04	-0.44	0.02	-0.01
Rn.64517	Tnfsf11	Tumor Necrosis Factor (Ligand) Superfamily, Member 11	0.81	0.81	0.89	0.09
Rn.30043	Tnfsf4	Tumor Necrosis Factor (Ligand) Superfamily, Member 4	-0.20	-0.44	-0.11	-0.22
Rn.31075	---	Tumor Necrosis Factor Alpha-Induced Protein 1-Like Protein	0.23	0.40	0.22	0.44
Rn.105040	Tnfrsf12a	Tumor Necrosis Factor Receptor Superfamily, Member 12A	0.17	0.09	-0.18	0.14

Unigene ID	Gene Symbol	Description	Log Ratio (CD/CS) 4 wks	12 wks	80 wks	Tumors
Rn.36610	Tpt1	Tumor Protein, Translationally-Controlled 1	-0.26	-0.13	-0.01	-0.28
Rn.2758	Txnip	Upregulated By 1,25-Dihydroxyvitamin D-3	-0.29	0.04	0.20	-0.41
Rn.93714	Jun	V-Jun Sarcoma Virus 17 Oncogene Homolog (Avian)	0.35	0.08	-0.39	-0.40
Rn.93714	Jun	V-Jun Sarcoma Virus 17 Oncogene Homolog (Avian)	-0.43	-0.17	-0.15	-0.23
Rn.93714	Jun	V-Jun Sarcoma Virus 17 Oncogene Homolog (Avian)	-0.13	-0.02	0.21	0.46
Rn.10725	Mafb	V-Maf Musculoaponeurotic Fibrosarcoma Oncogene Family, Protein B (Avian)	0.24	0.01	-0.02	-0.12
Rn.3818	Mafk	V-Maf Musculoaponeurotic Fibrosarcoma Oncogene Family, Protein K (Avian)	0.38	0.18	-0.56	-0.32
Rn.3193	Wfdc1	Wap Four-Disulfide Core Domain 1	0.35	0.23	-0.12	-0.46
Rn.11908	Zrf2	Zuotin Related Factor 2	-0.13	-0.32	0.09	-0.02
Tissue Remodeling						
Rn.54393	Adam23	A Disintegrin And Metalloprotease Domain 23	-0.05	-0.09	-0.13	-0.08
Rn.42918	Adam3	A Disintegrin And Metalloprotease Domain 3 (Cyritestin)	-0.34	-0.24	0.01	0.09
Rn.10357	Adam7	A Disintegrin And Metalloprotease Domain 7	-0.24	-0.27	0.07	0.08
Rn.42919	Adam1	A Disintegrin And Metalloproteinase Domain 1 (Fertilin Alpha)	-0.09	-0.25	-0.04	-0.03
Rn.98788	Adam15	A Disintegrin And Metalloproteinase Domain 15 (Metargidin)	-0.14	0.18	0.22	0.02
Rn.24102	Adam17	A Disintegrin And Metalloproteinase Domain 17 (Tumor Necrosis Factor, Alpha, Converting Enzyme)	0.53	0.56	0.10	0.15
Rn.42923	Adam18	A Disintegrin And Metalloproteinase Domain 18	0.01	-0.41	-0.09	-0.03
Rn.24189	Adam6	A Disintegrin And Metalloproteinase Domain 6	-0.12	-0.25	-0.23	-0.23
Rn.25221	Adam9	A Disintegrin And Metalloproteinase Domain 9 (Meltrin Gamma)	-0.16	-0.14	-0.16	-0.22
Rn.2090	Arpc1b	Actin Related Protein 2/3 Complex, Subunit 1B	1.25	1.68	0.91	0.34
Rn.94978	Actb	Actin, Beta	0.44	0.60	0.15	-0.13
Rn.94978	Actb	Actin, Beta	0.34	0.73	0.15	-0.51
Rn.11353	Add2	Adducin 2 (Beta)	-0.14	-0.19	-0.07	-0.08
Rn.76589	Add3	Adducin 3 (Gamma)	0.03	0.21	0.23	0.03
Rn.6993	Arf6	Adp-Ribosylation Factor 6	0.68	0.37	0.06	-0.08
Rn.54503	Agc1	Aggrecan 1	-0.03	-0.52	0.04	0.05
Rn.5812	Spna2	Alpha-Spectrin 2	-0.46	0.53	-0.36	-0.19
Rn.11149	Abtb2	Ankyrin Repeat And Btb (Poz) Domain Containing 2	-0.18	-0.29	0.06	-0.14
Rn.10624	Atp1b2	Atpase, Na+/K+ Transporting, Beta 2 Polypeptide	-0.01	-0.20	-0.16	-0.08
Rn.2269	Bsg	Basigin	0.27	0.37	-0.17	-0.44
Rn.48895	Bace	Beta-Site App Cleaving Enzyme	-0.08	-0.26	-0.13	-0.33
Rn.783	Bgn	Biglycan	1.24	1.80	0.43	-0.44
Rn.40101	Bcar1	Breast Cancer Anti-Estrogen Resistance 1	-0.17	-0.13	-0.49	1.09
Rn.10315	Bcan	Brevican	-0.18	-0.33	-0.09	-0.01
Rn.76726	Cdh17	Cadherin 17	1.26	0.66	0.10	0.48
Rn.10390	Cdh6	Cadherin 6	-0.05	-0.14	-0.15	-0.21
Rn.6822	Capn2	Calpain 2	0.65	1.21	0.59	-0.28
Rn.9726	Capn3	Calpain 3	-0.24	-0.32	0.03	-0.06
Rn.3430	Capns1	Calpain, Small Subunit 1	0.39	0.46	-0.17	-0.33
Rn.57635	Cnn3	Calponin 3, Acidic	0.65	1.17	0.22	-0.87
Rn.112585	Cap1	Cap, Adenylate Cyclase-Associated Protein 1 (Yeast)	0.94	1.16	0.74	0.43
Rn.10229	Cap2	Cap, Adenylate Cyclase-Associated Protein, 2 (Yeast)	-0.12	-0.12	-0.02	-0.03
Rn.42865	Capza3	Capping Protein (Actin Filament) Muscle Z-Line, Alpha 3	-0.32	-0.31	-0.04	0.02
Rn.12572	Cpb2	Carboxypeptidase B2 (Plasma)	-0.18	-0.36	-0.23	-0.39

Unigene ID	Gene Symbol	Description	Log Ratio (CD/CS) 4 wks	12 wks	80 wks	Tumors
Rn.41757	Cpn1	Carboxypeptidase N, Polypeptide 1, 50Kd	0.14	0.27	0.40	0.42
Rn.11056	Cpz	Carboxypeptidase Z	0.04	0.32	-0.06	-0.40
Rn.10343	Comp	Cartilage Oligomeric Matrix Protein	-0.70	-0.34	0.01	-0.18
Rn.107912	Ctsc	Cathepsin C	0.20	-0.16	-0.25	-0.97
Rn.11085	Ctsd	Cathepsin D	0.80	0.96	0.33	0.06
Rn.1997	Ctsh	Cathepsin H	-0.10	0.17	-0.29	-0.27
Rn.1294	Ctsl	Cathepsin L	0.35	0.63	0.49	0.60
Rn.1294	Ctsl	Cathepsin L	0.30	0.92	0.28	0.70
Rn.98382	Ctsql2	Cathepsin Q-Like 2	0.04	-0.15	-0.18	-0.11
Rn.1475	LOC252929	Cathepsin Y	0.83	0.97	1.24	0.12
Rn.98191	Cav3	Caveolin 3	-0.10	-0.25	-0.24	-0.29
Rn.60067	Cdc42	Cell Division Cycle 42 Homolog (S. Cerevisiae)	0.23	0.71	0.16	0.24
Rn.60067	Cdc42	Cell Division Cycle 42 Homolog (S. Cerevisiae)	0.40	0.62	0.19	0.17
Rn.63352	Ctrl	Chymotrypsin-Like	-0.09	-0.26	-0.01	0.03
Rn.105845	Ctrb	Chymotrypsinogen B	-0.25	-0.20	-0.03	-0.13
Rn.19943	Clasp2	Clip-Associating Protein 2	0.08	0.48	0.06	0.18
Rn.1780	Clu	Clusterin	0.88	0.62	-0.02	-0.43
Rn.2953	COLIA1	Collagen, Type 1, Alpha 1	0.53	0.90	0.13	-0.06
Rn.2953	COLIA1	Collagen, Type 1, Alpha 1	2.92	3.76	0.66	0.19
Rn.3247	Col3a1	Collagen, Type Iii, Alpha 1	1.50	1.91	0.13	-0.12
Rn.2875	Col5a2	Collagen, Type V, Alpha 2	0.45	0.62	0.18	0.25
Rn.2819	Coro1b	Coronin, Actin-Binding Protein, 1B	-0.16	-0.53	-0.09	-0.02
Rn.18514	Cst8	Cystatin 8	0.67	1.13	0.94	0.11
Rn.106351	Cst3	Cystatin C	-0.21	-0.13	-0.19	-0.24
Rn.86411	LOC257643	Cystatin Sc	-0.07	-0.08	-0.15	-0.06
Rn.58124	LOC266776	Cystatin Te-1	0.27	0.65	-0.67	-1.07
Rn.108075	Csrp1	Cysteine And Glycine-Rich Protein 1	0.65	0.64	0.45	0.26
Rn.22129	Cyr61	Cysteine Rich Protein 61	-0.05	0.34	0.40	0.21
Rn.9887	Krt21	Cytokeratin 21	1.40	2.55	0.87	-0.30
Rn.106103	Dcn	Decorin	-0.01	-0.06	-0.50	-1.24
Rn.91364	Dpp4	Dipeptidylpeptidase 4	-0.12	0.01	-0.29	-0.24
Rn.91364	Dpp4	Dipeptidylpeptidase 4	-0.11	-0.37	-0.09	-0.16
Rn.10076	Dpp6	Dipeptidylpeptidase 6	1.91	1.96	1.17	2.52
Rn.3363	Dpp7	Dipeptidylpeptidase 7	0.12	0.36	0.49	0.27
Rn.7807	Ddr1	Discoidin Domain Receptor Family, Member 1	-0.13	-0.22	-0.10	-0.26
Rn.74705	Dcbld2	Discoidin, Cub And Lccl Domain Containing 2	0.33	0.28	0.25	0.05
Rn.11247	Dbn1	Drebrin 1	0.39	0.49	0.12	0.05
Rn.4115	Dbnl	Drebrin-Like	0.45	0.65	0.04	0.18
Rn.11284	Dctn1	Dynactin 1	-0.17	-0.19	-0.09	-0.28
Rn.10307	Dmd	Dystrophin	0.20	0.28	1.80	3.39
Rn.6044	Ela1	Elastase 1, Pancreatic	0.25	0.42	0.22	0.21
Rn.16221	Emb	Embigin	1.42	1.51	-0.01	-1.64
Rn.3603	Ephx1	Epoxide Hydrolase 1	-0.09	-0.30	0.03	0.81
Rn.91373	Espn	Espin	1.11	1.54	0.29	-0.05
Rn.12759	Fbn1	Fibrillin-1	0.73	1.23	0.13	-0.17
Rn.12759	Fbn1	Fibrillin-1	-0.26	-0.22	0.06	-0.11
Rn.22906	Fbn2	Fibrillin-2	-0.14	-0.28	0.10	0.07
Rn.82756	Fap	Fibroblast Activation Protein	0.49	1.04	-0.06	-0.16

Unigene ID	Gene Symbol	Description	Log Ratio (CD/CS) 4 wks	12 wks	80 wks	Tumors
Rn.15709	Fgf13	Fibroblast Growth Factor 13	-0.12	-0.21	-0.03	0.03
Rn.44476	Fgf14	Fibroblast Growth Factor 14	2.54	-0.60	3.26	2.45
Rn.81231	Fgf21	Fibroblast Growth Factor 21	-0.27	-0.25	-0.05	-0.06
Rn.81232	Fgf22	Fibroblast Growth Factor 22	-0.12	-0.25	-0.12	-0.13
Rn.81229	Fgf23	Fibroblast Growth Factor 23	-0.23	-0.22	-0.09	-0.10
Rn.81236	Fgf3	Fibroblast Growth Factor 3	-0.11	-0.55	0.22	0.02
Rn.98842	Fgf7	Fibroblast Growth Factor 7	-0.15	-0.28	0.01	-0.12
Rn.73565	Fgf8	Fibroblast Growth Factor 8	-0.17	-0.33	-0.06	-0.09
Rn.25174	Fgf9	Fibroblast Growth Factor 9	-0.01	0.47	0.40	0.20
Rn.9797	Fgfr1	Fibroblast Growth Factor Receptor 1	0.01	0.20	0.24	0.13
Rn.9797	Fgfr1	Fibroblast Growth Factor Receptor 1	0.36	0.15	-0.13	-0.27
Rn.12732	Fgfr2	Fibroblast Growth Factor Receptor 2	0.15	0.49	1.16	0.38
Rn.23671	Fgfr3	Fibroblast Growth Factor Receptor 3	-0.31	-0.32	-0.24	-0.13
Rn.89278	Folh1	Folate Hydrolase	-1.09	-1.61	-0.96	-0.45
Rn.20140	Ftcd	Formiminotransferase Cyclodeaminase	0.23	0.28	-0.06	0.13
Rn.8411	Gabarap	Gamma-Aminobutyric Acid Receptor Associated Protein	0.29	-0.22	-0.40	-0.24
Rn.1437	Gc	Group Specific Component	-0.35	-0.37	-0.45	-0.43
Rn.11139	Hpn	Hepsin	-0.18	-0.24	-0.10	-0.08
Rn.50531	Hapln1	Hyaluronan And Proteoglycan Link Protein 1	-0.33	-0.29	-0.12	-0.19
Rn.76545	Hapln2	Hyaluronan And Proteoglycan Link Protein 2	-0.44	-0.60	-0.59	-1.04
Rn.7327	Igfals	Insulin-Like Growth Factor Binding Protein, Acid Labile Subunit	-0.15	-0.26	-0.23	-0.34
Rn.54492	Itga7	Integrin Alpha 7	-0.03	-0.41	-0.07	-0.33
Rn.54492	Itga7	Integrin Alpha 7	-0.20	-0.11	0.03	-0.17
Rn.54465	Itgam	Integrin Alpha M	0.93	1.12	0.56	0.09
Rn.25733	Itgb1	Integrin Beta 1	1.16	1.35	0.23	-0.49
Rn.25733	Itgb1	Integrin Beta 1	0.00	0.78	0.24	0.18
Rn.10727	Itgb4	Integrin Beta 4	-0.07	-0.18	-0.15	-0.06
Rn.9721	Ibsp	Integrin Binding Sialoprotein	0.83	0.59	-0.30	-1.00
Rn.12	Icam1	Intercellular Adhesion Molecule 1	-0.02	-0.10	-0.16	-0.06
Rn.64488	Impg1	Interphotoreceptor Matrix Proteoglycan 1	-0.31	-0.43	0.11	-0.20
Rn.41153	Ka14	Keratin Complex 1, Acidic, Gene 14	-0.09	1.80	1.86	1.05
Rn.9359	Krt1-19	Keratin Complex 1, Acidic, Gene 19	0.76	2.09	0.21	0.24
Rn.11083	Krt2-8	Keratin Complex 2, Basic, Gene 8	-0.24	-0.46	-0.26	-0.43
Rn.6526	Kif1b	Kinesin Family Member 1B	0.67	1.01	-0.01	0.30
Rn.89698	Kif1c	Kinesin Family Member 1C	0.01	0.04	0.08	-0.20
Rn.47400	Kif3a	Kinesin Family Member 3A	-0.06	-0.21	-0.20	-0.38
Rn.10894	Kif3c	Kinesin Family Member 3C	-0.27	-0.26	0.12	-0.04
Rn.41871	Klc3	Kinesin Light Chain 3	0.14	-0.02	0.32	0.21
Rn.45205	Knsl7	Kinesin-Like 7	0.46	0.61	-0.09	0.16
Rn.44161	Lmna	Lamin A	0.72	1.16	0.02	0.24
Rn.44161	Lmna	Lamin A	0.01	-0.06	0.03	-0.06
Rn.11362	Lmnb1	Lamin B1	0.20	-0.16	0.63	-0.07
Rn.10597	Lama3	Laminin, Alpha 3	1.52	2.28	2.43	-0.08
Rn.57	Lgals1	Lectin, Galactose Binding, Soluble 1	2.16	2.90	1.09	0.37
Rn.764	Lgals3	Lectin, Galactose Binding, Soluble 3	0.06	-0.04	0.16	0.72
Rn.64588	Lgals5 /// Lgals9	Lectin, Galactose Binding, Soluble 5 /// Lectin, Galactose Binding, Soluble 9	-0.09	-0.41	-0.26	-0.13
Rn.6336	Lgals7	Lectin, Galactose Binding, Soluble 7	1.56	1.84	1.37	1.11

Unigene ID	Gene Symbol	Description	Log Ratio (CD/CS) 4 wks	12 wks	80 wks	Tumors
Rn.2982	Lgals2	Lectin, Galactoside-Binding, Soluble, 2 (Galectin 2)	1.35	2.10	1.23	0.40
Rn.3251	Lgals3bp	Lectin, Galactoside-Binding, Soluble, 3 Binding Protein	-0.14	-0.21	-0.16	-0.17
Rn.9656	Lgals4	Lectin, Galactoside-Binding, Soluble, 4 (Galectin 4)	-0.18	-0.21	-0.03	0.05
Rn.47037	Lman2	Lectin, Mannose-Binding 2	1.36	3.42	1.55	0.49
Rn.2379	Mgp	Matrix Gla Protein	-0.27	-0.72	-0.10	-0.20
Rn.9946	Mmp10	Matrix Metalloproteinase 10	0.17	-0.09	-0.13	-0.14
Rn.11123	Mmp11	Matrix Metalloproteinase 11	3.28	3.39	0.86	0.62
Rn.33193	Mmp12	Matrix Metalloproteinase 12	0.05	0.26	-0.17	-0.35
Rn.74064	Mmp16	Matrix Metalloproteinase 16	-0.10	-0.34	-0.14	-0.22
Rn.6422	Mmp2	Matrix Metalloproteinase 2 (72 Kda Type Iv Collagenase)	1.46	2.40	0.45	0.00
Rn.6422	Mmp2	Matrix Metalloproteinase 2 (72 Kda Type Iv Collagenase)	0.20	0.69	0.33	0.00
Rn.22562	Mmp23	Matrix Metalloproteinase 23	0.00	-0.15	-0.20	-0.01
Rn.10282	Mmp7	Matrix Metalloproteinase 7	-0.06	-0.09	0.05	-0.19
Rn.10209	Mmp9	Matrix Metalloproteinase 9 (Gelatinase B, 92-Kda Type Iv Collagenase)	-1.39	-0.79	-0.03	1.06
Rn.33598	Mme	Membrane Metallo Endopeptidase	-0.04	-0.27	-0.15	-0.09
Rn.102300	LOC361170	Metalloprotease/Disintegrin	-0.21	-0.22	0.07	0.10
Rn.11402	Mtap1a	Microtubule-Associated Protein 1 A	0.78	1.20	0.26	0.65
Rn.3135	Map1lc3a	Microtubule-Associated Protein 1 Light Chain 3 Alpha	-0.15	-0.34	-0.09	-0.01
Rn.98152	Map1b	Microtubule-Associated Protein 1B	0.53	0.59	0.07	0.14
Rn.91417	LOC367171	Microtubule-Associated Protein 4	-0.01	-0.24	-0.11	-0.02
Rn.2455	Mapt	Microtubule-Associated Protein Tau	1.06	0.25	-0.24	-0.05
Rn.7652	Mapre1	Microtubule-Associated Protein, Rp/Eb Family, Member 1	0.87	0.99	0.54	0.29
Rn.3742	Mfge8	Milk Fat Globule-Egf Factor 8 Protein	-0.44	-0.13	0.04	0.24
Rn.17256	Map2k6	Mitogen-Activated Protein Kinase Kinase 6	-0.09	0.75	0.84	0.42
Rn.10779	Muc1	Mucin 1, Transmembrane	-0.25	-0.24	-0.04	-0.11
Rn.24930	Muc4	Mucin 4	-0.18	-0.47	0.03	-0.16
Rn.10789	Muc5ac	Mucin 5, Subtypes A And C, Tracheobronchial/Gastric	-0.06	1.11	0.04	1.31
Rn.18860	Mucdhl	Mucin And Cadherin-Like	-0.14	-0.21	0.02	-0.10
Rn.87175	Madcam1	Mucosal Vascular Addressin Cell Adhesion Molecule 1	-0.35	-0.20	-0.14	-0.25
Rn.8997	Mpz	Myelin Protein Zero	-0.07	-0.29	-0.22	-0.02
Rn.87331	Mag	Myelin-Associated Glycoprotein	0.85	0.90	0.72	0.28
Rn.98166	Myh10	Myosin Heavy Chain 10, Non-Muscle	-0.16	-0.36	-0.14	-0.05
Rn.94969	Myh11	Myosin Heavy Chain 11	-0.21	-0.07	0.11	-0.05
Rn.48756	Loc192253	Myosin Heavy Chain Myr 8	-0.21	-0.04	-0.15	-0.17
Rn.54399	Myh6	Myosin Heavy Chain, Polypeptide 6	-0.55	-0.24	0.11	-0.05
Rn.54399	Myh6 /// Myh7	Myosin Heavy Chain, Polypeptide 6 /// Myosin, Heavy Polypeptide 7, Cardiac Muscle, Beta	0.47	0.45	0.10	0.33
Rn.33782	Myo9b	Myosin Ixb	-0.04	-0.34	-0.07	-0.10
Rn.81191	Mylk2	Myosin Light Chain Kinase 2, Skeletal Muscle	0.59	0.57	0.13	0.59
Rn.6021	Mrlcb	Myosin Regulatory Light Chain	0.75	1.32	0.44	0.52
Rn.103179	Mrlcb	Myosin Regulatory Light Chain	-0.16	-0.32	-0.24	-0.13
Rn.34319	Myh13	Myosin, Heavy Polypeptide 13, Skeletal Muscle	-0.05	-0.17	-0.28	-0.11
Rn.10092	Myh4	Myosin, Heavy Polypeptide 4	0.78	0.87	0.20	-0.10
Rn.11385	Myh9	Myosin, Heavy Polypeptide 9	1.54	1.94	0.55	-0.45
Rn.9560	Marcks	Myristoylated Alanine Rich Protein Kinase C Substrate	0.84	1.16	0.39	-0.13
Rn.9560	Marcks	Myristoylated Alanine Rich Protein Kinase C Substrate	1.27	2.20	0.90	0.00
Rn.9560	Marcks	Myristoylated Alanine Rich Protein Kinase C Substrate	0.17	0.51	0.40	-0.25

Unigene ID	Gene Symbol	Description	Log Ratio (CD/CS) 4 wks	12 wks	80 wks	Tumors
Rn.17097	Napsa	Napsin A Aspartic Peptidase	-0.08	-0.14	0.00	0.03
Rn.11331	Ngfg	Nerve Growth Factor, Gamma	-0.08	-0.32	-0.09	-0.08
Rn.10926	Nrxn3	Neurexin 3	-0.10	-0.36	-0.18	0.00
Rn.3048	Nfasc	Neurofascin	-0.19	-0.27	-0.10	-0.19
Rn.10263	Nlgn3	Neuroligin 3	-0.17	-0.33	0.16	0.06
Rn.10263	Nlgn3	Neuroligin 3	-0.37	-0.51	-0.38	-0.95
Rn.11029	Nln	Neurolysin (Metallopeptidase M3 Family)	-0.18	-0.13	-0.22	-0.13
Rn.10691	Nrcam	Neuron-Glia-Cam-Related Cell Adhesion Molecule	-0.22	-0.29	-0.11	-0.01
Rn.44474	Mmp8	Neutrophil Collagenease	-0.08	0.10	-0.24	0.06
Rn.105658	Nid	Nidogen (Entactin)	0.60	0.46	-0.13	-0.16
Rn.11245	Ninj1	Ninjurin 1	-0.30	0.13	-0.38	0.86
Rn.31429	Ocln	Occludin	0.11	0.49	-0.14	-0.48
Rn.31429	Ocln	Occludin	0.08	0.04	-0.35	-0.59
Rn.31429	Ocln	Occludin	-0.10	-0.36	-0.18	-0.13
Rn.11366	Opcml	Opioid-Binding Protein/Cell Adhesion Molecule-Like	0.06	0.05	0.11	0.37
Rn.9149	Pak1	P21 (Cdkn1A)-Activated Kinase 1	0.24	-0.17	-0.19	-0.11
Rn.3840	Pak2	P21 (Cdkn1A)-Activated Kinase 2	-0.14	-0.22	-0.14	-0.31
Rn.43875	Pga5	Pepsinogen 5, Group I (Pepsinogen A)	-0.16	-0.16	0.05	-0.01
Rn.11086	Prph1	Peripherin 1	-0.85	-1.07	-1.10	-1.19
Rn.17112	Pgcp	Plasma Glutamate Carboxypeptidase	-0.02	-0.47	-0.55	-0.99
Rn.32103	Pls3	Plastin 3 (T-Isoform)	0.08	0.33	0.59	0.23
Rn.1085	Plec1	Plectin	0.06	0.20	0.39	0.42
Rn.13805	Podxl	Podocalyxin-Like	-0.38	-0.23	-0.15	-0.04
Rn.13805	Podxl	Podocalyxin-Like	0.45	0.55	0.30	0.06
Rn.2910	Pcolce	Procollagen C-Proteinase Enhancer Protein	1.00	1.66	0.47	0.16
Rn.12945	Plod2	Procollagen Lysine, 2-Oxoglutarate 5-Dioxygenase 2	0.02	-0.09	-0.05	0.03
Rn.107239	Col1a2	Procollagen, Type I, Alpha 2	-0.14	-0.13	0.08	0.02
Rn.107239	Col1a2	Procollagen, Type I, Alpha 2	0.52	0.56	0.20	0.52
Rn.23928	Col11a1	Procollagen, Type Xi, Alpha 1	0.23	0.14	0.08	0.11
Rn.11218	Col12a1	Procollagen, Type Xii, Alpha 1	0.93	1.06	0.12	0.04
Rn.4445	Plod	Procollagen-Lysine, 2-Oxoglutarate 5-Dioxygenase (Lysine Hydroxylase, Ehlers-Danlos Syndrome Type Vi)	0.32	0.23	0.10	0.14
Rn.90152	Plod3	Procollagen-Lysine, 2-Oxoglutarate 5-Dioxygenase 3	0.59	0.14	0.48	0.47
Rn.1152	Pfn1	Profilin 1	0.78	0.61	0.55	-0.02
Rn.3515	Pfn2	Profilin 2	-0.05	-0.27	0.00	-0.11
Rn.11310	Ptpn21	Protein Tyrosine Phosphatase 2E	0.02	1.15	1.08	-0.43
Rn.53971	Ptpns1	Protein Tyrosine Phosphatase, Non-Receptor Type Substrate 1	0.82	0.70	0.49	0.18
Rn.10674	Prg2	Proteoglycan 2, Bone Marrow	0.69	0.63	-0.24	-0.81
Rn.40122	Pgsg	Proteoglycan Peptide Core Protein	0.90	1.04	-0.11	-0.85
Rn.95071	Rap1b	Rap1B, Member Of Ras Oncogene Family	-0.18	-0.11	-0.09	-0.05
Rn.98353	Reln	Reelin	0.74	1.45	1.21	1.03
Rn.98353	Reln	Reelin	-0.05	0.00	0.28	0.19
Rn.93200	Ret	Ret Proto-Oncogene	-0.16	-0.18	-0.21	-0.25
Rn.2108	Risc	Retinoid-Inducible Serine Caroboxypetidase	0.46	0.59	0.72	0.02
Rn.34221	Ril	Reversion Induced Lim Gene	1.78	2.04	0.51	0.36
Rn.89756	Rock1	Rho-Associated Kinase Beta	0.29	1.01	0.05	-0.14
Rn.28912	Evl	Rnb6	0.00	0.11	-0.06	-0.19

Unigene ID	Gene Symbol	Description	Log Ratio (CD/CS) 4 wks	12 wks	80 wks	Tumors
Rn.98989	Sparc	Secreted Acidic Cysteine Rich Glycoprotein	-0.32	-0.30	-0.71	-0.98
Rn.98989	Sparc	Secreted Acidic Cysteine Rich Glycoprotein	-1.17	-1.17	-0.92	-1.20
Rn.1451	Sepp1	Selenoprotein P, Plasma, 1	-0.23	-0.29	-0.01	-0.07
Rn.1451	Sepp1	Selenoprotein P, Plasma, 1	0.00	0.96	0.58	0.11
Rn.109007	Sap	Serum Amyloid P-Component	0.37	0.97	0.15	-0.01
Rn.10467	Slc12a3	Solute Carrier Family 12, Member 3	0.18	1.28	0.31	-0.30
Rn.3091	Sparcl1	Sparc-Like 1 (Mast9, Hevin)	0.29	0.43	0.70	0.35
Rn.93208	Spnb2	Spectrin Beta 2	-0.31	-0.21	-0.18	0.06
Rn.93208	Spnb2	Spectrin Beta 2	-0.12	-0.30	-0.07	-0.12
Rn.49170	St14	Suppression Of Tumorigenicity 14	-0.22	-0.44	0.07	-0.04
Rn.3926	Sftpc	Surfactant Associated Protein C	0.42	0.43	-0.49	-0.40
Rn.11348	Sftpd	Surfactant Associated Protein D	0.46	0.06	-0.66	-0.13
Rn.11343	Sftpa1	Surfactant, Pulmonary-Associated Protein A1	-0.40	-0.86	-0.62	-0.34
Rn.11176	Sdc1	Syndecan 1	-0.63	-0.90	-0.61	-0.89
Rn.11176	Sdc1	Syndecan 1	0.00	-0.29	-0.33	-0.26
Rn.11127	Sdc2	Syndecan 2	-0.14	-0.15	-0.20	-0.15
Rn.11127	Sdc2	Syndecan 2	0.27	-0.08	-0.63	-0.01
Rn.10504	Sdc3	Syndecan 3	-0.07	-0.15	-0.18	-0.03
Rn.2029	Sdc4	Syndecan 4	-0.16	-0.20	-0.15	-0.11
Rn.70527	Ssx2ip	Synovial Sarcoma, X Breakpoint 2 Interacting Protein	-0.18	0.00	-0.07	-0.38
Rn.11028	Tnr	Tenascin R	0.50	0.94	0.37	-0.61
Rn.32098	Tpx1	Testis Specific Protein 1	2.18	2.66	0.52	-0.03
Rn.11207	Thbs4	Thrombospondin 4	1.07	1.63	0.68	0.00
Rn.2605	Tmsb4x	Thymosin Beta-4	-0.09	-0.23	-0.34	0.00
Rn.25754	Timp1	Tissue Inhibitor Of Metalloproteinase 1	0.15	0.11	0.20	0.86
Rn.10161	Timp2	Tissue Inhibitor Of Metalloproteinase 2	0.24	0.14	0.15	0.14
Rn.119634	Timp3	Tissue Inhibitor Of Metalloproteinase 3 (Sorsby Fundus Dystrophy, Pseudoinflammatory)	-0.18	-0.30	-0.03	-0.12
Rn.28991	Tpp2	Tripeptidyl Peptidase Ii	-0.12	-0.31	-0.18	-0.03
Rn.43122	Tpbg	Trophoblast Glycoprotein	-0.15	-0.09	0.04	-0.15
Rn.8816	Tpbpa	Trophoblast Specific Protein Alpha	-0.24	-0.24	-0.01	0.10
Rn.1646	Tmod1	Tropomodulin 1	0.89	1.91	0.43	0.42
Rn.74047	Tmod2	Tropomodulin 2	1.04	1.36	0.20	-0.28
Rn.74047	Tmod2	Tropomodulin 2	-0.07	0.05	0.06	0.10
Rn.87540	Tpm1	Tropomyosin 1, Alpha	-0.03	-0.31	0.13	-0.14
Rn.87540	Tpm1	Tropomyosin 1, Alpha	-0.35	-0.36	-0.11	-0.24
Rn.87540	Tpm1	Tropomyosin 1, Alpha	1.26	0.67	0.40	-0.11
Rn.37575	Tpm3	Tropomyosin 3, Gamma	0.79	0.56	0.20	-0.08
Rn.37575	Tpm3	Tropomyosin 3, Gamma	0.26	0.13	0.02	0.06
Rn.108199	Tpm4	Tropomyosin 4	0.50	0.46	0.33	0.07
---	LOC286890	Tropomyosin Isoform 6	1.22	0.85	0.25	-0.08
Rn.37575	Tpm3	Tropomyosin Isoform 6	1.50	0.82	0.20	0.04
---	LOC286890	Tropomyosin Isoform 6	-0.20	-0.23	0.28	-0.07
---	LOC286890	Tropomyosin Isoform 6	-0.05	-0.36	0.00	-0.08
Rn.37575	LOC286890 /// Tpm3	Tropomyosin Isoform 6 /// Tropomyosin 3, Gamma	0.93	1.14	0.70	0.61
Rn.10699	TPSB1	Tryptase Beta 1	1.48	1.74	1.16	0.93
Rn.35128	Ttl	Tubulin Tyrosine Ligase	0.21	0.26	0.32	0.48
Rn.54749	Tuba1	Tubulin, Alpha 1	0.75	0.76	0.07	0.25

			Log Ratio (CD/CS)			
Unigene ID	**Gene Symbol**	**Description**	**4 wks**	**12 wks**	**80 wks**	**Tumors**
Rn.2458	Tubb5	Tubulin, Beta 5	0.00	-0.08	-0.10	-0.13
Rn.8218	Tubg1	Tubulin, Gamma 1	1.23	2.05	2.25	1.12
Rn.8883	Tyro3	Tyro3 Protein Tyrosine Kinase 3	1.43	2.42	1.90	0.71
Rn.112600	Src	Tyrosine Protein Kinase Pp60-C-Src	-0.09	-0.12	0.02	-0.16
Rn.773	Vil2	Villin 2	0.57	0.64	0.63	-0.07
Rn.2710	Vim	Vimentin	0.65	0.40	0.16	0.06
Rn.9978	Wap	Whey Acidic Protein	2.54	3.08	0.55	-1.15
Rn.7914	Waspip	Wiskott-Aldrich Syndrome Protein Interacting Protein	2.16	2.82	0.46	-0.18
Rn.107363	Zyx	Zyxin	2.38	3.04	0.36	-0.08

APPENDIX 2

Biological processes associated with liver injury transition states in choline deficient rats

Significant gene lists were generated using SAM (FDR < 5%) for each transition state (transition state 1 – chronic liver injury; transition state 2 – tumors) and cross-compared using Venn diagram (Figure 4). Those genes lists were submitted to GoMiner (34) to identify significantly enriched ($p < 0.05$) biological processes unique to transition state 1 (Appendix 2A) and transition state 2 (Appendix 2B), or shared (Appendix 2C and 2D). Note that the genes in common between the two transitions states were directionally opposite in expression of one another and this is reflected in Appendices 2C and 2D.

Appendix 2A	**Transition State 1**	
Gene Ontology – Biological Processes	**Down-Regulated**	**Up-Regulated**
Cellular Physiological Process		0.0005
Transport	0.0374	
Ion Transport	<0.0001	
Cation Transport	<0.0001	
Metal Ion Transport	<0.0001	
Monovalent Inorganic Cation Transport	<0.0001	
Potassium Ion Transport	<0.0001	
Sodium Ion Transport	0.0038	
Di-, Tri-valent Inorganic Ion Transport	0.0091	
Transition Metal Ion Transport		0.0133
Iron Ion Transport		0.0024
Calcium Ion Transport	<0.0001	
Neurotransmitter Transport	0.0015	
Vesicle-Mediated Transport		
Exocytosis	0.0249	
Calcium Ion-Dependent Exocytosis	0.0388	
Regulation of Exocytosis		
Regulation of Calcium Ion-Dependent Exocytosis	0.0390	
Secretory Pathway		
Regulated Secretory Pathway	0.0480	
Intracellular Transport		0.0033
Intracellular Protein Transport		
Protein Import		0.0397
Protein-Nucleus Import		0.0259
Nucleocytoplasmic Transport		0.0380
Nuclear Import		0.0259

Appendix 2A *Gene Ontology – Biological Processes*	Transition State 1 Down-Regulated	Transition State 1 Up-Regulated
Cytoskeleton-Dependent Intracellular Transport		0.0404
Nuclear Transport		0.0227
Cell Cycle		<0.0001
Regulation of Cell Cycle		0.0004
Cell Cycle Arrest		0.0197
Regulation of Mitotic Cell Cycle		0.0240
Mitotic Cell Cycle		0.0001
M Phase of Mitotic Cell Cycle		0.0061
Mitosis		0.0045
M Phase		0.0329
Interphase		0.0478
Interphase of Mitotic Cell Cycle		0.0478
Chromosome Segregation		0.0429
Cell Death		0.0423
Programmed Cell Death		0.0397
Apoptosis		0.0343
Apoptotic Program		0.0304
Caspase Activation		0.0045
Regulation of Apoptosis		0.0017
Negative Regulation of Caspase Activation		0.0107
Negative Regulation of Apoptosis		0.0303
Positive Regulation of Apoptosis		0.0144
Regulation of Caspase Activation		0.0105
Regulation of Programmed Cell Death		0.0022
Negative Regulation of Programmed Cell Death		0.0303
Positive Regulation of Programmed Cell Death		0.0166
Induction of Programmed Cell Death		0.0128
Induction of Apoptosis		0.0128
Cell Proliferation		
Regulation of Cell Proliferation		
Negative Regulation of Cell Proliferation		0.0064
Cell Organization and Biogenesis		<0.0001
Organelle Organization and Biogenesis		<0.0001
Cytoskeleton Organization and Biogenesis		<0.0001
Microtubule-Based Process		0.0002
Microtubule Cytoskeleton Organization and Biogenesis		0.0015

Appendix 2A *Gene Ontology – Biological Processes*	Transition State 1 Down-Regulated	Up-Regulated
Microtubule Nucleation		0.0030
Spindle Organization and Biogenesis		0.0107
Mitotic Spindle Organization and Biogenesis		0.0107
Microtubule-Based Movement		0.0294
Actin Filament-Based Process		0.0020
Actin Cytoskeleton Organization and Biogenesis		0.0030
Actin Filament Severing		0.0209
Ribosome Biogenesis and Assembly		<0.0001
Ribosome Biogenesis		<0.0001
Chromosome Organization and Biogenesis		0.0175
Chromosome Organization and Biogenesis (Sensu Eukaryota)		0.0259
Cytoplasm Organization and Biogenesis		<0.0001
Cell Division		0.0021
Cytokinesis		0.0022
Response to Stimulus		
Response to Stress		
Response to Heat		0.0299
Response to Pain	0.0334	
Response to Wounding		
Wound Healing	0.0191	
Response to External Stimulus	0.0015	
Detection of External Stimulus	<0.0001	
Detection of Abiotic Stimulus	0.0013	
Detection of Chemical Substance	0.0034	
Detection of Mechanical Stimulus	0.0388	
Sensory Perception of Mechanical Stimulus	0.0388	
Response to Abiotic Stimulus		
Response to Organic Substance	0.0173	
Response to Biotic Stimulus		
Cellular Defense Response		
Cell-mediated Immune Response		0.0404
Antigen Presentation		
Antigen Presentation, Exogenous Antigen		0.0209
Antigen Processing		
Antigen Processing, Exogenous Antigen via MHC Class I		0.0209
Localization	0.0385	

Appendix 2A *Gene Ontology – Biological Processes*	Transition State 1 Down-Regulated	 Up-Regulated
Protein Localization		0.0056
Establishment of Protein Localization		0.0094
Protein Transport		0.0086
Intracellular Protein Transport		0.0076
Protein Targeting		0.0091
Establishment of Localization	0.0403	
Regulation of Cellular Physiological Process		0.0011
Negative Regulation of Cellular Physiological Process		0.0005
Cellular Process		0.0484
Cell Communication	<0.0001	
Cell Adhesion		
Cell-Cell Adhesion	0.0376	
Heterophilic Cell Adhesion	0.0074	
Negative Regulation of Cell Adhesion	0.0334	
Cell Recognition		0.0209
Neuronal Cell Recognition		0.0209
Signal Transduction	0.0001	
Cell Surface Receptor Linked Signal Transduction	<0.0001	
G-protein Coupled Receptor Protein Signaling Pathway	<0.0001	
G-protein Signaling, Coupled to Cyclic Nucleotide Second Messenger	0.0001	
G-protein Signaling, Coupled to cAMP Nucleotide Second Messenger	0.0001	
G-protein Signaling, Adenylate Cyclase Activating Pathway	0.0032	
Adenylate Cyclase Activation	0.0463	
G-protein Signaling, Adenylate Cyclase Inhibiting Pathway	0.0167	
Regulation of Adenylate Cyclase Activity	0.0134	
Gamma-aminobutyric Acid Signaling Pathway	0.0102	
Neuropeptide Signaling Pathway	0.0001	
Glutamate Signaling Pathway	0.0252	
Intracellular Signaling Cascade		
Small GTPase Mediated Signal Transduction		0.0026
Ras Protein Signal Transduction		0.0135
Regulation of Ras Protein Signal Transduction		0.0429
Second-Messenger-Mediated Signaling	<0.0001	
Cyclic-Nucleotide-Mediated Signaling	<0.0001	
cAMP-Mediated Signaling	<0.0001	
Cell-Cell Signaling	<0.0001	

Appendix 2A *Gene Ontology – Biological Processes*	Transition State 1 Down-Regulated	Up-Regulated
Regulation of Cellular Process		0.0006
Negative Regulation of Cellular Process		0.0006
Development	0.0403	
Sex Differentiation		
Development of Primary Male Sexual Characteristics	0.0173	
Morphogenesis		
Cellular Morphogenesis		0.0076
Cell Differentiation		
Neuron Cell Differentiation	0.0058	
Regulation of Cell Differentiation	0.0151	
Positive Regulation of Cell Differentiation	0.0075	
Positive Regulation of Myeloid Blood Cell Differentiation	0.0390	
Cell Development		
Cellular Morphogenesis during Differentiation		
Photoreceptor Cell Development	0.0034	
Organ Development	0.0237	
Organogenesis	0.0340	
Eye Morphogenesis		
Photoreceptor Cell Differentiation	0.0463	
Eye Photoreceptor Cell Differentiation		
Eye Photoreceptor Cell Development	0.0173	
Gonad Development		
Male Gonad Development	0.0173	
Physiological Process		0.0072
Metabolism		0.0001
Biosynthesis		<0.0001
Cellular Biosynthesis		<0.0001
Macromolecule Biosynthesis		<0.0001
Protein Biosynthesis		<0.0001
Translation		
Translational Elongation		0.0187
Pigment Biosynthesis	0.0077	
Heme Biosynthesis	0.0173	
Macromolecule Metabolism		<0.0001
Cellular Macromolecule Metabolism		<0.0001
Cellular Carbohydrate Metabolism		

Appendix 2A *Gene Ontology – Biological Processes*	Transition State 1 Down-Regulated	 Up-Regulated
Fructose Metabolism	0.0390	
Fructose 2,6-bisphosphate Metabolism	0.0390	
Glucose Metabolism	0.0497	
Biopolymer Metabolism		0.0028
Cellular Metabolism		<0.0001
Nucleobase, Nucleoside, Nucleotide and Nucleic Acid Metabolism		
DNA Metabolism		<0.0001
DNA Replication		0.0022
DNA-dependent DNA Replication		0.0083
DNA Replication Initiation		0.0209
Regulation of DNA Replication		0.0209
DNA Packaging		0.0197
Transcription		
Regulation of Transcription from RNA Polymerase II Promoter		0.0437
Amino Acid and Derivative Metabolism		
Amino Acid Metabolism		
Serine Family Amino Acid Metabolism		0.0299
L-Serine Metabolism		0.0240
L-Serine Biosynthesis		0.0107
Amino Acid Derivative Metabolism	0.0261	
Amino Acid Derivative Biosynthesis	0.0337	
Biogenic Amine Metabolism	0.0047	
Biogenic Amine Biosynthesis	0.0441	
Catecholamine Metabolism		
Catecholamine Biosynthesis	0.0334	
Phosphorus Metabolism		
Phosphate Metabolism		
Dephosphorylation		0.0366
Primary Metabolism		<0.0001
Lipid Metabolism		
Diacylglycerol Biosynthesis		0.0209
Acylglycerol Biosynthesis		0.0209
Neutral Lipid Biosynthesis		0.0209
Heterocycle Metabolism		
Porphyrin Biosynthesis	0.0034	
Protein Metabolism		<0.0001

Appendix 2A

Gene Ontology – Biological Processes

	Transition State 1	
	Down-Regulated	**Up-Regulated**
Cellular Protein Metabolism		<0.0001
Protein Folding		
Tubulin Folding		0.0209
Chaperone-mediated Tubulin Folding		0.0209
Posttranslational Protein Folding		0.0209
Chaperone Cofactor Dependent Protein Folding		0.0209
Protein Modification		
Autophosphorylation	0.0167	
Protein Polymerization		0.0187
Receptor Metabolism		0.0030
Coagulation	0.0193	
Blood Coagulation	0.0193	
Extracellular Structure Organization and Biogenesis	0.0261	
Extracellular Matrix Organization and Biogenesis	0.0261	
Organismal Physiological Process	<0.0001	
Cell Activation		0.0434
Immune Cell Activation		0.0434
Lymphocyte Activation		0.0350
Lymphocyte Differentiation		
Thymocyte Differentiation		0.0107
T-Cell Activation		0.0271
T-Cell Proliferation		0.0197
Digestion	0.0023	
Muscle Contraction		
Regulation of Muscle Contraction	0.0229	
Neurophysiological Process	<0.0001	
Sensory Perception	<0.0001	
Perception of Pain	0.0252	
Sensory Perception of Chemical Stimulus	<0.0001	
Perception of Smell	0.0002	
Perception of Smell, Sensory Transduction of Chemical Stimulus	0.0390	
Perception of Taste	0.0463	
Sensory Transduction	0.0034	
Sensory Transduction of Chemical Stimulus	0.0077	
Sensory Perception of Light	0.0288	
Visual Perception	0.0288	

Appendix 2A

Gene Ontology – Biological Processes

	Transition State 1	
	Down-Regulated	**Up-Regulated**
Transmission of Nerve Impulse	<0.0001	
Synaptic Transmission	<0.0001	
Nerve-nerve Synaptic Transmission	0.0441	
Regulation of Neurotransmitter Levels	0.0005	
Neurotransmitter Metabolism	0.0070	
Neurotransmitter Biosynthesis	0.0173	
Neurotransmitter Receptor Metabolism		0.0030
Regulation of Body Fluids	0.0097	
Hemostasis	0.0193	
Homeostasis		
Metal Ion Homeostasis		
Calcium Ion Homeostasis	0.0042	
Transition Metal Ion Homeostasis		0.0442
Secretion		
Neurotransmitter Secretion	0.0335	
Regulation of Neurotransmitter Secretion	0.0173	
Regulation of Biological Process		0.0010
Regulation of Gene Expression, Epigenetic		0.0404
Dosage Compensation		0.0107
Negative Regulation of Biological Process		0.0004
Regulation of Enzyme Activity		0.0461
Regulation of Cyclase Activity	0.0134	
Positive Regulation of Adenylate Cyclase Activity	0.0463	
Positive Regulation of Cyclase Activity	0.0463	
Regulation of Hydrolase Activity		0.0045
Positive Regulation of Hydrolase Activity		0.0045
Regulation of Caspase Activity		0.0045
Positive Regulation of Caspase Activity		0.0045
Regulation of Lyase Activity	0.0134	
Positive Regulation of Lyase Activity	0.0463	
Regulation of Development		
Positive Regulation of Development	0.0021	
Regulation of Physiological Process		0.0018
Regulation of Metabolism		
Regulation of Cellular Metabolism		
Negative Regulation of Metabolism		0.0164

Appendix 2A

Gene Ontology – Biological Processes	**Transition State 1** Down-Regulated	Up-Regulated
Negative Regulation of Cellular Metabolism		0.0484
Regulation of Nucleobase, Nucleoside, Nucleotide and Nucleic Acid Metabolism		
Negative Regulation of Nucleobase, Nucleoside, Nucleotide and Nucleic Acid Metabolism		0.0179
Regulation of Cellular Physiological Process		
Positive Regulation of Cellular Physiological Process		
Positive Regulation of Transport		
Positive Regulation of Endocytosis		0.0442
Negative Regulation of Physiological Process		0.0006

Appendix 2B

Gene Ontology – Biological Processes	**Transition State 2** Down-Regulated	Up-Regulated
Cellular Physiological Process		
Transport		
Di-, Tri-valent Inorganic Ion Transport		
Plasma Membrane Copper Ion Transport	0.0212	
Mitochondrial Calcium Ion Transport		0.0175
Cofactor Transport		0.0346
Vitamin Transport		
Carnitine Transport		0.0175
Intracellular Transport		
Protein-Nucleus Import		
Protein-Nucleus Import, Docking		0.0346
Mitochondrial Inner Membrane Protein Import		0.0346
Cell Death		
Induction of Apoptosis by Intracellular Signals	0.0114	
Cell Proliferation		0.0058
Regulation of Cell Proliferation		0.0263
Negative Regulation of Fibroblast Proliferation	0.0419	
Cell Organization and Biogenesis		
Mitochondrial Genome Maintenance	0.0212	
Peroxisome Membrane Biogenesis	0.0419	
Response to Stress		0.0470
Response to DNA Damage Stimulus	0.0354	0.0189
DNA Repair		0.0074
Base Excision Repair	0.0018	
Base Excision Repair, Gap-Filling	0.0212	

Appendix 2B *Gene Ontology – Biological Processes*	Transition State 2 Down-Regulated	Up-Regulated
Pyrimidine Dimer Repair	0.0212	
Transcription-Coupled Nucleotide-Excision Repair		0.0346
DNA Damage Response, Signal Transduction	0.0298	
DNA Damage Response, Signal Transduction Resulting in Induction of Apoptosis	0.0026	
DNA Damage Response, Signal Transduction by p53 Class Mediator	0.0212	
Response to Pest, Pathogen, or Parasite		
Response to Bacteria	0.0342	
Response to Virus		
Regulation of Antiviral Response		0.0175
Regulation of Antiviral Response by Host		0.0175
Response to External Stimulus		
Detection of Biotic Stimulus	0.0419	
Detection of Bacteria	0.0419	
Response to Abiotic Stimulus		
Response to X-ray	0.0419	
Response to UV	0.0419	
Response to Biotic Stimulus		
Humoral Immune Response		
Positive Regulation of Complement Activation		0.0175
Innate Immune Response		
Regulation of Innate Immune Response	0.0212	
Positive Regulation of Innate Immune Response	0.0212	
Antigen Presentation	0.0087	
Antigen Presentation, Endogenous Antigen	0.0026	
Antigen Presentation, Endogenous Peptide Antigen	0.0419	
Antigen Presentation, Lipid Antigen	0.0212	
Antigen Presentation, Endogenous Lipid Antigen	0.0212	
Antigen Processing	0.0063	
Response to Endogenous Stimulus		0.0274
Cellular Process		
Cell Communication		
Homophilic Cell Adhesion		0.0308
Development		
Morphogenesis		
Cellular Morphogenesis		0.0099
Cell Projection Organization and Biogenesis		

Appendix 2B *Gene Ontology – Biological Processes*	Transition State 2 Down-Regulated	Up-Regulated
Flagellum Biogenesis		0.0346
Axoneme Biogenesis		0.0175
Flagellum Axoneme Biogenesis		0.0175
Endothelial Cell Morphogenesis		0.0346
Regulation of Cell Size		
Negative Regulation of Cell Size		0.0308
Negative Regulation of Cell Growth		0.0308
Cell Differentiation		
Cardiac Cell Differentiation	0.0212	
Endothelial Cell Development		0.0346
Regulation of Cell Differentiation		
Positive Regulation of Osteoblast Differentiation		0.0175
Cell Development		
Sperm Axoneme Assembly		0.0175
Growth	0.0046	
Regulation of Growth	0.0166	
Regulation of Growth Rate	0.0212	
Negative Regulation of Growth		0.0345
Tube Development	0.0226	
Organ Development		
Blood Vessel Development		0.0479
Heart Development		
Embryonic Heart Tube Development	0.0013	
Myogenesis	0.0342	
Physiological Process		
Metabolism		
Nitrogen Fixation	0.0212	
Biosynthesis		
Protein Biosynthesis		
Selenocysteine Incorporation		0.0175
Translational Readthrough		0.0175
Regulation of Translation		0.0149
Regulation of Protein Biosynthesis		0.0192
Regulation of Biosynthesis		0.0361
Cellular Metabolism		
Alcohol Metabolism		
Glycerol Metabolism		

Appendix 2B *Gene Ontology – Biological Processes*	Transition State 2 Down-Regulated	Up-Regulated
Glycerol-3-phosphate Metabolism	0.0419	
Nucleobase, Nucleoside, Nucleotide and Nucleic Acid Metabolism		0.0071
DNA Metabolism		0.0263
Negative Regulation of DNA Metabolism	0.0419	
DNA Replication		
Regulation of DNA Replication	0.0419	
Negative Regulation of DNA Replication	0.0212	
DNA Packaging		
Covalent Chromatin Modification		0.0346
Transcription		0.0045
Transcription, DNA-dependent		0.0023
RNA Elongation		0.0346
RNA Elongation from RNA Polymerase II Promoter		0.0175
Regulation of Transcription, DNA-dependent		0.0050
Regulation of Transcription		0.0087
Transcription from RNA Polymerase II Promoter		0.0342
Regulation of Nucleobase, Nucleoside, Nucleotide and Nucleic Acid Metabolism		0.0096
Nucleobase Metabolism		
'de novo' pyrimidine base biosynthesis		0.0175
Pyrimidine Base Biosynthesis		0.0346
Nucleotide Metabolism		
cGMP Metabolism	0.0255	
Nucleotide Biosynthesis		
Cyclic Nucleotide Biosynthesis	0.0491	
cGMP Biosynthesis	0.0179	
Polyamine Metabolism		
Spermine Metabolism		0.0346
Spermine Biosynthesis		0.0175
Spermidine Biosynthesis		0.0346
Sulfur Metabolism		
Selenium Metabolism	0.0419	
Phosphorus Metabolism		
Polyphosphate Metabolism		0.0175
Polyphosphate Catabolism		0.0175
Phosphorylation		
Hyperphosphorylation		0.0175

Appendix 2B *Gene Ontology – Biological Processes*	Transition State 2 Down-Regulated	Up-Regulated
Cofactor Metabolism		
Coenzyme Metabolism		
Ubiquinone Metabolism	0.0419	
Uquinone Cofactor Biosynthesis	0.0419	
Ubiquinone Biosynthesis	0.0419	
Cofactor Catabolism		
Heme Oxidation	0.0419	
Primary Metabolism		
Lipid Metabolism		
Lipid Storage	0.0212	
Bile Acid Biosynthesis	0.0419	
Steroid Catabolism	0.0212	
Bile Acid Catabolism	0.0212	
Protein Metabolism		
Protein Modification		
Histone Modifcation		0.0346
Protein Amino Acid Acetylation		0.0175
Histone Acetylation		0.0175
Organismal Physiological Process		
Cell Activation		
Immune Cell Activation		
Astrocyte Activation		0.0175
Extrathymic T-Cell Selection		0.0175
T-Cell Activation		
NK T-Cell Proliferation		0.0175
Carbohydrate Utilization		0.0175
Circulation	0.0426	
Homeostasis	0.0362	
Cell Homeostasis	0.0109	
Ion Homeostasis	0.0180	
Cell Ion Homeostasis	0.0180	
Cation Homeostasis	0.0145	
Metal Ion Homeostasis	0.0270	
Transition Metal Ion Homeostasis	0.0179	
Di-, Tri-valent Inorganic Cation Homeostasis	0.0206	
Iron Ion Homeostasis	0.0087	
Regulation of Biological Process		0.0180

Appendix 2B *Gene Ontology – Biological Processes*	Transition State 2 Down-Regulated	 Up-Regulated
Regulation of Cellular Process		0.0082
Regulation of Physiological Process		0.0053
Regulation of Metabolism		0.0033
Regulation of Cellular Metabolism		0.0186
Regulation of Cellular Physiological Process		0.0055

Appendix 2C

Gene Ontology – Biological Processes	↑ Transition State 1 ↓ Transition State 2
Behavior	0.0015
Locomotory Behavior	0.0001
Locomotion	0.0001
Cell Motility	0.0001
Cell Migration	0.0001
Regulation of Cell Migration	0.0046
Positive Regulation of Cell Migration	0.0129
Regulation of Cell Motility	0.0046
Positive Regulation of Cell Motility	0.0129
Regulation of Locomotion	0.0059
Positive Regulation of Locomotion	0.0129
Regulation of Behavior	0.0075
Positive Regulation of Behavior	0.0129
Cellular Physiological Process	0.0310
Transport	
Ion Transport	
Phosphate Transport	0.0190
Lipid Transport	0.0477
Fatty Acid Transport	0.0302
Endocytosis	
Phagocytosis	0.0173
Phagocytosis, Engulfment	0.0001
Phagocytosis, Recognition	0.0001
Regulation of Phagocytosis	0.0051
Positive Regulation of Phagocytosis	0.0051
Regulation of Endocytosis	0.0384
Positive Regulation of Endocytosis	0.0102

Appendix 2C

Gene Ontology – Biological Processes	↑ Transition State 1 ↓ Transition State 2
Regulation of Transport	
Positive Regulation of Transport	0.0173
Cell Organization and Biogenesis	0.0270
Organelle Organization and Biogenesis	
Cytoskeleton Organization and Biogenesis	0.0199
Actin Filament-Based Process	0.0156
Actin Cytoskeleton Organization and Biogenesis	0.0111
Actin Filament Organization	0.0384
Response to Stimulus	0.0256
Response to Stress	
Response to Wounding	0.0307
Response to External Stimulus	
Response to Abiotic Stimulus	
Response to Chemical Substance	0.0292
Response to Biotic Stimulus	0.0141
Defense Response	0.0212
Immune Response	0.0204
Cytokine Production	
Regulation of Cytokine Production	
Positive Regulation of Cytokine Production	0.0302
Positive Regulation of Cytokine Biosynthesis	0.0302
Cellular Defense Response	0.0113
Cellular Defense Response (Sensu Vertebrata)	
Cell-Mediated Immune Response	0.0267
Antigen Presentation	0.0410
Taxis	0.0156
Chemotaxis	0.0156
Cellular Process	
Cell Communication	
Cell Adhesion	0.0096
Cell-Matrix Adhesion	0.0190
Regulation of Signal Transduction	
Regulation of G-protein Coupled Receptor Protein Signaling Pathway	0.0113
Positive Regulation of Small GTPase Mediated Signal Transduction	0.0129
Development	
Morphogenesis	

Appendix 2C

Gene Ontology – Biological Processes	↑ Transition State 1 ↓ Transition State 2
Cellular Morphogenesis	0.0044
Organ Development	
Vasculature Development	0.0073
Blood Vessel Development	0.0065
Blood Vessel Morphogenesis	0.0025
Angiogenesis	0.0057
Organogenesis	
Neurogenesis	
Gliogenesis	0.0173
Regulation of Axon Extension	0.0302
Physiological Process	0.0233
Regulation of Biosynthesis	0.0486
Macromolecule Metabolism	0.0320
Cellular Macromolecule Metabolism	0.0237
Nucleobase, Nucleoside, Nucleotide and Nucleic Acid Metabolism	
Chromatin Assembly or Disassembly	0.0410
Nucleosome Assembly	0.0208
Nucleoside Metabolism	0.0135
Purine Nucleoside Metabolism	0.0129
Ribonucleoside Metabolism	0.0010
Purine Ribonucleoside Metabolism	0.0129
Pyrimidine Ribonucleoside Metabolism	0.0480
Vitamin Metabolism	
Fat-Soluble Vitamin Metabolism	0.0384
Vitamin A Metabolism	0.0102
Retinoic Acid Metabolism	0.0410
Protein Metabolism	0.0043
Cellular Protein Metabolism	0.0057
Protein Complex Assembly	0.0136
Regulation of Protein Metabolism	
Positive Regulation of Protein Metabolism	0.0173
Organismal Physiological Process	
Cell Activation	
Immune Cell Activation	
Mast Cell Activation	0.0023
Bone Remodeling	

Appendix 2C

Gene Ontology – Biological Processes	↑ Transition State 1 ↓ Transition State 2
Regulation of Bone Remodeling	0.0323
Negative Regulation of Bone Remodeling	0.0208
Homeostasis	
Cell Homeostasis	
Ion Homeostasis	0.0258
Cell Ion Homeostasis	0.0258
Cation Homeostasis	0.0193
Metal Ion Homeostasis	0.0148
Di-, Tri-valent Inorganic Cation Homeostasis	0.0096
Secretion	
Hormone Secretion	0.0267

Appendix 2D

Gene Ontology – Biological Processes	↓ Transition State 1 ↑ Transition State 2
Cellular Physiological Process	
Transport	
Ion Transport	
Sulfate Transport	0.0357
Amine Transport	0.0405
Amino Acid Transport	0.0189
Basic Amino Acid Transport	0.0201
L-Amino Acid Transport	0.0447
Organic Acid Transport	0.0057
Carboxylic Acid Transport	0.0057
Dicarboxylic Acid Transport	0.0274
Physiological Process	
Metabolism	0.0020
Nitrogen Compound Metabolism	0.0064
Nitrogen Compound Biosynthesis	0.0085
Nitrogen Compound Catabolism	0.0085
Urea Cycle	0.0010
Urea Cycle Intermediate Metabolism	0.0028
Arginine Metabolism	0.0028
Nitrogen Fixation	

Appendix 2D

Gene Ontology – Biological Processes	**↓ Transition State 1 ↑ Transition State 2**
Catabolism	
Amine Catabolism	<0.0001
Glutamine Family Amino Acid Catabolism	0.0018
Arginine Catabolism	0.0085
Aromatic Amino Acid Family Catabolism	0.0010
Biosynthesis	
Amine Biosynthesis	
Amino Acid Biosynthesis	0.0302
Cellular Metabolism	0.0099
Sterol Metabolism	0.0103
Cholesterol Metabolism	0.0333
Organic Acid Metabolism	<0.0001
Carboxylic Acid Metabolism	<0.0001
Generation of Precursor Metabolites and Energy	0.0079
Electron Transport	0.0055
Amino Acid and Derivative Metabolism	<0.0001
Amino Acid Metabolism	<0.0001
Glutamine Family Amino Acid Metabolism	0.0012
Glutamine Family Amino Acid Biosynthesis	0.0137
Arginine Biosynthesis	0.0085
Aromatic Amino Acid Family Metabolism	0.0056
L-Phenylalanine Metabolism	0.0010
L-Phenylalanine Catabolism	0.0005
Tyrosine Metabolism	0.0137
Tyrosine Catabolism	0.0043
Aromatic Compound Metabolism	0.0004
Aromatic Compound Catabolism	0.0028
Amine Metabolism	<0.0001
Amino Acid Catabolism	<0.0001
Cofactor Metabolism	
Coenzyme Metabolism	0.0383
Acetyl-CoA Metabollism	0.0219
Primary Metabolism	0.0306
Lipid Metabolism	
Cellular Lipid Metabolism	0.0426

Appendix 2D

Gene Ontology – Biological Processes	**↓ Transition State 1** **↑ Transition State 2**
Steroid Metabolism	0.0189
Secretion	
Peptide Hormone Secretion	0.0357

APPENDIX 3

Gene list of orthologous genes shared between rat and human HCCs

Ensembl genome browser was used to identify orthologous genes shared between rat (this study) and human (160) HCC datasets. Of the 2,121 genes that SAM (FDR < 5%) identified as differentially expressed in CD-induced tumors, a total of 492 orthologous genes were found. Hierarchical clustering analysis of the integrated datasets (Figure 7) revealed two gene clusters of highly expressed genes that were shared between human and rat HCCs. Genes contained within those two clusters (outlined in red in Table below) were submitted to GoMiner (9) to identify significantly enriched biological processes. *Average gene expression ratios (log_2-transformed) between either human tumors and non-tumor liver tissue or choline deficient (CD) rat tumors and CD non-tumor liver tissue are shown.

Unigene		Gene Symbol			Log Ratio (A/B)*	
Human	**Rat**	**Human**	**Rat**	**Description**	**Human**	**Rat**
Hs.413924	Rn.10584	*CXCL10*	*Cxcl10*	Chemokine (C-X-C motif) ligand 10	1.053	0.165
Hs.77367	Rn.7391	*CXCL9*	*Cxcl9*	Chemokine (C-X-C motif) ligand 9	0.547	0.922
Hs.146668	Rn.2078	*TDE2*	*Tde2*	Tumor differentially expressed 2	0.549	0.865
Hs.6061	Rn.3619	*PRKAB1*	*Prkab1*	Protein kinase, AMP-activated, beta 1 non-catalytic subunit	0.904	1.622
Hs.192619	Rn.17036	*KIAA1600*		KIAA1600	0.019	-0.165
Hs.117747	Rn.97639	*MMAA*		Methylmalonic aciduria (cobalamin deficiency) type A	0.363	-0.368
Hs.487925	Rn.16575	*PDE4DIP*	*Pde4Dip*	Phosphodiesterase 4D interacting protein (myomegalin)	0.064	-0.409
Hs.480848	Rn.17881	*USP38*	*Usp38*	Ubiquitin specific protease 38	0.460	1.197
Hs.276916	Rn.29848	*NR1D1*	*Nr1d1*	Nuclear receptor subfamily 1, group D, member 1	0.616	-0.256
Hs.233325	Rn.3977	*HFE*	*Hfe*	Hemochromatosis	0.278	1.327
Hs.352018	Rn.10763	*TAP1*	*Tap1*	Transporter 1, ATP-binding cassette, sub-family B	0.300	0.368
Hs.7367	Rn.6057.2	*BTBD6*	*Btbd6*	BTB (POZ) domain containing 6	0.411	-0.489
Hs.442182	Rn.29976	*ABCC6*	*Abcc6*	ATP-binding cassette, sub-family C (CFTR/MRP), 6	0.383	1.350
Hs.76392	Rn.6132	*ALDH1A1*	*Aldh1a1*	Aldehyde dehydrogenase 1 family, member A1	0.756	-1.498
Hs.97432	Rn.34966	*PRKCE*	*Prkce*	Protein kinase C, epsilon	0.662	-0.186
Hs.476209	Rn.26773	*PLXNB1*	*Plxnb1*	Plexin B1	1.235	-1.022
Hs.315562	Rn.2460	*GCLM*	*Gclm*	Glutamate-cysteine ligase, modifier subunit	0.784	-0.759
Hs.29645	Rn.53355	*LOC90826*		Hypothetical protein BC004337	0.171	-0.173
Hs.520494	Rn.6137.2	*FLJ14525*		Hypothetical protein FLJ14525	-0.055	-0.692
Hs.78482	Rn.18947	*PALM*	*Palm*	Paralemmin	0.291	-0.059
Hs.437179	Rn.12866	*HTPAP*	*Htpap*	HTPAP protein	-0.008	-1.964
Hs.375108	Rn.6007	*CD24*	*Cd24*	CD24 antigen (small cell lung carcinoma cluster 4 antigen)	0.582	-1.226
Hs.468688	Rn.29813	*C10orf137*		Chromosome 10 open reading frame 137	-0.003	-0.128
Hs.528006	Rn.41053	*SPHK2*	*Sphk2*	Sphingosine kinase 2	-0.232	-0.328
Hs.253736	Rn.25344	*LRIG3*	*Lrig3*	Leucine-rich repeats and immunoglobulin-like domains 3	0.066	-0.117
Hs.162121	Rn.6104.2	*COPA*	*Copa*	Coatomer protein complex, subunit alpha	0.447	-1.064
Hs.156302	Rn.84872	*GTF2IRD1*	*Gtf2ird1*	GTF2I repeat domain containing 1	0.027	-0.316

Unigene		Gene Symbol			Log Ratio (A/B)*	
Human	**Rat**	**Human**	**Rat**	**Description**	**Human**	**Rat**
Hs.59757	Rn.22691	*ZNF281*	*Znf281*	Zinc finger protein 281	-0.154	0.143
Hs.527412	Rn.4158	*ASAH1*	*Asah*	N-acylsphingosine amidohydrolase (acid ceramidase) 1	0.278	0.825
Hs.368421	Rn.54555	*SMPD3*	*Smpd3*	Sphingomyelin phosphodiesterase 3, neutral membrane (neutral sphingomyelinase II)	0.394	-0.522
Hs.280342	Rn.14623	*PRKAR1A*	*Prkar1A*	Protein kinase, cAMP-dependent, regulatory, type I, alpha (tissue specific extinguisher 1)	-0.032	-0.174
Hs.162877	Rn.17106	*PACSIN2*	*Pacsin2*	Protein kinase C and casein kinase substrate in neurons 2	-0.256	-0.176
Hs.508461	Rn.11081	*MAP3K1*	*Map3k1*	Mitogen-activated protein kinase kinase kinase 1	-0.338	-0.551
Hs.79276	Rn.2473.2	*KIAA0232*		KIAA0232 gene product	-0.545	-0.152
Hs.503178	Rn.93208	*SPTBN1*	*Spnb2*	Spectrin, beta, non-erythrocytic 1	0.036	0.588
Hs.180878	Rn.3834	*LPL*	*Lpl*	Lipoprotein lipase	0.562	0.840
Hs.76090	Rn.18199	*TNFAIP1*	*Tnfaip1*	Tumor necrosis factor, alpha-induced protein 1 (endothelial)	-0.060	1.073
Hs.75372	Rn.55746	*NAGA*	*Naga*	N-acetylgalactosaminidase, alpha-	-0.095	0.254
Hs.368912	Rn.91364	*DPP4*	*Dpp4*	Dipeptidylpeptidase 4 (CD26, adenosine deaminase complexing protein 2)	0.156	1.690
Hs.62661	Rn.25736	*GBP1*	*Gbp2*	Guanylate binding protein 1, interferon-inducible, 67kDa	-0.118	0.196
Hs.513609	Rn.11020	*RBL2*	*Rbl2*	Retinoblastoma-like 2 (p130)	0.211	-0.850
Hs.349656	Rn.3957	*SCARB2*	*Scarb2*	Scavenger receptor class B, member 2	-0.053	0.594
Hs.314338	Rn.62770	*WDR9*	*Wdr9*	WD repeat domain 9	0.002	-0.220
Hs.93836	Rn.19866	*DFNB31*	*Dfnb31*	Deafness, autosomal recessive 31	-0.092	-0.041
Hs.440401	Rn.55275	*RetSat*	*Retsat*	All-trans-13,14-dihydroretinol saturase	0.439	-1.162
Hs.436061	Rn.6396	*IRF1*	*Irf1*	Interferon regulatory factor 1	0.103	1.656
Hs.12114	Rn.16319	*VNN1*	*Vnn1*	Vanin 1	-0.066	1.603
Hs.284712	Rn.11129	*BAAT*	*Baat*	Bile acid Coenzyme A: amino acid N-acyltransferase (glycine N-choloyltransferase)	0.227	-0.607
Hs.103502	Rn.6318	*GPT*	*Gpt*	Glutamic-pyruvate transaminase (alanine aminotransferase)	0.230	3.799
Hs.108969	Rn.98317	*PTD008*		PTD008 protein	-0.379	-1.228
Hs.251526	Rn.4772	*CCL7*	*Ccl2*	Chemokine (C-C motif) ligand 7	-0.395	0.181
Hs.315137	Rn.8645	*AARS*	*Aars*	Alanyl-tRNA synthetase	0.096	1.634
Hs.311958	Rn.2490	*IL15*	*Il15*	Interleukin 15	0.327	-0.212
Hs.624	Rn.10907	*IL8*	*Cxcl1*	Interleukin 8	-0.032	1.350
Hs.5509	Rn.7907	*EVI2B*	*Evi2B*	Ecotropic viral integration site 2B	-0.046	0.148
Hs.99528	Rn.28921	*RAB31*	*Rab31*	RAB31, member RAS oncogene family	0.304	1.160
Hs.43728	Rn.4130	*GPX7*	*Gpx7*	Glutathione peroxidase 7	-0.184	0.160
Hs.102308	Rn.118306	*KCNJ8*	*Kcnj8*	Potassium inwardly-rectifying channel, subfamily J, member 8	0.341	0.137
Hs.159430	Rn.87271	*FNDC3B*	*Fndc3B*	Fibronectin type III domain containing 3B	0.240	0.199
Hs.113912	Rn.23121	*RAPGEF2*	*Rapgef2*	Rap guanine nucleotide exchange factor (GEF) 2	0.090	1.848
Hs.471508	Rn.10476	*IRS1*	*Irs1*	Insulin receptor substrate 1	0.197	-0.027
Hs.1183	Rn.19118	*DUSP2*	*Dusp2*	Dual specificity phosphatase 2	0.353	0.063
Hs.110445	Rn.107123	*SBDS*	*Sbds*	Shwachman-Bodian-Diamond syndrome	0.594	1.748
Hs.128453	Rn.12034	*FRZB*	*Frzb*	Frizzled-related protein	0.645	0.125

Unigene		Gene Symbol			Log Ratio (A/B)*	
Human	**Rat**	**Human**	**Rat**	**Description**	**Human**	**Rat**
Hs.72912	Rn.10352	*CYP1A1*	*Cyp1a1*	Cytochrome P450, family 1, subfamily A, polypeptide 1	0.302	-0.211
Hs.502338	Rn.10240	*SLC1A2*	*Slc1a2*	Solute carrier family 1 (glial high affinity glutamate transporter), member 2	0.546	-0.001
Hs.525459	Rn.17605	*DLST*	*Dlst*	Dihydrolipoamide S-succinyltransferase (E2 component of 2-oxo-glutarate complex)	0.367	-1.071
Hs.6147	Rn.105953	*TENC1*	*Tenc1*	Tensin like C1 domain containing phosphatase	0.866	-0.763
Hs.182215	Rn.9538	*ARL3*	*Arl3*	ADP-ribosylation factor-like 3	0.341	-0.304
Hs.371723	Rn.10070	*ALDH5A1*	*Aldh5a1*	Aldehyde dehydrogenase 5 family, member A1 (succinate-semialdehyde dehydrogenase)	0.407	-0.816
Hs.444319	Rn.31429	*TPMT*	*Ocln*	Thiopurine S-methyltransferase	0.223	4.538
Hs.188553	Rn.95305	*RBBP6*	*Rbbp6*	Retinoblastoma binding protein 6	-0.293	-0.010
Hs.241579	Rn.98199	*SERPINH1*	*Serpinh1*	Serine (or cysteine) proteinase inhibitor, clade H (heat shock protein 47), member 1, (collagen binding protein 1)	-0.030	1.239
Hs.8309	Rn.11636	*MBC2*	*Mbc2*	Family with sequence similarity 62 (C2 domain containing), member A	-0.369	0.202
Hs.434326	Rn.24897	*EIF2AK3*	*Eif2ak3*	Eukaryotic translation initiation factor 2-alpha kinase 3	-0.109	0.331
Hs.429353	Rn.15108	*SEPN1*	*Sepn1*	Selenoprotein N, 1	-0.234	0.325
Hs.466391	Rn.6445	*C19orf2*		Chromosome 19 open reading frame 2	-0.019	-0.297
Hs.519909	Rn.9560	*MARCKS*	*Marcks*	Myristoylated alanine-rich protein kinase C substrate	-0.009	0.273
Hs.297324	Rn.3467	*TIMP3*	*Timp3*	Tissue inhibitor of metalloproteinase 3 (Sorsby fundus dystrophy, pseudoinflammatory)	-0.122	-0.001
Hs.9754	Rn.30491	*ATF5*	*Atf5*	Activating transcription factor 5	0.489	0.698
Hs.514220	Rn.5820	*GRN*	*Grn*	Granulin	0.502	-0.932
Hs.385986	Rn.20766	*UBE2B*	*LOC81816*	Ubiquitin-conjugating enzyme E2B (RAD6 homolog)	-0.184	1.359
Hs.130989	Rn.9808	*SCNN1A*	*Scnn1a*	Sodium channel, nonvoltage-gated 1 alpha	1.031	-0.027
Hs.29706	Rn.105727	*C14orf149*		Chromosome 14 open reading frame 149	0.159	-0.062
Hs.81337	Rn.64588	*LGALS9*	*Lgals5/9*	Lectin, galactoside-binding, soluble, 9 (galectin 9)	0.654	1.317
Hs.148330	Rn.35935	*ARF4*	*Arf4*	ADP-ribosylation factor 4	0.168	-0.840
Hs.298198	Rn.15332	*CKLFSF3*	*Cklfsf3*	Chemokine-like factor super family 3	0.158	0.661
Hs.529989	Rn.18019	*RNASET2*	*Rnaset2*	Ribonuclease T2	-0.112	-1.500
Hs.287362	Rn.24106	*TLE3*	*Tle3*	Transducin-like enhancer of split 3 (E(sp1) homolog, Drosophila)	0.068	0.562
Hs.485760	Rn.6598.2	*SLC17A5*	*Slc17A5*	Solute carrier family 17 (anion/sugar transporter), 5	-0.108	-0.263
Hs.24178	Rn.76362	*EML2*	*Eml2*	Echinoderm microtubule associated protein like 2	-0.321	0.072
Hs.75516	Rn.38688	*TYK2*	*Tyk2*	Tyrosine kinase 2	-0.473	-0.308
Hs.252682	Rn.6487	*TOR1B*	*Tor1B*	Torsin family 1, member B (torsin B)	-0.241	-0.085
Hs.57698	Rn.12640	*NSDHL*	*Nsdhl*	NAD(P) dependent steroid dehydrogenase-like	-0.216	0.696
Hs.521640	Rn.67042	*RAD23B*	*LOC298012*	RAD23 homolog B (S. cerevisiae)	-0.193	-0.634
Hs.473937	Rn.6452	*NDUFV3*	*Mipp65*	NADH dehydrogenase (ubiquinone) flavoprotein 3, 10kDa	-0.082	0.684
Hs.191887	Rn.103030	*SEC61B*	*Sec61B*	Sec61 beta subunit	-0.244	-0.539
Hs.51483	Rn.32292	*MGC17301*	*Mgc17301*	Hypothetical protein MGC17301	0.023	1.158
Hs.349150	Rn.3147	*PURB*	*Purb*	Purine-rich element binding protein B	-0.362	-0.212

Unigene		Gene Symbol			Log Ratio (A/B)*	
Human	Rat	Human	Rat	Description	Human	Rat
Hs.517240	Rn.23305	*IFNGR2*	*Ifngr2*	Interferon gamma receptor 2 -interferon gamma transducer	-0.162	0.132
Hs.368255	Rn.22555	*KIAA0368*		KIAA0368	-0.177	-0.515
Hs.313227	Rn.10301	*CHRNE*	*Chrne*	Cholinergic receptor, nicotinic, epsilon polypeptide	-0.100	-0.141
Hs.518267	Rn.91296	*TF*	*Tf*	Transferrin	-0.176	-0.176
Hs.381099	Rn.14256	*LCP1*	*Lcp1*	Lymphocyte cytosolic protein 1 (L-plastin)	0.195	-0.825
Hs.477128	Rn.2193	*URB*	*Ssg1*	Steroid sensitive gene 1	0.213	-0.972
Hs.529408	Rn.38581	*BACE2*	*Bace2*	Beta-site APP-cleaving enzyme 2	0.786	0.049
Hs.73677	Rn.22170	*RFX1*	*Rfx1*	Regulatory factor X, 1 influences HLA class II expression	0.040	0.477
Hs.134544	Rn.55497	*SLC25A21*	*Slc25a21*	Solute carrier family 25 (mitochondrial oxodicarboxylate carrier), member 21	-0.048	-0.323
Hs.255664	Rn.10893	*CYLN2*	*Cyln2*	Cytoplasmic linker 2	0.070	0.071
Hs.533934	Rn.126649	*FLJ20254*		Hypothetical protein FLJ20254	-0.318	1.099
Hs.470316	Rn.87899	*ACVR1*	*Acvr1*	Activin A receptor, type I	-0.134	0.059
Hs.386434	Rn.106184	*ANXA7*	*Anxa7*	Annexin A7	-0.096	1.686
Hs.91586	Rn.12071	*TM9SF1*	*Tm9Sf1*	Transmembrane 9 superfamily member 1	-0.310	-0.335
Hs.463964	Rn.12436	*WIPI49*	*Wipi49*	WD40 repeat protein Interacting with phosphoInositides of 49kDa	-0.171	-0.319
Hs.529846	Rn.63999	*CAMLG*	*Camlg*	Calcium modulating ligand	-0.174	-0.060
Hs.292949	Rn.19822	*INO80*	*Ino80*	Homolog of yeast INO80	-0.411	-0.273
Hs.165950	Rn.24104	*FGFR4*	*Fgfr4*	Fibroblast growth factor receptor 4	-0.156	-0.545
Hs.76111	Rn.2065	*DAG1*	*Dag1*	Dystroglycan 1 (dystrophin-associated glycoprotein 1)	-0.552	-1.438
Hs.492314	Rn.8123	*LAPTM4B*	*Laptm4B*	Lysosomal associated protein transmembrane 4 beta	-0.021	0.969
Hs.523443	Rn.102461	*HBB*	*Hbb*	Hemoglobin, beta	0.094	-3.100
Hs.524224	Rn.3918	*C1R*	*C1R*	Complement component 1, r subcomponent	-0.634	1.339
Hs.397153	Rn.39153	*LOC126208*		Hypothetical protein LOC126208	-0.385	-0.229
Hs.5462	Rn.11114	*SLC4A4*	*Slc4a4*	Solute carrier family 4, sodium bicarbonate cotransporter,4	-0.921	0.776
Hs.82614	Rn.2906	*GYS2*	*Gys2*	Glycogen synthase 2 (liver)	-1.319	-1.173
Hs.181128	Rn.17303	*ELK1*	*Elk1*	ELK1, member of ETS oncogene family	-0.059	-0.007
Hs.299878	Rn.34792	*DEGS1*	*Degs*	Degenerative spermatocyte homolog 1, lipid desaturase (Drosophila)	-0.044	1.702
Hs.374509	Rn.17785	*UBQLN4*	*Ubqln4*	Ubiquilin 4	-0.433	-0.329
Hs.458390	Rn.17962	*KIAA1698*		KIAA1698 protein	-0.096	-0.143
Hs.521608	Rn.14754	*CHPPR*	*Chppr*	Likely ortholog of chicken chondrocyte protein with a poly-proline region	-0.064	0.439
Hs.507087	Rn.5977	*SPPL3*	*Sppl3*	Signal peptide peptidase 3	-0.156	-1.362
Hs.3447	Rn.24570	*DKFZP564K1964*		DKFZP564K1964 protein	-0.180	-0.394
Hs.380929	Rn.43996	*LDHD*	*Ldhd*	Lactate dehydrogenase D	-0.674	-1.207
Hs.2899	Rn.3664	*HPD*	*Hpd*	4-hydroxyphenylpyruvate dioxygenase	-0.116	1.262
Hs.509718	Rn.28520	*ZNF318*	*Znf318*	Zinc finger protein 318	-0.292	-0.167
Hs.8821	Rn.7865	*HAMP*	*Hamp*	Hepcidin antimicrobial peptide	-2.580	-2.236
Hs.144567	Rn.9931	*AGXT*	*Agxt*	Alanine-glyoxylate aminotransferase (oxalosis I; hyperoxaluria I; glycolicaciduria; serine-pyruvate aminotransferase)	-1.664	2.878
Hs.522099	Rn.34735	*PIGO*	*Pigo*	Phosphatidylinositol glycan, class O	-0.401	-0.133

Unigene		Gene Symbol			Log Ratio (A/B)*	
Human	Rat	Human	Rat	Description	Human	Rat
Hs.236030	Rn.20004	*SMARCC2*	*Smarcc2*	SWI/SNF related, matrix associated, actin dependent regulator of chromatin, subfamily c, member 2	-0.292	-0.447
Hs.192326	Rn.7581	*SNX27*	*Snx27*	Sorting nexin family member 27	-0.553	-0.070
Hs.389461	Rn.8798	*SMAP-1*	*Smap-1*	Smooth muscle cell associated protein-1	-0.264	-0.785
Hs.439127	Rn.67071	*CACH-1*	*rACH*	Cytosolic acetyl-CoA hydrolase	-0.344	0.540
Hs.103934	Rn.3625	*FKBP9*	*Fkbp9*	FK506 binding protein 9, 63 kDa	-0.201	0.760
Hs.507681	Rn.17231	*MAP3K7IP1*	*Map3K7Ip1*	Mitogen-activated protein kinase kinase kinase 7 interacting protein 1	-0.204	-0.188
Hs.386404	Rn.18962	*UBE4B*	*Ube4B*	Ubiquitination factor E4B (UFD2 homolog, yeast)	-0.099	-2.213
Hs.503022	Rn.23976	*C11orf23*		Chromosome 11 open reading frame 23	-0.019	-0.867
Hs.96513	Rn.9343	*USP40*	*Usp40*	Ubiquitin specific protease 40	-0.225	-0.634
Hs.12970	Rn.101332	*PSMD3*	*Psmd3*	Proteasome (prosome, macropain) 26S subunit, non-ATPase, 3	-0.029	-1.597
Hs.369373	Rn.8735	*SEC23B*	*Sec23B*	Sec23 homolog B (S. cerevisiae)	-0.016	-1.701
Hs.146806	Rn.68078	*CUL1*	*Cul1*	Cullin 1	0.084	-0.761
Hs.163867	Rn.42942	*CD14*	*Cd14*	CD14 antigen	-0.782	1.053
Hs.378505	Rn.3309	*MOSPD1*	*Mospd1*	Motile sperm domain containing 1	-0.096	-0.635
Hs.238432	Rn.15048	*SP192*		Hypothetical protein SP192	-0.142	-0.316
Hs.164410	Rn.18619	*C16orf7*		Chromosome 16 open reading frame 7	0.232	-2.077
Hs.198158	Rn.2417	*MAWBP*	*Mawbp*	MAWD binding protein	-0.517	1.122
Hs.449076	Rn.39242	*PWP2H*	*Pwp2H*	PWP2 periodic tryptophan protein homolog (yeast)	0.132	-0.072
Hs.159699	Rn.25752	*FBXO21*	*Serpinb5*	F-box protein 21	0.470	-0.297
Hs.381072	Rn.2923	*PPIF*	*Ppif*	Peptidylprolyl isomerase F (cyclophilin F)	0.350	0.472
Hs.512815	Rn.8074	*AP3D1*	*Ap3D1*	Adaptor-related protein complex 3, delta 1 subunit	0.340	0.424
Hs.310591	Rn.8844	*SLC22A4*	*Slc22a5*	Solute carrier family 22 (organic cation transporter), member 4	-0.047	-0.557
Hs.531615	Rn.34645	*MtFMT*	*Mtfmt*	Methionyl-tRNA formyltransferase, mitochondrial	0.184	-0.092
Hs.1422	Rn.11309	*FGR*	*Fgr*	Gardner-Rasheed feline sarcoma viral (v-fgr) oncogene homolog	0.141	0.399
Hs.16004	Rn.8704	*C10orf76*		Chromosome 10 open reading frame 76	-0.030	-0.111
Hs.507916	Rn.3545	*TGFB1I4*	*Tgfb1i4*	TSC22 domain family 1	-0.055	-1.202
Hs.508545	Rn.2539	*PHGDHL1*	*Phgdhl1*	Phosphoglycerate dehydrogenase like 1	0.008	-0.572
Hs.157351	Rn.5874	*PTD004*	*Ptd004*	GTP-binding protein PTD004	0.175	-0.802
Hs.307734	Rn.33598	*MME*	*Mme*	Membrane metallo-endopeptidase (neutral endopeptidase, enkephalinase, CALLA, CD10)	0.169	-0.272
Hs.391561	Rn.4258	*FABP4*	*Fabp4*	Fatty acid binding protein 4, adipocyte	0.364	0.970
Hs.181301	Rn.11347	*CTSS*	*Ctss*	Cathepsin S	0.873	-1.944
Hs.433300	Rn.9277	*FCER1G*	*Fcer1g*	Fc fragment of IgE, high affinity I, receptor for; gamma polypeptide	0.299	-2.848
Hs.372679	Rn.23977	*FCGR3B*	*LOC304966*	Fc fragment of IgG, low affinity IIIb, receptor (CD16b)	0.154	0.307
Hs.375115	Rn.20089	*HLA-DQB2*	*RT1-Bb*	Major histocompatibility complex, class II, DQ beta 2	1.576	0.681
Hs.128846	Rn.53971	*PTPNS1*	*Ptpns1*	Protein tyrosine phosphatase, non-receptor type substrate 1	0.706	0.556
Hs.1166	Rn.10576	*THPO*	*Thpo*	Thrombopoietin (myeloproliferative leukemia virus oncogene ligand, megakaryocyte growth and development	1.086	-0.040

Unigene		Gene Symbol			Log Ratio (A/B)*	
Human	Rat	Human	Rat	Description	Human	Rat
				factor)		
Hs.91109	Rn.37820	*LOC222171*		Hypothetical protein LOC222171	0.058	-0.956
Hs.42853	Rn.18179	*CREBL1*	*Crebl1*	CAMP responsive element binding protein-like 1	-0.192	-0.249
Hs.529285	Rn.15324	*SLC40A1*	*Slc40a1*	Solute carrier family 40 (iron-regulated transporter), member 1	1.871	-2.049
Hs.5710	Rn.3532	*CREG1*	*Creg1*	Cellular repressor of E1A-stimulated genes 1	2.169	0.812
Hs.8867	Rn.22129	*CYR61*	*Cyr61*	Cysteine-rich, angiogenic inducer, 61	1.095	0.139
Hs.490892	Rn.9048	*MCPH1*	*Agpt2*	Microcephaly, primary autosomal recessive 1	-0.040	-0.020
Hs.386866	Rn.18956	*PTPRG*	*Ptprg*	Protein tyrosine phosphatase, receptor type, G	0.117	-0.064
Hs.369615	Rn.21048	*FLJ20551*		Hypothetical protein FLJ20551	0.065	-1.246
Hs.76206	Rn.7055	*CDH5*	*Cdh5*	Cadherin 5, type 2, VE-cadherin (vascular epithelium)	0.620	0.539
Hs.310421	Rn.38834	*APBB1IP*	*Apbb1Ip*	Amyloid beta (A4) precursor protein-binding, family B, member 1 interacting protein	-0.346	0.500
Hs.77890	Rn.87228	*GUCY1B3*	*Gucy1b3*	Guanylate cyclase 1, soluble, beta 3	0.203	0.073
Hs.338182	Rn.14938	*UNQ9217*		AASA9217	-0.032	0.088
Hs.546267	Rn.74064	*MMP16*	*Mmp16*	Matrix metalloproteinase 16 (membrane-inserted)	0.113	0.029
Hs.50282	Rn.11259	*RRAGB*	*RragB*	Ras-related GTP binding B	0.100	-0.006
Hs.11170	Rn.15446	*RBM14*	*Rbm14*	RNA binding motif protein 14	0.063	-0.178
Hs.479634	Rn.19979	*SLC30A9*	*Slc30A9*	Solute carrier family 30 (zinc transporter), member 9	0.125	-0.248
Hs.516341	Rn.34623	*FLJ10081*		Hypothetical protein FLJ10081	0.004	-0.279
Hs.443057	Rn.31988	*CD53*	*Cd53*	CD53 antigen	0.351	1.121
Hs.481980	Rn.14763	*DAB2*	*Dab2*	Disabled homolog 2, mitogen-responsive phosphoprotein (Drosophila)	0.161	1.356
Hs.550470	Rn.32777	*CP*	*Cp*	Ceruloplasmin (ferroxidase)	-0.185	-1.008
Hs.325404	Rn.1652	*PAH*	*Pah*	Phenylalanine hydroxylase	0.064	0.751
Hs.128065	Rn.107912	*CTSC*	*Ctsc*	Cathepsin C	0.094	-1.165
Hs.516700	Rn.94956	*CYP27A1*	*Cyp27a1*	Cytochrome P450, family 27, subfamily A, polypeptide 1	0.041	0.770
Hs.146447	Rn.12759	*FBN1*	*Fbn1*	Fibrillin 1 (Marfan syndrome)	0.087	0.204
Hs.489142	Rn.107239	*COL1A2*	*Col1a2*	Collagen, type I, alpha 2	0.122	1.034
Hs.410037	Rn.17145	*CTGF*	*Ctgf*	Connective tissue growth factor	0.408	0.658
Hs.430551	Rn.12233	*IQGAP1*	*Iqgap1*	IQ motif containing GTPase activating protein 1	0.243	0.495
Hs.389733	Rn.10995	*RAB8B*	*Rab8b*	RAB8B, member RAS oncogene family	0.131	0.079
Hs.498143	Rn.3547	*TBCE*	*Tbce*	Tubulin-specific chaperone e	-0.155	-0.234
Hs.500526	Rn.1237	*BTAF1*	*Btaf1*	BTAF1 RNA polymerase II, B-TFIID transcription factor-associated, 170kDa (Mot1 homolog, S. cerevisiae)	0.101	-0.189
Hs.515469	Rn.98750	*VASP*	*Vasp*	Vasodilator-stimulated phosphoprotein	0.179	1.341
Hs.5353	Rn.54474	*CASP10*	*Casp8*	Caspase 10, apoptosis-related cysteine protease	-0.041	0.129
Hs.90232	Rn.7646	*ProSAPiP1*		ProSAPiP1 protein	-0.063	-0.199
Hs.131933	Rn.3413	*FLJ22662*		Hypothetical protein FLJ22662	0.200	-1.350
Hs.529044	Rn.37799	*RAB22A*	*Rab22A*	RAB22A, member RAS oncogene family	0.077	0.865
Hs.410092	Rn.3798	*KIAA0652*		KIAA0652 gene product	0.431	-3.839

Unigene		Gene Symbol			Log Ratio (A/B)*	
Human	**Rat**	**Human**	**Rat**	**Description**	**Human**	**Rat**
Hs.135087	Rn.1716	*IL6R*	*Il6r*	Interleukin 6 receptor	1.602	-1.852
Hs.436410	Rn.127	*TBRG1*	*Tbrg1*	Transforming growth factor beta regulator 1	0.187	-2.094
Hs.477009	Rn.24190	*USP24*	*Usp24*	Ubiquitin specific protease 24	0.123	0.841
Hs.98041	Rn.16048	*ZFYVE26*	*Zfyve26*	Zinc finger, FYVE domain containing 26	-0.131	-1.309
Hs.19383	Rn.6319	*AGT*	*Agt*	Angiotensinogen (serine (or cysteine) proteinase inhibitor, clade A (alpha-1 antiproteinase, antitrypsin), member 8)	1.638	1.891
Hs.84928	Rn.90077	*NFYB*	*Nfyb*	Nuclear transcription factor Y, beta	-0.093	0.021
Hs.482043	Rn.3128	*NNT*	*Nnt*	Nicotinamide nucleotide transhydrogenase	0.143	-00.859
Hs.88025	Rn.1508	*VPS39*	*Vps39*	Vacuolar protein sorting 39 (yeast)	0.105	-0.047
Hs.481371	Rn.8633	*FAT*	*Fat*	FAT tumor suppressor homolog 1 (Drosophila)	0.100	-1.146
Hs.546303	Rn.8796	*ST13*	*St13*	Suppression of tumorigenicity 13 (colon carcinoma) (Hsp70 interacting protein)	-0.052	-1.591
Hs.173859	Rn.1806	*FZD7*	*Fzd7*	Frizzled homolog 7 (Drosophila)	0.215	-0.226
Hs.482976	Rn.17425	*LOC90355*		Hypothetical gene supported by AF038182; BC009203	0.230	0.614
Hs.43670	Rn.47400	*KIF3A*		Kinesin family member 3A	0.022	0.070
Hs.146339	Rn.3973	*PPP2R2A*	*Rpl29*	Protein phosphatase 2 (formerly 2A), regulatory subunit B (PR 52), alpha isoform	0.191	-0.574
Hs.26333	Rn.38478	*CXorf37*		Chromosome X open reading frame 37	-0.113	-0.449
Hs.524579	Rn.2283	*LYZ*	*Lyz*	Lysozyme (renal amyloidosis)	0.521	-1.387
Hs.510833	Rn.12180	*TJP1*	*Tjp1*	Tight junction protein 1 (zona occludens 1)	0.130	-1.614
Hs.434951	Rn.6294	*USP15*	*Usp15*	Ubiquitin specific protease 15	0.309	-0.194
Hs.516119	Rn.22161	*GCS1*	*Gcs1*	Glucosidase I	-0.108	1.608
Hs.403010	Rn.15339	*TTRAP*	*Ttrap*	TRAF and TNF receptor associated protein	-0.117	-0.058
Hs.406590	Rn.3393	*PGR1*	*Pgr1*	Mof4 family associated protein 1	0.108	-0.823
Hs.348921	Rn.3080	*PHF3*	*Phf3*	PHD finger protein 3	-0.005	-0.113
Hs.332138	Rn.81052	*PPT2*	*Ppt2*	Palmitoyl-protein thioesterase 2	-0.068	-0.165
Hs.500066	Rn.8027	*TADA2L*	*Tada2L*	Transcriptional adaptor 2 (ADA2 homolog, yeast)-like	0.094	-0.048
Hs.437084	Rn.29454	*NKRF*	*Nkrf*	NF-kappaB repressing factor	0.214	-0.426
Hs.273621	Rn.31762	*CNP*	*Cnp1*	2',3'-cyclic nucleotide 3' phosphodiesterase	0.022	1.255
Hs.311072	Rn.8870	*MRPS35*	*Mrps35*	Mitochondrial ribosomal protein S35	0.207	-0.713
Hs.52788	Rn.93013	*FXR2*	*Fxr2*	Fragile X mental retardation, autosomal homolog 2	0.104	-0.252
Hs.80720	Rn.1725	*GAB1*	*Gab1*	GRB2-associated binding protein 1	0.216	-0.872
Hs.201398	Rn.53880	*C1QTNF1*	*C1Qtnf1*	C1q and tumor necrosis factor related protein 1	0.339	0.082
Hs.478150	Rn.1176	*PDCD10*	*Pdcd10*	Programmed cell death 10	0.038	0.682
Hs.277721	Rn.7811	*M17S2*	*M17S2*	Neighbor of BRCA1 gene 1	0.021	1.180
Hs.471851	Rn.122675	*HDLBP*	*Hdlbp*	High density lipoprotein binding protein (vigilin)	0.075	0.865
Hs.524491	Rn.3668	*PAPSS2*	*Papss2*	3'-phosphoadenosine 5'-phosphosulfate synthase 2	0.075	1.735
Hs.440961	Rn.17481	*CAST*	*Cast*	Calpastatin	-0.013	0.376
Hs.250009	Rn.6283	*ARL10C*	*Arl10C*	ADP-ribosylation factor-like 10C	0.091	0.784
Hs.114033	Rn.25091	*SSR1*	*Ssr1*	Signal sequence receptor, alpha (translocon-associated protein alpha)	-0.008	-1.077

Unigene		Gene Symbol			Log Ratio (A/B)*	
Human	**Rat**	**Human**	**Rat**	**Description**	**Human**	**Rat**
Hs.191334	Rn.6357	*UNG*	*Ung*	Uracil-DNA glycosylase	-0.005	1.114
Hs.180877	Rn.9454	*H3F3B*	*H3F3B*	H3 histone, family 3B (H3.3B)	0.146	-1.674
Hs.155827	Rn.6165	*GOLGA2*	*Golga2*	Golgi autoantigen, golgin subfamily a, 2	-0.048	-0.100
Hs.201641	Rn.37779	*BASP1*	*Basp1*	Brain abundant, membrane attached signal protein 1	0.609	0.032
Hs.104879	Rn.95177	*SERPINB9*	*Serpinb9*	Serine (or cysteine) proteinase inhibitor, clade B (ovalbumin), member 9	0.269	-0.760
Hs.79769	Rn.8926	*PCDH1*	*Pcdh1*	Protocadherin 1 (cadherin-like 1)	0.074	-0.340
Hs.210850	Rn.36797	*HECTD1*	*Hectd1*	HECT domain containing 1	0.226	0.619
Hs.546298	Rn.5958	*SUMO2*	*Sumo2*	SMT3 suppressor of mif two 3 homolog 2 (yeast)	0.122	-1.341
Hs.464595	Rn.16065	*PPP4R1*	*Ppp4r1*	Protein phosphatase 4, regulatory subunit 1	0.177	-0.320
Hs.500842	Rn.1048	*MGEA5*	*Mgea5*	Meningioma expressed antigen 5 (hyaluronidase)	0.108	1.970
Hs.212046	Rn.22211	*KIAA0433*		KIAA0433 protein	0.179	-0.199
Hs.216653	Rn.3335	*FBXO9*	*Fbxo9*	F-box protein 9	0.017	1.715
Hs.109051	Rn.18564	*SH3BGRL3*	*Sh3Bgrl3*	SH3 domain binding glutamic acid-rich protein like 3	0.212	1.748
Hs.462278	Rn.36639	*COX10*	*Cox10*	COX10 homolog, cytochrome c oxidase assembly protein, heme A: farnesyltransferase (yeast)	0.218	-0.306
Hs.469537	Rn.13913	*MRPS9*	*Mrps9*	Mitochondrial ribosomal protein S9	0.287	-0.229
Hs.471675	Rn.17832	*DGKD*	*Dgkd*	Diacylglycerol kinase, delta 130kDa	0.164	-0.089
Hs.85951	Rn.2238	*XPOT*	*Xpot*	Exportin, tRNA (nuclear export receptor for tRNAs)	0.199	0.713
Hs.432424	Rn.28991	*TPP2*	*Tpp2*	Tripeptidyl peptidase II	0.325	-0.474
Hs.268849	Rn.108014	*GLO1*	*Glo1*	Glyoxalase I	0.179	-0.810
Hs.549238	Rn.46749	*LOC126731*		LOC126731	0.084	-0.050
Hs.445000	Rn.10361	*PTGER3*	*Ptger3*	Prostaglandin E receptor 3 (subtype EP3)	0.161	0.432
Hs.433653	Rn.106312	*MDC1*	*Mdc1*	Mediator of DNA damage checkpoint 1	0.077	-0.037
Hs.474069	Rn.11954	*PCNT2*	*Pcnt2*	Pericentrin 2 (kendrin)	0.106	-0.031
Hs.412707	Rn.47	*HPRT1*	*Hprt*	Hypoxanthine phosphoribosyltransferase 1 (Lesch-Nyhan syndrome)	0.296	-1.194
Hs.466714	Rn.40291	*PD2*	*Pd2*	Hypothetical protein F23149_1	0.157	-0.117
Hs.46523	Rn.94638	*ELK3*	*Elk3*	ELK3, ETS-domain protein (SRF accessory protein 2)	0.164	0.246
Hs.444870	Rn.13505	*ORC2L*	*Orc2L*	Origin recognition complex, subunit 2-like (yeast)	0.304	-0.233
Hs.523594	Rn.5598	*CTSK*	*Ctsk*	Cathepsin K (pycnodysostosis)	0.312	0.096
Hs.83286	Rn.14013	*KDELC2*	*Kdelc2*	KDEL (Lys-Asp-Glu-Leu) containing 2	0.212	0.110
Hs.79402	Rn.22044	*POLR2C*	*Polr2C*	Polymerase (RNA) II (DNA directed) polypeptide C, 33kDa	0.273	-0.263
Hs.301419	Rn.2055	*TERF2IP*	*Terf2Ip*	Telomeric repeat binding factor 2, interacting protein	0.298	-1.062
Hs.377360	Rn.22855	*KIAA1971*		Similar to junction-mediating and regulatory protein p300 JMY	0.242	-0.101
Hs.433269	Rn.55623	*C14orf11*		Chromosome 14 open reading frame 11	0.155	-0.255
Hs.549082	Rn.13007	*BCL10*	*Bcl10*	B-cell CLL/lymphoma 10	0.153	0.903
Hs.427284	Rn.4237	*ZNRF1*	*Znrf1*	Zinc and ring finger 1	0.217	-0.064
Hs.6877	Rn.7690	*C14orf130*		Chromosome 14 open reading frame 130	0.207	-0.138
Hs.516468	Rn.39047	*ARL6IP6*	*Arl6Ip6*	ADP-ribosylation-like factor 6 interacting protein 6	0.179	0.009
Hs.406461	Rn.8024	*ALG1*	*Alg1*	Asparagine-linked glycosylation 1	0.159	-0.025

Unigene		Gene Symbol			Log Ratio (A/B)*	
Human	Rat	Human	Rat	Description	Human	Rat
				homolog (yeast, beta-1,4-mannosyltransferase)		
Hs.323583	Rn.20514	*DKFZp434L142*	*MGC72614*	Hypothetical protein DKFZp434L142	0.170	0.383
Hs.270543	Rn.10844	*GNB4*	*Gnb4*	Guanine nucleotide binding protein (G protein), beta polypeptide 4	0.300	0.146
Hs.336916	Rn.870	*DAXX*	*Daxx*	Death-associated protein 6	0.167	0.289
Hs.525238	Rn.2583	*C14orf119*		Chromosome 14 open reading frame 119	0.149	-0.156
Hs.410406	Rn.7758	*SMARCAD1*	*Smarcad1*	SWI/SNF-related, matrix-associated actin-dependent regulator of chromatin, subfamily a, containing DEAD/H box 1	0.303	-0.094
Hs.173162	Rn.6292	*NOC4*	*Noc4*	Neighbor of COX4	0.268	-0.376
Hs.469030	Rn.11744	*MTHFD2*	*Mthfd2*	Methylenetetrahydrofolate dehydrogenase (NADP+ dependent) 2, methenyltetrahydrofolate cyclohydrolase	0.350	0.281
Hs.81791	Rn.9792	*TNFRSF11B*	*Tnfrsf11b*	Tumor necrosis factor receptor superfamily, member 11b (osteoprotegerin)	0.437	0.373
Hs.87595	Rn.41817	*TIMM22*	*Timm22*	Translocase of inner mitochondrial membrane 22 homolog (yeast)	0.322	-0.025
Hs.74471	Rn.10346	*GJA1*	*Gja1*	Gap junction protein, alpha 1, 43kDa (connexin 43)	0.336	0.218
Hs.435215	Rn.6913	*VEGFC*	*Vegfc*	Vascular endothelial growth factor C	0.378	0.186
Hs.494173	Rn.1792	*ANXA1*	*Anxa1*	Annexin A1	0.416	1.472
Hs.156519	Rn.3174	*MSH2*	*Msh2*	MutS homolog 2, colon cancer, nonpolyposis type 1 (E. coli)	0.221	-0.034
Hs.289044	Rn.106264	*LOC493869*		Similar to RIKEN cDNA 2310016C16	0.332	0.068
Hs.425427	Rn.33249	*LYAR*	*Lyar*	Hypothetical protein FLJ20425	0.303	-0.268
Hs.12109	Rn.108832	*WDR39*	*Ciao1*	WD repeat domain 39	0.225	-0.302
Hs.474436	Rn.49122	*HPS4*	*Hps4*	Hermansky-Pudlak syndrome 4	0.237	-0.326
Hs.409137	Rn.5910	*EIF2B2*	*Eif2b2*	Eukaryotic translation initiation factor 2B, subunit 2 beta, 39kDa	0.214	1.285
Hs.258209	Rn.31889	*RAB3IP*	*RABIN3*	RAB3A interacting protein (rabin3)	0.129	-0.099
Hs.76556	Rn.2232	*PPP1R15A*	*Myd116*	Protein phosphatase 1, regulatory (inhibitor) subunit 15A	0.209	-0.131
Hs.406423	Rn.103341	*SF3B2*	*Sf3B2*	Splicing factor 3b, subunit 2, 145kDa	0.085	0.107
Hs.181112	Rn.6309	*MED4*	*Med4*	Mediator of RNA polymerase II transcription, subunit 4 homolog (yeast)	0.289	-0.335
Hs.425091	Rn.27518	*FAM44B*	*Fam44B*	Family with sequence similarity 44, member B	0.102	-0.168
Hs.284141	Rn.22402	*TSPYL4*	*Tspyl4*	TSPY-like 4	0.241	-0.514
Hs.396447	Rn.47229	*FLJ32065*		Hypothetical protein FLJ32065	0.195	-0.905
Hs.461361	Rn.123614	*CFDP1*	*Cfdp1*	Craniofacial development protein 1	0.191	-0.688
Hs.3100	Rn.46563	*KARS*	*Kars*	Lysyl-tRNA synthetase	0.309	3.232
Hs.12013	Rn.2961	*ABCE1*	*Abce1*	ATP-binding cassette, sub-family E (OABP), member 1	0.367	2.339
Hs.127092	Rn.35093	*DHX38*	*Dhx38*	DEAH (Asp-Glu-Ala-His) box polypeptide 38	0.245	2.134
Hs.75890	Rn.2362	*MBTPS1*	*Mbtps1*	Membrane-bound transcription factor protease, site 1	0.247	1.731
Hs.16355	Rn.98166	*MYH10*	*Myh10*	Myosin, heavy polypeptide 10, non-muscle	0.371	0.378
Hs.401509	Rn.8822	*RBM10*	*Rbm10*	RNA binding motif protein 10	0.116	-0.166
Hs.482390	Rn.8191	*TGFBR3*	*Tgfbr3*	Transforming growth factor, beta receptor III (betaglycan, 300kDa)	0.236	0.415
Hs.292493	Rn.27023	*G22P1*	*G22p1*	Thyroid autoantigen 70kDa (Ku antigen)	0.163	-0.043
Hs.380403	Rn.19047	*PCGF4*	*Pcgf4*	Polycomb group ring finger 4	0.128	-0.473
Hs.497039	Rn.7145	*LAMC1*	*Lamc1*	Laminin, gamma 1 (formerly LAMB2)	0.240	0.146

Unigene		Gene Symbol			Log Ratio (A/B)*	
Human	**Rat**	**Human**	**Rat**	**Description**	**Human**	**Rat**
Hs.435413	Rn.94848	*MTA3*	*Mta3*	Metastasis associated 1 family, member 3	0.124	0.320
Hs.472010	Rn.3936	*PRNP*	*Prnp*	Prion protein (p27-30) (Creutzfeld-Jakob disease, Gerstmann-Strausler-Scheinker syndrome, fatal familial insomnia)	0.477	0.947
Hs.500572	Rn.8225	*FER1L3*	*Fer1L3*	Fer-1-like 3, myoferlin (C. elegans)	0.337	0.142
Hs.332197	Rn.8933	*D2S448*	*D2S448*	Melanoma associated gene	0.347	0.690
Hs.101302	Rn.11218	*COL12A1*	*Col12a1*	Collagen, type XII, alpha 1	0.283	0.084
Hs.500013	Rn.21289	*DNAJB12*	*Dnajb12*	DnaJ (Hsp40) homolog, subfamily B, member 12	0.124	-0.094
Hs.173001	Rn.8773	*ZNF644*	*Znf644*	Zinc finger protein 644	0.135	-0.299
Hs.27184	Rn.11039	*GFER*	*Gfer*	Growth factor, augmenter of liver regeneration (ERV1 homolog, S. cerevisiae)	0.198	-0.591
Hs.443625	Rn.3247	*COL3A1*	*Col3a1*	Collagen, type III, alpha 1 (Ehlers-Danlos syndrome type IV, autosomal dominant)	0.259	-2.945
Hs.269512	Rn.95652	*FSTL1*	*Fstl1*	Follistatin-like 1	0.235	0.317
Hs.511952	Rn.12512	*CBX6*	*Cbx7*	Chromobox homolog 6	0.265	-0.005
Hs.381985	Rn.56270		*Amd1*	Homo sapiens, clone IMAGE:4337652, mRNA	0.198	-1.085
Hs.509909	Rn.24380	*NUMB*	*Numb*	Numb homolog (Drosophila)	0.209	-1.141
Hs.416049	Rn.8631	*TNPO2*	*Tnpo2*	Transportin 2 (importin 3, karyopherin beta 2b)	0.148	1.986
Hs.55041	Rn.102111	*MRPL2*	*Mrpl2*	Mitochondrial ribosomal protein L2	0.095	-0.883
Hs.158688	Rn.107482	*EIF5B*	*Eif5b*	Eukaryotic translation initiation factor 5B	0.144	-0.741
Hs.406534	Rn.79731	*HMG20B*	*Hmg20B*	High-mobility group 20B	0.250	-1.722
Hs.532091	Rn.11685	*AP3B1*	*Ap3B1*	Adaptor-related protein complex 3, beta 1 subunit	0.079	1.000
Hs.435231	Rn.11634	*ZFR*	*Zfr*	Zinc finger RNA binding protein	0.155	-1.049
Hs.6076	Rn.3963	*COPS3*	*Cops3*	COP9 constitutive photomorphogenic homolog subunit 3 (Arabidopsis)	0.347	0.669
Hs.445748	Rn.2386	*FCHSD2*	*Fchsd2*	FCH and double SH3 domains 2	0.209	0.556
Hs.5120	Rn.35769	*DNCL1*	*Pin*	Dynein, cytoplasmic, light polypeptide 1	0.026	-2.154
Hs.474949	Rn.8068	*RBX1*	*Rbx1*	Ring-box 1	0.144	-0.962
Hs.268177	Rn.11243	*PLCG1*	*Plcg1*	Phospholipase C, gamma 1	0.178	-2.454
Hs.250493	Rn.47120	*ZNF219*	*Znf219*	Zinc finger protein 219	0.124	-0.078
Hs.187763	Rn.9365	*BRD4*	*Brd4*	Bromodomain containing 4	0.127	-1.451
Hs.106674	Rn.3382	*BAP1*	*Bap1*	BRCA1 associated protein-1 (ubiquitin carboxy-terminal hydrolase)	0.036	-0.537
Hs.496068	Rn.16871	*PCTK1*	*Pctk1*	PCTAIRE protein kinase 1	0.016	-1.054
Hs.475401	Rn.6207	*TATDN2*	*Tatdn2*	TatD DNase domain containing 2	0.041	-0.565
Hs.378532	Rn.2852	*HBS1L*	*Hbs1L*	HBS1-like (S. cerevisiae)	0.231	-0.408
Hs.534312	Rn.20041	*TOR1A*	*Dyt1*	Torsin family 1, member A (torsin A)	0.165	-0.056
Hs.133044	Rn.18832	*RAPTOR*		Raptor	0.031	-0.727
Hs.532216	Rn.64629	*MTERF*	*Mterf*	Transcription termination factor, mitochondrial	0.213	-0.690
Hs.63348	Rn.99346	*EMILIN1*	*Emilin1*	Elastin microfibril interfacer 1	0.204	1.740
Hs.75231	Rn.6085	*SLC16A1*	*Slc16a1*	Solute carrier family 16 (monocarboxylic acid transporters), member 1	0.286	-1.217
Hs.160958	Rn.17982	*CDC37*	*Cdc37*	CDC37 cell division cycle 37 homolog (S. cerevisiae)	0.135	-0.477
Hs.131151	Rn.24127	*PSMD9*	*Psmd9*	Proteasome (prosome, macropain) 26S subunit, non-ATPase, 9	-0.005	1.468

Unigene		Gene Symbol			Log Ratio (A/B)*	
Human	Rat	Human	Rat	Description	Human	Rat
Hs.522418	Rn.40526	*GLE1L*	*Gle1L*	GLE1 RNA export mediator-like (yeast)	0.163	-0.036
Hs.150749	Rn.9996	*BCL2*	*Bcl2*	B-cell CLL/lymphoma 2	0.237	0.056
Hs.474053	Rn.107165	*COL6A1*	*Col6A1*	Collagen, type VI, alpha 1	0.298	1.162
Hs.198281	Rn.1556	*PKM2*	*Pkm2*	Pyruvate kinase, muscle	0.173	1.561
Hs.146585	Rn.94288	*LEPROTL1*	*Leprotl1*	Leptin receptor overlapping transcript-like 1	0.225	2.123
Hs.270532	Rn.29982	*PEX12*	*Pex12*	Peroxisomal biogenesis factor 12	0.006	-0.065
Hs.413801	Rn.16691	*PSME4*	*Psme4*	Proteasome (prosome, macropain) activator subunit 4	0.121	0.601
Hs.500419	Rn.28390	*FAM35A*	*Fam35A*	Family with sequence similarity 35, member A	0.112	-0.127
Hs.443240	Rn.8177.2	*FLJ12716*		FLJ12716 protein	0.188	-0.080
Hs.192039	Rn.14233	*PTPRC*	*Ptprc*	Protein tyrosine phosphatase, receptor type, C	0.344	0.522
Hs.128067	Rn.7914	*WASPIP*	*Waspip*	Wiskott-Aldrich syndrome protein interacting protein	0.227	0.318
Hs.515524	Rn.1492	*NUCB1*	*Nucb*	Nucleobindin 1	0.172	-0.802
Hs.9731	Rn.8395	*NFKBIB*	*Nfkbib*	Nuclear factor of kappa light polypeptide gene enhancer in B-cells inhibitor, beta	0.182	-0.140
Hs.2411	Rn.10217	*P2RY1*	*P2ry1*	Purinergic receptor P2Y, G-protein coupled, 1	0.294	0.038
Hs.429581	Rn.1348	*RTN4*	*Rtn4*	Reticulon 4	0.184	0.686
Hs.132439	Rn.98353	*RELN*	*Reln*	Reelin	0.480	0.324
Hs.483454	Rn.57635	*CNN3*	*Cnn3*	Calponin 3, acidic	-0.008	-1.361
Hs.368808	Rn.7771	*EHD3*	*Ehd3*	EH-domain containing 3	0.666	0.261
Hs.472854	Rn.106880	*C20orf161*		Chromosome 20 open reading frame 161	-0.167	-0.150
Hs.189915	Rn.22664	*KIF13A*	*Kif13A*	Kinesin family member 13A	0.117	-0.181
Hs.529959	Rn.11982	*KIAA0274*		KIAA0274	-0.028	-0.072
Hs.274184	Rn.9231.2	*TFE3*	*Tfe3*	Transcription factor binding to IGHM enhancer 3	-0.163	-0.291
Hs.239663	Rn.19646	*MLLT7*	*Mllt7*	Myeloid/lymphoid or mixed-lineage leukemia (trithorax homolog, Drosophila); translocated to, 7	-0.173	-0.432
Hs.44070	Rn.8770	*SFXN2*	*Sfxn2*	Sideroflexin 2	0.066	0.965
Hs.12457	Rn.91990	*NUP133*	*Nup133*	Nucleoporin 133kDa	0.121	-0.082
Hs.469386	Rn.11215	*INPP4A*	*Inpp4a*	Inositol polyphosphate-4-phosphatase, type I, 107kDa	0.097	-0.396
Hs.153310	Rn.14163	*PREX1*	*Prex1*	Phosphatidylinositol 3,4,5-trisphosphate-dependent RAC exchanger 1	0.233	0.244
Hs.502876	Rn.2042	*RHOB*	*Rhob*	Ras homolog gene family, member B	-0.183	-0.103
Hs.95120	Rn.105938	*CYGB*	*Cygb*	Cytoglobin	0.399	0.802
Hs.190783	Rn.10037	*HAL*	*Hal*	Histidine ammonia-lyase	0.605	1.314
Hs.513153	Rn.3220	*FURIN*	*Pcsk3*	Furin (paired basic amino acid cleaving enzyme)	1.317	2.113
Hs.369440	Rn.2009	*SFXN1*	*Sfxn1*	Sideroflexin 1	0.283	1.690
Hs.440332	Rn.9093	*ERF*	*Erf*	Ets2 repressor factor	0.050	-0.303
Hs.474536	Rn.8338	*MTMR3*	*Mtmr3*	Myotubularin related protein 3	0.179	-1.121
Hs.497159	Rn.35474	*C1orf21*		Chromosome 1 open reading frame 21	0.182	0.216
Hs.350756	Rn.73714	*STAU2*	*Stau2*	Staufen, RNA binding protein, homolog 2 (Drosophila)	-0.272	-0.875
Hs.3416	Rn.101967	*ADFP*	*ADRP*	Adipose differentiation-related protein	-0.600	-0.676
Hs.528299	Rn.6629	*HTATIP*	*Htatip*	HIV-1 Tat interacting protein, 60kDa	-0.089	-0.186

Unigene		Gene Symbol			Log Ratio (A/B)*	
Human	**Rat**	**Human**	**Rat**	**Description**	**Human**	**Rat**
Hs.137427	Rn.3765	*IRF8*	*Irf8*	Interferon regulatory factor 8	-0.319	0.384
Hs.494163	Rn.24783	*GDA*	*Gda*	Guanine deaminase	1.362	-1.212
Hs.78824	Rn.13171	*TIE1*	*Tie1*	Tyrosine kinase with immunoglobulin-like and EGF-like domains 1	1.260	0.120
Hs.24258	Rn.1974	*GUCY1A3*	*Gucy1a3*	Guanylate cyclase 1, soluble, alpha 3	1.084	0.629
Hs.385861	Rn.8854	*KLHL7*	*Klhl7*	Kelch-like 7 (Drosophila)	0.124	-0.048
Hs.169378	Rn.6684	*MPDZ*	*Mpdz*	Multiple PDZ domain protein	0.500	-0.229
Hs.546248	Rn.11085	*CTSD*	*Ctsd*	Cathepsin D (lysosomal aspartyl protease)	1.639	-1.069
Hs.3873	Rn.1574	*PPT1*	*Ppt*	Palmitoyl-protein thioesterase 1 (ceroid-lipofuscinosis, neuronal 1, infantile)	1.018	1.616
Hs.272062	Rn.11386	*PTPRF*	*Ptprf*	Protein tyrosine phosphatase, receptor type, F	1.212	0.999
Hs.408062	Rn.16800	*KNSL8*	*Knsl8*	Kinesin-like 8	0.898	1.950
Hs.76364	Rn.32080	*AIF1*	*Aif1*	Allograft inflammatory factor 1	1.262	0.383
Hs.126521	Rn.10945	*HCK*	*Hck*	Hemopoietic cell kinase	1.053	0.335
Hs.514193	Rn.107168	*RAMP2*	*Ramp2*	Receptor (calcitonin) activity modifying protein 2	1.543	0.242
Hs.124649	Rn.8398	*ABCG1*	*Abcg1*	ATP-binding cassette, sub-family G (WHITE), member 1	2.250	0.666
Hs.24678	Rn.8423	*SGPP1*	*Sgpp1*	Sphingosine-1-phosphate phosphatase 1	0.586	1.611
Hs.433702	Rn.40123	*EIF5*	*Eif5*	Eukaryotic translation initiation factor 5	0.666	0.651
Hs.200841	Rn.21475	*LAMA2*	*Lama2*	Laminin, alpha 2 (merosin, congenital muscular dystrophy)	0.900	0.296
Hs.74615	Rn.55127	*PDGFRA*	*Pdgfra*	Platelet-derived growth factor receptor, alpha polypeptide	1.195	0.522
Hs.23388	Rn.32388	*DKFZP434F0318*		Hypothetical protein DKFZp434F0318	1.656	-0.294
Hs.422688	Rn.13092	*RBP7*	*Rbp7*	Retinol binding protein 7, cellular	3.399	-0.740
Hs.75799	Rn.107364	*PRSS8*	*Prss8*	Protease, serine, 8 (prostasin)	1.609	1.443
Hs.512843	Rn.17097	*NAPSA*	*Napsa*	Napsin A aspartic peptidase	0.853	0.179
Hs.162963	Rn.6715	*ANTXR2*	*Antxr2*	Anthrax toxin receptor 2	1.207	2.110
Hs.172631	Rn.54465	*ITGAM*	*Itgam*	Integrin, alpha M (complement component receptor 3, alpha; also known as CD11b (p170), macrophage antigen alpha polypeptide)	1.088	0.074
Hs.90753	Rn.103263	*HTATIP2*	*Htatip2*	HIV-1 Tat interactive protein 2, 30kDa	2.240	0.666
Hs.522730	Rn.7755	*GPRASP1*	*Gprasp1*	G protein-coupled receptor associated sorting protein 1	1.484	0.024
Hs.194121	Rn.22496	*RCL1*	*Rcl1*	RNA terminal phosphate cyclase-like 1	1.021	0.789
Hs.82407	Rn.7070	*CXCL16*	*Cxcl16*	Chemokine (C-X-C motif) ligand 16	1.856	0.627
Hs.221847	Rn.16393	*SLC38A2*	*Slc38a2*	Solute carrier family 38, member 2	0.859	0.882
Hs.523332	Rn.1430	*OAT*	*Oat*	Ornithine aminotransferase (gyrate atrophy)	0.731	3.815
Hs.370666	Rn.102196	*FOXO1A*	*Foxo1a*	Forkhead box O1A (rhabdomyosarcoma)	0.778	-0.178
Hs.42217	Rn.3622	*CDA08*	*Cda08*	T-cell immunomodulatory protein	1.603	-0.397
Hs.75294	Rn.10349	*CRH*	*Crh*	Corticotropin releasing hormone	0.825	0.003
Hs.1799	Rn.11120	*CD1D*	*Cd1d1*	CD1D antigen, d polypeptide	0.528	0.791
Hs.514535	Rn.3251	*LGALS3BP*	*Lgals3bp*	Lectin, galactoside-binding, soluble, 3 binding protein	1.093	1.517
Hs.118681	Rn.12019	*ERBB3*	*Erbb3*	V-erb-b2 erythroblastic leukemia viral oncogene homolog 3 (avian)	0.805	1.799
Hs.247460	Rn.11029	*NLN*	*Nln*	Neurolysin (metallopeptidase M3 family)	0.203	0.221
Hs.489849	Rn.9699	*SLC13A1*	*Slc13a1*	**Solute carrier family 13 (sodium/sulfate	0.451	0.003

Unigene		Gene Symbol			Log Ratio (A/B)*	
Human	Rat	Human	Rat	Description	Human	Rat
				symporters), member 1		
Hs.516376	Rn.22892	*WDR33*	*Wdr33*	WD repeat domain 33	0.128	-0.532
Hs.396740	Rn.6506	*NIP30*	*Nip30*	NEFA-interacting nuclear protein NIP30	0.058	-0.258
Hs.131776	Rn.23058	*PGPEP1*	*Pgpep1*	Pyroglutamyl-peptidase I	0.934	0.459
Hs.524625	Rn.6500	*GRK5*	*Gprk5*	G protein-coupled receptor kinase 5	0.361	0.051
Hs.9688	Rn.11988	*CMRF-35H*	*Cmrf-35H*	CD300A antigen	0.212	0.598
Hs.500101	Rn.13776	*VCL*	*Vcl*	Vinculin	0.167	1.033
Hs.357128	Rn.100030	*MOCS1*	*Mocs1*	Molybdenum cofactor synthesis 1	1.532	-0.929
Hs.408846	Rn.18573	*SEMA4A*	*Sema4A*	Sema domain, immunoglobulin domain (Ig), transmembrane domain (TM) and short cytoplasmic domain, (semaphorin) 4A	0.041	-2.042
Hs.75275	Rn.102204	*UBE4A*	*Ube4a*	Ubiquitination factor E4A (UFD2 homolog, yeast)	-0.124	-0.994
Hs.351558	Rn.21476	*U2AF1L3*		U2(RNU2) small nuclear RNA auxiliary factor 1-like 3	0.025	0.091
Hs.102402	Rn.3279	*MXD4*	*Mxd4*	MAX dimerization protein 4	-0.250	1.064
Hs.110849	Rn.53888	*ESRRA*	*Esrra*	Estrogen-related receptor alpha	-0.030	-0.288
Hs.296169	Rn.3016	*RAB4A*	*Rab4a*	RAB4A, member RAS oncogene family	-0.333	-0.459
Hs.380906	Rn.106161	*MYADM*	*Myadm*	Myeloid-associated differentiation marker	0.420	-0.818
Hs.303669	Rn.17455	*MGC26694*		Hypothetical protein MGC26694	0.738	1.490
Hs.418198	Rn.6410	*PAPD4*	*Papd4*	PAP associated domain containing 4	0.274	-0.010
Hs.8261	Rn.8693	*SSB1*	*Ssb1*	SPRY domain-containing SOCS box protein SSB-1	0.238	-0.367
Hs.125039	Rn.4896	*CROT*	*Crot*	Carnitine O-octanoyltransferase	0.141	0.822
Hs.55131	Rn.20696	*DKFZp313N0621*		Chromosome 3 open reading frame 23	-0.041	-0.337
Hs.149414	Rn.5825	*CR1L*	*Crry*	Complement component (3b/4b) receptor 1-like	-0.344	1.109
Hs.300834	Rn.12691	*GALNT2*	*Galnt2*	UDP-N-acetyl-alpha-D-galactosamine:polypeptide N-acetylgalactosaminyltransferase 2 (GalNAc-T2)	0.565	-0.691
Hs.304376	Rn.23619	*PPP1R15B*	*Ppp1R15B*	Protein phosphatase 1, regulatory (inhibitor) subunit 15B	-0.111	2.001
Hs.514373	Rn.2567	*MTMR4*	*Mtmr4*	Myotubularin related protein 4	-0.108	-0.494
Hs.471917	Rn.17460	*PSMF1*	*Psmf1*	Proteasome inhibitor subunit 1 PI31	-0.150	-1.270
Hs.253903	Rn.16958	*STOM*	*Stom*	Stomatin	0.181	0.119
Hs.821	Rn.783	*BGN*	*Bgn*	Biglycan	-0.155	-2.507
Hs.522578	Rn.6312	*STS*	*Sts*	Steroid sulfatase microsomal, arylsulfatase C, isozyme S	-0.081	-0.668
Hs.499222	Rn.2549	*CES1*	*Es2*	Carboxylesterase 1 (monocyte/macrophage serine esterase 1)	0.702	-0.911
Hs.149387	Rn.18047	*MYO6*	*Myo6*	Myosin VI	0.579	-0.252
Hs.264	Rn.16693	*PNPLA4*	*Pnpla4*	Patatin-like phospholipase domain containing 4	0.338	-0.022
Hs.434961	Rn.88438	*ATXN1*	*Sca1*	Ataxin 1	-0.202	-0.011
Hs.410388	Rn.73451	*LACTB*	*Lactb*	Lactamase, beta	0.780	0.169
Hs.453951	Rn.37438	*NRG1*	*Nrg1*	Neuregulin 1	1.188	0.044
Hs.414473	Rn.15657	*C6orf110*		Chromosome 6 open reading frame 110	0.281	-0.639
Hs.533055	Rn.4126	*PCAF*	*Pcaf*	P300/CBP-associated factor	0.119	0.288
Hs.232194	Rn.2250	*KIAA0174*		KIAA0174 gene product	-0.181	1.440

Unigene		Gene Symbol			Log Ratio (A/B)*	
Human	**Rat**	**Human**	**Rat**	**Description**	**Human**	**Rat**
Hs.132314	Rn.8731	*ELTD1*	*Etl*	EGF, latrophilin and seven transmembrane domain containing 1	0.578	0.213
Hs.2006	Rn.9158	*GSTM3*	*Gstm5*	Glutathione S-transferase M3 (brain)	0.208	0.078
Hs.398157	Rn.12100	*PLK2*	*Plk2*	Polo-like kinase 2 (Drosophila)	0.099	0.950
Hs.270570	Rn.8820	*DBT*	*Dbt*	Dihydrolipoamide branched chain transacylase E2	0.268	-0.626
Hs.76494	Rn.65510	*PRELP*	*Prelp*	Proline arginine-rich end leucine-rich repeat protein	-0.622	0.908
Hs.19156	Rn.28222	*DAAM1*	*Daam1*	Dishevelled associated activator of morphogenesis 1	0.654	1.157
Hs.1041	Rn.87436	*ROS1*	*Ros1*	V-ros UR2 sarcoma virus oncogene homolog 1 (avian)	0.444	-0.042
Hs.529735	Rn.11133	*AADAT*	*Aadat*	Aminoadipate aminotransferase	0.502	1.624
Hs.160562	Rn.6282	*IGF1*	*Igf1*	Insulin-like growth factor 1 (somatomedin C)	-0.923	0.600
Hs.519276	Rn.6276	*MAPKAPK2*	*Mapkapk2*	Mitogen-activated protein kinase-activated protein kinase 2	0.171	2.764
Hs.408312	Rn.54443	*TP53*	*Tp53*	Tumor protein p53 (Li-Fraumeni syndrome)	0.001	0.303
Hs.517033	Rn.10	*TGM2*	*Tgm2*	Transglutaminase 2 (C polypeptide, protein-glutamine-gamma-glutamyltransferase)	-2.015	-2.435
Hs.46319	Rn.37473	*SHBG*	*Shbg*	Sex hormone-binding globulin	-1.162	-0.058
Hs.481342	Rn.24612	*ARGBP2*	*Argbp2*	Arg/Abl-interacting protein ArgBP2	1.252	-0.864
Hs.156727	Rn.81030	*ANKH*	*Ank*	Ankylosis, progressive homolog (mouse)	0.941	0.996
Hs.5476	Rn.17644	*SLC25A25*	*Pcscl*	Solute carrier family 25 (mitochondrial carrier; phosphate carrier), member 25	0.597	2.431
Hs.446077	Rn.73202	*SLC38A4*	*Slc38A4*	Solute carrier family 38, member 4	-0.099	3.487
Hs.494496	Rn.15319	*FBP1*	*Fbp2*	Fructose-1,6-bisphosphatase 1	-0.594	-0.879
Hs.514489	Rn.12104	*WBP2*	*Wbp2*	WW domain binding protein 2	0.317	0.132
Hs.8375	Rn.3219	*TRAF4*	*Traf4*	TNF receptor-associated factor 4	0.005	0.542
Hs.498543	Rn.6923	*FBXO18*	*Fbxo18*	F-box protein, helicase, 18	-0.059	-1.000
Hs.189641	Rn.24238	*SEC24D*	*Sec24D*	SEC24 related gene family, member D (S. cerevisiae)	0.338	-2.250
Hs.193566	Rn.15254	*ZDHHC9*	*Zdhhc9*	Zinc finger, DHHC domain containing 9	1.370	0.145

APPENDIX 4

Unsupervised hierarchical clustering of 15,866 genes in liver distinguishes between choline sufficient (CS) and choline deficient (CD) treated rats

Hierarchical clustering analysis was conducted on control choline sufficient (CS) or choline deficient (CD) liver samples collected between 4 and 80 weeks. Tumor (T) samples were collected at 80 weeks from CD-treated rats. The dendrogram shows that the samples clustered into two groups according to treatment. The color of each gene is proportional to the mean expression level (in $\log_2$ units, see color bar) of the gene across the entire set of samples (red - median, black – no change, and green - below median value).

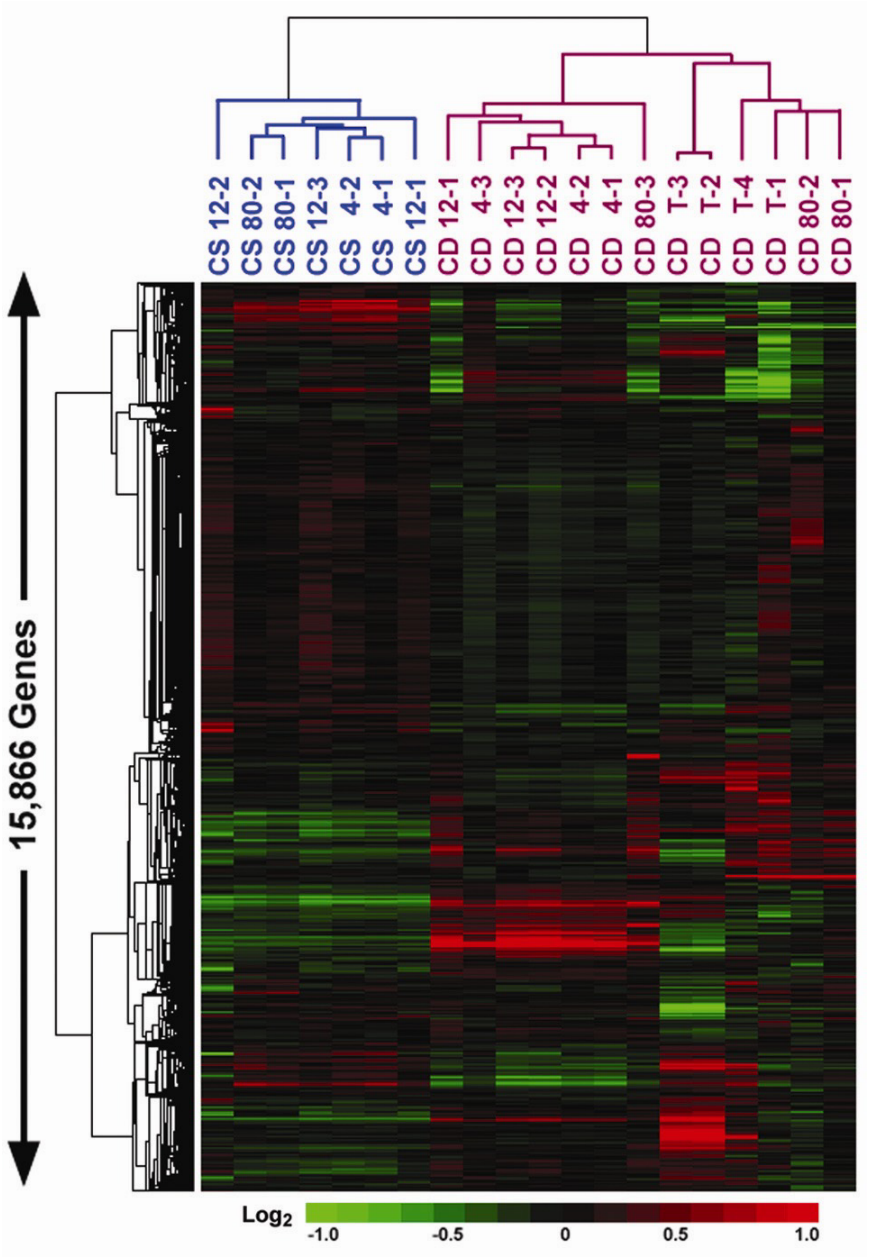

APPENDIX 5

KEGG-annotated pathways that are significantly enriched in CD rats

Two significant gene lists were generated using intrinsic gene identifier (white bar) or SAM (grey bar) and the number of genes (as identified by each procedure) for a given KEGG pathway is shown in comparison to a total number of genes in that representative pathway (black bar).

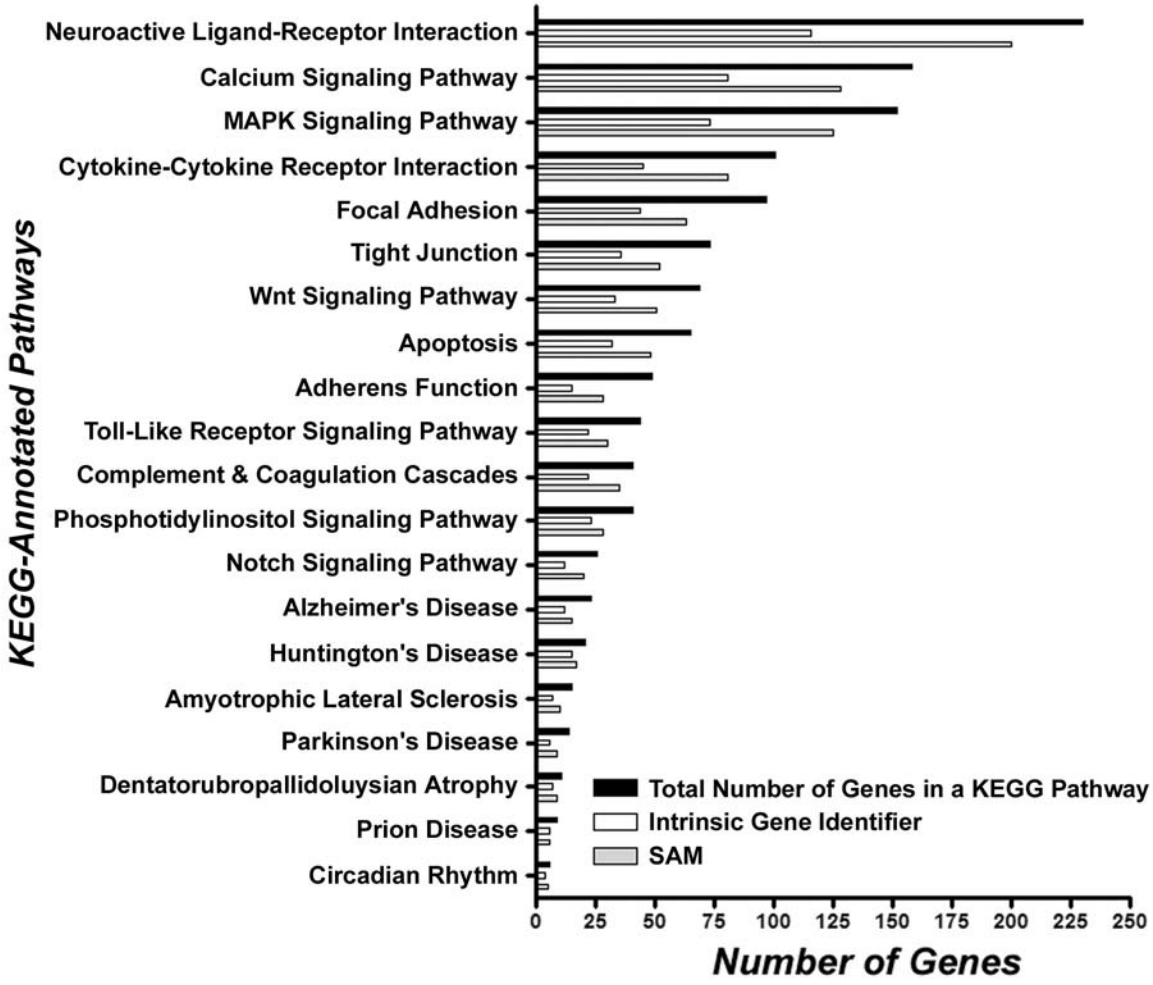

Reference List

1. National Academy of Sciences. Toxicogenomics: the "new biology" revolution in environmental health sciences. Washington, DC: The National Academy of Science; 2002.

2. Tennant RW. The National Center for Toxicogenomics: using new technologies to inform mechanistic toxicology. Environ Health Perspect 2002 Jan;110(1):A8-10.

3. Waters M, Boorman G, Bushel P, Cunningham M, Irwin R, Merrick A, et al. Systems toxicology and the Chemical Effects in Biological Systems (CEBS) knowledge base. EHP Toxicogenomics 2003 Jan;111(1T):15-28.

4. Paules R. Phenotypic anchoring: Linking cause and effect. Environ Health Perspect 2003;111(6):A338-A339.

5. Hamadeh HK, Bushel PR, Jayadev S, DiSorbo O, Bennett L, Li L, et al. Prediction of compound signature using high density gene expression profiling. Toxicol Sci 2002 Jun;67(2):232-240.

6. Hamadeh HK, Bushel PR, Jayadev S, Martin K, DiSorbo O, Sieber S, et al. Gene expression analysis reveals chemical-specific profiles. Toxicol Sci 2002 Jun;67(2):219-231.

7. Hamadeh HK, Bushel P, Paules R, Afshari CA. Discovery in toxicology: mediation by gene expression array technology. J Biochem Mol Toxicol 2001;15(5):231-242.

8. Boverhof DR, Zacharewski TR. Toxicogenomics in risk assessment: applications and needs. Toxicol Sci 2006 Feb;89(2):352-360.

9. Zeeberg BR, Feng W, Wang G, Wang MD, Fojo AT, Sunshine M, et al. GoMiner: a resource for biological interpretation of genomic and proteomic data. Genome Biol 2003;4(4):R28.

10. Orphanides G, Kimber I. Toxicogenetics: applications and opportunities. Toxicol Sci 2003 Sep;75(1):1-6.

11. Cooke MS, Evans MD, Dizdaroglu M, Lunec J. Oxidative DNA damage: mechanisms, mutation, and disease. FASEB J 2003 Jul;17(10):1195-1214.

12. von Sonntag C. The Chemical Basis of Radiation Biology. London: Taylor and Francis, 1987.

13. Valko M, Izakovic M, Mazur M, Rhodes CJ, Telser J. Role of oxygen radicals in DNA damage and cancer incidence. Mol Cell Biochem 2004 Nov;266(1-2):37-56.

14. Sies H. Oxidative Stress. New York: Academic Press, 1985.

15. Friedberg EC. DNA damage and repair. Nature 2003 Jan 23;421(6921):436-440.

16. Slupphaug G, Kavli B, Krokan HE. The interacting pathways for prevention and repair of oxidative DNA damage. Mutat Res 2003 Oct 29;531(1-2):231-251.

17. Palmer HJ, Paulson KE. Reactive oxygen species and antioxidants in signal transduction and gene expression. Nutr Rev 1997 Oct;55(10):353-361.

18. Poli G, Leonarduzzi G, Biasi F, Chiarpotto E. Oxidative stress and cell signalling. Curr Med Chem 2004 May;11(9):1163-1182.

19. Kamata H, Hirata H. Redox regulation of cellular signalling. Cell Signal 1999 Jan;11(1):1-14.

20. Liou JS, Chen CY, Chen JS, Faller DV. Oncogenic ras mediates apoptosis in response to protein kinase C inhibition through the generation of reactive oxygen species. J Biol Chem 2000 Dec 15;275(50):39001-39011.

21. Staal FJ, Anderson MT, Staal GE, Herzenberg LA, Gitler C, Herzenberg LA. Redox regulation of signal transduction: tyrosine phosphorylation and calcium influx. Proc Natl Acad Sci U S A 1994 Apr 26;91(9):3619-3622.

22. Anderson MT, Staal FJ, Gitler C, Herzenberg LA, Herzenberg LA. Separation of oxidant-initiated and redox-regulated steps in the NF-kappa B signal transduction pathway. Proc Natl Acad Sci U S A 1994 Nov 22;91(24):11527-11531.

23. Powis G, Gasdaska JR, Baker A. Redox signaling and the control of cell growth and death. Adv Pharmacol 1997;38:329-359.

24. Helbock HJ, Beckman KB, Shigenaga MK, Walter PB, Woodall AA, Yeo HC, et al. DNA oxidation matters: the HPLC-electrochemical detection assay of 8-oxo-deoxyguanosine and 8-oxo-guanine. Proc Natl Acad Sci U S A 1998 Jan 6;95(1):288-293.

25. Kawanishi S, Hiraku Y, Oikawa S. Mechanism of guanine-specific DNA damage by oxidative stress and its role in carcinogenesis and aging. Mutat Res 2001 Mar;488(1):65-76.

26. Marnett LJ. Oxyradicals and DNA damage. Carcinogenesis 2000 Mar;21(3):361-370.

27. Fraga CG, Shigenaga MK, Park JW, Degan P, Ames BN. Oxidative damage to DNA during aging: 8-hydroxy-2'-deoxyguanosine in rat organ DNA and urine. Proc Natl Acad Sci U S A 1990 Jun;87(12):4533-4537.

28. Von Sonntag C. New aspects in the free-radical chemistry of pyrimidine nucleobases. Free Rad Res Comm 1987;2(4-6):217-224.

29. Dizdaroglu M. Oxidative damage to DNA in mammalian chromatin. Mutat Res 1992;275:331-342.

30. Demple B, Harrison L. Repair of oxidative damage to DNA: Enzymology and biology. Annu Rev Biochem 1994;63:915-948.

31. Cadet J, Douki T, Gasparutto D, Ravanat JL. Oxidative damage to DNA: formation, measurement and biochemical features. Mutat Res 2003 Oct 29;531(1-2):5-23.

32. Hussain SP, Hofseth LJ, Harris CC. Radical causes of cancer. Nat Rev Cancer 2003 Apr;3(4):276-285.

33. Halliwell B, Aruoma OI. DNA damage by oxygen-derived species. Its mechanism and measurement in mammalian systems. FEBS Lett 1991 Apr 9;281(1-2):9-19.

34. Dizdaroglu M. Quantitative determination of oxidative base damage in DNA by stable isotope-dilution mass spectrometry. FEBS Lett 1993;315(1):1-6.

35. Steenken S. Structure, acid/base properties and transformation reactions of purine radicals. Free Rad Res Comm 1989;6(2-3):117-120.

36. von Sonntag C. The Chemical Basis of Radiation Biology. London: Taylor & Francis, 1987.

37. Halliwell B, Gutteridge JMC. Free Radicals in Biology and Medicine. 2 ed. Oxford: Clarendon Press, 1989.

38. Michaels ML, Miller JH. The GO system protects organisms from the mutagenic effect of the spontaneous lesion 8-hydroxyguanine (7,8-dihydro-8-oxoguanine). J Bacteriol 1992;174:6321-6325.

39. Thomas D, Scot AD, Barbey R, Padula M, Boiteux S. Inactivation of OGG1 increases the incidence of G:C to T:A transversions in Saccharomyces cerevisiae: evidence for endogenous oxidative damage to DNA in eukaryotic cells. Mol Gen Genet 1997 Mar 26;254(2):171-178.

40. Inoue S, Kawanishi S. Oxidative DNA damage induced by simultaneous generation of nitric oxide and superoxide. FEBS Lett 1995 Aug 28;371(1):86-88.

41. Yermilov V, Rubio J, Ohshima H. Formation of 8-nitroguanine in DNA treated with peroxynitrite in vitro and its rapid removal from DNA by depurination. FEBS Lett 1995 Dec 4;376(3):207-210.

42. Salgo MG, Stone K, Squadrito GL, Battista JR, Pryor WA. Peroxynitrite causes DNA nicks in plasmid pBR322. Biochem Biophys Res Commun 1995 May 25;210(3):1025-1030.

43. Douki T, Cadet J. Peroxynitrite mediated oxidation of purine bases of nucleosides and isolated DNA. Free Radic Res 1996 May;24(5):369-380.

44. Tretyakova NY, Wishnok JS, Tannenbaum SR. Peroxynitrite-induced secondary oxidative lesions at guanine nucleobases: chemical stability and recognition by the Fpg DNA repair enzyme. Chem Res Toxicol 2000 Jul;13(7):658-664.

45. Uppu RM, Cueto R, Squadrito GL, Salgo MG, Pryor WA. Competitive reactions of peroxynitrite with 2'-deoxyguanosine and 7,8-dihydro-8-oxo-2'-

deoxyguanosine (8-oxodg) - relevance to the formation of 8-oxodG in DNA exposed to peroxynitrite. Free Radic Biol Med 1996;21(3):407-411.

46. Burney S, Niles JC, Dedon PC, Tannenbaum SR. DNA damage in deoxynucleosides and oligonucleotides treated with peroxynitrite. Chem Res Toxicol 1999 Jun;12(6):513-520.

47. Juedes MJ, Wogan GN. Peroxynitrite-induced mutation spectra of pSP189 following replication in bacteria and in human cells. Mutat Res 1996 Jan 17;349(1):51-61.

48. Dedon PC, Plastaras JP, Rouzer CA, Marnett LJ. Indirect mutagenesis by oxidative DNA damage: formation of the pyrimidopurinone adduct of deoxyguanosine by base propenal. Proc Natl Acad Sci USA 1998 Sep 15;95(19):11113-11116.

49. Singer B. The role of cyclic nucleic acid adducts in carcinogenesis and mutagenesis. Lyon, France: International Agency for Research on Cancer; 1986. Report No.: 70.

50. Marnett LJ. DNA Adducts: Identification and Biological Significance. Lyon, France: International Agency for Research on Cancer; 1994. Report No.: 125.

51. Esterbauer H, Eckl P, Ortner A. Possible mutagens derived from lipids and lipid precursors. Mutat Res 1990 May;238(3):223-233.

52. Spalding JW. Toxicology and carcinogenesis studies of malondialdehyde sodium salt (3-hydroxy-2-propenal, sodium salt) in F344/N rats and B6C3F1 mice. 1988. Report No.: 331.

53. Griffiths HR. Antioxidants and protein oxidation. Free Radic Res 2000 Nov;33 Suppl:S47-S58.

54. Naskalski JW, Bartosz G. Oxidative modifications of protein structures. Adv Clin Chem 2000;35:161-253.

55. Stadtman ER. Oxidation of free amino acids and amino acid residues in proteins by radiolysis and by metal-catalyzed reactions. Annu Rev Biochem 1993;62:797-821.

56. Stadtman ER. Protein oxidation and aging. Free Radic Res 2006 Dec;40(12):1250-1258.

57. Stadtman ER. Metal ion-catalyzed oxidation of proteins: biochemical mechanism and biological consequences. Free Radic Biol Med 1990;9(4):315-325.

58. Greenacre SA, Ischiropoulos H. Tyrosine nitration: localisation, quantification, consequences for protein function and signal transduction. Free Radic Res 2001 Jun;34(6):541-581.

59. Levine RL, Mosoni L, Berlett BS, Stadtman ER. Methionine residues as endogenous antioxidants in proteins. Proc Natl Acad Sci U S A 1996 Dec 24;93(26):15036-15040.

60. Stadtman ER, Levine RL. Protein oxidation. Ann N Y Acad Sci 2000;899:191-208.

61. Cheeseman KH. Lipid Peroxidation and Cancer. In: Halliwell B, Aruoma OI, eds. DNA and Free Radicals.Chichester: Ellis Horwood Limited, 1993. 109-144.

62. Kaneko T, Honda S, Nakano S, Matsuo M. Lethal effects of a linoleic acid hydroperoxide and its autoxidation products, unsaturated aliphatic aldehydes, on human diploid fibroblasts. Chem Biol Interact 1987;63(2):127-137.

63. Valko M, Rhodes CJ, Moncol J, Izakovic M, Mazur M. Free radicals, metals and antioxidants in oxidative stress-induced cancer. Chem Biol Interact 2006 Mar 10;160(1):1-40.

64. Tomkinson AE, Mackey ZB. Structure and function of mammalian DNA ligases. Mutat Res 1998 Feb;407(1):1-9.

65. Friedberg EC, Walker GC, Siede W. DNA Repair and Mutagenesis. Washington, D.C.: American Society for Microbiology, 1995.

66. Cairns J. The contribution of bacterial hypermutators to mutation in stationary phase. Genetics 2000 Oct;156(2):923-926.

67. Glassner BJ, Rasmussen LJ, Najarian MT, Posnick LM, Samson LD. Generation of a strong mutator phenotype in yeast by imbalanced base excision repair. Proc Natl Acad Sci USA 1998 Aug 18;95(17):9997-10002.

68. Posnick LM, Samson LD. Imbalanced base excision repair increases spontaneous mutation and alkylation sensitivity in Escherichia coli. J Bacteriol 1999 Nov;181(21):6763-6771.

69. Canitrot Y, Cazaux C, Frechet M, Bouayadi K, Lesca C, Salles B, et al. Overexpression of DNA polymerase beta in cell results in a mutator phenotype and a decreased sensitivity to anticancer drugs. Proc Natl Acad Sci U S A 1998 Oct 13;95(21):12586-12590.

70. Armitage P, Doll R. The age distribution of cancer and a multi-stage theory of carcinogenesis. Br J Cancer 1954 Mar;8(1):1-12.

71. Schwarz M, Peres G, Kunz W, Furstenberger G, Kittstein W, Marks F. On the role of superoxide anion radicals in skin tumour promotion. Carcinogenesis 1984 Dec;5(12):1663-1670.

72. Coussens LM, Werb Z. Inflammation and cancer. Nature 2002 Dec 19;420(6917):860-867.

73. Rusyn I, Rose ML, Bojes HK, Thurman RG. Novel role of oxidants in the molecular mechanism of action of peroxisome proliferators. Antiox Redox Signal 2000;2:607-621.

74. Cerutti PA, Trump BF. Inflammation and oxidative stress in carcinogenesis. Cancer Cells 1991 Jan;3(1):1-7.

75. Weisburger JH. Antimutagenesis and anticarcinogenesis, from the past to the future. Mutat Res 2001 Sep 1;480-481:23-35.

76. Balkwill F, Mantovani A. Inflammation and cancer: back to Virchow? Lancet 2001 Feb 17;357(9255):539-545.

77. Klaunig JE, Xu Y, Bachowski S, and Jiang J. Free-Radical Oxygen-Induced Changes in Chemical Carcinogenesis. In: Wallace KB, ed. Free Radical Toxicology. Taylor & Francis, 1997. 375-400.

78. IARC Working Group. Benzene. Lyon, France: International Agency for Research on Cancer; 1987. Report No.: 7.

79. Kolachana P, Subrahmanyam VV, Meyer KB, Zhang L, Smith MT. Benzene and its phenolic metabolites produce oxidative DNA damage in HL60 cells in vitro and in the bone marrow in vivo. Cancer Res 1993 Mar 1;53(5):1023-1026.

80. Goode EL, Ulrich CM, Potter JD. Polymorphisms in DNA repair genes and associations with cancer risk. Cancer Epidemiol Biomarkers Prev 2002 Dec;11(12):1513-1530.

81. Collins A, Cadet J, Epe B, Gedik C. Problems in the measurement of 8-oxoguanine in human DNA. Report of a workshop, DNA oxidation, held in Aberdeen, UK, 19-21 January, 1997. Carcinogenesis 1997 Sep;18(9):1833-1836.

82. Hofer T, Moller L. Reduction of oxidation during the preparation of DNA and analysis of 8-hydroxy-2'-deoxyguanosine. Chem Res Toxicol 1998 Aug;11(8):882-887.

83. Nakamura J, Swenberg JA. Endogenous apurinic/apyrimidinic sites in genomic DNA of mammalian tissues. Cancer Res 1999 Jun 1;59(11):2522-2526.

84. Rusyn I, Denissenko MF, Wong VA, Butterworth BE, Cunningham ML, Upton PB, et al. Expression of base excision repair enzymes in rat and mouse liver is induced by peroxisome proliferators and is dependent upon carcinogenic potency. Carcinogenesis 2000 Dec;21(12):2141-2145.

85. Hofseth LJ, Khan MA, Ambrose M, Nikolayeva O, Xu-Welliver M, Kartalou M, et al. The adaptive imbalance in base excision-repair enzymes generates microsatellite instability in chronic inflammation. J Clin Invest 2003 Dec;112(12):1887-1894.

86. Pastore A, Federici G, Bertini E, Piemonte F. Analysis of glutathione: implication in redox and detoxification. Clin Chim Acta 2003 Jul 1;333(1):19-39.

87. Olson H, Betton G, Robinson D, Thomas K, Monro A, Kolaja G, et al. Concordance of the toxicity of pharmaceuticals in humans and in animals. Regul Toxicol Pharmacol 2000 Aug;32(1):56-67.

88. Waring JF, Jolly RA, Ciurlionis R, Lum PY, Praestgaard JT, Morfitt DC, et al. Clustering of hepatotoxins based on mechanism of toxicity using gene expression profiles. Toxicol Appl Pharmacol 2001 Aug 15;175(1):28-42.

89. Chung CH, Bernard PS, Perou CM. Molecular portraits and the family tree of cancer. Nat Genet 2002 Dec;32 Suppl:533-540.

90. Holleman A, Cheok MH, den Boer ML, Yang W, Veerman AJ, Kazemier KM, et al. Gene-expression patterns in drug-resistant acute lymphoblastic leukemia cells and response to treatment. N Engl J Med 2004 Aug 5;351(6):533-542.

91. Heinloth AN, Irwin RD, Boorman GA, Nettesheim P, Fannin RD, Sieber SO, et al. Gene expression profiling of rat livers reveals indicators of potential adverse effects. Toxicol Sci 2004 Jul;80(1):193-202.

92. Simopoulos AP. Essential fatty acids in health and chronic disease. Am J Clin Nutr 1999 Sep;70(3 Suppl):560S-569S.

93. Boorman GA, Haseman JK, Waters MD, Hardisty JF, Sills RC. Quality review procedures necessary for rodent pathology databases and toxicogenomic studies: the National Toxicology Program experience. Toxicol Pathol 2002 Jan;30(1):88-92.

94. Bammler T, Beyer RP, Bhattacharya S, Boorman GA, Boyles A, Bradford BU, et al. Standardizing global gene expression analysis between laboratories and across platforms. Nat Methods 2005;2(5):351-356.

95. Nakamura J, La DK, Swenberg JA. 5'-nicked apurinic/apyrimidinic sites are resistant to b-elimination by b-polymerase and are persistent in human cultured cells after oxidative stress. J Biol Chem 2000 Feb 25;275(8):5323-5328.

96. Liao S. Quantification of 8-hydroxy-2'-deoxyguanosine in DNA by capillary liquid chromatography-electrospray tandem mass spectrometry. University of North Carolina at Chapel Hill; 2003.

97. Radi R, Beckman JS, Bush KM, Freeman BA. Peroxynitrite-induced membrane lipid peroxidation: the cytotoxic potential of superoxide and nitric oxide. Arch Biochem Biophys 1991 Aug 1;288(2):481-487.

98. Pryor WA, Squadrito GL. The chemistry of peroxynitrite: a product from the reaction of nitric oxide with superoxide. Am J Physiol 1995 May;268(5 Pt 1):L699-L722.

99. Mitchell JR, Jollow DJ, Potter WZ, Davis DC, Gillette JR, Brodie BB. Acetaminophen-induced hepatic necrosis. I. Role of drug metabolism. J Pharmacol Exp Ther 1973 Oct;187(1):185-194.

100. ESCODD. Measurement of DNA oxidation in human cells by chromatographic and enzymic methods. Free Radic Biol Med 2003 Apr 15;34(8):1089-1099.

101. Pogozelski WK, Tullius TD. Oxidative strand scission of nucleic acids: Routes initiated by hydrogen abstraction from the sugar moiety. Chemical Review 1998;98:1089-1107.

102. Khan MF, Wu X, Tipnis UR, Ansari GA, Boor PJ. Protein adducts of malondialdehyde and 4-hydroxynonenal in livers of iron loaded rats: quantitation and localization. Toxicology 2002 May 1;173(3):193-201.

103. Ostapowicz G, Fontana RJ, Schiodt FV, Larson A, Davern TJ, Han SH, et al. Results of a prospective study of acute liver failure at 17 tertiary care centers in the United States. Ann Intern Med 2002 Dec 17;137(12):947-954.

104. Dahlin DC, Miwa GT, Lu AY, Nelson SD. N-acetyl-p-benzoquinone imine: a cytochrome P-450-mediated oxidation product of acetaminophen. Proc Natl Acad Sci U S A 1984 Mar;81(5):1327-1331.

105. Cohen SD, Pumford NR, Khairallah EA, Boekelheide K, Pohl LR, Amouzadeh HR, et al. Selective protein covalent binding and target organ toxicity. Toxicol Appl Pharmacol 1997 Mar;143(1):1-12.

106. Qiu Y, Benet LZ, Burlingame AL. Identification of the hepatic protein targets of reactive metabolites of acetaminophen in vivo in mice using two-dimensional gel electrophoresis and mass spectrometry. J Biol Chem 1998 Jul 10;273(28):17940-17953.

107. Donnelly PJ, Walker RM, Racz WJ. Inhibition of mitochondrial respiration in vivo is an early event in acetaminophen-induced hepatotoxicity. Arch Toxicol 1994;68(2):110-118.

108. Jaeschke H. Glutathione disulfide formation and oxidant stress during acetaminophen-induced hepatotoxicity in mice in vivo: the protective effect of allopurinol. J Pharmacol Exp Ther 1990 Dec;255(3):935-941.

109. Hinson JA, Pike SL, Pumford NR, Mayeux PR. Nitrotyrosine-protein adducts in hepatic centrilobular areas following toxic doses of acetaminophen in mice. Chem Res Toxicol 1998 Jun;11(6):604-607.

110. Gardner CR, Heck DE, Yang CS, Thomas PE, Zhang XJ, DeGeorge GL, et al. Role of nitric oxide in acetaminophen-induced hepatotoxicity in the rat. Hepatology 1998 Mar;27(3):748-754.

111. O'Donnell VB, Chumley PH, Hogg N, Bloodsworth A, Darley-Usmar VM, Freeman BA. Nitric oxide inhibition of lipid peroxidation: kinetics of reaction with lipid peroxyl radicals and comparison with alpha-tocopherol. Biochemistry 1997 Dec 9;36(49):15216-15223.

112. James LP, Mayeux PR, Hinson JA. Acetaminophen-induced hepatotoxicity. Drug Metab Dispos 2003 Dec;31(12):1499-1506.

113. James LP, McCullough SS, Lamps LW, Hinson JA. Effect of N-acetylcysteine on acetaminophen toxicity in mice: relationship to reactive nitrogen and cytokine formation. Toxicol Sci 2003 Oct;75(2):458-467.

114. Gaut JP, Byun J, Tran HD, Lauber WM, Carroll JA, Hotchkiss RS, et al. Myeloperoxidase produces nitrating oxidants in vivo. J Clin Invest 2002 May;109(10):1311-1319.

115. Whiteman M, Kaur H, Halliwell B. Protection against peroxynitrite dependent tyrosine nitration and alpha 1-antiproteinase inactivation by some anti-inflammatory drugs and by the antibiotic tetracycline. Ann Rheum Dis 1996 Jun;55(6):383-387.

116. Lakshmi VM, Hsu FF, Davis BB, Zenser TV. Nitrating reactive nitric oxygen species transform acetaminophen to 3-nitroacetaminophen. Chem Res Toxicol 2000 Sep;13(9):891-899.

117. Fritz G, Grosch S, Tomicic M, Kaina B. APE/Ref-1 and the mammalian response to genotoxic stress. Toxicology 2003 Nov 15;193(1-2):67-78.

118. Wendell GD, Thurman RG. Effect of ethanol concentration on rates of ethanol elimination in normal and alcohol-treated rats in vivo. Biochem Pharmacol 1979;28(2):273-279.

119. Knight TR, Fariss MW, Farhood A, Jaeschke H. Role of lipid peroxidation as a mechanism of liver injury after acetaminophen overdose in mice. Toxicol Sci 2003 Nov;76(1):229-236.

120. Hinson JA, Bucci TJ, Irwin LK, Michael SL, Mayeux PR. Effect of inhibitors of nitric oxide synthase on acetaminophen-induced hepatotoxicity in mice. Nitric Oxide 2002 Mar;6(2):160-167.

121. Henry CJ, Phillips R, Carpanini F, Corton JC, Craig K, Igarashi K, et al. Use of genomics in toxicology and epidemiology: findings and recommendations of a workshop. Environ Health Perspect 2002 Oct;110(10):1047-1050.

122. Nakae D. Endogenous liver carcinogenesis in the rat. Pathol Int 1999 Dec;49(12):1028-1042.

123. Zeisel SH, Albright CD, Shin OH, Mar MH, Salganik RI, da Costa KA. Choline deficiency selects for resistance to p53-independent apoptosis and causes tumorigenic transformation of rat hepatocytes. Carcinogenesis 1997 Apr;18(4):731-738.

124. Chandar N, Amenta J, Kandala JC, Lombardi B. Liver cell turnover in rats fed a choline-devoid diet. Carcinogenesis 1987 May;8(5):669-673.

125. Ghoshal AK, Farber E. Liver biochemical pathology of choline deficiency and of methyl group deficiency: A new orientation and assessment. Histol Histopathol 1995;10(2):457-462.

126. Nakae D, Yoshiji H, Mizumoto Y, Horiguchi K, Shiraiwa K, Tamura K, et al. High incidence of hepatocellular carcinomas induced by a choline deficient L-amino acid defined diet in rats. Cancer Res 1992 Sep 15;52(18):5042-5045.

127. Floyd RA, Kotake Y, Hensley K, Nakae D, Konishi Y. Reactive oxygen species in choline deficiency induced carcinogenesis and nitrone inhibition. Mol Cell Biochem 2002 May;234-235(1-2):195-203.

128. da Costa KA, Cochary EF, Blusztajn JK, Garner SC, Zeisel SH. Accumulation of 1,2-sn-diradylglycerol with increased membrane-associated protein kinase C may be the mechanism for spontaneous hepatocarcinogenesis in choline-deficient rats. J Biol Chem 1993 Jan 25;268(3):2100-2105.

129. Endoh T, Tang Q, Denda A, Noguchi O, Kobayashi E, Tamura K, et al. Inhibition by acetylsalicylic acid, a cyclo-oxygenase inhibitor, and p-bromophenacylbromide, a phospholipase A2 inhibitor, of both cirrhosis and enzyme-altered nodules caused by a choline-deficient, L-amino acid-defined diet in rats. Carcinogenesis 1996 Mar;17(3):467-475.

130. Dizik M, Christman JK, Wainfan E. Alterations in expression and methylation of specific genes in livers of rats fed a cancer promoting methyl-deficient diet. Carcinogenesis 1991 Jul;12(7):1307-1312.

131. Tsujiuchi T, Tsutsumi M, Sasaki Y, Takahama M, Konishi Y. Hypomethylation of CpG sites and c-myc gene overexpression in hepatocellular carcinomas, but not hyperplastic nodules, induced by a choline-deficient L-amino acid-defined diet in rats. Jpn J Cancer Res 1999 Sep;90(9):909-913.

132. Alizadeh AA, Ross DT, Perou CM, van de RM. Towards a novel classification of human malignancies based on gene expression patterns. J Pathol 2001 Sep;195(1):41-52.

133. Garber ME, Troyanskaya OG, Schluens K, Petersen S, Thaesler Z, Pacyna-Gengelbach M, et al. Diversity of gene expression in adenocarcinoma of the lung. Proc Natl Acad Sci U S A 2001 Nov 20;98(24):13784-13789.

134. Sorlie T, Perou CM, Tibshirani R, Aas T, Geisler S, Johnsen H, et al. Gene expression patterns of breast carcinomas distinguish tumor subclasses with clinical implications. Proc Natl Acad Sci U S A 2001 Sep 11;98(19):10869-10874.

135. Bertucci F, Finetti P, Rougemont J, Charafe-Jauffret E, Nasser V, Loriod B, et al. Gene expression profiling for molecular characterization of inflammatory breast cancer and prediction of response to chemotherapy. Cancer Res 2004 Dec 1;64(23):8558-8565.

136. Denda A, Kitayama W, Murata A, Kishida H, Sasaki Y, Kusuoka O, et al. Increased expression of cyclooxygenase-2 protein during rat hepatocarcinogenesis caused by a choline-deficient, L-amino acid-defined diet and chemopreventive efficacy of a specific inhibitor, nimesulide. Carcinogenesis 2002 Feb;23(2):245-256.

137. Irizarry RA, Hobbs B, Collin F, Beazer-Barclay YD, Antonellis KJ, Scherf U, et al. Exploration, normalization, and summaries of high density oligonucleotide array probe level data. Biostatistics 2003 Apr;4(2):249-264.

138. Eisen MB, Spellman PT, Brown PO, Botstein D. Cluster analysis and display of genome-wide expression patterns. Proc Natl Acad Sci U S A 1998 Dec 8;95(25):14863-14868.

139. Sorlie T, Tibshirani R, Parker J, Hastie T, Marron JS, Nobel A, et al. Repeated observation of breast tumor subtypes in independent gene expression data sets. Proc Natl Acad Sci U S A 2003 Jul 8;100(14):8418-8423.

140. Tusher VG, Tibshirani R, Chu G. Significance analysis of microarrays applied to the ionizing radiation response. Proc Natl Acad Sci U S A 2001 Apr 24;98(9):5116-5121.

141. Zielinska-Park J, Nakamura J, Swenberg JA, Aitken MD. Aldehydic DNA lesions in calf thymus DNA and HeLa S3 cells produced by bacterial quinone metabolites of fluoranthene and pyrene. Carcinogenesis 2004 Sep;25(9):1727-1733.

142. Khatri P, Bhavsar P, Bawa G, Draghici S. Onto-Tools: an ensemble of web-accessible, ontology-based tools for the functional design and interpretation of high-throughput gene expression experiments. Nucleic Acids Res 2004 Jul 1;32(Web Server issue):W449-W456.

143. Lombardi B, Pani P, Schlunk FF. Choline-deficiency fatty liver: impaired release of hepatic triglycerides. J Lipid Res 1968 Jul;9(4):437-446.

144. Nishizuka Y. Studies and perspectives of protein kinase C. Science 1986 Jul 18;233(4761):305-312.

145. Weinstein IB. The role of protein kinase C in growth control and the concept of carcinogenesis as a progressive disorder in signal transduction. Adv Second Messenger Phosphoprotein Res 1990;24:307-316.

146. Yen CL, Mar MH, Craciunescu CN, Edwards LJ, Zeisel SH. Deficiency in methionine, tryptophan, isoleucine, or choline induces apoptosis in cultured cells. J Nutr 2002 Jul;132(7):1840-1847.

147. Lotersztajn S, Julien B, Teixeira-Clerc F, Grenard P, Mallat A. Hepatic Fibrosis: Molecular Mechanisms and Drug Targets. Annu Rev Pharmacol Toxicol 2004 Oct 7.

148. Kershenobich SD, Weissbrod AB. Liver fibrosis and inflammation. A review. Ann Hepatol 2003 Oct;2(4):159-163.

149. Iredale JP, Murphy G, Hembry RM, Friedman SL, Arthur MJ. Human hepatic lipocytes synthesize tissue inhibitor of metalloproteinases-1. Implications for regulation of matrix degradation in liver. J Clin Invest 1992 Jul;90(1):282-287.

150. Herbst H, Wege T, Milani S, Pellegrini G, Orzechowski HD, Bechstein WO, et al. Tissue inhibitor of metalloproteinase-1 and -2 RNA expression in rat and human liver fibrosis. Am J Pathol 1997 May;150(5):1647-1659.

151. Rusyn I, Asakura S, Pachkowski B, Bradford BU, Denissenko MF, Peters JM, et al. Expression of base excision DNA repair genes is a sensitive biomarker for in vivo detection of chemical-induced chronic oxidative stress: Identification of the molecular source of radicals responsible for DNA damage by peroxisome proliferators. Cancer Res 2004;64(3):1050-1057.

152. Lopatina NG, Vanyushin BF, Cronin GM, Poirier LA. Elevated expression and altered pattern of activity of DNA methyltransferase in liver tumors of rats fed methyl-deficient diets. Carcinogenesis 1998 Oct;19(10):1777-1781.

153. Wakasugi N, Tagaya Y, Wakasugi H, Mitsui A, Maeda M, Yodoi J, et al. Adult T-cell leukemia-derived factor/thioredoxin, produced by both human T-lymphotropic virus type I- and Epstein-Barr virus-transformed lymphocytes, acts as an autocrine growth factor and synergizes with interleukin 1 and interleukin 2. Proc Natl Acad Sci U S A 1990 Nov;87(21):8282-8286.

154. European Standards Committee on Oxidative DNA Damage (ESCODD). Measurement of DNA oxidation in human cells by chromatographic and enzymic methods. Free Radic Biol Med 2003 Apr 15;34(8):1089-1099.

155. Yoshiji H, Nakae D, Mizumoto Y, Horiguchi K, Tamura K, Denda A, et al. Inhibitory effect of dietary iron deficiency on inductions of putative preneoplastic lesions as well as 8-hydroxydeoxyguanosine in DNA and lipid peroxidation in the livers of rats caused by exposure to a choline-deficient L-amino acid defined diet. Carcinogenesis 1992 Jul;13(7):1227-1233.

156. Cheng KC, Cahill DS, Kasai H, Nishimura S, Loeb LA. 8-Hydroxyguanine, an abundant form of oxidative DNA damage, causes G----T and A----C substitutions. J Biol Chem 1992 Jan 5;267(1):166-172.

157. Luczaj W, Skrzydlewska E. DNA damage caused by lipid peroxidation products. Cell Mol Biol Lett 2003;8(2):391-413.

158. Zindy P, Andrieux L, Bonnier D, Musso O, Langouet S, Campion JP, et al. Upregulation of DNA repair genes in active cirrhosis associated with hepatocellular carcinoma. FEBS Lett 2005 Jan 3;579(1):95-99.

159. Jungst C, Cheng B, Gehrke R, Schmitz V, Nischalke HD, Ramakers J, et al. Oxidative damage is increased in human liver tissue adjacent to hepatocellular carcinoma. Hepatology 2004 Jun;39(6):1663-1672.

160. Chen X, Cheung ST, So S, Fan ST, Barry C, Higgins J, et al. Gene expression patterns in human liver cancers. Mol Biol Cell 2002 Jun;13(6):1929-1939.

161. Ford ES. Risks for all-cause mortality, cardiovascular disease, and diabetes associated with the metabolic syndrome: a summary of the evidence. Diabetes Care 2005 Jul;28(7):1769-1778.

162. Singh B, Mallika V, Goswami B. Metabolic syndrome: Diagnosis, potential markers and management-an update. Clin Chim Acta 2006 Sep 1.

163. James PT. Obesity: the worldwide epidemic. Clin Dermatol 2004 Jul;22(4):276-280.

164. Institute of Medicine of the National Academies. Dietary fats: total fats and fatty acids. Dietary reference intakes for energy, carbohydrate, fiber, fat, fatty acids, cholesterol, protein, and amino acids (macronutrients).Washington, DC: The National Academy Press, 2002. 335-432.

165. Kris-Etherton PM, Taylor DS, Yu-Poth S, Huth P, Moriarty K, Fishell V, et al. Polyunsaturated fatty acids in the food chain in the United States. Am J Clin Nutr 2000 Jan;71(1 Suppl):179S-188S.

166. Curtis CL, Hughes CE, Flannery CR, Little CB, Harwood JL, Caterson B. n-3 fatty acids specifically modulate catabolic factors involved in articular cartilage degradation. J Biol Chem 2000 Jan 14;275(2):721-724.

167. Demaison L, Moreau D. Dietary n-3 polyunsaturated fatty acids and coronary heart disease-related mortality: a possible mechanism of action. Cell Mol Life Sci 2002 Mar;59(3):463-477.

168. Connor WE, Prince MJ, Ullmann D, Riddle M, Hatcher L, Smith FE, et al. The hypotriglyceridemic effect of fish oil in adult-onset diabetes without adverse glucose control. Ann N Y Acad Sci 1993 Jun 14;683:337-340.

169. Bartsch H, Nair J, Owen RW. Dietary polyunsaturated fatty acids and cancers of the breast and colorectum: emerging evidence for their role as risk modifiers. Carcinogenesis 1999 Dec;20(12):2209-2218.

170. Xu H, Barnes GT, Yang Q, Tan G, Yang D, Chou CJ, et al. Chronic inflammation in fat plays a crucial role in the development of obesity-related insulin resistance. J Clin Invest 2003 Dec;112(12):1821-1830.

171. Furukawa S, Fujita T, Shimabukuro M, Iwaki M, Yamada Y, Nakajima Y, et al. Increased oxidative stress in obesity and its impact on metabolic syndrome. J Clin Invest 2004 Dec;114(12):1752-1761.

172. Browning LM. n-3 Polyunsaturated fatty acids, inflammation and obesity-related disease. Proc Nutr Soc 2003 May;62(2):447-453.

173. Ailhaud G, Massiera F, Weill P, Legrand P, Alessandri JM, Guesnet P. Temporal changes in dietary fats: role of n-6 polyunsaturated fatty acids in excessive adipose tissue development and relationship to obesity. Prog Lipid Res 2006 May;45(3):203-236.

174. Curzio M, Esterbauer H, Poli G, Biasi F, Cecchini G, Di Mauro C, et al. Possible role of aldehydic lipid peroxidation products as chemoattractants. Int J Tissue React 1987;9(4):295-306.

175. Gonzalez MJ, Gray JI, Schemmel RA, Dugan L, Jr., Welsch CW. Lipid peroxidation products are elevated in fish oil diets even in the presence of added antioxidants. J Nutr 1992 Nov;122(11):2190-2195.

176. BLIGH EG, DYER WJ. A rapid method of total lipid extraction and purification. Can J Biochem Physiol 1959 Aug;37(8):911-917.

177. Tacconi M, Wurtman RJ. Rat brain phosphatidyl-N,N-dimethylethanolamine is rich in polyunsaturated fatty acids. J Neurochem 1985 Sep;45(3):805-809.

178. Berger JA, Hautaniemi S, Jarvinen AK, Edgren H, Mitra SK, Astola J. Optimized LOWESS normalization parameter selection for DNA microarray data. BMC Bioinformatics 2004 Dec 9;5:194.

179. Powell CL, Kosyk O, Ross PK, Schoonhoven R, Boysen G, Swenberg JA, et al. Phenotypic anchoring of acetaminophen-induced oxidative stress with gene expression profiles in rat liver. Toxicol Sci 2006 Sep;93(1):213-222.

180. Dignam JD, Lebovitz RM, Roeder RG. Accurate transcription initiation by RNA polymerase II in a soluble extract from isolated mammalian nuclei. Nucleic Acids Res 1983 Mar 11;11(5):1475-1489.

181. Inestrosa NC, Bronfman M, Leighton F. Detection of peroxisomal fatty acyl-coenzyme A oxidase activity. Biochem J 1979 Sep 15;182(3):779-788.

182. Niture SK, Velu CS, Smith QR, Bhat GJ, Srivenugopal KS. Increased expression of the MGMT repair protein mediated by cysteine prodrugs and chemopreventative natural products in human lymphocytes and tumor cell lines. Carcinogenesis 2006 Aug 31.

183. Kliewer SA, Sundseth SS, Jones SA, Brown PJ, Wisely GB, Koble CS, et al. Fatty acids and eicosanoids regulate gene expression through direct interactions with peroxisome proliferator-activated receptors alpha and gamma. Proc Natl Acad Sci U S A 1997 Apr 29;94(9):4318-4323.

184. Forman BM, Chen J, Evans RM. Hypolipidemic drugs, polyunsaturated fatty acids, and eicosanoids are ligands for peroxisome proliferator-activated receptors alpha and delta. Proc Natl Acad Sci U S A 1997 Apr 29;94(9):4312-4317.

185. Xu HE, Lambert MH, Montana VG, Parks DJ, Blanchard SG, Brown PJ, et al. Molecular recognition of fatty acids by peroxisome proliferator-activated receptors. Mol Cell 1999 Mar;3(3):397-403.

186. Clarke SD. Nonalcoholic steatosis and steatohepatitis. I. Molecular mechanism for polyunsaturated fatty acid regulation of gene transcription. Am J Physiol Gastrointest Liver Physiol 2001 Oct;281(4):G865-G869.

187. Cho HY, Jedlicka AE, Reddy SP, Zhang LY, Kensler TW, Kleeberger SR. Linkage analysis of susceptibility to hyperoxia. Nrf2 is a candidate gene. Am J Respir Cell Mol Biol 2002 Jan;26(1):42-51.

188. Anderson SP, Howroyd P, Liu J, Qian X, Bahnemann R, Swanson C, et al. The transcriptional response to a peroxisome proliferator-activated receptor alpha agonist includes increased expression of proteome maintenance genes. J Biol Chem 2004 Dec 10;279(50):52390-52398.

189. Chen C, Hennig GE, Whiteley HE, Corton JC, Manautou JE. Peroxisome proliferator-activated receptor alpha-null mice lack resistance to acetaminophen hepatotoxicity following clofibrate exposure. Toxicol Sci 2000 Oct;57(2):338-344.

190. Lai DY. Rodent carcinogenicity of peroxisome proliferators and issues on human relevance. J Environ Sci Health C Environ Carcinog Ecotoxicol Rev 2004 May;22(1):37-55.

191. Devchand PR, Keller H, Peters JM, Vazquez M, Gonzalez FJ, Wahli W. The PPARalpha-leukotriene B4 pathway to inflammation control. Nature 1996 Nov 7;384(6604):39-43.

192. Cunard R, Ricote M, DiCampli D, Archer DC, Kahn DA, Glass CK, et al. Regulation of cytokine expression by ligands of peroxisome proliferator activated receptors. J Immunol 2002 Mar 15;168(6):2795-2802.

193. Delerive P, De Bosscher K, Besnard S, Vanden Berghe W, Peters JM, Gonzalez FJ, et al. Peroxisome proliferator-activated receptor alpha negatively regulates the vascular inflammatory gene response by negative cross-talk with transcription factors NF-kappaB and AP-1. J Biol Chem 1999 Nov 5;274(45):32048-32054.

194. Spencer NF, Poynter ME, Im SY, Daynes RA. Constitutive activation of NF-kappa B in an animal model of aging. Int Immunol 1997 Oct;9(10):1581-1588.

195. Delerive P, Gervois P, Fruchart JC, Staels B. Induction of IkappaBalpha expression as a mechanism contributing to the anti-inflammatory activities of peroxisome proliferator-activated receptor-alpha activators. J Biol Chem 2000 Nov 24;275(47):36703-36707.

196. Youn CK, Kim SH, Lee DY, Song SH, Chang IY, Hyun JW, et al. Cadmium down-regulates human OGG1 through suppression of Sp1 activity. J Biol Chem 2005 Jul 1;280(26):25185-25195.

197. Bravard A, Vacher M, Gouget B, Coutant A, de Boisferon FH, Marsin S, et al. Redox regulation of human OGG1 activity in response to cellular oxidative stress. Mol Cell Biol 2006 Oct;26(20):7430-7436.

198. Cabelof DC, Raffoul JJ, Yanamadala S, Guo Z, Heydari AR. Induction of DNA polymerase beta-dependent base excision repair in response to oxidative stress in vivo. Carcinogenesis 2002 Sep;23(9):1419-1425.

199. Powell CL, Swenberg JA, Rusyn I. Expression of base excision DNA repair genes as a biomarker of oxidative DNA damage. Cancer Lett 2005 Nov 8;229(1):1-11.

200. Srivastava DK, Berg BJ, Prasad R, Molina JT, Beard WA, Tomkinson AE, et al. Mammalian abasic site base excision repair. Identification of the reaction sequence and rate-determining steps. J Biol Chem 1998 Aug 14;273(33):21203-21209.

201. Blount BC, Mack MM, Wehr CM, MacGregor JT, Hiatt RA, Wang G, et al. Folate deficiency causes uracil misincorporation into human DNA and chromosome breakage: implications for cancer and neuronal damage. Proc Natl Acad Sci USA 1997 Apr 1;94(7):3290-3295.

202. Keaney JF, Jr., Larson MG, Vasan RS, Wilson PW, Lipinska I, Corey D, et al. Obesity and systemic oxidative stress: clinical correlates of oxidative stress in the Framingham Study. Arterioscler Thromb Vasc Biol 2003 Mar 1;23(3):434-439.

203. Olusi SO. Obesity is an independent risk factor for plasma lipid peroxidation and depletion of erythrocyte cytoprotectic enzymes in humans. Int J Obes Relat Metab Disord 2002 Sep;26(9):1159-1164.

204. Nikitin A, Egorov S, Daraselia N, Mazo I. Pathway studio--the analysis and navigation of molecular networks. Bioinformatics 2003 Nov 1;19(16):2155-2157.

205. Aardema MJ, MacGregor JT. Toxicology and genetic toxicology in the new era of "toxicogenomics": impact of "-omics" technologies. Mutat Res 2002 Jan 29;499(1):13-25.

206. Knight TR, Ho YS, Farhood A, Jaeschke H. Peroxynitrite is a critical mediator of acetaminophen hepatotoxicity in murine livers: protection by glutathione. J Pharmacol Exp Ther 2002 Nov;303(2):468-475.

207. Powell CL, Kosyk O, Bradford BU, Parker JS, Lobenhofer EK, Denda A, et al. Temporal correlation of pathology and DNA damage with gene expression in a choline-deficient model of rat liver injury. Hepatology 2005 Nov;42(5):1137-1147.

208. Yarden Y. The EGFR family and its ligands in human cancer. signalling mechanisms and therapeutic opportunities. Eur J Cancer 2001 Sep;37 Suppl 4:S3-S8.

209. Lee JS, Thorgeirsson SS. Comparative and integrative functional genomics of HCC. Oncogene 2006 Jun 26;25(27):3801-3809.

210. Tsipas G, Morphake P. Beneficial effects of a diet rich in a mixture of n - 6/n - 3 essential fatty acids and of their metabolites on cyclosporine - nephrotoxicity. J Nutr Biochem 2003 Nov;14(11):626-632.

211. Hennig B, Hammock BD, Slim R, Toborek M, Saraswathi V, Robertson LW. PCB-induced oxidative stress in endothelial cells: modulation by nutrients. Int J Hyg Environ Health 2002 Mar;205(1-2):95-102.

212. Farooqui MY, Ybarra B, Piper J, Tamez A. Effect of dosing vehicle on the toxicity and metabolism of unsaturated aliphatic nitriles. J Appl Toxicol 1995 Sep;15(5):411-420.

213. Casciano DA, Woodcock J. Empowering microarrays in the regulatory setting. Nat Biotechnol 2006 Sep;24(9):1103.

214. Shi L, Tong W, Fang H, Scherf U, Han J, Puri RK, et al. Cross-platform comparability of microarray technology: intra-platform consistency and appropriate data analysis procedures are essential. BMC Bioinformatics 2005 Jul 15;6 Suppl 2:S12.

215. Shi L, Reid LH, Jones WD, Shippy R, Warrington JA, Baker SC, et al. The MicroArray Quality Control (MAQC) project shows inter- and intraplatform reproducibility of gene expression measurements. Nat Biotechnol 2006 Sep;24(9):1151-1161.

216. Kuo WP, Liu F, Trimarchi J, Punzo C, Lombardi M, Sarang J, et al. A sequence-oriented comparison of gene expression measurements across different hybridization-based technologies. Nat Biotechnol 2006 Jul;24(7):832-840.

217. Tong W, Lucas AB, Shippy R, Fan X, Fang H, Hong H, et al. Evaluation of external RNA controls for the assessment of microarray performance. Nat Biotechnol 2006 Sep;24(9):1132-1139.

218. Qin LX, Beyer RP, Hudson FN, Linford NJ, Morris DE, Kerr KF. Evaluation of methods for oligonucleotide array data via quantitative real-time PCR. BMC Bioinformatics 2006;7:23.

219. Canales RD, Luo Y, Willey JC, Austermiller B, Barbacioru CC, Boysen C, et al. Evaluation of DNA microarray results with quantitative gene expression platforms. Nat Biotechnol 2006 Sep;24(9):1115-1122.

220. Budhraja V, Spitznagel E, Schaiff WT, Sadovsky Y. Incorporation of gene-specific variability improves expression analysis using high-density DNA microarrays. BMC Biol 2003;1:1.

221. Guo L, Lobenhofer EK, Wang C, Shippy R, Harris SC, Zhang L, et al. Rat toxicogenomic study reveals analytical consistency across microarray platforms. Nat Biotechnol 2006 Sep;24(9):1162-1169.

222. Liu G, Zhou W, Park S, Wang LI, Miller DP, Wain JC, et al. The SOD2 Val/Val genotype enhances the risk of nonsmall cell lung carcinoma by p53 and XRCC1 polymorphisms. Cancer 2004 Dec 15;101(12):2802-2808.

223. Meyers DA, Larj MJ, Lange L. Genetics of asthma and COPD. Similar results for different phenotypes. Chest 2004 Aug;126(2 Suppl):105S-110S.

224. Weber WW. Effect of pharmacogenetics on medicine. Environ Mol Mutagen 2001;37(3):179-184.